MIMO ANTENNAS FOR MOBILE HANDSET AND TABLET APPLICATIONS

Sultan Shoaib

A thesis presented in partial fulfillment of the requirements for the Degree of Doctor of Philosophy

January, 2016

Antennas and Electromagnetic Research Group
School of Electronic Engineering and Computer Science, Queen Mary,
University of London, Mile End Road, London, United Kingdom, E1 4NS.

DECLARATION

I, Sultan Shoaib, confirm that the research included within this thesis is my own work or that where it has been carried out in collaboration with, or supported by others, that this is duly acknowledged below and my contribution indicated. Previously published material is also acknowledged below.

I attest that I have exercised reasonable care to ensure that the work is original, and does not to the best of my knowledge break any UK law, infringe any third party's copyright or other Intellectual Property Right, or contain any confidential material.

I accept that the College has the right to use plagiarism detection software to check the electronic version of the thesis.

I confirm that this thesis has not been previously submitted for the award of a degree by this or any other university.

Signature: *Sultan Shoaib*

Date: 29/01/16

TO MY BELOVED PARENTS

ABSTRACT

The fast development of wireless communication technologies is pressing the antenna engineers to investigate and design compact multiband antennas for the multiple-input multiple-output (MIMO) systems, which is the key technology for the next generation of mobile communications. The growing increase in the demand for transmitting and exchanging large volume data, such as multimedia and interactive materials is constantly fueling the need for higher data rates. MIMO systems have demonstrated the capability to increase channel capacity, with a simultaneous increase in range and reliability, without taking any additional bandwidth thus resulting in improved data throughput. However, the performance of a MIMO system is highly dependent on the nature of its propagation environment and the placement of antennas on device platform. The true benefits of MIMO can be exploited through a smart design that can adapt with changing system requirements or environmental conditions.

This research project has investigated the methods to make multiband MIMO and multiband reconfigurable antennas on small mobile terminals with high communication performance. This involves the methods for avoiding coupling between multiple antennas and possible tuning of the antennas for next generation mobile handsets. The aim of this work is to develop MIMO and reconfigurable antennas for wireless terminals such as mobile handsets and tablets. The project is divided in two phases with the first phase involving the development of multiband MIMO antennas for handheld terminals and the second phase involves the design of reconfigurable antenna for mobile handsets. Several prototypes of handset antennas, capable of covering various cellular frequency bands, have been developed. The research involves a substantial work on theoretical analysis, computer simulation and experimental verification.

ACKNOWLDEGMENTS

Foremost, I would like to express my sincere thanks to my supervisor *Prof. Xiaodong Chen* for his continuous support and encouragement throughout my years of PhD. His guidance has made this a thoughtful and rewarding journey.

I would also like to thank my co-supervisors *Prof. Clive Parini* and *Dr. Robert Donnan* for their encouragement, insightful comments and helping questions.

Besides my supervisor, I would like to thank *Dr. Rostyslav Dubrovka* the manager of Terahertz and Quasi-Optics Research Unit, *Mr. Tony Stone* of the Mechanical Laboratory, *Mr. Ho Heun* of the Electronics Laboratory and *Dr. Massimo Candotti* of the Antenna Laboratory for their valuable help and support in the fabrication and measurements of antennas.

I would also like to thank my brothers *Mr. Imran Shoaib* and *Dr. Nosherwan Shoaib* who always guide me in my problems and difficulty.

I would like to thank my *parents* and all my *family members* for their moral support and undying love because without it, I do not think I would have been able to accomplish anything. Their prayers always keep my confidence high and helped me achieving my goals.

Lastly, I would like to thank my *friends* and *members* of the School of Electronic Engineering at QMUL for their infinite support and an incredible experience.

TABLE OF CONTENTS

LIST OF FIGURES

LIST OF TABLES

LIST OF ABBREVIATIONS

- MIMO Multiple-Input Multiple-Output
- SISO Single-Input Single-Output
- SIMO Single-Input Multiple-Output
- MISO Multiple-Input Single-Output
- 2G Second Generation (Wireless communication system)
- 3G Third Generation (Wireless communication system)
- 4G Fourth Generation (Wireless communication system)
- LTE Long Term Evolution
- GSM Global System for Mobile Communications
- UMTS *Universal Mobile Telecommunications System*
- DCS Digital Cellular Service
- PCS Personal Communications Service
- HSDPA High-Speed Downlink Packet Access
- WiMAX Worldwide Interoperability for Microwave Access
- LAN Local Area Network
- HyperLAN High Performance Radio Local Area Network
- GPS Global Positioning System
- WLAN Wireless Local Area Network
- PIFA Planar Inverted-F Antenna
- RF Radio Frequency
- ECC Envelope Correlation Coefficient
- PIN Positive - Intrinsic – Negative
- CST Computer Simulation Technology

- VNA Vector Network Analyzer
- AUT Antenna Under Test
- QMUL Queen Mary, University of London
- FR-4 Flame Retardant 4
- PCB Printed Circuit Board
- IP Internet Protocol
- IEEE Institute of Electrical and Electronics Engineers

CHAPTER 1
INTRODUCTION AND OVERVIEW

1.1 Introduction

Wireless communication is probably the fastest growing part of the modern communication technology. Currently there are around 4.4 billion mobile users worldwide which will increase to 5.1 billion by 2019 [1]. In earlier days of development, the wireless communication was limited to military and security applications. With the development of the various communication standards, the wireless communication was expanded to the commercial applications for making businesses more profitable. Further advancements in wireless communication such as 2G Global System for Mobile communications (GSM) resulted in the evolution of handheld wireless terminals such as mobile phones. The mobile phone industry is now perhaps one of the fastest growing industries with a rapidly increasing number of consumers. Mobile phone technology has experienced a rapid growth over the last decade. The first mobile phone was developed by Motorola in 1973 which cost around modern day $10000 and had the size of 330 x 45 x 89 mm^3 [2]. Initially mobile devices were only able to provide voice communication services. Also the size of mobile handset was bulky and the concept of a pocket held device was not introduced. As the technology advanced, the size of the mobile device started reducing with an improved capability to support numerous communication services. A few examples of early mobile handsets are shown in figure 1.1. It can be seen from the figure that the handset size reduced with the advancement of the wireless technology. Earlier mobile devices were manufactured with antennas outside the

mobile housing. With the developments in antenna technology, it became possible to place the antenna inside mobile handset. Later on, the portability requirements of the users also changed. The users now demand a slim and compact mobile handset that can be used in indoor and outdoor environments at both pedestrian and vehicular speeds. Also, the average time spent by each user on mobile device is radically increased over the last five years. A mobile device now is not only a source of multimedia communication but also a source of entertainment. This in turn requires a high data rate communication to keep the user entertainment seamless and uninterrupted. Certain modern communication standards were thus evolved to meet the user requirements.

Figure 1.1: Evolution of mobile handsets. (*Source: Google Images*)

With the introduction of modern wireless communication standards such as universal mobile telecommunication system (UMTS), high-speed downlink packet access (HSDPA) and Advanced Long Term Evolution (LTE), the mobile handset is now reduced to a compact pocket held device. Figure 1.2 presents numerous uses of modern mobile handsets. Today's mobile devices can provide seamless audio, video and large sized data communication services on the go. Meanwhile, the number of users also started increasing over the last five years. We are now living in a dense environment of wireless communication where mobile phone use is an integrated part of everyone's life. Studies have shown that the number of mobile users increased from 4.01 billion to 4.43 billion in the last 3 years [1]. Also the size of mobile handsets is getting smaller which has induced the requirement of having an advanced and compact antenna technology. A comparison between various generations of mobile communication is shown in table 1.1.

Figure 1.2: Uses of mobile devices. (*Source: Google Images*)

Table 1.1: Comparison between various generations of cellular communication.[3]-[4]

Technology Name	Key Features	Data Rate
1st generation (1G) 	- Deployed in 1981 - Analog protocols - Voice communication only - Large sized handsets - No security - Poor handoff reliability - Antenna outside handset - No roaming facility	2.4 kbps
2nd generation (2G) 	- Deployed in 1992 - Digital protocols - Voice communication and text messaging - Better voice quality than 1G - Better range than 1G - Improved security - More reliable than 1G	64 kbps
3rd generation (3G) 	- Deployed in 2001 - Digital broadband and packet data - First mobile broadband technology - Voice, text and multimedia communication - Better voice quality than 1G and 2G - Better range than 1G and 2G - Enhanced security - More reliable than 1G and 2G	3.1 Mbps
4th generation (4G) 	- Deployed in 2011 - Specialized in data communication - On the go large volume multimedia services - IP based protocols - Excellent range - Excellent handoff reliability - Advanced antenna technology	100 Mbps

Multiple Input Multiple Output (MIMO) is a technology that promises an increased capacity without requiring any additional bandwidth and transmission power. The MIMO technology was developed more than 10 years ago and it has been successfully employed in WLAN terminals [5]. However, the implementation of MIMO in a mobile handset is not yet successful due to the size limitations. It is rather a big challenge to place multiple antennas inside a mobile handset with acceptable isolation. This is because the close spacing between the antennas increases the mutual coupling. The design of closely spaced MIMO antennas requires certain decoupling techniques to achieve an acceptable isolation. This introduces a challenge as the decoupling structure alters the return loss of the antennas. It is therefore necessary to develop MIMO antennas with acceptable return loss and isolation performance for multiband mobile phones. The 4G LTE advanced is the newest standard of wireless communication that can provide a high data rate from a portable mobile handset [6]. The benefits of 4G LTE advanced can be exploited by developing compact MIMO antennas for slim mobile handsets. Therefore, the antenna designs need to be improved so as to occupy less space and provide good performance.

1.2 Motivation

With the advancements in the modern communication standards such as LTE advanced, wireless communication becomes more convenient and with more rapid data transfer. Today's wireless terminals come with a capability of supporting voice and large sized data communications simultaneously [7]-[9]. Modern day users are not only able to access and download data on the mobile handset but also enjoy high quality video streaming. However, with the increasingly changing environment such as large buildings and obstacles and increase in the number of users, the amount of interference to the communication is increased. This largely degrades the quality of the communication link. Strong, continued growth in wireless usage, particularly data and multimedia services on smartphones and tablets, has motivated the wireless industry to improve existing wireless communication systems for achieving unprecedented network speed and have good connectivity indoors or outdoors. Multiple Input Multiple Output is the key technology which utilizes the signal scatterings from the obstacles to enhance the communication capacity. Research in wired and wireless communications with high spectral

efficiency has been gaining increasingly intense efforts since the findings of Claude E. Shannon on the channel capacity in 1948, [7]. The pioneering work by Foschini [8]-[9] and Telatar [10] has proven that MIMO systems have significant higher capacity than conventional single-input single-output (SISO) systems. MIMO technology assures a high data rate, increased channel capacity and enhanced coverage without a need of having additional channel bandwidth. Nevertheless, the performance of a MIMO system is highly dependent on the nature of its propagation environment and the placement of the antennas on the device platform. Real propagation environments do not match the uncorrelated independent and identically distributed channel models and the varying channel conditions largely limit the channel capacity of a MIMO system. The choice of an antenna also imposes restrictions on the overall system performance that arises because the antenna characteristics are fixed. The main problem with newly released wireless terminals is their tendency to become compact, which limits the total size of the antenna design. A consequence of this is that the multiple antennas required have to be more closely spaced. This increases the undesired signal correlation between the antennas which significantly degrades the MIMO system throughput.

Adaptive MIMO systems, which can dynamically adapt themselves to time-varying channel conditions, will be the key for the future generation of mobile communication systems. An excellent discussion on adaptive MIMO systems is given in [11]. In this reference, some parameters such as the modulation level, coding rate and transmission signaling schemes are dynamically adapted to the time-varying channel conditions. The antenna elements in such systems are fixed by the initial design and cannot reconfigure their properties, that is, radiation pattern, polarization, and operating frequency.

Reconfigurable antennas have the capacity to alter their properties over varying channel conditions. This feature of reconfigurable antennas made their development imperative in future wireless communication systems. Their agility and diversity created new horizons for different types of applications especially when employed in MIMO systems. Recent studies have shown that reconfigurable antennas offer an additional degree of freedom in improving performance of an adaptive MIMO system and selection of the optimum antenna properties and configuration together with other

system parameters with respect to the varying channel conditions [12]-[16]. Thus Reconfigurable antennas can be employed in mobile handsets to further enhance the quality of data communication.

The aim of this work is to develop MIMO and reconfigurable antennas for new generation multiband mobile handsets. The project is divided in two phases in which the first phase involves the development of multiband MIMO antennas for handheld mobile terminals such as tablets and smartphones. Whereas, the second phase includes the design of the reconfigurable antennas for mobile handsets. Several prototypes of multiband MIMO and reconfigurable antennas for mobile handsets/tablets, capable of covering various cellular frequency bands to provide seamless services, have been developed. The research involves a substantial work based on theoretical analysis, computer simulation and experimental verification.

1.3 Outline of the report

Chapter 2 gives an introduction to the fundamentals of antenna theory and the MIMO technology. This chapter is divided in two major sections. The first section presents the basic concepts and the working mechanism of antennas. The key parameters used in the testing of an antenna such as return loss, isolation, bandwidth and radiation patterns will also be discussed in this section. This section will provide a basic knowledge of antennas and wave propagation to the readers. The second section of this chapter presents the introduction and working mechanism of MIMO technology. What is MIMO and how it works will be discussed in this section along with the applications and the requirements of MIMO antenna design.

Chapter 3 includes a detailed review of various designs that have been proposed in the literature for achieving multiband operations for mobile terminals. This chapter includes three sections which include a discussion on single antenna, MIMO and reconfigurable antenna designs for mobile handsets that have been presented recently in the literature.

Chapter 4 presents the designs of multiband MIMO antennas for mobile handsets. Three designs of the MIMO antennas are presented in this chapter covering 2G, 3G and 4G cellular frequency bands. The chapter is divided in three sections. The first

section presents the design of multiband MIMO antennas based on multi-branch monopole configuration whereas, the second section will present the design of compact MIMO antennas in meandered monopole configuration. Likewise, the third section presents the design of MIMO antennas based on coupled loop configuration. Each design is presented in detail including the simulation and measurement results along with a comprehensive simulation analysis of each MIMO design.

Chapter 5 presents two designs of the MIMO antennas for mobile tablets. This chapter includes two sections. The first section presents a design of MIMO antennas for 2G and 3G cellular coverage whereas, the second section presents the MIMO antennas for covering 2G, 3G and 4G cellular frequency bands. This chapter will include the simulation and measurement results along with the simulation analysis of the proposed MIMO antennas for mobile tablets.

Chapter 6 presents the design of pattern reconfigurable MIMO antennas for mobile handsets. The design is based on meandered monopole configuration with additional metallic branches that can be connected or disconnected to achieve pattern reconfigurability. This chapter will include the simulation and measurement results along with a comprehensive simulation analysis of the proposed reconfigurable antennas.

Chapter 7 presents the conclusions and the plans and improvements for future work.

1.4 Contributions

The research work presented in this thesis introduced new designs of multiband MIMO antennas for portable terminals such as mobile handsets and tablets. The designs proposed in the work are planar and compact. The design methodology is based on meandering monopole and loop strips for achieving compact volume, suitable for slim mobile handsets. The antennas possess good cellular coverage with acceptable return loss and isolation performances. The decoupling structures used in the designs are new and provide better isolation then most of the designs presented in the literature. The antennas cover most of the commercially available 2G, 3G and 4G cellular frequency bands.

1.5 List of publications

a) Conference Papers:

[1] *Design and Performance Study of MIMO Antennas for Next Generation Mobile Tablets*, in IEEE URSI Commission B International Symposium on Electromagnetic Theory, February 2016, (Under Review)

[2] *MIMO Antennas for New Generation Smartphones*, in IEEE 10th European Conference on Antennas and Propagation (EuCAP), April 2016

[3] *Compact and printed MIMO antennas for 2G/3G and 4G — LTE mobile tablets*, in IEEE-APS Topical Conference on Antennas and Propagation in Wireless Communications (APWC), September 2015

[4] *Compact and printed multiband antennas for 2G/3G/4G smartphones*, in IEEE International Symposium on Antennas and Propagation & USNC/URSI National Radio Science Meeting, July 2015

[5] *Pattern reconfigurable antenna for mobile handsets*, in IEEE Loughborough Antennas and Propagation Conference (LAPC), November 2014

[6] *A 4×4 MIMO antenna system for mobile tablets*, in IEEE European Conference on Antennas and Propagation (EuCAP), April 2014

[7] *A single-element frequency and radiation pattern reconfigurable antenna*, in IEEE European Conference on Antennas and Propagation (EuCAP), April 2013

[8] *A printed hybrid loop planar inverted-F antenna for next generation handheld terminals*, in IEEE European Conference on Antennas and Propagation (EuCAP), April 2013

[9] *A switched-beam three element printed loop antenna array for MIMO systems*, in IEEE European Conference on Antennas and Propagation (EuCAP), April 2013

(b) Invited Papers:

[1] *MIMO antennas for mobile handsets*, in Antennas and Propagation (APCAP), 2014 3rd Asia-Pacific Conference on , Harbin, China, July 2014

[2] *Compact dual printed MIMO antennas for mobile handsets covering GSM/UMTS/WLAN and LTE*, Invited abstract paper and presentation, Progress in Electromagnetics Research Symposium (PIERS), Stockholm, Sweden, August, 2013

(c) Journal Papers:

[1] *Reconfigurable MIMO Antennas for Mobile Smartphones*, in Microwave and Optical Technology Letters (MOTL), Wiley Online Library, 2015-16 (Under Review)

[2] *MIMO Antennas for Mobile Handsets*, in Antennas and Wireless Propagation Letters (AWPL), IEEE , Vol. 14, pp.799-802, 2015

[3] *Design and Performance Study of a Dual-Element Multiband Printed Monopole Antenna Array for MIMO Terminals*, in Antennas and Wireless Propagation Letters (AWPL), IEEE , Vol. 13, pp.329-332, 2014

References

[1] Telecommunications report, “Number of mobile phone users worldwide”, online, Available at: http://www.statista.com/statistics/274774/forecast-of-mobile-phone-users-worldwide/.

[2] Wikipedia article, “History of Mobile phones”, online, Available at: https://en.wikipedia .org/wiki/History_of_mobile_phones.

[3] 1G, 2G, 3G, 4G: The evolution of wireless generations, http://www.phonearena.com/news/1G-2G-3G-4G-The-evolution-of-wireless-generations_id46952

[4] S. Shukla, V. Khare, “Comparative Study of 1G, 2G, 3G and 4G”, Journal of Engineering, Computers & Applied Sciences (JEC&AS), ISSN No: 2319-5606, Vol. 2, No.4, April 2013

[5] Gesbert, D.; Shafi, M.; Da-shan Shiu; Smith, P.J.; Naguib, A., "From theory to practice: an overview of MIMO space-time coded wireless systems," in Selected Areas in Communications, IEEE Journal on , vol.21, no.3, pp.281-302, Apr 2003.

[6] Ghosh, A.; Ratasuk, R.; Mondal, B.; Mangalvedhe, N.; Thomas, T., "LTE-advanced: next-generation wireless broadband technology [Invited Paper]," in Wireless Communications, IEEE , vol.17, no.3, pp.10-22, June 2010.

[7] C. E. Shannon, “A mathematical theory of communication,” Bell System Technology Journal, vol. 27, pp. 623–656, 1948.

[8] G. J. Foschini and M. J. Gans, “On limits of wireless communications in a fading environment when using multiple antennas,” Wireless Personal Communi-cations, vol. 6, no. 3, pp. 311–335, 1998.

[9] D.-S. Shiu, G. J. Foschini, M. J. Gans, and J. M. Kahn, “Fading correlation and its effect on the capacity of multielement antenna systems,” IEEE Transactions on Commununications, vol. 48, no. 3, pp. 502–513, 2000.

[10] E. Telatar, “Capacity of multi-antenna gaussian channels,” European Transactions on Telecommunications, vol. 10, no. 6, pp. 585–595, 1999.

[11] S. Catreux, V. Erceg et al., “Adaptive Modulation and MIMO Coding for Broadband Wireless Data Networks,” IEEE Communications Magazine, vol. 40, no. 6, pp. 108–115, 2002.

[12] Zhengyi Li, Xuan Wang, Zhengwei Du and Ke Gong, “Performance Evaluation of a Four-Element Antenna Array with Selection Circuits for Adaptive

MIMO Systems," Tsinghua Science & Technology Journal, vol. 15, no. 3, pp. 294–298, 2010.

[13] H. K. Pan, G. Huff et al., "Increasing channel capacity on MIMO system employing adaptive pattern/polarization reconfigurable antenna," in Proceedings of the IEEE Antennas and Propagation Society International Symposium, pp. 481–484, 2007.

[14] D. Piazza, P. Mookiah, M. D'Amico, and K. R. Dandekar, "Experimental Analysis of Pattern and Polarization Reconfigurable Circular Patch Antennas for MIMO Systems," IEEE Transactions on Vehicular Technology, vol. 59, no. 5, pp. 2352–2362, 2010.

[15] F. Mubasher, Shihua Wang, Xiaodong Chen, and Zhinong Ying, "Study of reconfigurable antennas for MIMO systems," in Proceedings of the International Workshop on Antenna Technology (iWAT), 2010.

[16] D. Piazza, N. Kirsch, A. Forenza, R. Heath, and K. R. Dandekar, "Design and Evaluation of a Reconfigurable Antenna Array for MIMO Systems," IEEE Transactions on Antennas and Propagation, vol. 56, no. 3, pp. 869–881, 2008.

CHAPTER 2
THEORETICAL BACKGROUND

This chapter gives an introduction to the fundamentals of antenna theory and the multiple input multiple output (MIMO) technology. This chapter is divided in two major sections. The first section presents the basic concepts and the radiation mechanism of antenna. Key parameters used in the testing of an antenna such as return loss, isolation, bandwidth and radiation patterns will also be discussed in this section. This section will provide a basic knowledge of antennas and wave propagation to the readers. The second section of this chapter will present the introduction and working mechanism of MIMO technology: what is MIMO and how it works, along with the applications and the requirements of MIMO antenna design.

2.1 Fundamentals of antenna theory:

2.1.1 What is an Antenna?

An antenna is a metallic device that is used to transmit or receive electromagnetic waves. Electromagnetic waves are also known as radio waves. When a radio frequency signal is applied to antenna, it converts it into the electromagnetic radiation that travels through the free space. Conversely, a receiving antenna transforms an electromagnetic radiation back to a radio signal. The antenna is thus a passive device which can be used as a transmitter and a receiver. An antenna just redirects the power to get more radiation in specific directions without adding any additional power to it [1]-[3]. Each antenna is designed or tuned to cover either single or multiple frequency bands other than which it cannot transmit or receive. The antenna size is usually expressed in terms of wavelength for example, half wavelength dipole. Wavelength is

symbolically represented as λ. It is the distance that a radio signal travels in one cycle. An antenna is an interface between the transmission line and the free space through which the signal travels. Antenna is used in all devices which involve transmission or reception of communication signal wirelessly. Typical examples of antennas include dipole antenna, loop antenna, patch antenna, helical antenna, reflector antenna and Yagi antenna [1]-[3].

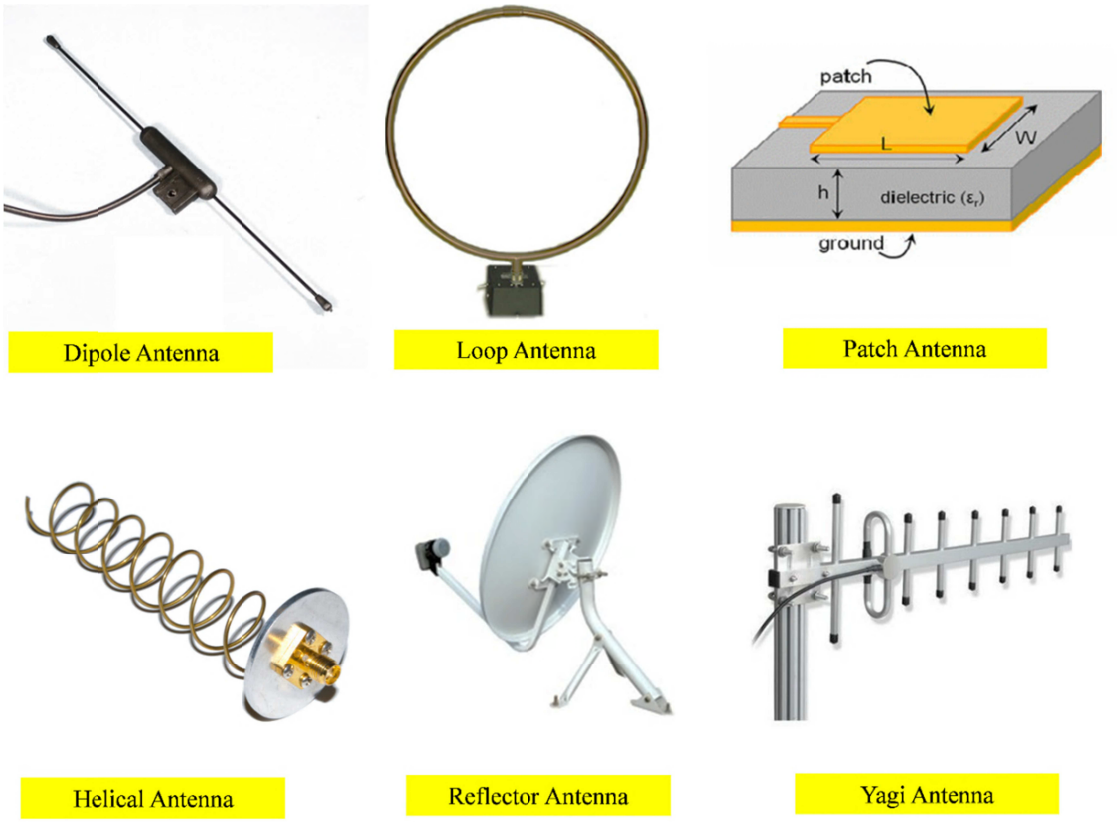

Figure 2.1: Typical examples of antennas. [1]-[3]

2.1.2 Principles of Electromagnetic radiation

An antenna works by the oscillations of the electrons back and forth on its metallic surface. Every metal has atoms with outer shells made up of weakly held electrons which can be detached to float in free space. This happens when electrons are subjected to an excitation signal which changes their energy level. In antennas, when an alternating voltage is applied to the input of antenna, the electrons on the surface of metals oscillate due to the alternation of the electric polarity. As the polarity of the electric current changes the magnetic field is created and the field starts oscillating [1]-[4].

If we feed an antenna with AC current, the electron flow will set up in it. Due to the alternating nature of the feeding signal, the direction in which maximum concentration of electrons flow occurs changes alternatingly. This cycle repeats itself at signal frequency. This electron flow creates a fluctuating magnetic field. The direction of the magnetic field reverses with the change in the polarity. The magnetic field thus reverses its direction at each half cycle of the signal frequency. This is known as H field whose strength is proportional to the amplitude of the current standing wave. The current standing wave is out of phase of the voltage standing wave. As the polarity changes on the surface of antenna, the electric field lines are produced which change the direction with the direction of polarity. This is known as E field. The E and H fields thus build and collapse 90^0 out of phase to each other and constitute the antenna's immediate field. This immediate field then produces radiating patterns which propagate outwards into the free space in the form of bubbles of energy. The radiation mechanism can be understood by taking example of a half wavelength dipole antenna. Figure 2.2 shows the formation and detachment of electric field lines from the surface of a half wavelength dipole antenna [1]-[4].

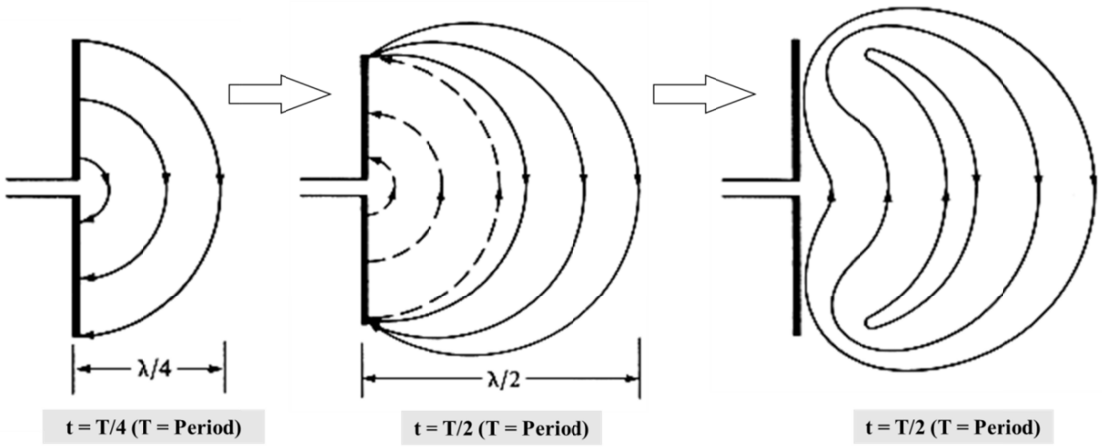

Figure 2.2: Radiation mechanism of a half wavelength dipole antenna [1].

2.1.3 Key antenna parameters

(a) Input impedance:

When an input radio frequency signal is applied to an antenna it excites the electrons on its surface thereby generating a current distribution which is then radiated to the free space. However, besides this radiation there are certain losses associated with an antenna. These losses include the power dissipation due to ohmic or dielectric losses in the antenna and also a part of input voltage creates a reactive field around the antenna. The antenna can thus be

modelled as equivalent complex impedance Z_c which takes the same power from input transmission line as the amount of power drawn by antenna. This complex impedance is known as input impedance of antenna. Input impedance refers to the ratio of voltage and current at the feeding point of antenna. It has no physical existence. The real part of the input impedance is the resistive part which represents the power radiated in the free space and the power dissipated in the antenna whereas, the imaginary part is the reactive part which represents the reactive power stored in the antenna's near field. If the imaginary part is zero, the antenna is said to be resonant. For an efficient transmission and reception of radio signal, the input impedance of the feeding source and the antenna must be well matched. In case of impedance mismatch, the radiation will be impaired and an impedance matching circuit will be needed. Usually the feeding sources are designed with an impedance of 50 Ω. If an antenna is designed to radiate a single or multiple frequency bands then its impedance must be matched to the impedance of the feeding source at single or multiple frequencies [1]-[4].

(b) Return loss:

The return loss (R_L) is defined as the ratio of power reflected to the input power. It represents how much mismatch exists between the antenna and feed line and is usually expressed in decibels (dB). The return loss can be calculated by using the magnitude of the reflection coefficient (Γ). The mathematical equation relating return loss and reflection coefficient is:

$$R_L = -20 * \log|\Gamma| \tag{2.1}$$

The reflection coefficient can be defined as the ratio of amplitudes of the signal reflected back to the input signal. It can be calculated by using the source and load impedances. The mathematical equation for calculating the reflection coefficient using impedances can be represented as [1]-[4]:

$$\Gamma = \frac{Z_L - Z_s}{Z_L + Z_s} \tag{2.2}$$

(c) Bandwidth:

The term bandwidth refers to the frequency bands in which an antenna can operate. It is the difference of the highest frequency from the lowest frequency. However, antenna can operate in multiple frequency bandwidths that are usually defined with respect to the return loss value

of 10 dB for most antennas. However, for low profile antennas such as handset antennas, the bandwidth is usually defined with respect to a return loss of 6 dB [1]-[4].

(d) Radiation pattern:

The term radiation pattern refers to the mathematical or graphical illustration of the strength of the electromagnetic field radiated by an antenna relative to the direction. It represents the radiation properties of an antenna as a function of space coordinates. The radiation pattern of an antenna is usually presented as a 3D graphical diagram. However, the measurement of 3D radiation patterns is usually very time consuming so, a 2D polar or rectangular plot can be used to represent the radiation of antenna in the principal planes which include E-plane (Elevation plane) and H-plane (Azimuthal plane). The E-plane contains the electric field vector, whereas, the H-plane contains the magnetic field vector. Both E-plane and H-plane are usually defined with respect to the direction of maximum radiation [1]-[4]. An example of radiation pattern is shown in Figure 2.3.

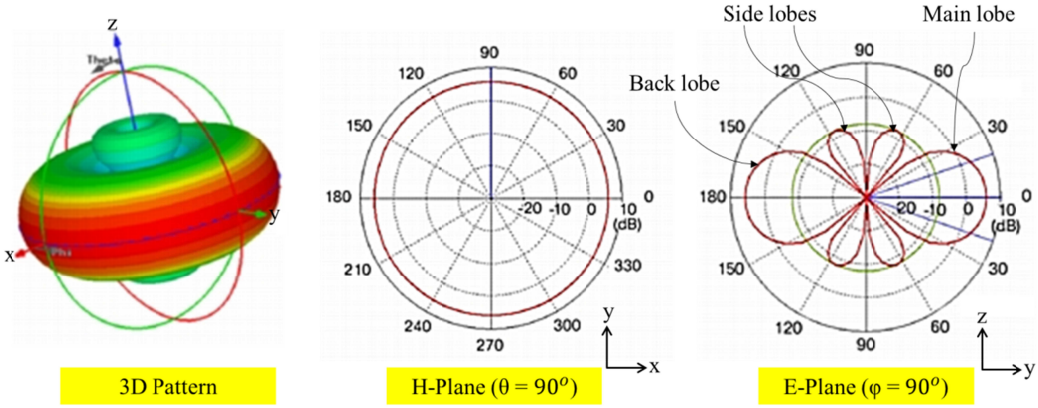

Figure 2.3: An example of an antenna's radiation pattern. [1]-[3]

The radiation pattern gives information about the side lobes level, the beamwidth and the directivity of an antenna.

(e) Directivity:

Directivity is the ability of an antenna to direct or concentrate the radiated power in a particular direction and is a dimensionless parameter having a value greater than or equal to one [3]-[4]. It is the ratio of the power density of an antenna in its strongest emission zone to the power density radiated by an isotropic radiator [1]-[2]. An isotropic radiator radiates uniformly in all directions and has the lowest definable directivity. Antennas can be omni-directional, sectorial or directive. Directive antennas radiate significantly more strongly in one direction than the others. Directivity depends only on the radiation pattern of the antenna

and for a given radiation efficiency directive antennas possess a higher gain than omni-directional antennas. An example of an omni-directional antenna is a dipole antenna, whereas, a horn antenna is a good example of a high gain directive antenna.

(f) Efficiency:

Efficiency is defined as the ratio of the power radiated by an antenna in free space to the power delivered to the antenna input. It is a measure of an antenna's ability to transform the input radio signal into electromagnetic radiation. The efficiency can be mathematically represented as [1]:

$$\eta = \frac{P_{radiated}}{P_{input}} \tag{2.3}$$

Antenna efficiency always has a value between 0 and 1. A highly efficient antenna is one in which most of the power delivered to the antenna is radiated. The efficiency of an antenna largely depends on its radiation area and can be changed by altering the radiation area. It also depends on the number and type of the electronic components surrounding the antenna as they can absorb the radiated power leading to a less efficient antenna. The efficiency in the above equation is usually termed as the radiation efficiency and it does not consider any loss due to the impedance mismatch. However, in practical applications this loss is considered with the radiation efficiency to determine the total efficiency of an antenna. The efficiency of an antenna is directly proportional to its gain [2]-[4].

(g) Antenna gain:

According to Balanis, the gain of an antenna is defined as "*the ratio of the radiation intensity in a given direction to the radiation intensity that would be obtained if the power accepted (input) by the antenna were radiated isotropically*" [1]. A gain of 3 dB means that at a given distance the power radiated by an antenna will be 3 dB higher than that radiated by a lossless isotropic radiator owing to an equal input power to both radiators. The gain of an antenna is actually its directivity (D) after considering the total efficiency and can be mathematically represented as:

$$Gain = \eta * D \tag{2.4}$$

According to the IEEE, the gain of an antenna does not take in account the losses due to impedance mismatch. This leads to two definitions of gain, one from the IEEE known as

'Gain' and the other which considers the reflection losses known as *'Realized gain'*. Gain is usually expressed in decibels and is directly related to the radiation pattern of an antenna. A high gain antenna is usually more directional as compared to a low gain antenna which means that the transmission range of a high gain antenna is more than a low gain antenna [1]-[2].

2.2 Introduction to MIMO technology

The introduction of high definition interactive multimedia services into wireless terminals has placed a need of having transceiver systems with high data rates and transmission efficiency. To meet this requirement, multiple input multiple output (MIMO) technology has been introduced that is capable of providing a high data throughput and efficient transmission than conventional single input single output (SISO) systems.

2.2.1 Conventional wireless communication system (SISO)

Conventional wireless communication system involves the use of one antenna at the transmitter and one antenna at the receiver side. Such type of system is known as Single Input Single Output (SISO). An illustration of the SISO is shown in Figure 2.5. The capacity of a conventional wireless communication system is given by the Shannon's capacity theorem as [5]:

$$C = W * log\left(1 + \frac{S}{N}\right), \tag{2.5}$$

where 'W' is the bandwidth of the channel and 'S/N' is signal to noise ratio (SNR). It can be seen from the equation 2.5 that the channel capacity is directly proportional to the channel bandwidth and the signal transmission power. As we increase the signal power or bandwidth, the channel capacity will increase. However, the frequency spectrum is limited and also the signal power cannot be increased without limit as it introduces co-channel interference.

2.2.2 Multipath propagation and the need for multiple antennas

The transmission and reception of radio signals through a wireless channel is influenced by multiple propagation paths which occur due to the presence of obstacles between the transmitter and receiver in the propagation path. This is known as multipath propagation and as a result of which multiple copies of the same signal may arrive at the receiver end at different times with probably different phase and attenuation. An illustration of line of sight and non-line of sight propagation is shown in Figure 2.4. In the line of sight propagation, the receiver can receive a direct component of the signal from the transmitter, whereas, in non-line of sight propagation the signal is received only after diffraction and reflection from the obstacles and there is no direct transmission path available. In mobile communication, the signal transmission is mostly non-line of sight and the received radio signal is usually a vector sum of all the signal components received from multiple paths. As a result of this, the actual signal power level fluctuates which is known as fading.

Different diversity techniques are used to lessen the effects of multipath fading experienced in SISO wireless systems. These techniques employ the technique of transmitting and receiving multiple copies of the same signal through different channels instead of one channel as in SISO. As a result of transmission and reception through multiple channels the probability of having a reliable wireless link and increased data throughput increases due to the fact that while some signal copies may experience deep fades, others may not.

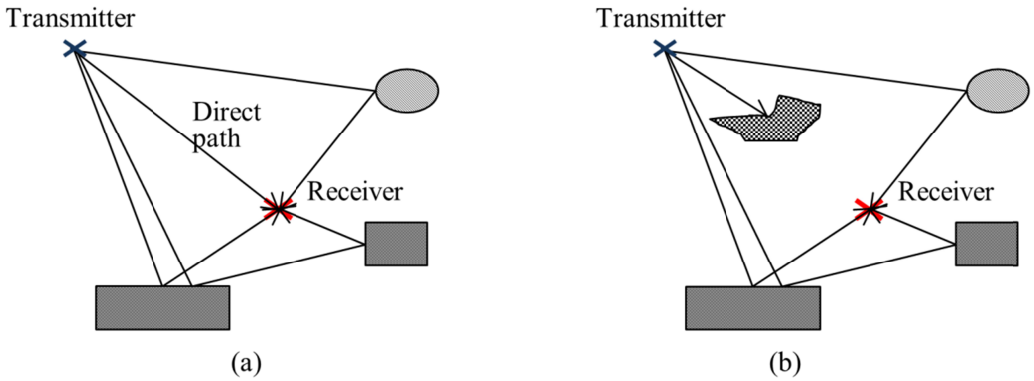

Figure 2.4: An illustration of (a): Line of sight and (b): Non-line of sight radio signal propagation.

Three kinds of diversity techniques are usually discussed in wireless communications [6]:

(a) Frequency diversity.

In frequency diversity, the radio signal is modulated at different carrier frequencies. This leads to multiple copies of the same signal with different and independent fading envelopes.

(b) Time diversity.

In time diversity technique, multiple copies of the radio signal are transmitted at different intervals of time. Each copy has independent fading.

(c) Space diversity.

In space diversity, multiple copies of the same information signal are transmitted through multiple antennas. The antennas should be spaced far enough apart so that received copies of the same signal must have independent fading. This type of diversity technique does not require any extra channel bandwidth or transmission power. An illustration of the space diversity is shown in Figure 2.5.

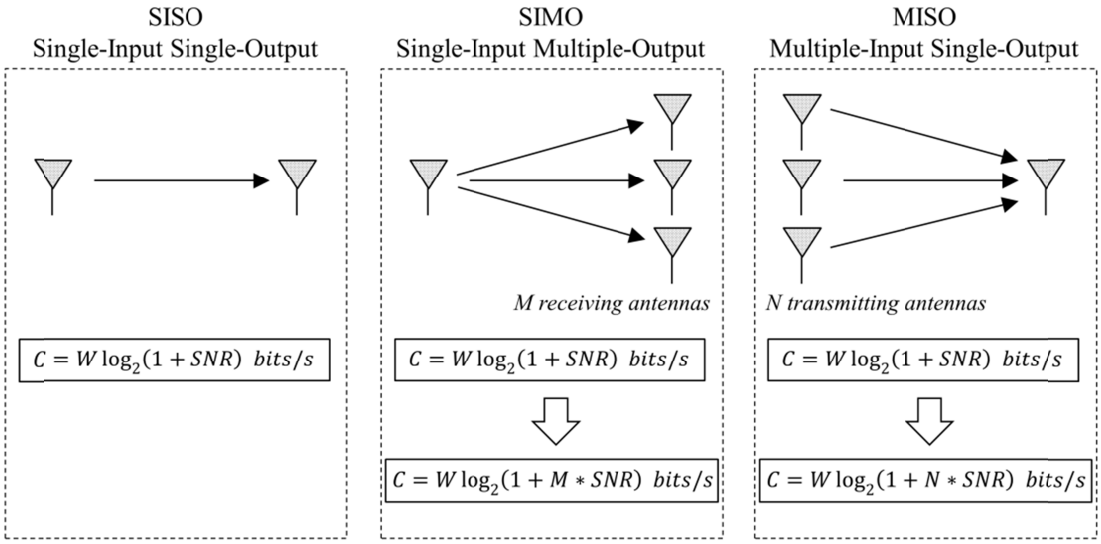

Figure 2.5: An illustration of spatial diversity [6].

An illustration of how two copies of an incoming signal combine to achieve better mean SNR than that of an individual signal component is shown in Figure 2.6. The signal processor at the receiver combines multiple copies of the transmitted signal received through different paths. Each signal being uncorrelated to the others possesses different nulls pattern than the other signals and the probability of the multiple signals having deep nulls at the same time is

very low. This leads to an increased signal level as compared to the conventional SISO system.

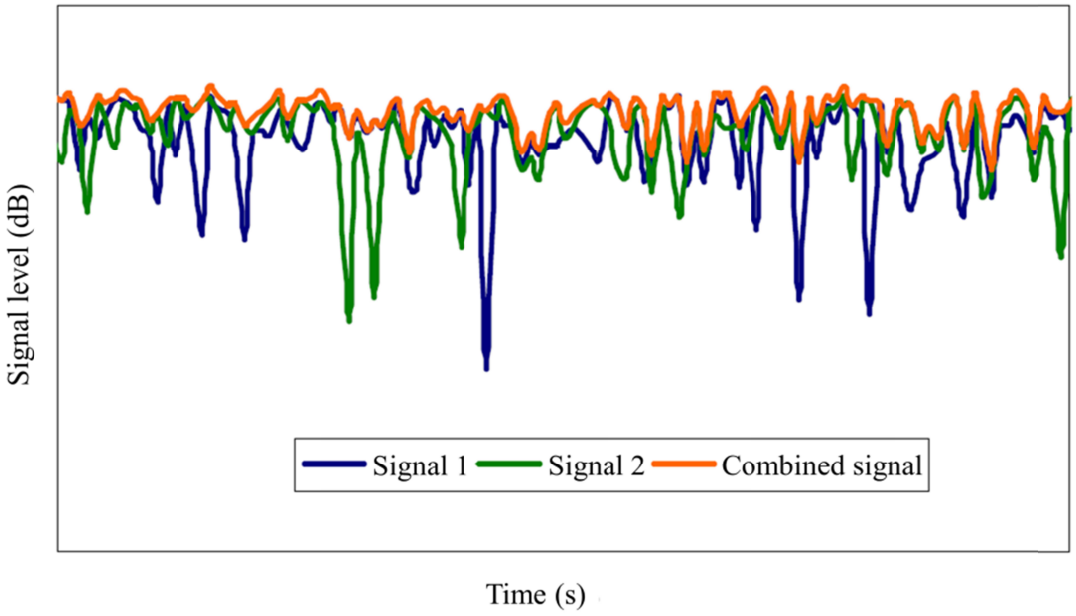

Figure 2.6: An illustration of how two copies of an incoming signal combine to achieve better mean SNR [7].

2.2.3 Multiple Input Multiple Output (MIMO)

The term MIMO is the acronym of Multiple Input Multiple Output. It is a system of transmission and reception in which more than one antenna is used at the transmitter and receiver sides. The use of multiple antennas at the transmitter and receiver using same the frequency channel greatly increases the channel capacity as each antenna receives not only the signal which is transmitted to it but also components of the signal transmitted to other antennas. This has the advantage of increased signal level and transmission efficiency [5]-[9]. An illustration of a MIMO antenna system is shown in Figure 2.8. The capacity of a MIMO system, consisting of 'M' number of 'transmit' and 'receive' antennas, is given by Shannon's capacity theorem as [13]-[16]:

$$C = M * W * log\left(1 + \frac{S}{N}\right) \tag{2.6}$$

2.2.4 Why MIMO?

In wireless communication, the propagation of RF signals through a channel is characterized by the multiple paths of propagation which result due to the scattering from certain obstacles

in the signal path to the receiver as shown in Figure 2.7. This results in wireless technologies facing problems such as signal fading, multipath and increased channel interference which largely degrades spectral efficiency, signal power and range. MIMO technology offers many advantages over conventional SISO. Some of these are discussed below [5]-[10].

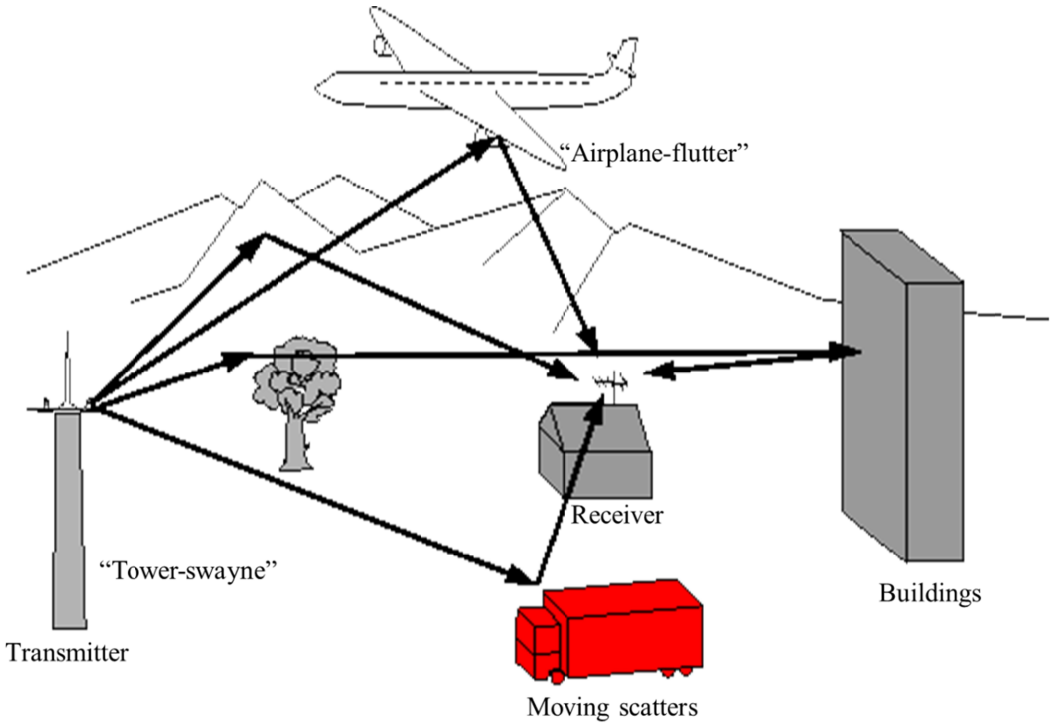

Figure 2.7: Multipath Signal Propagation from certain obstacles in real world environment [8].

(a) Increased Data Throughput and Channel Capacity:

In a SISO system, there is a single radio transmission over a channel but in MIMO there are multiple transmissions on a single channel analogous to multiple virtual wires carrying the same signal. This increases data throughput without the requirement of additional power or frequency spectrum. The power of the signal is increased as compared to conventional SISO. Moreover a single high data rate signal can be split up into low rate multiple data streams and transmitted from multiple transmit antennas simultaneously. This largely increases channel capacity owing to a better use of the frequency channel as compared to conventional SISO [5]-[16].

(b) Increased Range:

In a SISO system, the signal level is highly degraded by the obstacles and multipath fading, whereas, in MIMO the signal reflecting off the obstacles is also received as there are multiple propagation paths within the same channel. In conventional SISO, the system receiver cannot

easily separate the echoes of the signal through multiple paths, whereas, a MIMO receiver being more sensitive than SISO, makes use of the same signal echoes to increase range and throughput in a multipath environment [5]-[11]. A comparison of MIMO and single radio range is shown in Figure 2.8.

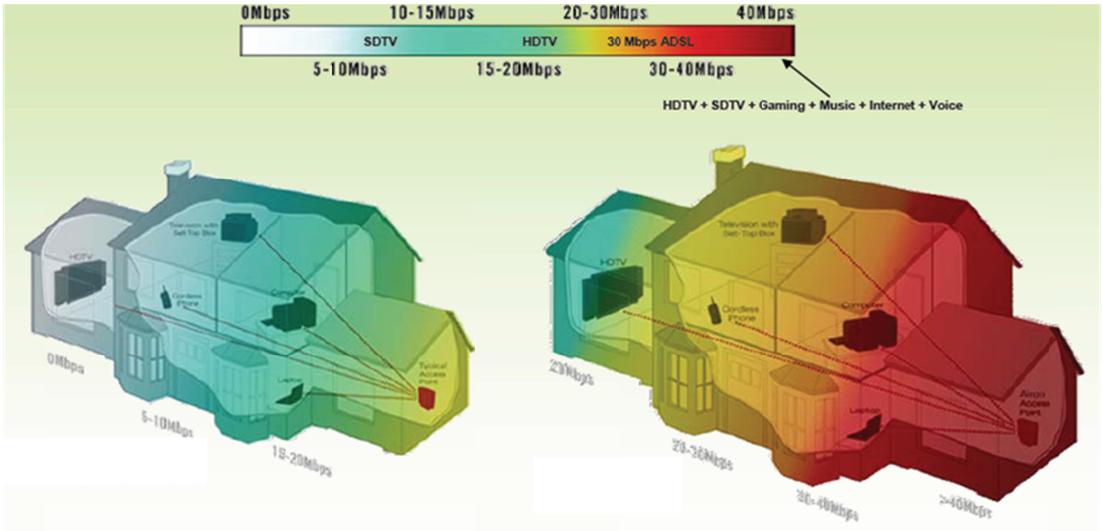

Figure 2.8: Comparison of Range between MIMO and SISO [10].

2.2.5 Principles of MIMO

MIMO technology employs several signal processing techniques to utilize all the multipath signals received by the multiple receivers to reconstruct the originally sent signal with more gain and power as compared to conventional wireless communication systems [5]-[16]. An illustration of MIMO transmission and reception is shown in Figure 2.9.

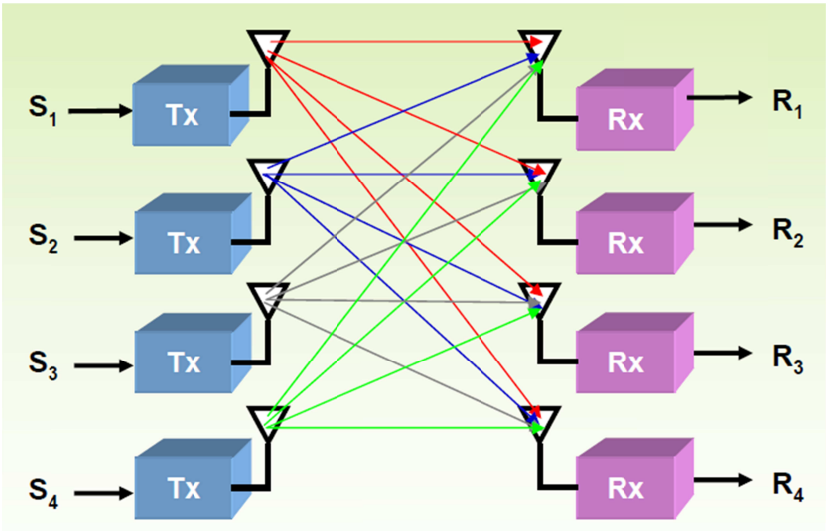

Figure 2.9: Utilization of Multiple Propagation Paths by MIMO increasing data throughput [9].

Three types of transmission technique used in MIMO are:

(a) Pre-coding
(b) Spatial Multiplexing
(c) Diversity Coding

(a) Pre-coding:

Pre-coding is the beam-forming of multiple data streams. This occurs at the transmitter side. In this scheme of transmission, the same signal is transmitted from each transmitter antenna but with different phase and gain. This results in an increased signal power at the receiver. The main benefit of pre-coding or multi-stream beam forming is that it increases the received signal strength by constructively combining all the received signals thereby reducing multipath fading effect.

(b) Spatial Multiplexing:

Spatial multiplexing is another transmission technique in MIMO. In this scheme the original high data rate signal is split up into a number of lower data rate streams and then each stream is transmitted through different transmit antennas using the same frequency channel. Each of these streams is received by the receiver antennas with a relatively different spatial signature making them appear to be many parallel channels at the receiver end. Spatial multiplexing greatly increases channel capacity and also improves signal to noise ratio (SNR).

(c) Diversity Coding:

The above discussed transmission techniques require channel state information (CSI) at the transmitter side. In wireless communication, CSI describes how radio signal propagates from the transmitter side to the receiver side. It represents the combined effect of scattering, fading and power decay as a function of distance. Diversity coding works without requiring CSI at the transmit end. In this scheme of transmission, the signal is not broken up into multiple streams. So, a single stream of signal is transmitted from all the transmit antennas but with nearly orthogonal space time coding. This scheme enhances signal diversity by taking into account the fading in each antenna link.

2.2.6 MIMO channel model and capacity formulation

(a) MIMO channel model:

MIMO wireless communication link employs *M* number of antennas at the receiver side and *N* number of antennas at the transmitter side. A typical MIMO channel model consisting of *M* number of antennas at receiver and *N* number of antennas at the transmitter with $M = N$ is illustrated in Figure 2.10.

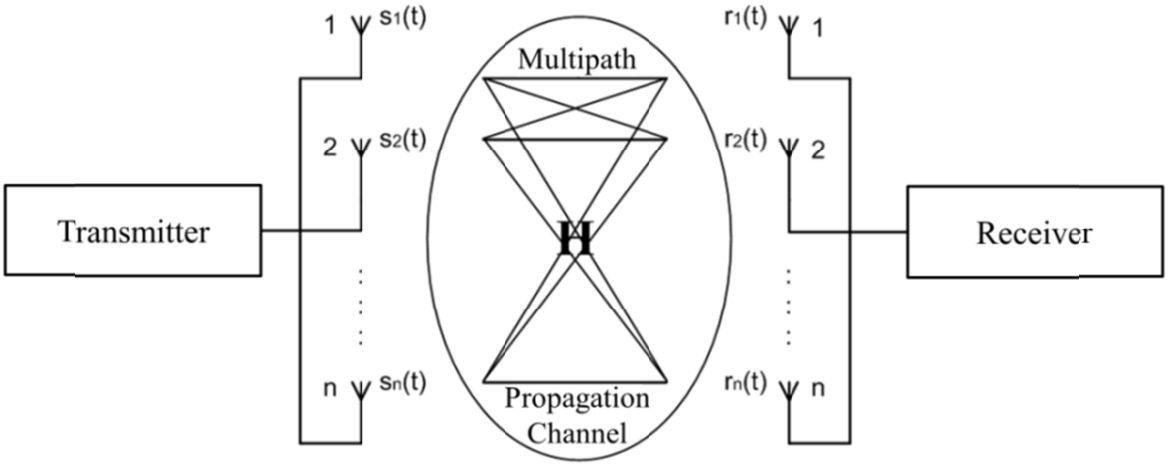

Figure 2.10: An illustration a typical MIMO channel model [7].

where, $s(t)$ and $r(t)$ are the transmit and receive signal vectors, respectively, defined as:

$$s(t) = [s_1(t), s_2(t), \dots\dots\dots, s_n(t)]^T \tag{2.7}$$

$$r(t) = [r_1(t), r_2(t), \dots\dots\dots, r_n(t)]^T \tag{2.8}$$

Where, *T* is transpose operator.

The received signal vector is expressed as:

$$r(t) = H(t) * s(t) + v(t) \tag{2.9}$$

In the above equation, $H(t)$ represents the MIMO channel propagation matrix and $v(t)$ represents the additive white Gaussian noise. The *H* matrix can be expressed as:

$$H = \begin{bmatrix} h_{11} & h_{12} & h_{1j} \\ h_{21} & h_{22} & h_{2j} \\ h_{i1} & h_{i2} & h_{ij} \end{bmatrix}_{M*N} \tag{2.10}$$

The h_{ij} in the above matrix represent the frequency response comprising the complex path gain from the transmit point *j* to the receive point *i*, for $i = 1,2,\ldots,M$ and $j = 1,2,\ldots,N$. The frequency response of a narrowband channel at a known carrier frequency f_0 is given in [9] as:

$$h_{ij} = \sum_{k=1}^{m} \sqrt{P_k} \; . e^{i\left(\frac{2\pi}{\lambda_o}\right) l_k} . e^{i(2\pi f_o)\tau_k} \tag{2.11}$$

where, *m* is the number of propagation paths between each transmitter and receiver pair, f_o is the operating frequency, λ_o is the wavelength, P_k is the received power, l_k is the length of the k^{th} ray, τ_k is the time delay corresponding to the k^{th} ray and the term $e^{i(2\pi/\lambda_0)l_k}$ represents the phase progression due to ray length l_k.

(b) MIMO channel capacity:

The narrowband channel capacity for an $N \times N$ MIMO system, assuming that the channel state information is unavailable on the transmitter side and the total transmit power is uniformly distributed among all transmit points, is expressed as: [13]

$$C(\xi) = log_2 \left(det \left[I_N + \frac{\xi}{N} H_n H^{\dagger} \right] \right) \qquad bits/s/Hz \tag{2.12}$$

where, ξ represents the average signal-to-noise ratio (SNR) at each receive point, det$[*]$ denotes the determinant operator, I_N is the identity matrix of $N \times N$ size, H_n is the normalized $N \times N$ propagation matrix such that $\sum_{j=1}^{N} \left|h_{ij}\right|^2 = 1$, and $H^{\dagger}$ indicates the conjugate transpose of *H* i.e. The Hermitian operator.

A simplified form of (2.12) using the singular value decomposition method (SVD) is expressed in [3] as:

$$C(\xi) = \sum_{i=1}^{N} log_2 \left[1 + \frac{\xi}{N} \lambda_i \right] \qquad bits/s/Hz \tag{2.13}$$

Where, λ_i represents the eigenvalues of $H_n H^{\dagger}$ for $i = 1, 2\ldots N$, corresponding to each parallel orthogonal sub-channel.

According to (2.13), MIMO technology has the capacity to obtain almost *N* more bits per second per Hertz for every 3 dB increase in SNR in a rich multipath environment as compared to conventional SISO in which only one additional bit per second per Hertz for every 3 dB increase in SNR can be achieved [14]. A comparison of the channel capacity for SISO and MIMO is shown in Figure 2.11. It can be seen that the channel capacity increases by increasing the number of antennas at the transmitter and receiver sides. The capacity of 4 x 4 MIMO is almost five times the capacity of SISO.

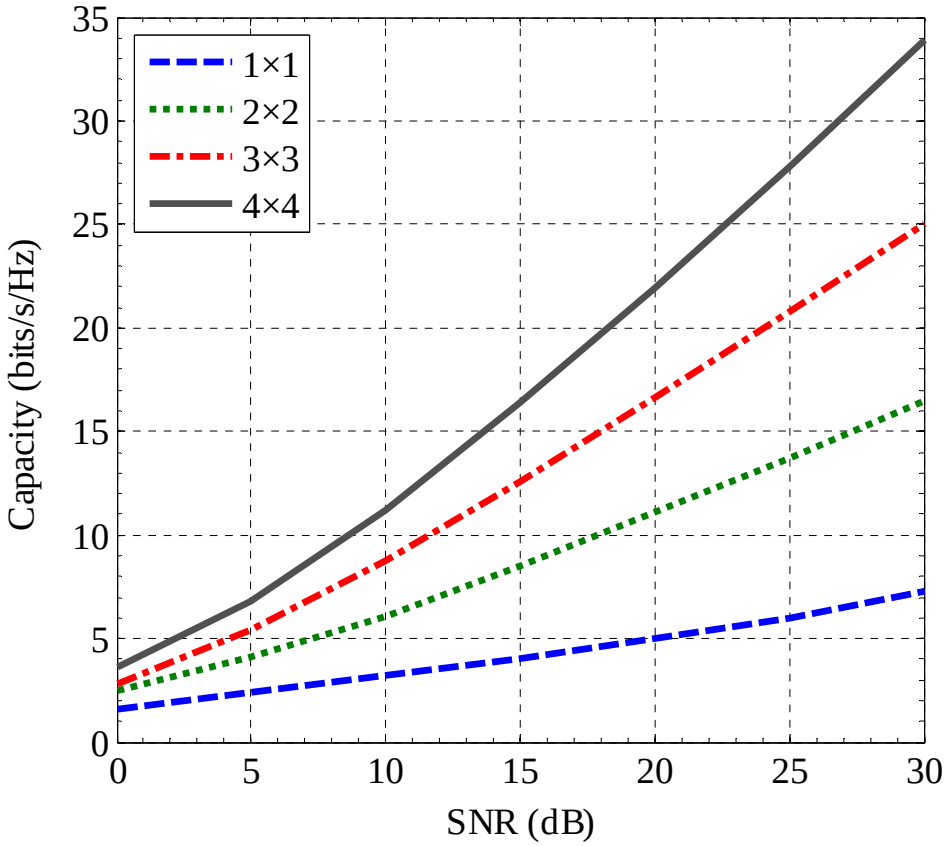

Figure 2.11: An illustration of increase in channel capacity with increase in number of transmitter and receiver antennas [3].

2.2.7 Requirements of MIMO Antenna Design:

The placement of multiple antennas on a compact platform imposes many design challenges such as low correlation between multiple antennas, good efficiencies and good return losses. In MIMO, the multiple antennas have to perform with a low coupling, not majorly affecting the radiation characteristics of each other. The multiple antennas on the same platform should have the same frequency bandwidths, isolation performance and radiation characteristics such as the gain and radiation efficiency. In order to meet these criteria, techniques proposed in the

literature include various decoupling structures etched between MIMO antennas and the relative orientation of the MIMO antennas to improve polarization decoupling. According to the research work done by Saunders, the maximum permissible value of correlation should be less than 0.7 so that there is no more than 3 dB loss in the diversity gain [17]-[19]. Also the isolation between multiple antennas in MIMO should be better than 15 dB. Likewise, the return loss criterion for the bandwidths accommodated by MIMO antennas should be better than 10 dB to meet the practical requirements [20]-[23]. However, for compact antennas such as for mobile handset, the bandwidth is usually defined with reference to a return loss of 6 dB.

2.2.8 Applications of MIMO:

The major applications in which MIMO technology has been successfully employed are:

- WLAN 802.11n
- Mesh Networks
- WMAN – WiMAX 802.16e
- 4G Mobile Internet
- Digital Home

In mobile communication, the downlink MISO has already been realized in some practical smartphones where multiple antennas are used at the transmitter base station and a single antenna is used at the receiver of the mobile handset [10]. However, the implementation of uplink MIMO with multiple transmit antennas is not yet successful in mobile handsets due to the size limitations. In uplink MIMO, the mobile handset acts as transmitter and the base station acts as receiver [10]. It is a major challenge to place multiple antennas inside mobile handset while achieving acceptable isolation and return loss performances. It is therefore a research problem yet to be resolved especially at the lower frequency bands such as GSM 850 and LTE 700.

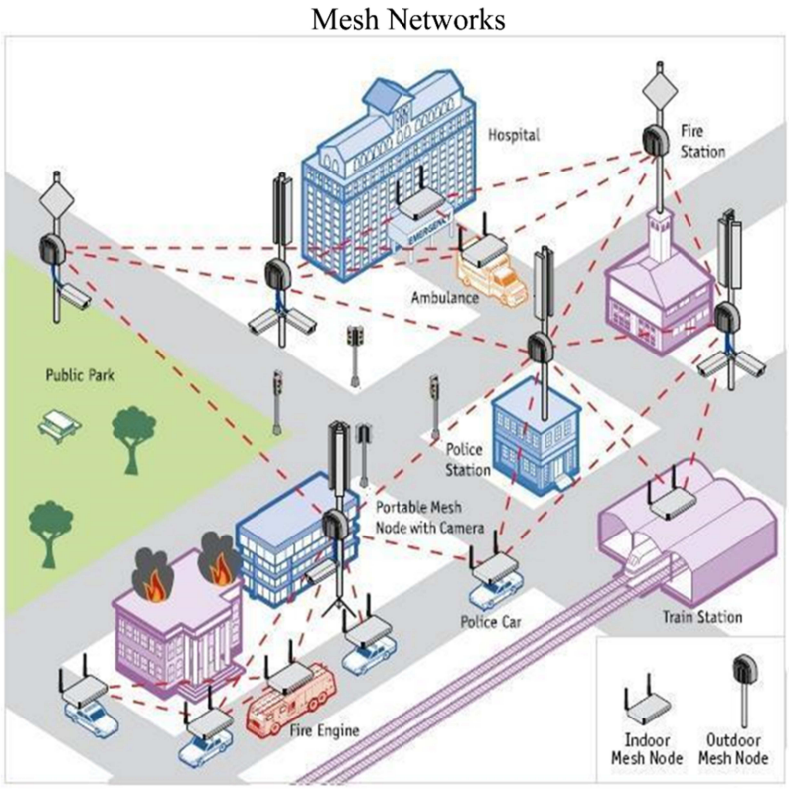

Wireless LAN Terminals

4G Mobile Broadband Dongles

Digital Home Automation

Figure 2.12: Applications of Multiple-Input Multiple-Output (MIMO) [11].

References

[1] Balanis, C. A., "Antenna Theory Analysis and Design", Edition, 3rd, A John Wiley & Sons, Inc., Publication, ISBN 0-471-66782-X, 2005.

[2] David K. Cheng, Field and Wave Electromagnetic, Addison Wesley Pub. Co., New York, 1989.

[3] Antenna fundamentals, Online, Available at: http://www.antenna-theory.com/ basics/ main.php

[4] Antennas basic concepts, Pulse electronics, Online, Available at: www.pulseelectronics. com/download/3248/antenna_basic/pdf

[5] Agilent, Transforming MIMO Test with Fast, Accurate Signal Creation, Signal Analysis, and Protocol Development and Conformance, August 26, 2009, available at: http://www.agilent.com/about/newsroom/tmnews/background/N5106A/.

[6] T. S. Rappaport, Wireless Communications Principles and Practice, IEEE Publications, United States, 1996.

[7] Y. Gao, “Characterisation of multiple antennas and channel for small mobile terminals,” Ph.D. thesis, Department of Electronic Engineering, Queen Mary University of London, United Kingdom, 2007.

[8] Institute for communication technologies and embedded systems, OFDM and the orthogonality principle, 2012, available at http://www.ice.rwth-aachen.de/research /algorithms-projects/ofdm/ofdm-and-the-orthogonality-principle/

[9] MATLAB Central, MIMO Rayleigh fading Channel Capacity, 04 Oct 2006, Available at: http://www.mathworks.com/matlabcentral/fileexchange/12491-mimo-rayleigh-fading-channel-capacity

[10] David, T., Viswanath, P., "Fundamentals of Wireless Communication", Cambridge University Press, ISBN 978-0521845274, May 2005.

[11] EEWeb Electrical Engineering Community, Antenna and wireless communication, Available at: http://www.eeweb.com/project/joel_abraham/ antenna-and-wireless-communication-presentation

[12] CEWIT - Center of Excellence in Wireless and Information Technology, Introduction to Wireless MIMO–Theory and Applications, Nov 15 2006, Available at: www.ieee.li/pdf/viewgraphs/wireless_mimo.pdf

[13] C. E. Shannon, “A mathematical theory of communication,” Bell System Techno-logy Journal, vol. 27, pp. 623–656, 1948.

[14] G. J. Foschini and M. J. Gans, “On limits of wireless communications in a fading environment when using multiple antennas,” Wireless Personal Communi-cations, vol. 6, no. 3, pp. 311–335, 1998.

[15] A. Paulraj, R. Nabar, and D. Gore, Introduction to Space-time Wireless Communications, Cambridge University Press, 2003.

[16] D.-S. Shiu, G. J. Foschini, M. J. Gans, and J. M. Kahn, “Fading correlation and its effect on the capacity of multielement antenna systems,” IEEE Transactions on Commununications, vol. 48, no. 3, pp. 502–513, 2000.

[17] E. Telatar, “Capacity of multi-antenna gaussian channels,” European Transac-tions on Telecommunications, vol. 10, no. 6, pp. 585–595, 1999.

[18] S.R. Saunders, “Antennas and propagation for wireless communication systems”, Wiley, 1999.

[19] M. Schwartz, W. R. Bennet and S. Stein, “Communication systems and techniques”, McGraw Hill, 1996.

[20] C. C. Chiau , “Study of the Diversity Antenna Array for the MIMO Wireless communication Systems”, Ph.D. Thesis, Queen Mary University of London, April 2006.

[21] Jamil, A.; Yusoff, M.Z.; Yahya, N.; Zakariya, M.A.; , "Design and performance evaluation of multiband MIMO antennas," *National Postgraduate Conference (NPC), 2011* , pp.1-5, 19-20 Sept. 2011

[22] Qin-Xin Chu; Jian-Feng Li; , "A compact wider dual-band MIMO antenna array for mobile phone," *Wireless Information Technology and Systems (ICWITS), 2010 IEEE International Conference on* , pp.1-4, Aug. 28 2010-Sept. 3 2010

[23] MinSeok Han; Jaehoon Choi; , "Compact multiband MIMO antenna for next generation USB dongle application," *Antennas and Propagation Society International Symposium (APSURSI), 2010 IEEE* , pp.1-4, 11-17 July 2010

[24] Qinghao Zeng, Yuan Yao, Shaohua Liu, Junsheng Yu, Peng Xie, and Xiaodong Chen, “Tetraband Small-Size Printed Strip MIMO Antenna for Mobile Handset Application,” International Journal of Antennas and Propagation, 2012, Article ID 320582, 8 pages, 2012

CHAPTER 3
LITERATURE REVIEW

This chapter provides a review on multiband antennas for mobile handsets that have been proposed recently in the literature. A comprehensive analysis for both single and MIMO antennas will be presented. Also, a literature review on the reconfigurable antennas using different switching techniques is also included.

3.1 Review of the State-of-Art

Research and development in multiband mobile phone antennas has been an area of intense undertaking by many groups over the last few years due to the demand of having sleek designs capable of covering the 2G, 3G and 4G cellular services. The detailed literature reviews on the current single (SISO), MIMO and reconfigurable antenna designs presented in the references [1]-[79] will be discussed. The single antenna designs include PIFA antennas [1]-[14], loop antennas [15]-[20], monopole antennas [21]-[31], slot antennas [32]-[37], dielectric antennas [38] and coupled fed antennas [39]-[43]. There are fewer MIMO and reconfigurable antenna designs for handset applications due to the potential problem of having designs with acceptable isolation between multiple antennas. This makes the reconfigurability of radiation pattern from a mobile antenna a big challenge especially when dealing with multiple frequency bands. The objective of this literature review is to analyze the designs of current handset antennas and to examine the major issues associated with the design of multiband antennas in a compact volume.

3.1.1 Single antenna (SISO) designs:

A planar inverted-F antenna (PIFA) is presented in [7]. The antenna shown in figure 3.1 is composed of a helical feed, folded patch and two slots for improved bandwidth. The antenna is capable of covering only GSM 850/900/1900. The geometry of the antenna is such that it is 7 mm high from the ground plane which makes is not suitable for new generation sleek designs of mobile handsets. Also the antenna does not provide any bandwidth for covering 3G and 4G cellular services.

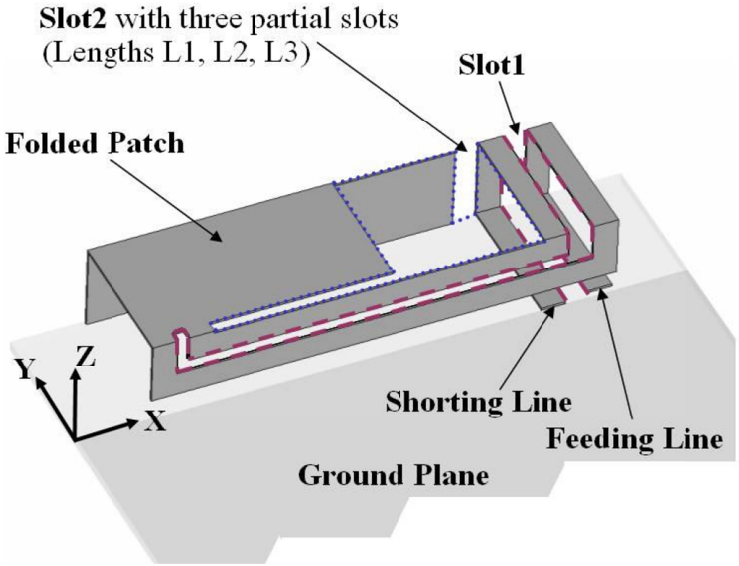

Figure 3.1: Compact five band internal antenna for mobile phone [7].

Another PIFA for mobile phones has been presented in [14]. The antenna is comprised of a ground plane and a radiating patch. The feed is provided to the radiating patch and shorting stub is connected between antenna and ground plane as shown in figure 3.2. Though the antenna is very simple to fabricate with a low manufacturing cost, the antenna is giving a narrow bandwidth covering only GSM 1850/1900.

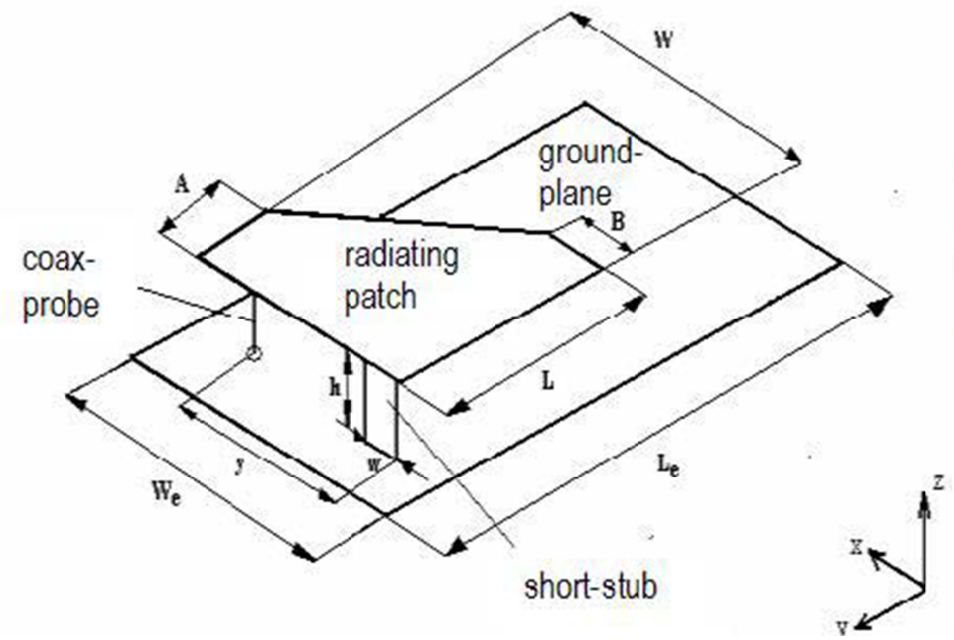

Figure 3.2: Tapered PIFA for handset terminals [14].

The size of the traditional PIFA antennas is not suitable to be mounted inside thin mobile housings. In order to improve this, the printed PIFA was introduced. One such antenna is shown in [9]. The antenna is a λ/8 PIFA capable of covering GSM 850/900, GSM 1850/1900 and UMTS. The antenna comprises of a microstrip, feeding two folded radiation strips by coupling as shown in figure 3.3. The two strips are coupled fed to generate λ/8 and λ/4 resonant modes. These two resonant modes give 6 dB bandwidths covering GSM 850/900 and GSM 1850/1900 and UMTS.

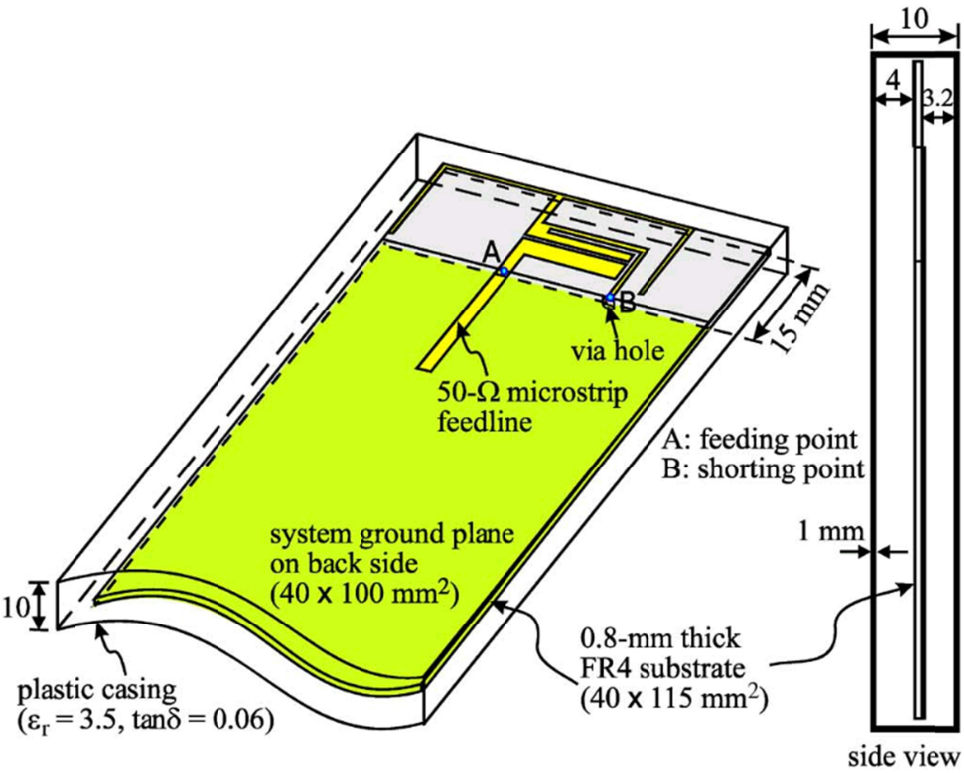

Figure 3.3: Printed λ/8-PIFA for Internal Penta-Band Mobile Phone Antenna [9].

The major drawback of the PIFA designs presented earlier is the narrow bandwidth which makes the designs highly unsuitable for smartphone applications. The bandwidth can be significantly improved by employing a coupled feed or by use of some parasitic structures. Also the PIFA antennas occupy a large volume. To improve this, loop antennas are found to be more suitable for multiband mobile phone communication. Loop antennas are one of the most promising candidates for achieving multiband operation in a mobile phone. Unlike traditional PIFAs, loop antennas can operate at 1λ and 0.5λ modes with a fairly compact volume. Loop antennas consist of thin metallic strips, folded to form a very compact configuration with a wide bandwidth [15]-[20]. One such antenna is presented in [19]. The antenna is composed of a folded loop strip and an internal matching circuit formed by a coupling strip and an inductive strip as shown in figure 3.4. The folded loop strip resonates at lower frequency band. The internal matching circuit increases the bandwidth at upper frequency bands. The bandwidth thus achieved is 600 MHz ranging from 1650 MHz to 2250 MHz covering GSM 900, DCS, PCS and UMTS cellular frequency bands.

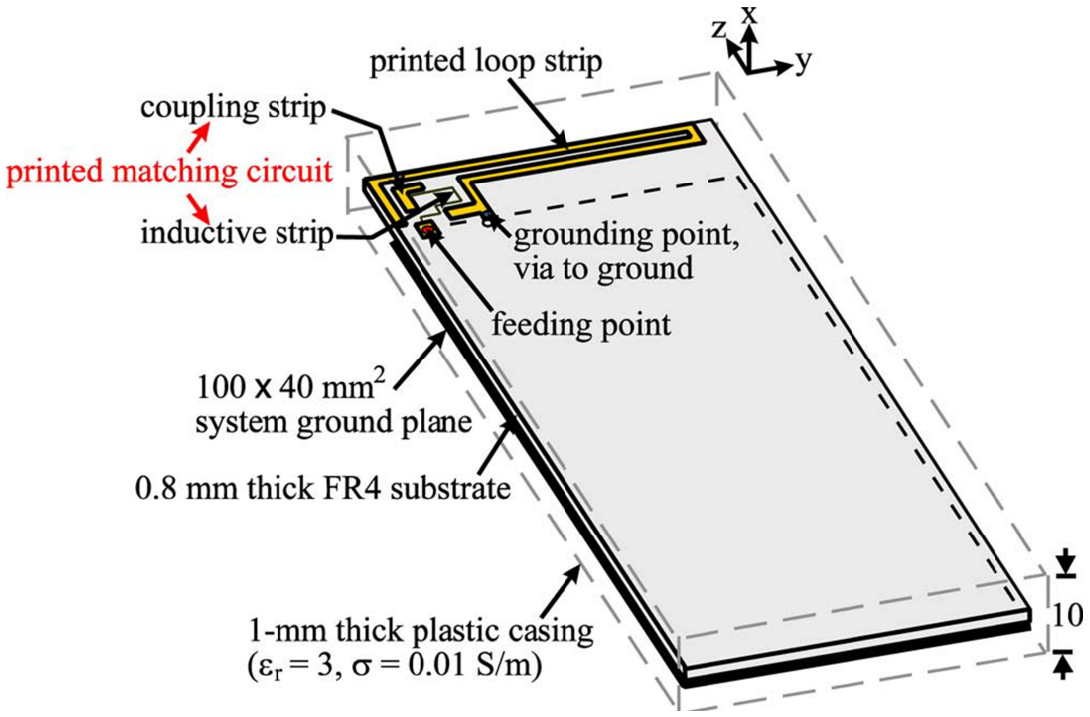

Figure 3.4: Quarter-Wavelength Printed Loop Antenna with an Internal Printed Matching Circuit for GSM/DCS/PCS/UMTS Operation in the Mobile Phone [19].

Another loop antenna has been presented in [16]. The antenna geometry is shown in figure 3.5. The antenna is composed of a loop antenna that generates a 0.5λ resonant mode at 900 MHz and a 1λ mode at 1900 MHz. However the bandwidth of the loop antenna is not wide enough to cover DCS, PCS and UMTS bands. For this purpose two side tuning sections and one central tuning section is introduced which provides 1.5λ resonant mode covering DCS, PCS and UMTS.

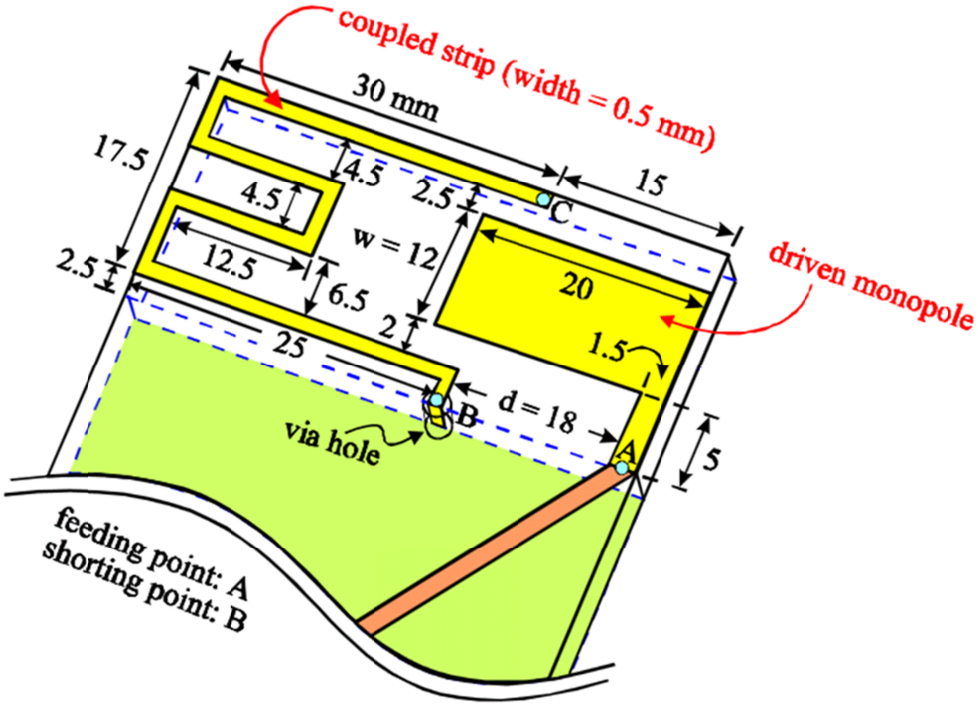

Figure 3.5: Internal Penta-Band Printed Loop-Type Mobile Phone Antenna [16].

The loop antenna can be folded to make an inverted-F configuration. One such design is described in [20] and is composed of a folded loop structure as shown in figure 3.6. The antenna is capable of operating in two modes of which one is the loop mode and the other is the inverted-F mode. A pin diode is used to control these modes. When the pin diode is 'ON' the antenna works in the loop mode, whereas, the antenna operates in the inverted-F mode when the diode is 'OFF' thereby making antenna structure as two IFAs. A shorting bridge is used to connect the antenna feed point with the shorting point to widen the frequency bandwidth. Moreover a tuning pad is also used for good impedance matching. The antenna operates in the 0.5λ resonant mode at the lower band for covering GSM 850/900, whereas, 1λ and 1.5λ modes are obtained to achieve the higher frequency bandwidths for covering GPS, DCS, PCS, UMTS and WLAN. The configuration of the antenna requires a supporting structure and also the presence of the diode switch requires biasing circuit and possibly an insertion loss will be introduced.

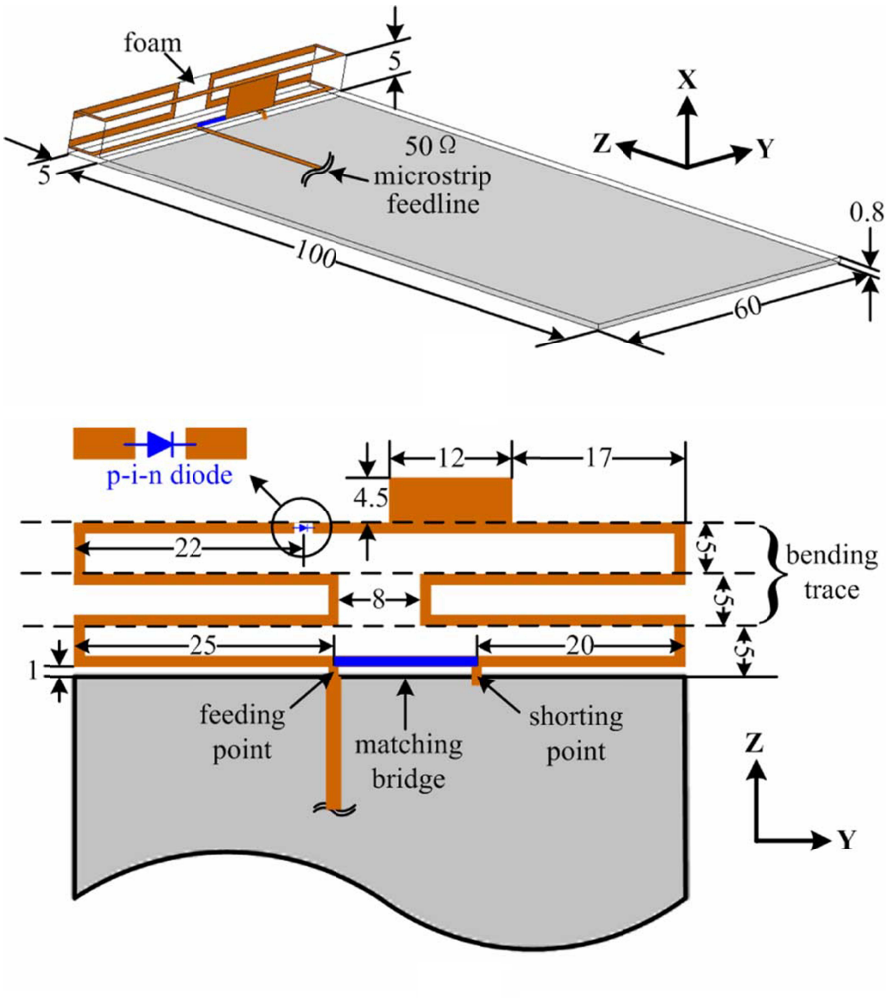

Figure 3.6: A Compact Hepta-Band Loop-Inverted F Reconfigurable Antenna for Mobile Phone [20].

Another type of antenna commonly designed for mobile phone applications is the monopole antenna which usually possesses a wide bandwidth thus making them suitable for handset applications. One such design is presented in [28]. The antenna is composed of a T-slit monopole that is printed on the non-grounded portion of the substrate as shown in figure 3.7. The design comprises a slotted ground plane etched on the backside of the substrate. To cover the lower GSM band, an additional L-shaped copper strip is soldered at the end of the monopole. The slot and slit in the ground portion leads to some additional excited modes. The proposed antenna resonates in two frequency bands. The lower band ranges from 840 MHz to 965 MHz covering GSM 850/900, whereas, the upper band ranges from 1705 MHz to 2175 MHz covering GSM 1850/1900 and UMTS. The reason for having a good bandwidth at the upper band is the presence of the slotted ground plane which contributes to a

0.25λ resonant mode at 1920 MHz. However, practically the radiation of the ground plane is not desirable as it can be affected by the presence of the components on the circuit board which largely changes the behavior of the antenna in practice.

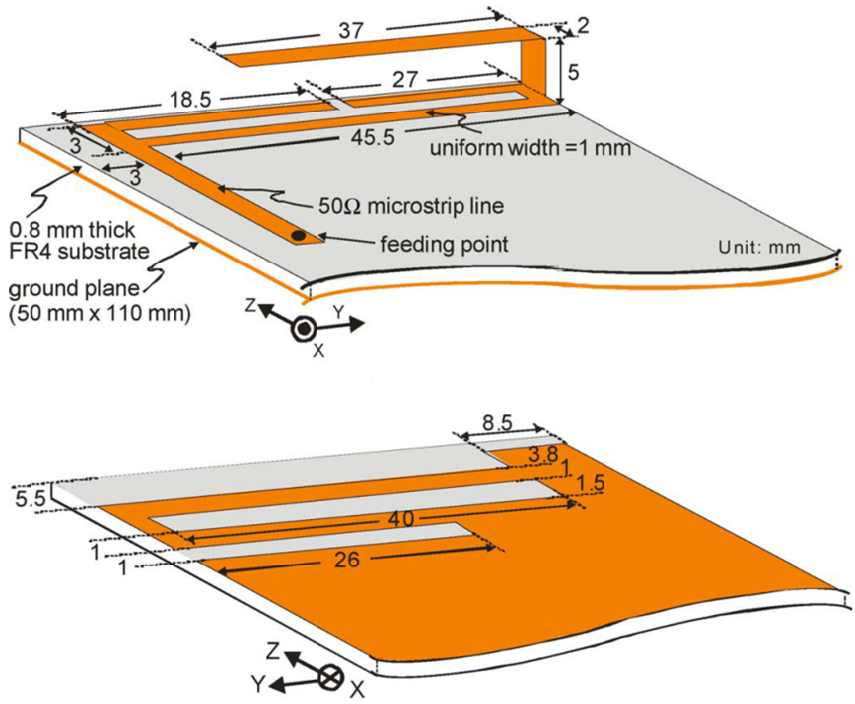

Figure 3.7: Miniature Internal Penta-Band Monopole Antenna for Mobile Phones [28].

Another design of monopole antenna capable of hepta-band operation has been presented in [31]. The antenna is composed of a single radiator composed of two branches and a floating element that is printed on the back side as shown in figure 3.8. The antenna is resonating in three frequency bandwidths thus covering GSM 900, GPS, DCS, PCS, UMTS, WLAN and WiMAX. The antenna operates in the quarter wavelength mode. The floating element makes a magnetic dipole of length close to 0.5λ at 3.5 GHz. The floating element is coupled to the antenna at the front side thus improving its frequency bandwidth.

Another antenna employing monopole slots is discussed in [32]. The antenna shown in figure 3.9 is composed of two monopole slots of different length cut at the upper edge of the substrate. The longer slot excites the lower band covering GSM 850/900 while DCS, PCS, UMTS and WLAN are due to the radiation of the shorter slot. The feed used in the design is a microstrip line that is printed at the backside with an

additional tuning stub to improve the impedance matching at the lower and upper bands.

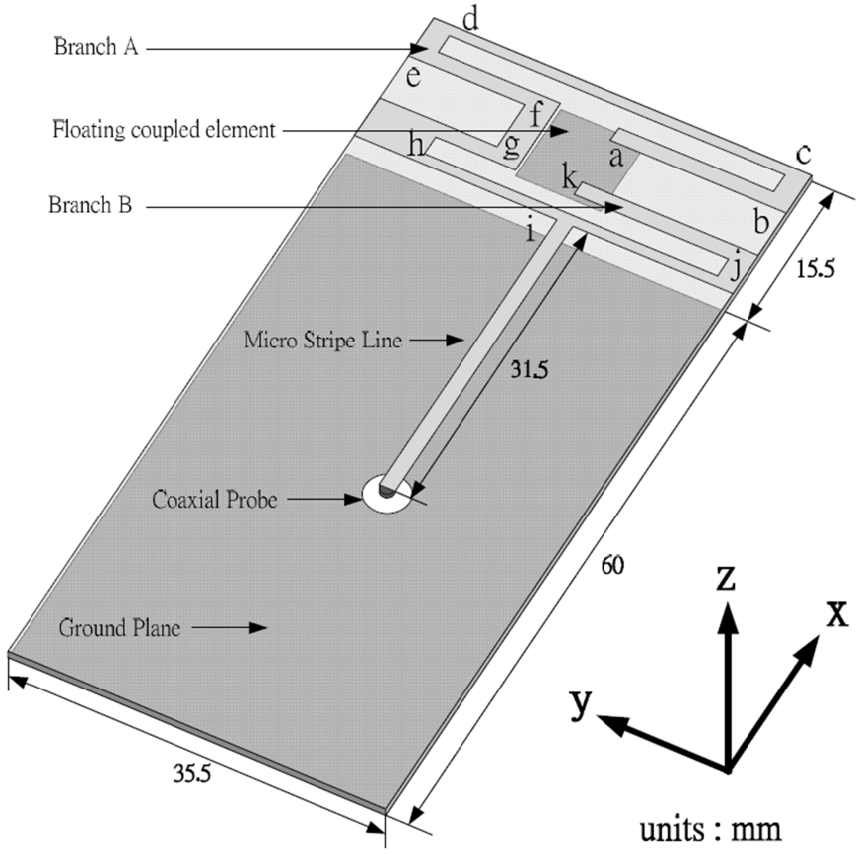

Figure 3.8: Compact Printed Hepta-Band Monopole Antenna for Mobile Devices [31].

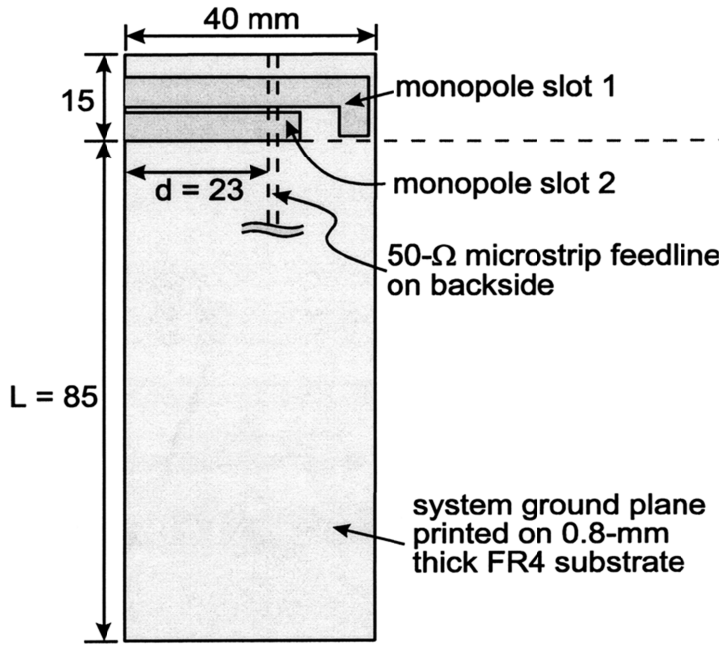

Figure 3.9: Printed Monopole Slot Antenna for Internal Multiband Mobile Phone Antenna [32].

Besides the previously discussed design approaches, the use of dielectric material is also researched. One such design is presented in [38]. The antenna is a PIFA antenna with a high Q dielectric ceramic puck placed at the feeding point as shown in figure 3.10. The introduction of the ceramic puck increases the bandwidth at the lower frequency band. The ceramic puck used is based on $BaO\text{-}PbO\text{-}Nd_2O_3\text{-}TiO_2$. When signal flows through the ceramic puck, it operates as a dielectric resonator due to which the signal power is widely spread and delivered from the feed to the antenna elements. The antenna is capable of covering GSM 850/900 and GSM 1800/1900 when referenced to a return loss of 6 dB. The design however is not suitable for handset applications due to the compact size of a mobile handset. Also the use of the ceramic puck increases the price.

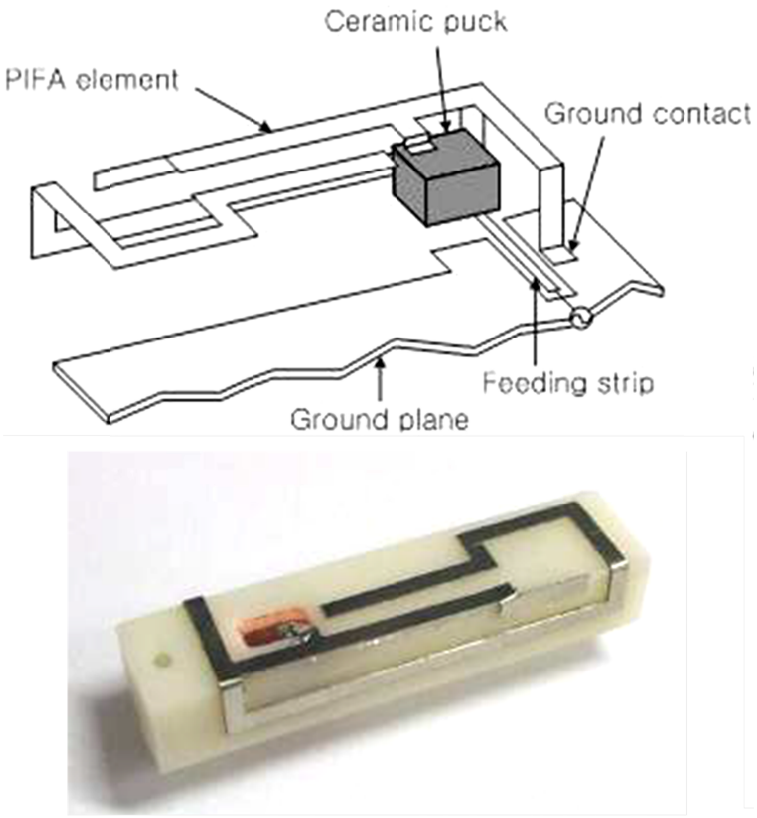

Figure 3.10: Multiband Internal Antenna for Mobile Phones Using a High Dielectric Material [38].

The designs discussed above are mostly direct fed in which the feeding branch is directly connected to the radiating element. However, it is seen from the above designs and their results that the bandwidth achievement is a big issue especially at the low frequency band. The compact size of a mobile phone is largely limiting the

size of the antenna. Recently some designs have been proposed in which the radiating strip of the antenna is fed through coupling and a coupling gap is adjusted between the feeding strip and the radiating strip [39]-[43]. One such design is presented in [39]. The antenna is a coupled feed printed PIFA as shown in figure 3.11 and is composed of a T-shaped monopole patch that is feeding two meandered monopoles through coupling. One of the strips is shorted to the ground and is etched at the bottom layer of the substrate, whereas, the second strip is printed at the front layer. This strip and the T-shaped patch contribute a wide bandwidth at the higher frequency. The strip etched at the backside is slightly longer in length thus contributing to a bandwidth at lower frequency. The antenna resonates in two frequency bands with the lower band ranging from 698 MHz to 960 MHz covering LTE 700, GSM 850/900 and the upper band ranging from 1810-2690 MHz covering GSM 1850/1900, UMTS and LTE 2300/2500. Though the antenna is covering most of the 2G, 3G and 4G cellular frequencies, the practical implementation of the design is difficult due to its complex structure.

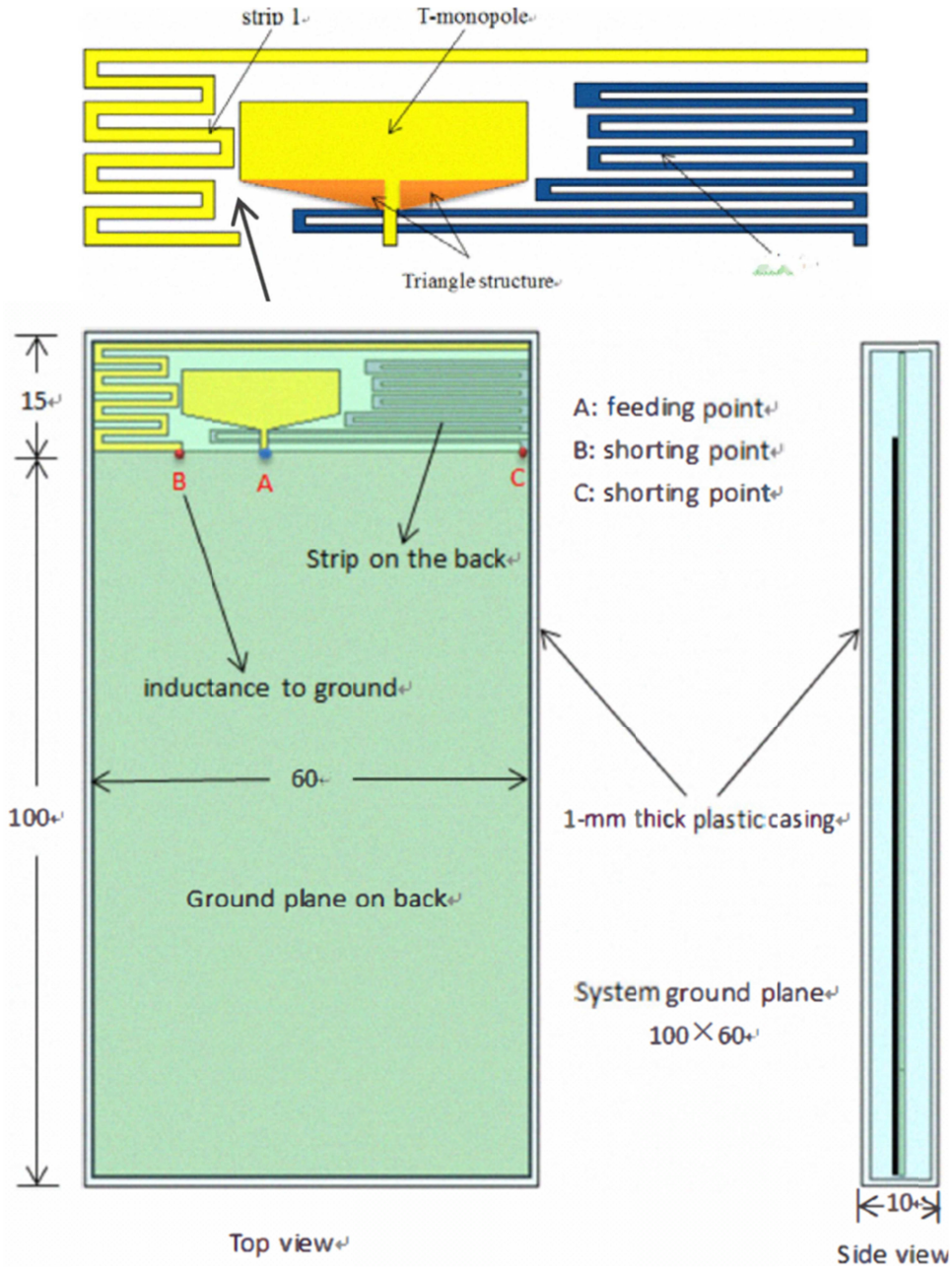

Figure 3.11: Low-Profile Coupled-Fed Printed PIFA for Internal Seven-Band LTE/GSMIUMTS Mobile Phone Antenna [39].

3.1.2 MIMO Antenna Designs:

Multiple-input and multiple-output antenna systems are a key mobile transmission technology being under research over the last 20 years. The use of multiple antennas at the transmitter and receiver largely improve the channel capacity and reliability in a rich scattering real world environment by reducing multipath fading and co-channel interference [50]-[68]. The antennas that were discussed in the previous section were single element (SISO) multiband antennas for mobile phones. In this section some of the MIMO antenna designs for handset applications that have already been proposed in the literature will be discussed. The main difference between a MIMO antenna for base station and one for a mobile handset is the size limitation of the handset. This in turn induces more limitations for the design engineers the major of which is the mutual coupling between the multiple antennas within the compact volume [50]-[68]. Numerous MIMO antenna designs have been proposed over the last few years. Different types of decoupling techniques have been discussed for achieving an acceptable isolation.

A MIMO antenna design has been presented in [55] with the geometry as shown in figure 3.12, where two antennas are mirrored on the top and no-ground portion of the substrate. Each antenna is composed of two resonant units, one etched on the front side and other on the back side of the substrate. In order to decrease the coupling, the antennas are placed at 45^0 to each other. A slot has been made to further improve the isolation at the lower frequency band. Each antenna resonates in two frequency bands with the lower ranging from 1620 MHz to 3600 MHz and the upper from 4400 MHz to 5920 MHz. Each antenna covers the GSM 1800/1900, UMTS, WLAN and WiMAX bands. Though the antennas are compact and covering most of the cellular frequency bands, the isolation is very poor and needs to be improved.

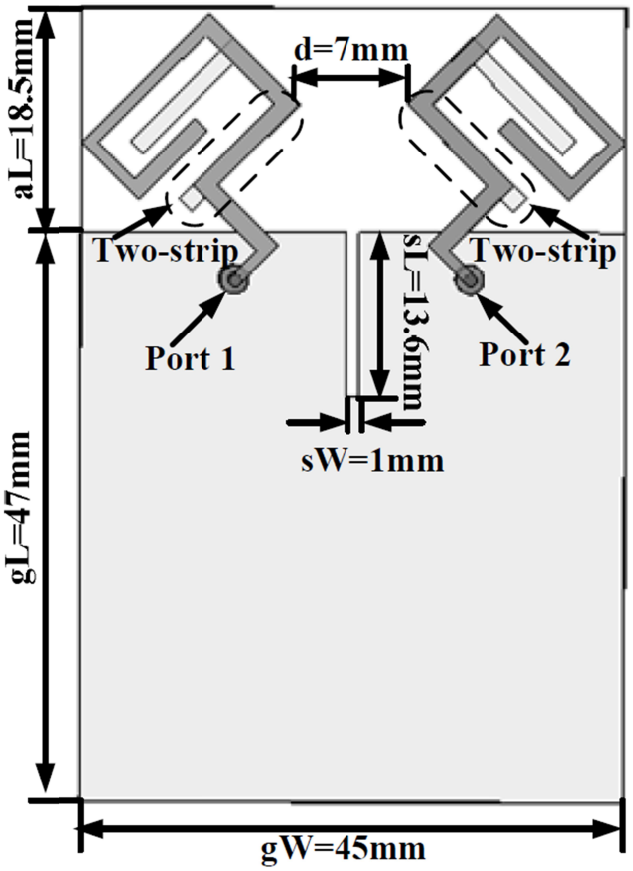

Figure 3.12: A Compact Wider Dual-Band MIMO Antenna Array for Mobile Phone [55].

Another design of the concurrent 2-port / 3-port MIMO antennas for mobile phone has been presented in [56]. The design is composed of two back to back printed symmetrical hybrid antennas and a dual loop antenna arranged with them as shown in figure 3.13. The hybrid structure is formed by a printed coupled fed PIFA and a Microstrip coupled monopole slot. The coupled feed PIFA is composed of an inverted L-shaped radiating branch that is printed on the back side while the feeding strip is printed on the front side of the substrate. The proposed antennas cover UMTS and LTE 2500 bands. Despite satisfactory isolation, the fabrication of the antennas due to the complex structure is very difficult. Also the antennas cover few cellular frequency bands.

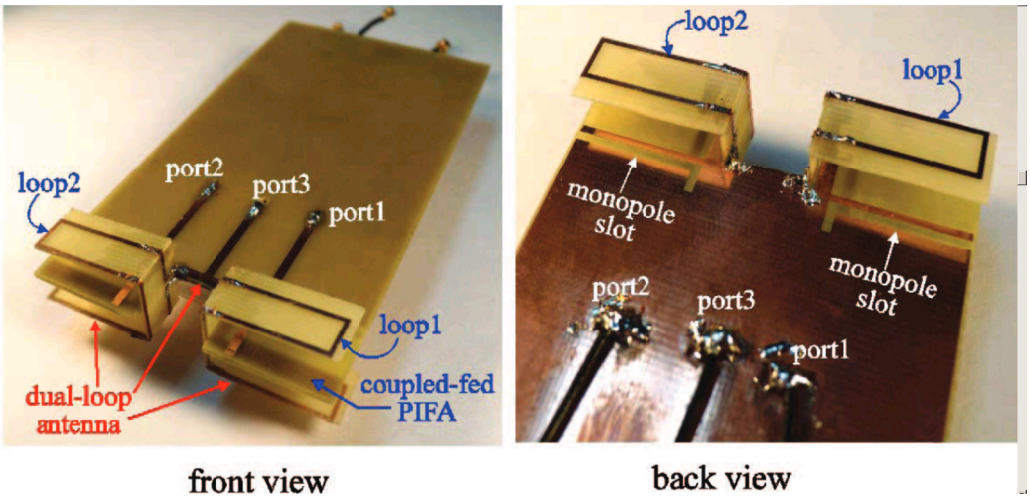

Figure 3.13: Concurrent 2-Port/3-Port MIMO Antenna System for UMTS/LTE2500 Operation in the Mobile Phone [56].

A fairly compact and less complex design of MIMO antennas for multiband applications is presented in [57]. The antennas possess a simpler isolation technique. The design is composed of two multi-patch monopole antennas placed 90^0 apart for orthogonal radiation. To improve isolation, a T-shaped ground branch is used to block the coupling path thereby restricting the current from the antenna 1 to the antenna 2. The proposed antenna system is shown in figure 3.14. The antennas are resonating in three bands covering GSM 850/900, DCS, PCS, UMTS, WLAN and LTE 2500 with isolation better than 15 dB. However, the width of the substrate can be reduced to make the design suitable for smartphones.

Another design with a novel decoupling structure has been presented in [59]. The antenna is tetra-band covering GSM 900/1800/1900 and UMTS when referenced to a return loss of 6 dB and the isolation achieved is better than 10 dB. The design presents two coupled feed loop antennas arranged in symmetry as shown in figure 3.16. A slot and a dual inverted-L shaped ground branch were etched at the back side of the substrate for the improvement of isolation. The slot also contributes to a resonance at 1.05 GHz.

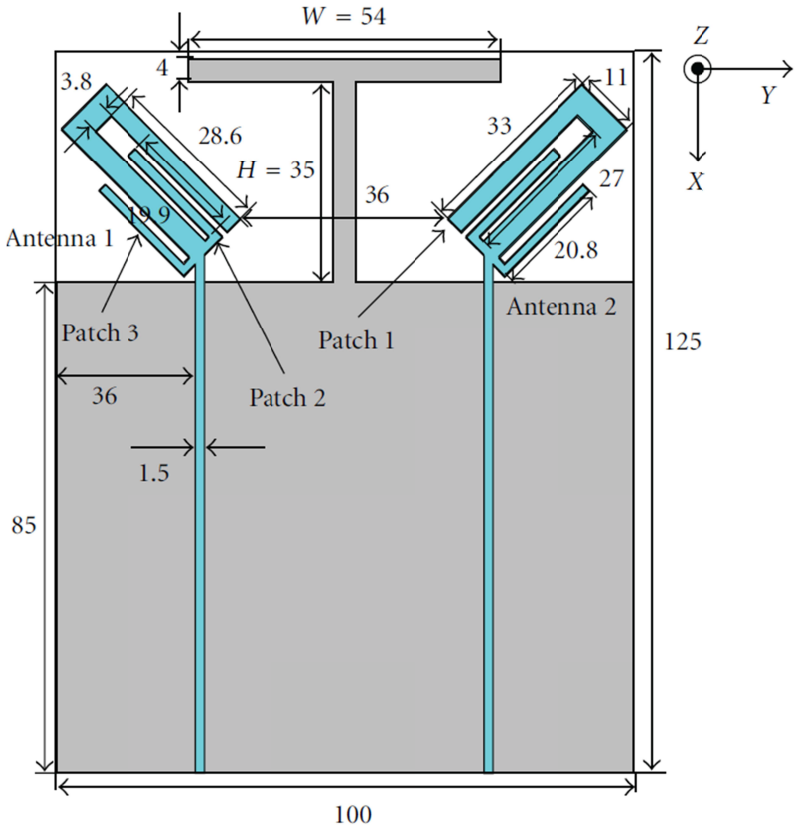

Figure 3.14: Novel Compact Multiband MIMO Antenna for Mobile Terminal [57].

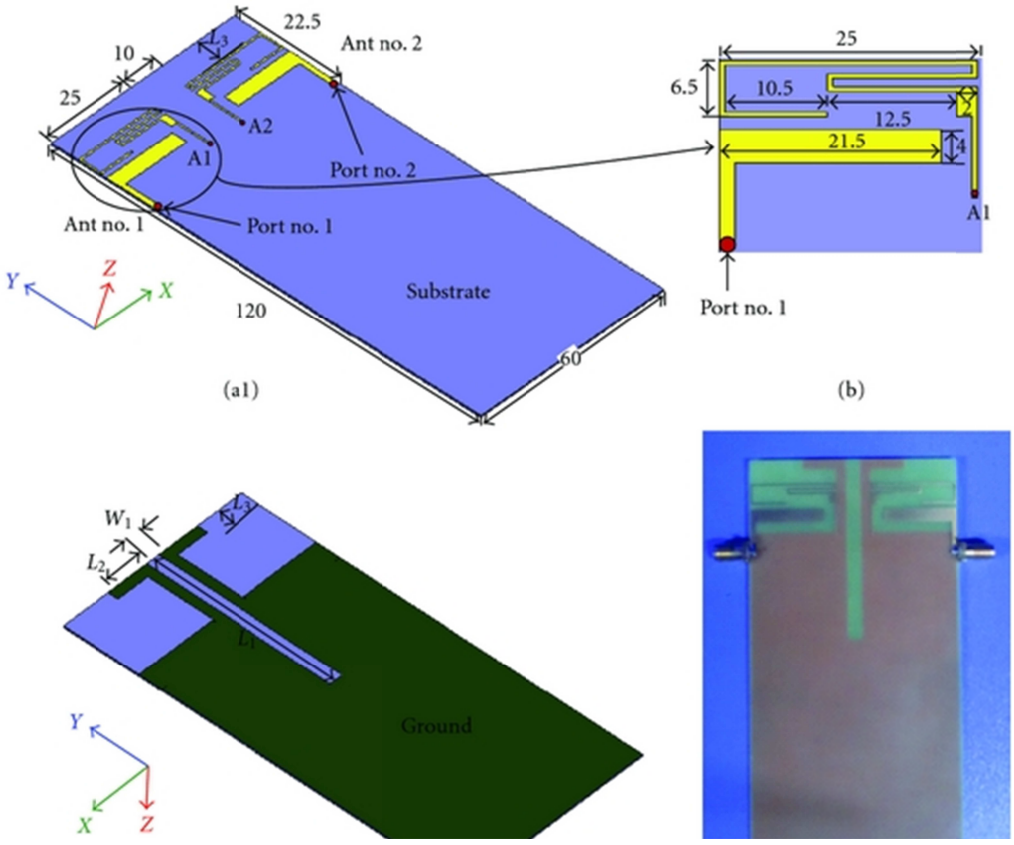

Figure 3.16: Tetra-band Small-Size Printed Strip MIMO Antenna for Mobile Handset Application [59].

A recent MIMO antenna design for mobile handsets is presented in [63]. The antennas proposed in this design are planar monopoles in MIMO configuration. Each antenna consists of coupled feed monopole strips which are continuing from the front side to the back side of the substrate as shown in figure 3.17. The antennas are capable of covering the lower LTE band. The overall bandwidth is 51 MHz ranging from 745 MHz to 796 MHz. The antennas proposed in this design are compact with an overall volume of 55 x 100 x 1.6 mm^3. The antennas however have limited cellular coverage covering only the LTE lower band which makes the implementation not suitable for multiband smartphones.

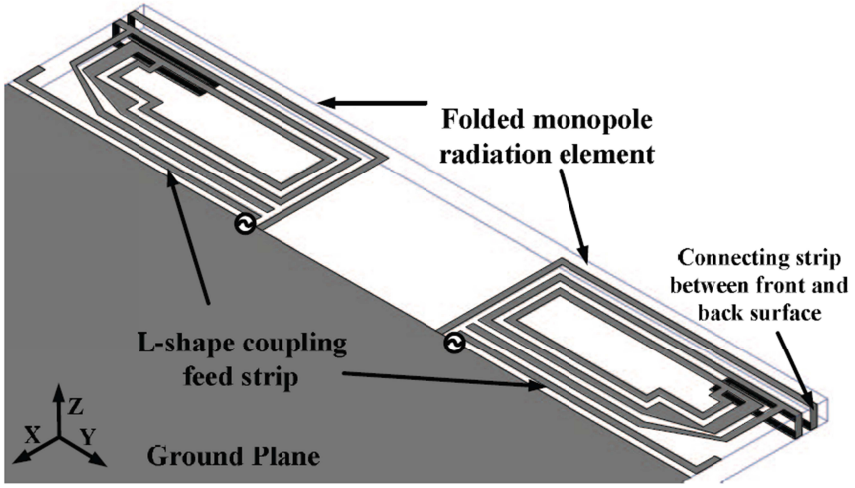

Figure 3.17: Compact Planar MIMO Antenna for LTE Mobile Application [63].

Another MIMO antenna design was presented recently in [64]. The antennas of the proposed MIMO configuration are PIFAs as shown in figure 3.18. Each antenna occupies an area of 17 x 9.75 mm^2 at the top edge of the FR-4 substrate with an overall volume of 100 x 50 x 0.8 mm^3. The antennas are placed above the ground plane using a support structure. Each antenna covers LTE band 13 (765-798 MHz), PCS 1900 and WiMAX (3.05-3.65 GHz) frequency bands. The antennas do not cover the basic cellular frequency bands and have a poor isolation at the upper frequency bands. Also, the antennas are folded PIFAs which makes the fabrication more difficult. As the antennas are placed at a height above the ground plane, the design is not suitable for slim housed mobile handsets.

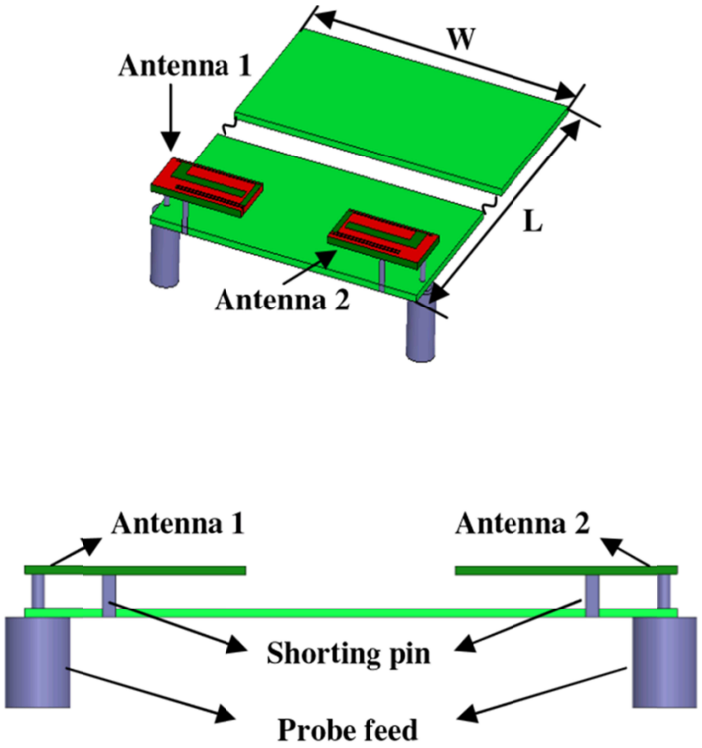

Figure 3.18: A Compact Tri-Band MIMO/Diversity Antenna for Mobile Handsets [64].

A MIMO antenna design using ceramic material for LTE communication was presented recently in [65]. The overall design is shown in figure 3.19 where folded strip antennas have an overall volume of 35 x 11 x 5 mm^3. The antenna utilizes a new ceramic material which gives a shorter guided wavelength and a wider frequency bandwidth. The ceramic is fed through coupling using a microstrip line which then excites the antenna. The height of the antenna is 5mm, which makes it unsuitable for slender designs. Also the isolation between the antennas is poor at the lower and upper frequency bands.

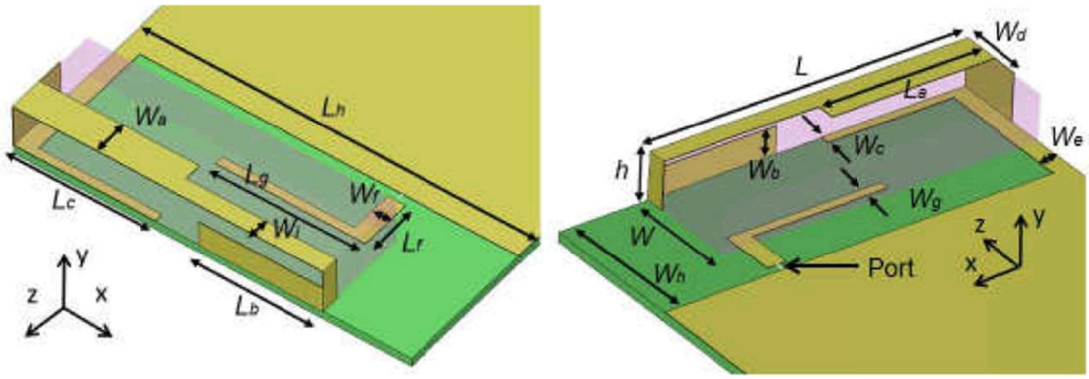

Figure 3.19: Ceramic Based Small LTE MIMO Handset Antenna [65].

A MIMO antenna design consisting of 2 x 2 pairs is presented in [67] and the geometry is shown in figure 3.20. The two antennas at the top no-ground edge of the substrate are identical and so as the two antennas at the bottom. Each antenna resonates at 2.4 GHz covering the 2.4 GHz LTE band only. The proposed MIMO antennas are compact but due to poor band coverage and isolation, the design is not suitable for multiband mobile handsets.

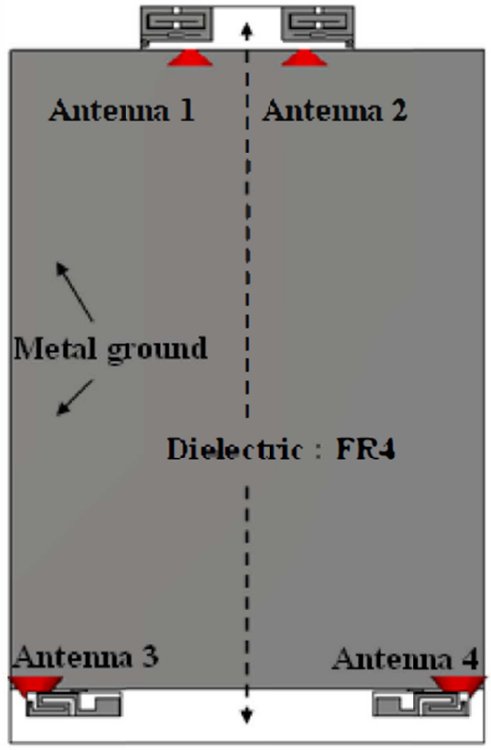

Figure 3.20: Four MIMO Handset Antennas [67].

3.1.3 Reconfigurable Antennas for Mobile Handsets:

This section presents a literature review of reconfigurable antennas for mobile handsets. The antenna designs reviewed include PIN diodes, MEMS and optical switching techniques. The reviewed designs are mostly of frequency reconfigurable antennas. Pattern reconfigurable designs are rare due to the size limitation of a mobile handset which makes it difficult to achieve with MIMO antennas.

A design of frequency and beam reconfigurable antenna using optical switches is presented in [69]. The antenna is a printed dipole as shown in figure 3.21(a). A wideband coplanar waveguide (CPW) to coplanar stripline (CPS) transition is used to feed the antenna. Two silicon photo diode switches are used on the arms of the dipole

and the activation of the switches is achieved using infrared laser diodes through optical fibre. The radiation patterns of the antenna are shown in figure 3.24 (b). When both switches are 'ON', the antenna resonates at 2.26 GHz, whereas when both switches are 'OFF', the antenna operating frequency shifts from 2.26 GHz to 3.15 GHz. Also the radiation patterns show that the antenna is beam reconfigurable. When the left switch is 'ON' the left arm of the antenna becomes longer than the right thus rotating the pattern to the left. Likewise, the pattern is rotated to the right when the right switch is 'ON'. The proposed design is a good example for achieving pattern reconfigurability within a compact volume. However, due to limited frequency coverage, the antenna cannot be employed in multiband cellular handsets.

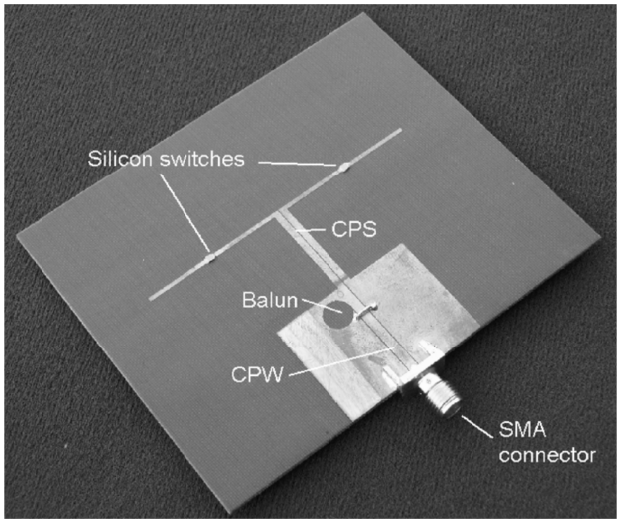

(a)

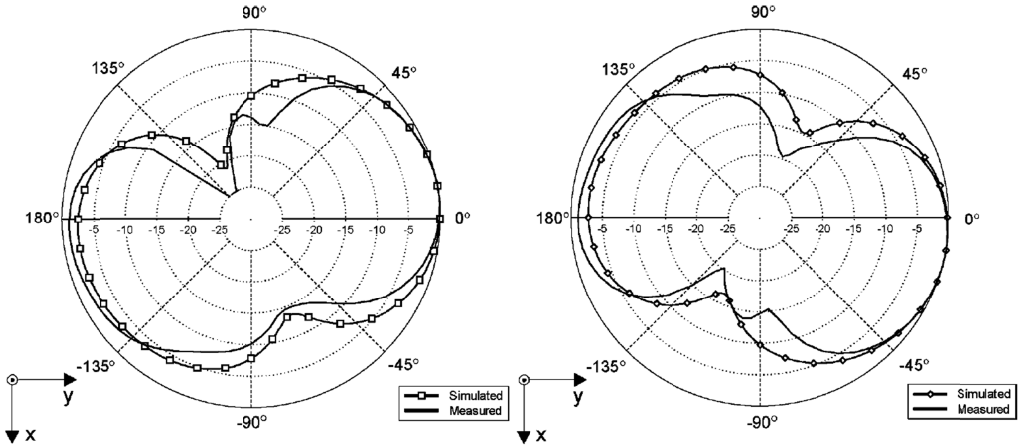

(Only Left Switch is ON) (Only Right Switch is ON)

(b)

Figure 3.21: Frequency and Beam Reconfigurable Antenna Using Photo-conducting Switches [69]. (a): Proposed antenna geometry. (b): Radiation patterns of the proposed antenna.

A frequency reconfigurable antenna for mobile handsets is presented in [70]. The proposed design operates in two modes, the PIFA mode and the loop mode. Switching between the modes is done using two PIN diode switches. The overall geometry of the antenna is shown in figure 3.22. When the PIN diode 1 is 'ON' and the PIN diode 2 is 'OFF', the antenna operates in the PIFA mode covering GSM 900 only. When the PIN diode 1 is 'OFF' and the PIN diode 2 is 'ON', the antenna operates in loop mode covering GSM 1800/1900 and UMTS 2100 frequency bands. A major shortfall in the proposed design is the height above the ground which is 6mm making it not suitable for sleek handsets.

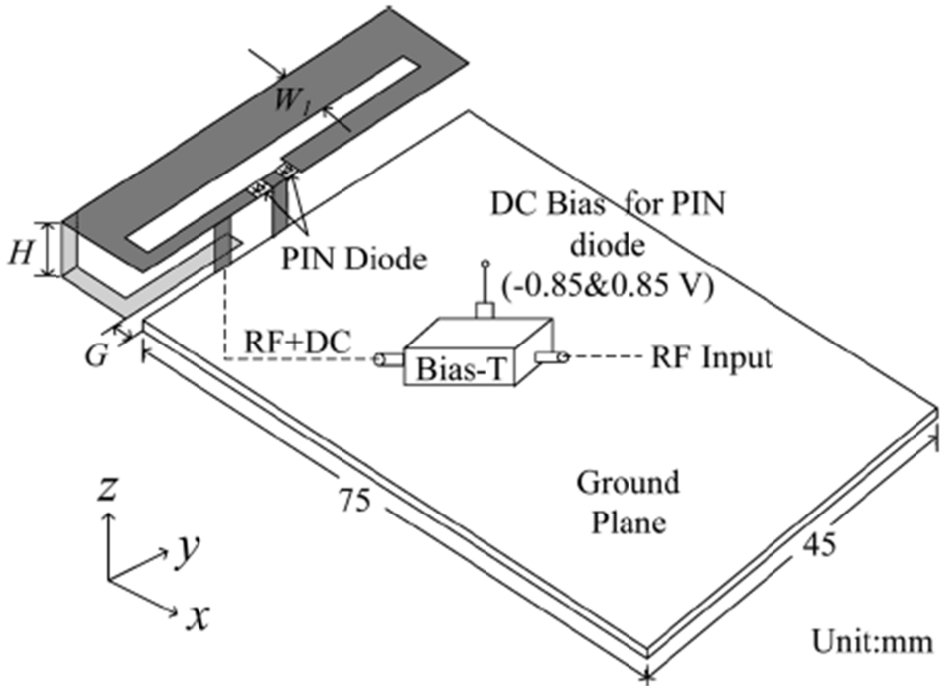

Figure 3.22: A Reconfigurable Antenna for Quad-Band Mobile Handset [70].

A recent reconfigurable antenna for mobile handsets was presented in [71] and the geometry is shown in figure 3.23. The proposed antenna is composed of a PIFA antenna with an overall volume of 40 x 16 x 5 mm^3. A PIN diode is used to control the electrical length of the antenna thereby changing the operating frequency of the antenna. When the PIN diode is 'OFF', the proposed antenna covers GSM 850/900, DCS, PCS and UMTS frequency bands. By switching the PIN diode 'ON', the electrical length of the antenna increases making the antenna capable of covering the lower LTE band (698-787 MHz).

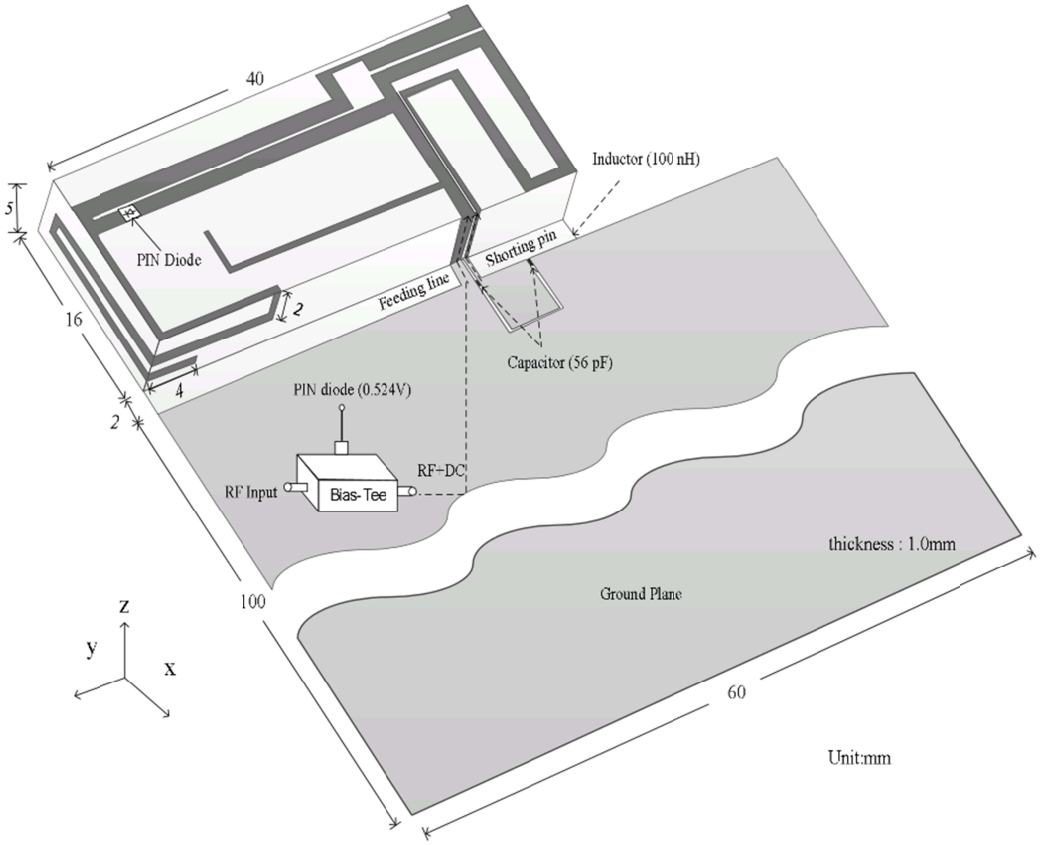

Figure 3.23: A Reconfigurable PIFA Using a PIN-Diode for LTE/GSM850/GSM900/DCS /PCS/ UMTS [71].

Two frequency reconfigurable antenna designs have been presented in [72]. Each design covers two frequency bands with the first ranging from 700 MHz to 960 MHz and the second from 1.7 GHz to 2.7 GHz. The operating band reconfigurability is achieved using micro-electro-mechanical switches (MEMS). The first design is made up of a driven monopole that is capacitively coupled to a parasitic strip as shown in figure 3.24. The input impedance of the parasitic strip is changed using a two-branch matching network and the branch selection is done using MEMS switches. The second design is composed of two driven strips. One of the driven strips is capacitively coupled to the parasitic strip as shown in figure 3.25. In this design, a selection is made between driven strips using MEMS switches thereby increasing or decreasing the length of the radiator, thus enabling or disabling the antenna to cover the lower LTE band. Though the designs proposed in this work are compact, the use of MEMS switches in mobile handsets is not suitable due to the high insertion loss, high biasing voltage (50-70V) and complex matching network required.

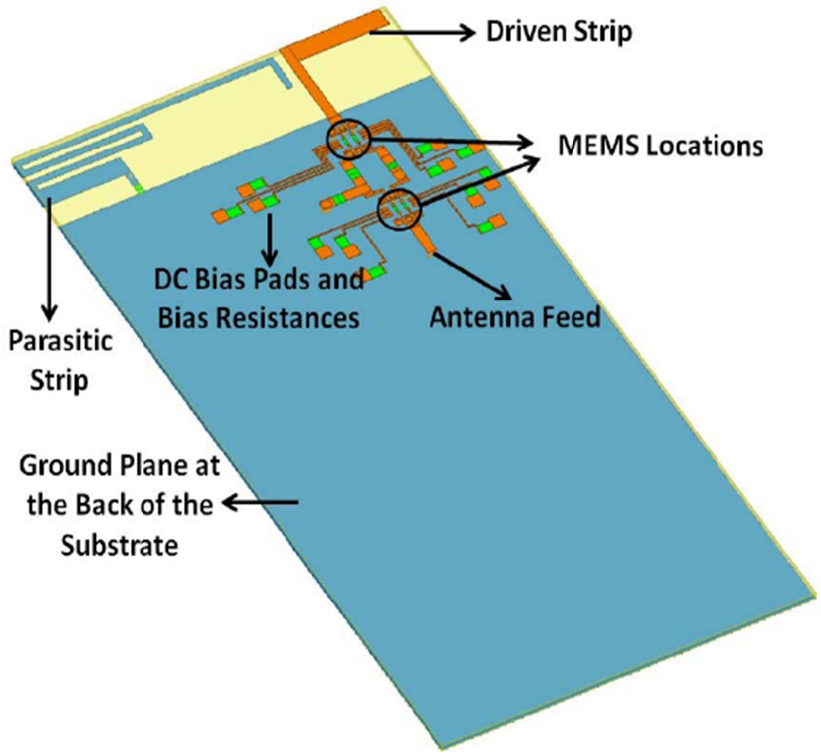

Figure 3.24: A Tuneable Antenna Using MEMS Switches for LTE Mobile Terminals [72].

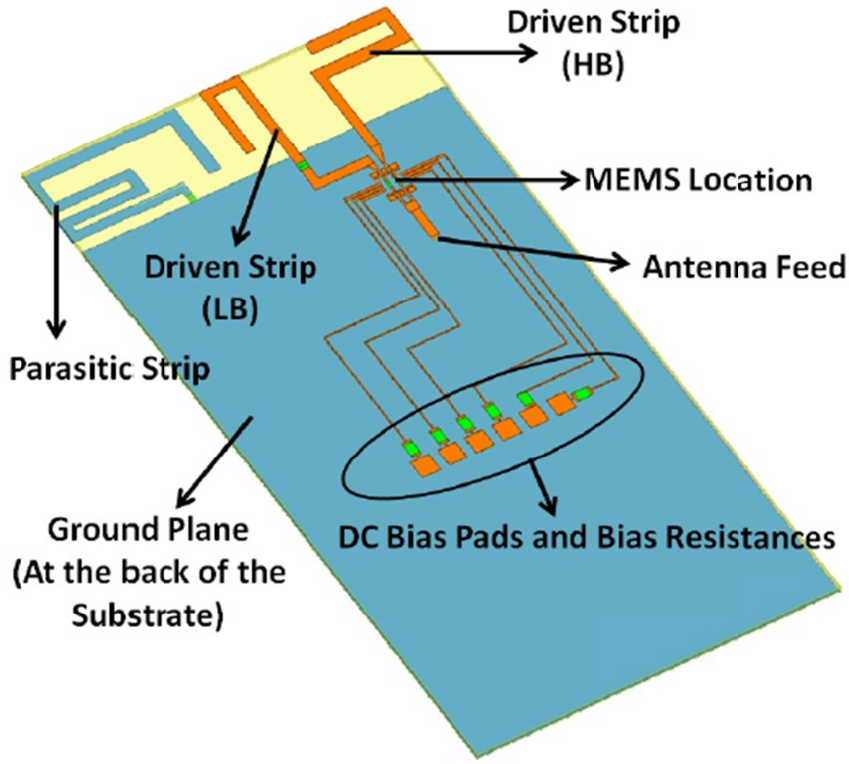

Figure 3.25: A Tuneable Antenna Using MEMS Switches for LTE Mobile Terminals [72].

Other recent designs of the reconfigurable antennas have been presented in [74]-[78]. A pattern reconfigurable antenna in MIMO configuration for mobile applications has been presented in [75]. The geometry of the antennas is shown in figure 3.26.

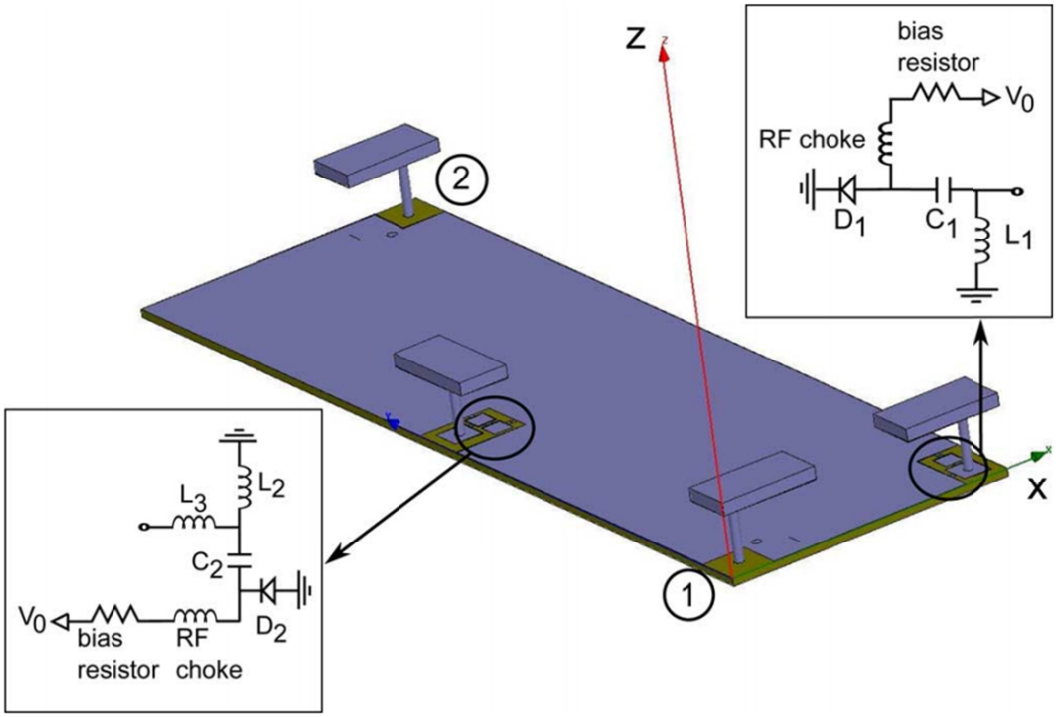

Figure 3.26: A Pattern Reconfigurable Chassis-Mode MIMO Antenna [75].

The design is composed of two MIMO antennas placed diagonally at the no-ground portion of the substrate. In order to achieve a better decoupling, two parasitic elements are also designed and tuned. Furthermore, a four-port network is loaded with reactive loads at the two ports. This leads to two sets of loads decoupling the antennas and thus obtaining two states for the reconfigurable antenna. The selection between the loads is done using PIN diodes and LC networks for achieving orthogonal and highly de-correlated radiation patterns. The radiation patterns of the reconfigurable antenna in the different states are shown in figure 3.27. Despite pattern reconfigurability and good decoupling performance of the MIMO antennas, the cellular coverage is restricted with a resonance at 2.36 GHz only. Also the height of the antennas above the ground plane is 6 mm which makes the design not suitable for sleek smartphones.

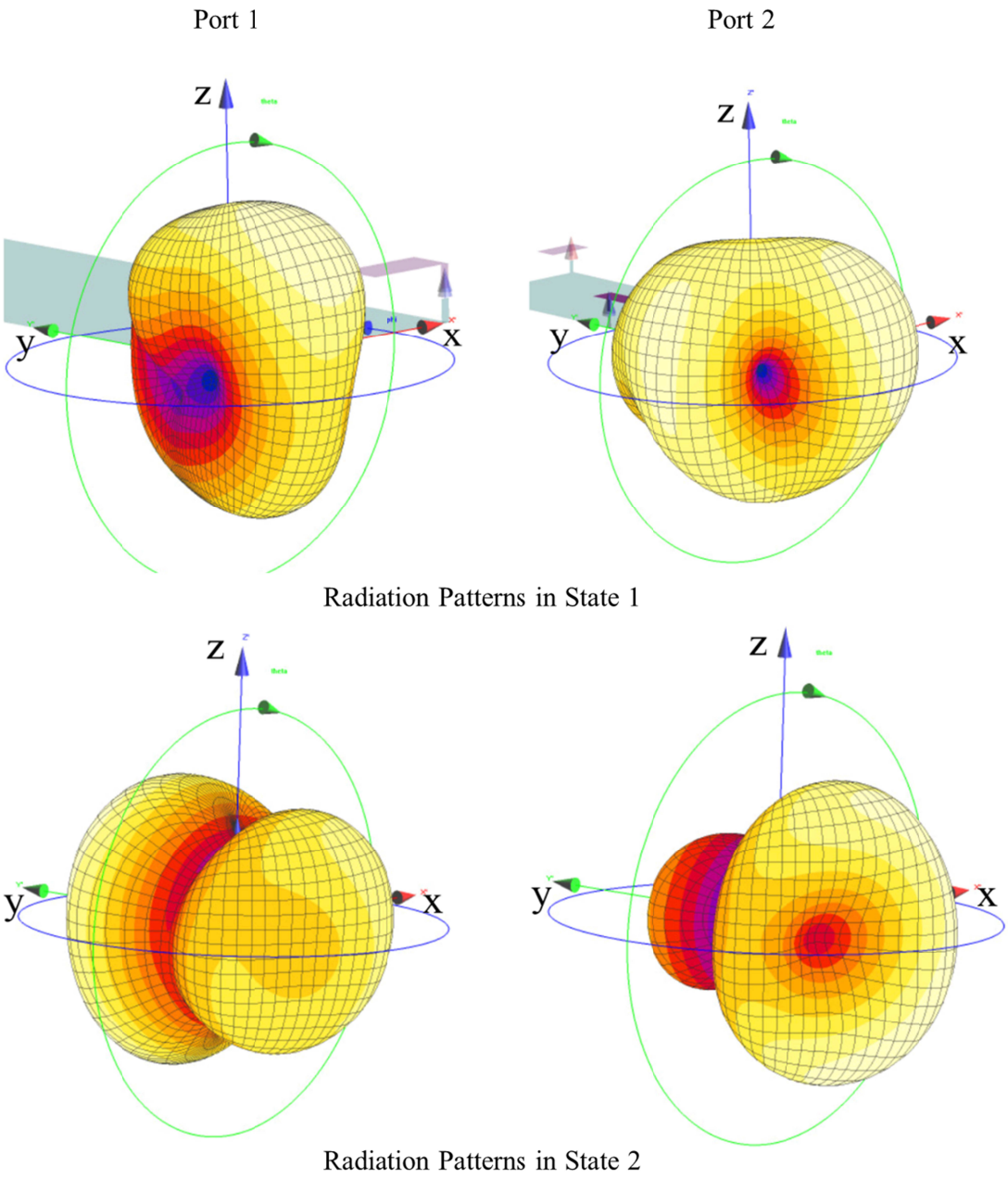

Figure 3.27: Radiation patterns of Pattern Reconfigurable Chassis-Mode MIMO Antenna [75].

The design presented in [76] is of pattern reconfigurable antennas that are very compact and printed but the operating bandwidth is 5.15 – 5.35 GHz which is not suitable for cellular handsets.

A detailed comparison of the various switching techniques reported in this review is shown in Table 3.1.

Table 3.1: Comparison of various Switching techniques used in reconfigurable antennas [79]-[90].

Switch	Theory of operation	Advantages	Disadvantages
P-i-n Diode	Heavily doped p-type and n-type regions; Lightly doped intrinsic region; Low forward biased resistance; Open circuit in reverse biased state.	Low loss when forward biased (ON state); Low capacitance when reverse biased (OFF state); Reasonable linearity; Low biasing voltage; Cheaper technology; Readily available; Easier implementation.	Large DC power consumption due to a large biasing current; May reduce antenna's gain and efficiency.
FET	Operated by the flow of current between source and drain when a voltage is applied at the gate.	Low loss when forward biased (ON state); Low capacitance when reverse biased (OFF state); Low power consumption; Good linearity.	Availability at various frequencies is limited especially in the range of 1.5 – 2.1 GHz.
MEMS	Miniature electro-mechanical switch; An electrostatic force results which connects the beam when a biasing voltage is applied.	Low insertion loss when forward biased (ON state); Low capacitance when reverse biased (OFF state); Excellent linearity.	Large biasing voltage; Slow switching; Complex biasing circuitry; Poor reliability; Temperature sensitive.
Varactor	The capacitance of varactor switch changes inversely with the applied voltage; A thin depletion region.	Continuous tuning for wide bandwidth; Low consumption of DC power.	Poor linearity; Bias voltage needs to be analog.
Silicon Photo-diode	This switch gets forward biased when the silicon is subjected to a source of light.	Extremely low insertion loss; No biasing wires; Fast switching.	Not easy implementation for some wireless devices; May not work properly if the intensity and power of the light source changes.

Summary

A comprehensive literature review was presented in this chapter which included both single and MIMO antenna designs for handset applications. Single antenna designs are widely available. However, MIMO and the reconfigurable designs with acceptable performance and isolation are less common and this is a potential task that is under research. The single antenna designs discussed in the literature review were mostly simple PIFA, loop antennas and monopole antennas. It was observed that the bandwidth with a coupling feed is more than that with the direct feed. Also the coupling feed makes the antenna structure much simpler and more compact. So coupled fed antennas seem to be more suitable for the small volume of a mobile handset. Also, to obtain a single antenna capable of covering all the cellular frequency bands is a challenging task in itself.

The MIMO designs discussed in this chapter involved various decoupling techniques. It is concluded that the current designs are not covering most of the cellular frequency bands while simultaneously showing a good isolation between the MIMO antennas. The potential problem to be solved is to obtain compact MIMO antennas capable of covering multiple mobile communication frequencies with an acceptable isolation performance.

The reconfigurable antenna designs that have been included in this chapter are mostly of frequency reconfigurable antennas using PIN diodes, MEMS and optical switching schemes. However, these designs for smartphone applications are rare due to the compact size of a mobile handset which makes the design challenging. To achieve pattern reconfigurability from a compact handset antenna is a very challenging task. The close spacing between MIMO antennas in a mobile handset largely increases the farfield correlation which in turn results in poor diversity performance thus hindering the capability of the MIMO antennas to achieve pattern reconfigurability while assuring multiband cellular coverage. It is therefore a challenging research problem yet to be resolved.

References

[1] Tarvas, S.; Isohatala, A., "An internal dual-band mobile phone antenna," *Antennas and Propagation Society International Symposium, 2000. IEEE* , vol.1, pp.266-269 vol.1, 2000

[2] Massey, P.J.; , "GSM fabric antenna for mobile phones integrated within clothing," *Antennas and Propagation Society International Symposium, 2001. IEEE* , vol.3, pp.452-455 vol.3, 2001

[3] Shih-Huang Yeh; Kin-Lu Wong; Tzung-Wern Chiou; Shyh-Tirng Fang; , "Dual-band planar inverted-F antenna for GSM/DCS mobile phones," *Antennas and Propagation, IEEE Transactions on* , vol.51, no.5, pp. 1124- 1126, May 2003

[4] Ciais, P.; Staraj, R.; Kossiavas, G.; Luxey, C.; , "Design of an internal quad-band antenna for mobile phones," *Microwave and Wireless Components Letters, IEEE* , vol.14, no.4, pp. 148- 150, April 2004

[5] Shao-Lun Chien; Hong-Twu Chen; Chih-Ming Su; Fu-Ren Hsiao; Kin-Lu Wong; , "Planar inverted-F antenna with a hollow shorting cylinder for internal mobile phone antenna," *Antennas and Propagation Society International Symposium, 2004. IEEE* , vol.2, pp. 1947- 1950 Vol.2, 20-25 June 2004

[6] Kin-Lu Wong; Saou-Wen Su; Chia-Lun Tang; Shih-Huang Yeh; , "Internal shorted patch antenna for a UMTS folder-type mobile phone," *Antennas and Propagation, IEEE Transactions on* , vol.53, no.10, pp. 3391- 3394, Oct. 2005

[7] Min-Seok Han; Hong-Teuk Kim; , "Compact Five Band Internal Antenna for Mobile Phone," *Antennas and Propagation Society International Symposium 2006, IEEE* , pp.4381-4384, 9-14 July 2006

[8] Yildirim, B.; Cetiner, B.; Qingzhou Xu; , "Reconfigurable planar inverted-F antenna for mobile phones," *Antennas and Propagation Society International Symposium, 2007 IEEE* , pp.5207-5210, 9-15 June 2007

[9] Kin-Lu Wong; Chih-Hua Chang; , "Printed λ/8-PIFA for internal penta-band mobile phone antenna," *Antennas and Propagation, 2009. EuCAP 2009. 3rd European Conference on* , pp.533-537, 23-27 March 2009

[10] Chih-Hua Chang; Kin-Lu Wong; , "Penta-band one-eighth wavelength PIFA for internal mobile phone antenna," *Antennas and Propagation Society International Symposium, 2009. APSURSI '09. IEEE* , pp.1-4, 1-5 June 2009

[11] Chien-Wen Chiu; Yu-Jen Chi; , "Planar Hexa-Band Inverted-F Antenna for Portable Device Applications," *Antennas and Wireless Propagation Letters, IEEE* , vol.8, pp.1099-1102, 2009

[12] Yongyan Du; Anping Zhao; , "An Internal Quad-Band Antenna for Oval-Shaped Mobile Phones," *Antennas and Wireless Propagation Letters, IEEE* , vol.9, pp.830-833, 2010

[13] Saidatu, N.A.; Soh, P.J.; Sun, Y.; Lauder, D.; Azremi, A.A.H.; , "Multiband Fractal PIFA (Planar Inverted F Antenna) for mobile phones," *Wireless Communication Systems (ISWCS), 2010 7th International Symposium on* , pp.671-675, 19-22 Sept. 2010

[14] Krzysztofik, W.J.; Skikiewicz, A.; , "Tapered PIFA antenna for handsets terminals," Microwaves, Radar and Wireless Communications, 2008. MIKON 2008. 17th International Conference on , pp.1-4, 19-21 May 2008

[15] Chi, Y.-W.; Kin-Lu Wong; , "Internal Compact Dual-Band Printed Loop Antenna for Mobile Phone Application," *Antennas and Propagation, IEEE Transactions on* , vol.55, no.5, pp.1457-1462, May 2007

[16] Wei-Yu Li; Kin-Lu Wong; , "Internal penta-band printed loop-type mobile phone antenna," *TENCON 2007 - 2007 IEEE Region 10 Conference* , pp.1-4, Oct. 30 2007-Nov. 2 2007

[17] Kin-Lu Wong; Chih-Hong Huang; , "Penta-Band Printed Loop Antenna for Mobile Phone," *Antenna Technology: Small Antennas and Novel Metamaterials, 2008. iWAT 2008. International Workshop on* , pp.99-102, 4-6 March 2008

[18] Yun-Wen Chi; Kin-Lu Wong; , "Small-size multiband folded loop antenna for small-size mobile phone," *Antennas and Propagation Society International Symposium, 2008. AP-S 2008. IEEE* , pp.1-4, 5-11 July 2008

[19] Yun-Wen Chi; Kin-Lu Wong; , "Quarter-Wavelength Printed Loop Antenna With an Internal Printed Matching Circuit for GSM/ DCS/PCS/UMTS Operation in the Mobile Phone," *Antennas and Propagation, IEEE Transactions on* , vol.57, no.9, pp.2541-2547, Sept. 2009

[20] Yue Li; Zhijun Zhang; Jianfeng Zheng; Zhenghe Feng; Iskander, M.F.; , "A Compact Hepta-Band Loop-Inverted F Reconfigurable Antenna for Mobile Phone," *Antennas and Propagation, IEEE Transactions on* , vol.60, no.1, pp.389-392, Jan. 2012

[21] Lee, G.; Chiou, T.; Wong, K.; Wang, C.; , "Low-profile planar monopole antenna for GSM/DCS/PCS triple-band mobile phone," *Antennas and Propagation Society International Symposium, 2002. IEEE* , vol.3, pp.26, 16-21 June 2002

[22] Hao-Chun Tung; Chi-Yin Fang; Kin-Lu Wong; , "Dual-band inverted-L monopole antenna for GSM/DCS mobile phone," *Antennas and Propagation Society International Symposium, 2002. IEEE* , vol.3, pp.30, 16-21 June 2002

[23] Hao-Chun Tung; Shih-Wen Lu; Ji-Fuh Liang; Kin-Lu Wong; , "Internal monopole plastic chip antenna for GSM/DCS/PCS mobile phone," *Antennas and Propagation*

Society International Symposium, 2005 IEEE , vol.2A, pp. 434- 437 vol. 2A, 3-8 July 2005

[24] Shyh-Tirng Fang; Meng-Hann Shieh; , "Compact monopole antenna for GSM/DCS/PCS mobile phone," *Microwave Conference Proceedings, 2005. APMC 2005. Asia-Pacific Conference Proceedings* , vol.4, pp. 4 pp., 4-7 Dec. 2005

[25] Hao-Chun Tung; Tzung-Fang Huang; Chao-Yung Lin; Shih-Wen Lu; Fu-Ji Yang; , "Shorted Monopole Dual Band Antenna for Ultra-Thin Profile Slider Mobile Phone," *Antennas and Propagation Society International Symposium 2006, IEEE* , pp.4693-4696, 9-14 July 2006

[26] Chih-Hsien Wu; Kin-Lu Wong; , "Low-profile printed monopole antenna for penta-band operation in the mobile phone," *Antennas and Propagation Society International Symposium, 2007 IEEE* , pp.3540-3543, 9-15 June 2007

[27] Bhatti, R.A.; Park, S.-O.; , "Octa-band internal monopole antenna for mobile phone applications," *Electronics Letters* , vol.44, no.25, pp.1447-1448, December 4 2008

[28] Chia-Ling Liu; Yi-Fang Lin; Chia-Ming Liang; Shan-Cheng Pan; Hua-Ming Chen; , "Miniature Internal Penta-Band Monopole Antenna for Mobile Phones," *Antennas and Propagation, IEEE Transactions on* , vol.58, no.3, pp.1008-1011, March 2010

[29] Jie Ma; Ying Zeng Yin; Jing Li Guo; You Huo Huang; , "Miniature Printed Octaband Monopole Antenna for Mobile Phones," *Antennas and Wireless Propagation Letters, IEEE* , vol.9, pp.1033-1036, 2010

[30] Wen-Shan Chen; Li-Yu Yeh; Bai-Chen Chen; Yu-Hung Huang; Wen-Hsiu Hsu; , "Five-band printed monopole antenna for mobile phone application," *Antenna Technology (iWAT), 2011 International Workshop on* , pp.437-440, 7-9 March 2011

[31] Yu-Jen Chi; Fu-Chiarng Chen; , "Compact printed hepta-band monopole antenna for mobile devices," Microwave Conference Proceedings (APMC), 2010 Asia-Pacific , pp.2216-2219, 7-10 Dec. 2010

[32] Chun-I Lin; Kin-Lu Wong; , "Printed Monopole Slot Antenna for Internal Multiband Mobile Phone Antenna," *Antennas and Propagation, IEEE Transactions on* , vol.55, no.12, pp.3690-3697, Dec. 2007

[33] Chun-I Lin; Kin-Lu Wong; Shih-Huang Yeh; , "Printed monopole slot antenna for multiband operation in the mobile phone," *Antennas and Propagation Society International Symposium, 2007 IEEE* , pp.629-632, 9-15 June 2007

[34] Fang-Hsien Chu; Kin-Lu Wong; , "Simple Folded Monopole Slot Antenna for Penta-Band Clamshell Mobile Phone Application," *Antennas and Propagation, IEEE Transactions on* , vol.57, no.11, pp.3680-3684, Nov. 2009

[35] Kin-Lu Wong; Yun-Wen Chi; Shu-Yang Tu; , "Printed folded slot antenna for internal multiband mobile phone antenna," *Antennas and Propagation Society International Symposium, 2007 IEEE* , pp.2622-2625, 9-15 June 2007

[36] Rhyu, H.; Byun, J.; Harackiewicz, F.J.; Park, M.J.; Jung, K.; Kim, D.; Kim, N.; Kim, T.; Lee, B.; , "Multi-band hybrid antenna for ultra-thin mobile phone applications," *Electronics Letters* , vol.45, no.15, pp.773-774, July 16 2009

[37] Bau-Yi Lee; Wen-Shan Chen; Wen-Lin Chang; Fu-Lai Yen; Yuan-Chih Lin; , "Five-band printed antenna for mobile phone and WLAN applications," *Antennas and Propagation Society International Symposium (APSURSI), 2010 IEEE* , pp.1-4, 11-17 July 2010

[38] Shinho Yoon; Chulwoo Park; Minsu Kim; Kyungwon Kim; Youngoo Yang; , "Multiband internal antenna for mobile phones using a high dielectric material," *Microwave Conference Proceedings (APMC), 2010 Asia-Pacific* , pp.219-222, 7-10 Dec. 2010

[39] Li-Jun Ying; Yong-Ling Ban; Jin-Hua Chen; , "Low-profile coupled-fed printed PIFA for internal seven-band LTE/GSM/UMTS mobile phone antenna," *Cross Strait Quad-Regional Radio Science and Wireless Technology Conference (CSQRWC), 2011* , vol.1, pp.418-421, 26-30 July 2011

[40] Chia-Lun Tang; Jia-Yi Sze; Yi-Feng Wu; , "A compact coupled-fed penta-band antenna for mobile phone application," *Microwave Conference Proceedings (APMC), 2010 Asia-Pacific* , pp.2260-2263, 7-10 Dec. 2010

[41] Hai Zhao; Gui Lin; Beckman, C.; , "Design of a coupling element based penta-band mobile phone antenna," *Antennas & Propagation Conference, 2009. LAPC 2009. Loughborough* , pp.209-212, 16-17 Nov. 2009

[42] Jeong-Ho Lee; Jong-Gwan Yook; , "Improvement of radiation performance of mobile phone antenna using parasitic element," *Consumer Electronics, IEEE Transactions on* , vol.56, no.4, pp.2411-2415, November 2010

[43] Kin-Lu Wong; Yu-Wei Chang; Chun-Yih Wu; Wei-Yu Li; , "A small-size penta-band WWAN antenna integrated with USB connector for mobile phone applications," *Applications of Electromagnetism and Student Innovation Competition Awards (AEM2C), 2010 International Conference on* , pp.147-151, 11-13 Aug. 2010

[44] Tzortzakakis, M.; Langley, R.J.; , "Quad-band Antenna for a Foldable Mobile Phone," *Wireless Technology, 2006. The 9th European Conference on* , pp.281-284, 10-12 Sept. 2006

[45] Tzortzakakis, M.; Langley, R.J.; , "Quad-Band Internal Mobile Phone Antenna," *Antennas and Propagation, IEEE Transactions on* , vol.55, no.7, pp.2097-2103, July 2007

[46] Zhijun Zhang; Langer, J.-C.; Li, K.; Iskander, M.F.; , "Design of Ultrawideband Mobile Phone Stubby Antenna (824 MHz-6 GHz)," *Antennas and Propagation, IEEE Transactions on* , vol.56, no.7, pp.2107-2111, July 2008

[47] Chia-Lun Tang; Chi-Ming Chiang; , "Penta-band folded antenna for mobile phone application," *Antennas and Propagation Society International Symposium, 2008. AP-S 2008. IEEE* , pp.1-4, 5-11 July 2008

[48] Cho, J.; Jung, C.W.; Kim, K.; , "Frequency-reconfigurable two-port antenna for mobile phone operating over multiple service bands," *Electronics Letters* , vol.45, no.20, pp.1009-1011, September 24 2009

[49] Ben Ahmed, M.; El Ouaai, F.; Bouhorma, M.; Mamouni, A.; , "Compact internal antenna for multi standard operations in the mobile phone," *Microwave Symposium (MMS), 2009 Mediterrannean* , pp.1-7, 15-17 Nov. 2009

[50] Simanee, K.; Uthansakul, M.; Uthansakul, P.; , "A switched-beam microstrip antenna for 3G mobile phone," *Intelligent Signal Processing and Communications Systems (ISPACS), 2011 International Symposium on* , pp.1-4, 7-9 Dec. 2011

[51] Ding Yuan; Du Zhengwei; Gong Ke; Feng Zhenghe; , "A Four-Element Antenna System for Mobile Phones," *Antennas and Wireless Propagation Letters, IEEE* , vol.6, pp.655-658, 2007

[52] Kulkarni, A.N.; Sharma, S.K.; , "A compact multiband antenna with MIMO implementation for USB size 4G LTE wireless devices," *Antennas and Propagation (APSURSI), 2011 IEEE International Symposium on* , pp.2215-2218, 3-8 July 2011

[53] Jamil, A.; Yusoff, M.Z.; Yahya, N.; Zakariya, M.A.; , "Design and performance evaluation of multiband MIMO antennas," *National Postgraduate Conference (NPC), 2011* , pp.1-5, 19-20 Sept. 2011

[54] Sanguk Park; Jungyup Lee; Joonghee Lee; Kim, A.S.; , "Dual-port LCP multi-band antenna for Wibro/mWiMax MIMO, Bluetooth and GPS applications in mobile phone," *Antennas and Propagation Society International Symposium, 2009. APSURSI '09. IEEE* , pp.1-4, 1-5 June 2009

[55] Qin-Xin Chu; Jian-Feng Li; , "A compact wider dual-band MIMO antenna array for mobile phone," *Wireless Information Technology and Systems (ICWITS), 2010 IEEE International Conference on* , pp.1-4, Aug. 28 2010-Sept. 3 2010

[56] Wei-Yu Li; Wei-Ji Chen; , "Concurrent 2-port/3-port MIMO antenna system for UMTS/LTE2500 operation in the mobile phone," *Antennas and Propagation (APSURSI), 2011 IEEE International Symposium on* , pp.1918-1921, 3-8 July 2011

[57] Cheng Yang, Yuan Yao, Junsheng Yu, and Xiaodong Chen, “Novel Compact Multiband MIMO Antenna for Mobile Terminal,” International Journal of Antennas and Propagation, Article ID 691681, 9 pages, 2012

[58] MinSeok Han; Jaehoon Choi; , "Compact multiband MIMO antenna for next generation USB dongle application," *Antennas and Propagation Society International Symposium (APSURSI), 2010 IEEE* , pp.1-4, 11-17 July 2010

[59] Qinghao Zeng, Yuan Yao, Shaohua Liu, Junsheng Yu, Peng Xie, and Xiaodong Chen, “Tetraband Small-Size Printed Strip MIMO Antenna for Mobile Handset Application,” International Journal of Antennas and Propagation, Article ID 320582, 8 pages, 2012

[60] Neyestanak, A.; Danideh, A.; Sadeghifakhr, R.; , "Compact size microstrip array MIMO antenna operable in multiband," *Communications, 2008 24th Biennial Symposium on* , pp.158-161, 24-26 June 2008

[61] Boyle, K.R.; Massey, P.J.; , "Nine-band antenna system for mobile phones," *Electronics Letters* , vol.42, no.5, pp. 265- 266, 2 March 2006

[62] Yimin Zhao; Yuanpeng Li; , "A novel multi-band smart antenna with compact size for mobile phones," *Electrical and Control Engineering (ICECE), 2011 International Conference on* , pp.1917-1919, 16-18 Sept. 2011

[63] Xing Zhao; Youngki Lee; Jaehoon Choi, "Design of a compact planar MIMO antenna for LTE mobile application," Antennas and Propagation (ISAP), 2012 International Symposium on , pp.1365,1368, Oct. 29 2012-Nov. 2 2012

[64] Singh, H.S.; Bharti, P.K.; Pandey, G.K.; Meshram, M.K., "A compact tri-band MIMO/diversity antenna for mobile handsets," *Electronics, Computing and Communication Technologies (CONECCT), 2013 IEEE International Conference on* , pp.1,6, 17-19 Jan. 2013

[65] Yu-Jiun Ren, "Ceramic Based Small LTE MIMO Handset Antenna," *Antennas and Propagation, IEEE Transactions on* , vol.61, no.2, pp.934,938, Feb. 2013

[66] Ahmed, F.; Feng, Y.; Li, R.; "Dual Wide-Band Four-unit MIMO Antenna System for 4G/LTE and WLAN Mobile Phone Applications," In proceedings, Loughborough Antennas & Propagation Conference, Nov. 2013

[67] Kyungseok Kahng; Inkyu Yang; Sungtek Kahng; Anguera, J.; Ju Yong Lee, "Design of four MIMO handset antennas," *Antennas and Propagation (EuCAP), 2013 7th European Conference on* , pp.723,725, 8-12 April 2013

[68] Di Wu; Cheung, S.W.; Yuk, T.I.; Liu, L., "Design of a printed multiband MIMO antenna," *Antennas and Propagation (EuCAP), 2013 7th European Conference on* , pp.2020,2023, 8-12 April 2013

[69] Panagamuwa, C.J.; Chauraya, A.; Vardaxoglou, J.C., "Frequency and beam reconfigurable antenna using photoconducting switches," *Antennas and Propagation, IEEE Transactions on* , vol.54, no.2, pp.449,454, Feb. 2006

[70] Park, Y. K.; Sung, Y., "A Reconfigurable Antenna for Quad-Band Mobile Handset Applications," *Antennas and Propagation, IEEE Transactions on* , vol.60, no.6, pp.3003,3006, June 2012

[71] Lee, J. H.; Sung, Y., "A reconfigurable PIFA using a PIN-diode for LTE/GSM850/ GSM900/ DCS/PCS/UMTS," *Antennas and Propagation Society International Symposium (APSURSI), 2012 IEEE* , pp.1,2, 8-14 July 2012

[72] Aykut, C.; Ferrero, F.; Cyril, L.; Gilles, J.; Larique, E.; Robin, R.; Patrice, B.; "Tunable Antennas Using MEMS switches for LTE Mobile Terminals," In proceedings, Loughborough Antennas & Propagation Conference, Nov. 2013

[73] Lee, S.W.; Sung, Y.; Park, J.Y.; Lee, S.J.; Hur, B.J., "Frequency reconfigurable antenna using a PIN diode for mobile handset application," Antennas and Propagation (EuCAP), 2013 7th European Conference on , pp.2053,2054, 8-12 April 2013

[74] Yu-Jiun Ren, "Ceramic Based Small LTE MIMO Handset Antenna," Antennas and Propagation, IEEE Transactions on , vol.61, no.2, pp.934,938, Feb. 2013

[75] Kumar Kishor, K.; Hum, S.V., "A Pattern Reconfigurable Chassis-Mode MIMO Antenna," Antennas and Propagation, IEEE Transactions on , vol.62, no.6, pp.3290,3298, June 2014

[76] Changyong Rhee; Yongjin Kim; Taejoon Park; Sung-su Kwoun; Byeonggwi Mun; Byungje Lee; Changwon Jung, "Pattern-Reconfigurable MIMO Antenna for High Isolation and Low Correlation," Antennas and Wireless Propagation Letters, IEEE , vol.13, pp.1373,1376, 2014

[77] Yan Wang; Zhengwei Du, "A Wideband Quad-Antenna System for Mobile Terminals," Antennas and Wireless Propagation Letters, IEEE , vol.13, pp.1521,1524, 2014

[78] Shuai Zhang; Kun Zhao; Zhinong Ying; Sailing He, "Investigation of Diagonal Antenna-Chassis Mode in Mobile Terminal LTE MIMO Antennas for Bandwidth Enhancement," Antennas and Propagation Magazine, IEEE , vol.57, no.2, pp.217,228, April 2015

[79] J. Desjardins, D. McNamara, S. Thirakoune, and A. Petosa, “Electronically frequency-reconfigurable rectangular dielectric resonator antennas,” IEEE Trans. Antennas Propag., vol. 60, no. 6, pp. 2997-3002, 2012

[80] M. Zamudio, Y. Tawk, J. Costantine, J. Kim, and C. Christodoulou,”Integrated cognitive radio antenna using reconfigurable band pass filters,” in Proc. 5th Eur. Conf. Antennas and Propag. (EUCAP), Apr. 2011, pp. 2108-2112

[81] H. AbuTarboush, R. Nilavalan, S. W. Cheung, K. Nasr, T. Peter, D. Budimir, and H. Al-Raweshidy, “A reconfigurable wideband and multiband antenna using dual-patch

elements for compact wireless devices," IEEE Trans. Antennas Propag., vol. 60, no. 1, pp. 36-43, Jan. 2012

[82] L. Pringle, P. Harms, S. Blalock, G. Kiesel, E. Kuster, P. Friederich, R. Prado, J. Morris, and G. Smith, "A reconfigurable aperture antenna based on switched links between electrically small metallic patches," IEEE Trans. Antennas Propag., vol. 52, no. 6, pp. 1434-1445, 2004

[83] E. Erdil, K. Topalli, M. Unlu, O. Civi, and T. Akin, "Frequency tunable microstrip patch antenna using rf MEMS technology," IEEE Trans. Antennas Propag., vol. 55, no. 4, pp. 1193-1196, Apr. 2007

[84] N. Behdad and K. Sarabandi, "A varactor-tuned dual-band slot antenna," IEEE Trans. Antennas Propag., vol. 54, no. 2, pp. 401-408, Feb. 2006

[85] C. Panagamuwa, A. Chauraya, and J. Vardaxoglou, "Frequency and beam reconfigurable antenna using photoconducting switches," IEEE Trans. Antennas Propag., vol. 54, no. 2, pp. 449-454, Feb. 2006

[86] Y. Tawk, J. Costantine, and C. Christodoulou, "A frequency reconfigurable rotatable microstrip antenna design," in Antennas and Propagation Society International Symposium (APSURSI), 2010 IEEE, pp. 1-4, 2010

[87] L. Liu and R. Langley, "Liquid crystal tunable microstrip patch antenna," Electron. Lett., vol. 44, no. 20, pp. 1179-1180, 2008

[88] D. Pozar and V. Sanchez, "Magnetic tuning of a microstrip antenna on a ferrite substrate," Electron. Lett., vol. 24, no. 12, pp. 729-731, 1988

[89] A. M. Yadav, C. Panagamuwa, and R. Seager, "Investigating the effects of control lines on a frequency reconfigurable patch antenna," in Antennas and Propagation Conference (LAPC), 2010 Loughborough, pp. 605-608, 2010

[90] R. Haupt and M. Lanagan, "Reconfigurable antennas," IEEE Antennas Propag. Mag., vol. 55, no. 1, pp. 49-61, 2013

CHAPTER 4
MIMO ANTENNAS FOR MOBILE HANDSETS

This chapter will present three new MIMO multiband antenna designs for mobile handsets. The antennas are designed to cover 2G, 3G and 4G cellular frequency bands. Simulation and measurement results are given along with a comprehensive simulation analysis of each design.

4.1 Quad-band MIMO multi-branch monopole antennas

Motivated by the features of the multiband and MIMO antennas discussed in Chapter 3, a multiband antenna for mobile handsets is designed in a MIMO configuration. The antenna covers four different frequency bands thereby providing coverage for most of the cellular services. The antenna is primarily designed as single element configuration in [1] by Jie Ma et. al. and is a miniature printed monopole on an FR-4 substrate as shown in Figure 4.1.

The antenna is quad band, covering the GSM 850/900, GSM 1800/1900, UMTS, WLAN and WiMAX frequency bands. In this chapter the design proposed in [1] is remodeled in a 2-element MIMO configuration on the top layer of a FR-4 substrate of thickness 0.8 mm. In addition, a decoupling structure is designed on the bottom layer of the substrate to achieve an acceptable isolation performance. The following sections will present the design of the MIMO antennas and a discussion of the simulation and measurement results.

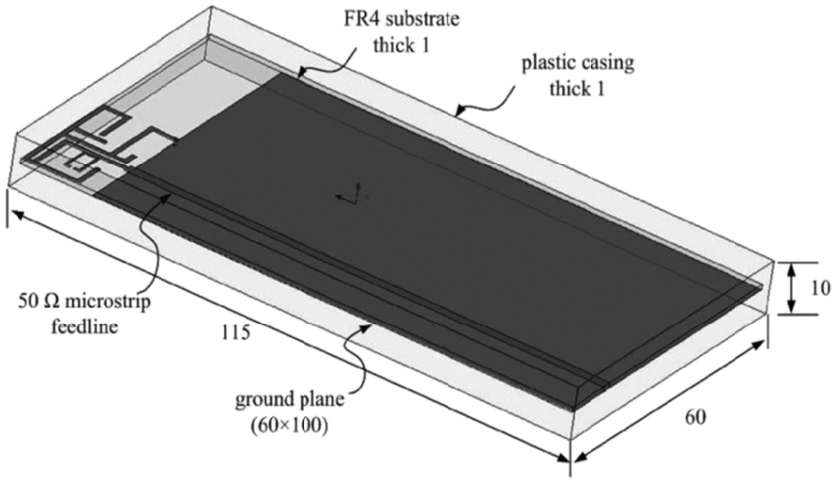

Figure 4.1: Miniature Printed Octa-band Monopole Antenna for Mobile Phones [1].

4.1.1 Antenna Design:

The antenna was designed and optimized in MIMO configuration through simulations in CST® Microwave Studio [2]. Figure 4.2 shows the simulation model and geometry of the multiband MIMO antennas for mobile handsets. The detailed dimensions of the antennas are presented in Figure 4.3.

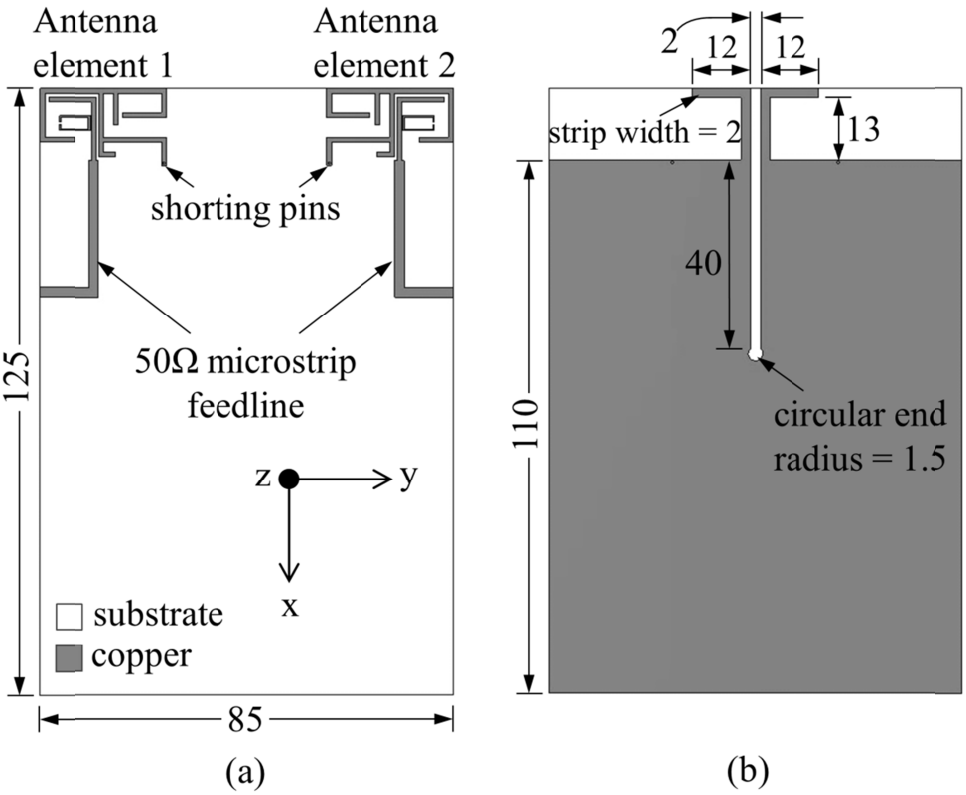

Figure 4.2: Simulated model of the quad-band MIMO multi-branch monopole antennas. (a): Top layer. (b): Bottom layer. [Units: mm]

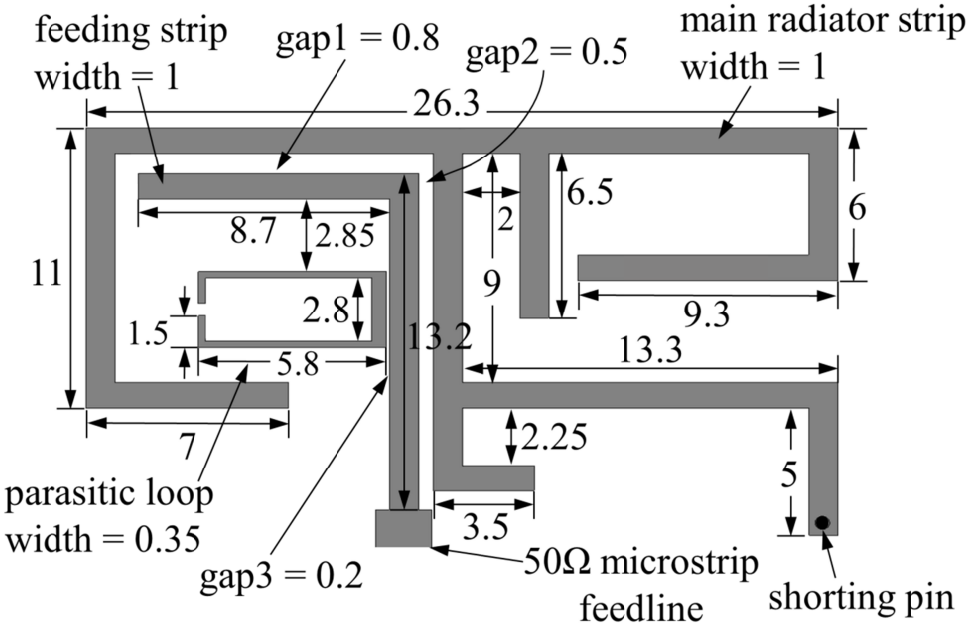

Figure 4.3: Detailed dimensions of each antenna of the MIMO configuration. [Units: mm]

The top layer of the substrate is composed of two MIMO antennas arranged in mirror configuration at the no-ground portion. Each antenna is a coupled feed monopole based on multi-branch configuration. The gaps between the feed line and the antenna and the width of the feed line have been selected through simulations in CST® Microwave Studio to achieve an optimum impedance bandwidth. The bottom layer of the substrate is composed of the ground plane and the decoupling structure for reducing the coupling between the two antennas. The decoupling structure consists of two inverted L-shaped ground branches that extend into the no-ground portion on the bottom layer of the substrate. The Width of the inverted L-shaped ground branches is 2 mm. A slot of length 42 mm and width 2 mm is also cut in to the ground plane for achieving a better decoupling between the antennas. For further enhancement of isolation, a circular slot is added at the end of the ground slot. The diameter of the circular slot is 3 mm. The decoupling structure thus improves the isolation performance of the MIMO antennas especially at the lower frequency. The length and depth of the ground slot, the radius of the circular slot and the length of the inverted L-shaped branches have been optimized to achieve an optimum decoupling between the MIMO antennas. The substrate material used in the design is FR-4 with relative permittivity of 4.3 – 4.4 and loss tangent of 0.02. The overall volume of the substrate board is 125 x 85 x 0.8 mm^3 with each antenna occupying an area of 26.3 x 16 mm^2. The edge to edge separation between the two antennas is 32.4 mm. A prototype of MIMO antennas has been developed and shown in Figure 4.4. For the measurements

of the S-parameters, the antennas were connected to an Agilent® Technologies 2-port network analyzer placed in the antenna laboratory at Queen Mary, University of London (QMUL). The radiation pattern and gain measurements were performed inside anechoic chamber set up at QMUL. It is anticipated that there will be some discrepancies in the experimental results due to the fabrication imperfections and the measurement setup.

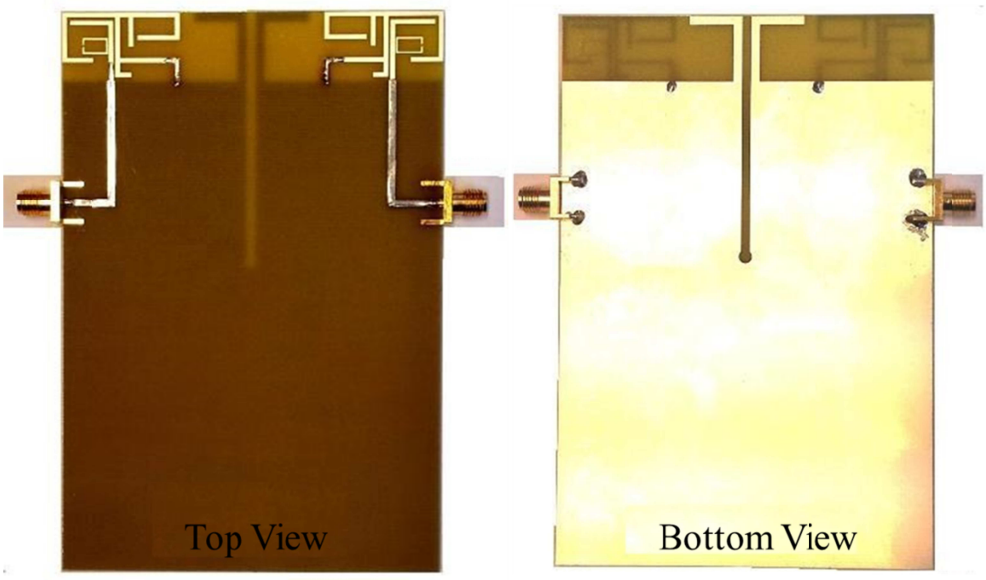

Figure 4.4: Fabricated prototype of the quad-band MIMO multi-branch monopole antennas.

4.1.2 Working Mechanism:

Each antenna of the MIMO configuration is composed of various lengths of monopole strips that are connected to have resonance at different frequencies. The surface current distribution provides the information about different parts of the antenna radiating relative to the frequency. It can be seen from the surface current distribution in Figure 4.5 that at 900 MHz the strip lengths 'a-b-d-e' and some parts of strips 'b-c' and 'd-g' are radiating. The combined length thus calculated is 76 mm which is nearly 0.25λ at 900 MHz. Likewise, at 2.1 GHz the strip lengths that are radiating are 'd-e-f', 'd-g' and some part of 'd-b'. The combined length thus obtained is 34 mm which is 0.25λ at 2.1 GHz. The part of the strip length 'b-d-e' radiating at 3.5 GHz is 23 mm which is close to 0.25λ. For the radiation at 5.4 GHz, a strip length 'o-x' is introduced that is placed at a gap of 0.2 mm from the feed line. The length of the strip 'o-x' is 13 mm which is near to 0.25λ at 5.4 GHz.

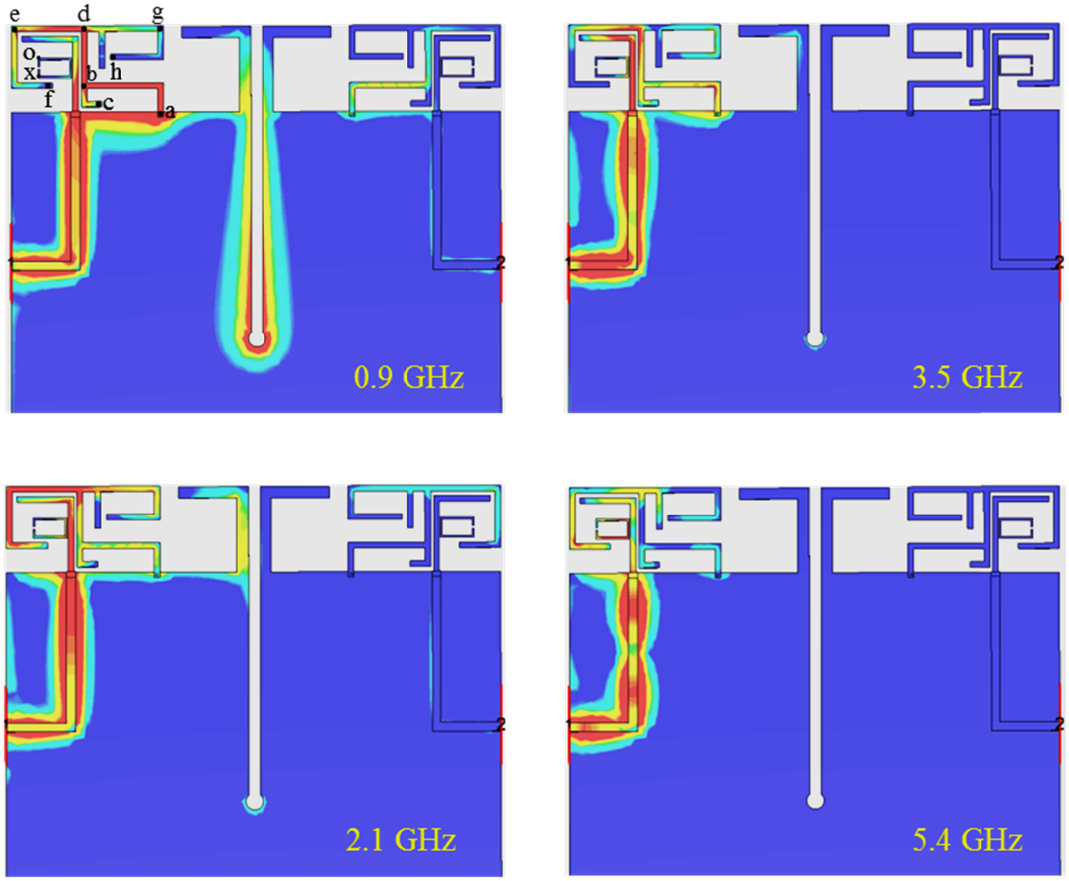

Figure 4.5: Surface current distributions of the quad-band MIMO multi-branch monopole antennas.

It can be seen that a minor current is propagating in the ground plane. If the current is large in the ground plane then it can be affected by the electronic components. So the decoupling technique should not introduce current in the ground plane. The decoupling technique used in this design includes a slot that cuts into the ground plane and inverted L-shaped metallic branches that extend from the ground plane into the no-ground part on the bottom layer of the substrate. The ground slot along with the inverted-L branches draws a large amount of current thereby restricting the flow of current from one port to the other. This largely improves the isolation performance of the MIMO antennas.

4.1.3 Parametric Study:

(a) Effect of Decoupling Structure:

A stepwise approach for modelling the proposed decoupling structure is shown in Figure 4.6. The effect of each part of the decoupling structure on the S-parameters is

plotted in Figures 4.7 and 4.8. The decoupling structure has no significant impact on S_{11} and the 6 dB bandwidths almost stay the same as shown in Figure 4.7. However, it does impact significantly on $S_{21.}$ It can be seen from Figure 4.8 that the inverted L-shaped ground branches and the slot contribute to the improvement of isolation. Without any decoupling structure the isolation is poorer than 15 dB in the first two frequency bands. With the introduction of the simple slot in the ground plane the isolation is slightly improved but it is still poorer and below 15 dB. If the slot is removed and only the L-shaped ground branches are added, the isolation in the first band is slightly improved while it becomes better than 15 dB in the second band. In order to improve isolation at the lower frequency band, a slot is introduced along with the L-shaped ground branches which significantly improve the isolation in both the first and second frequency bands. For further improvement of isolation, a circular slot is added at the end of the main slot and that makes the isolation better than 15 dB over all the frequency bandwidths covered by the MIMO antennas.

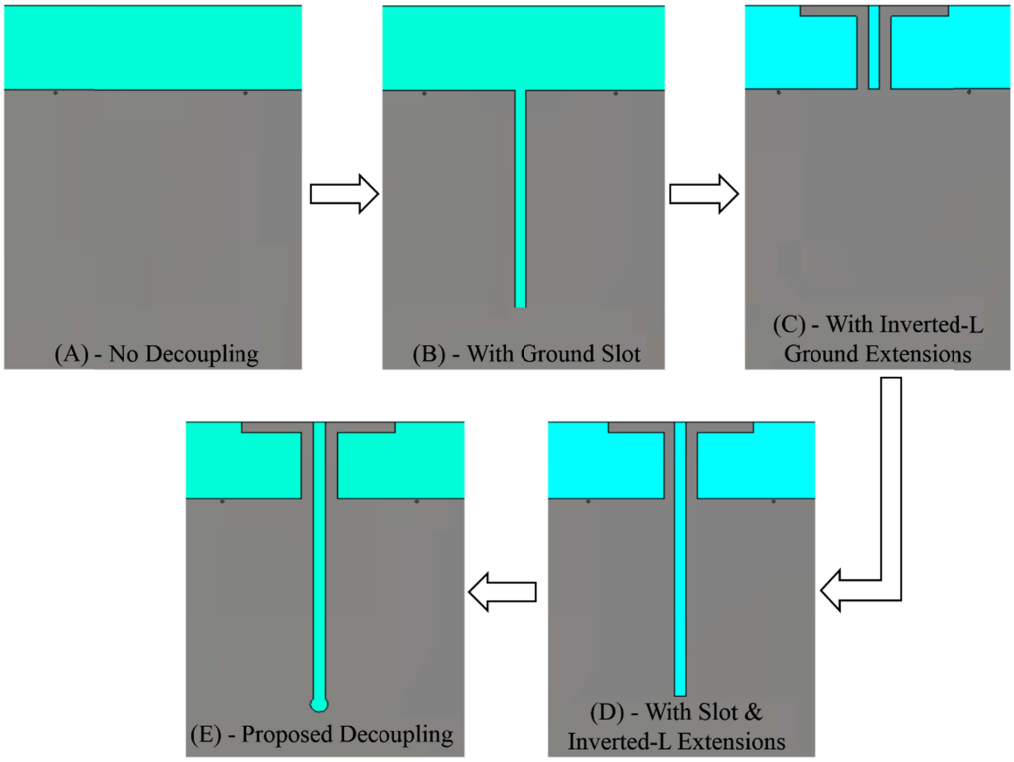

Figure 4.6: A stepwise approach for achieving the proposed decoupling structure.

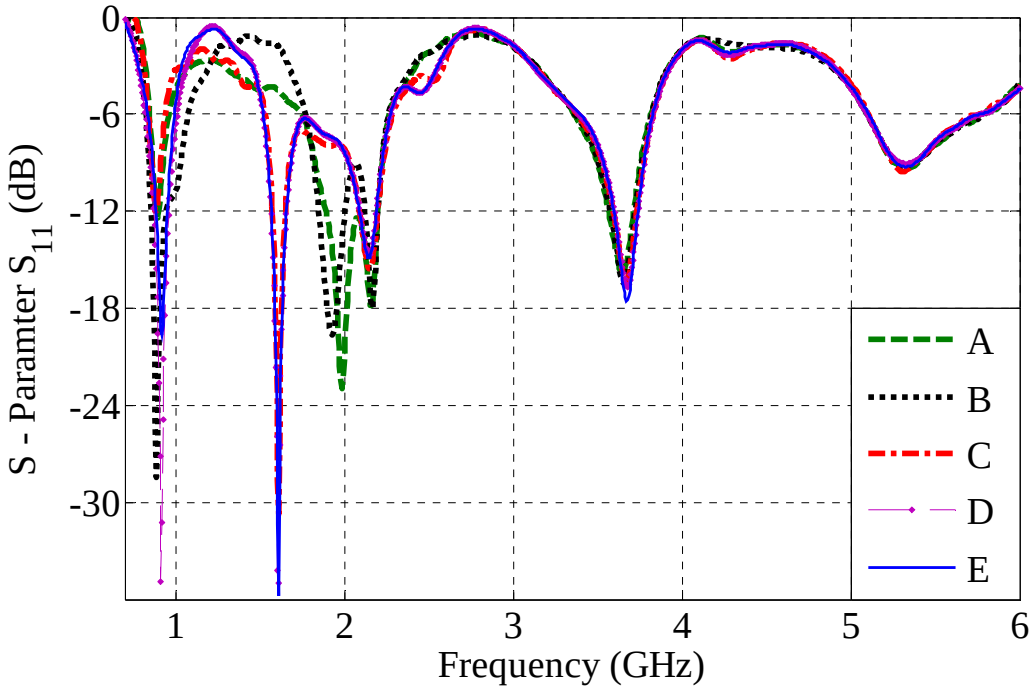

Figure 4.7: Effect of decoupling structure on the S-parameters (S_{11}) of the quad-band MIMO multi-branch monopole antennas.

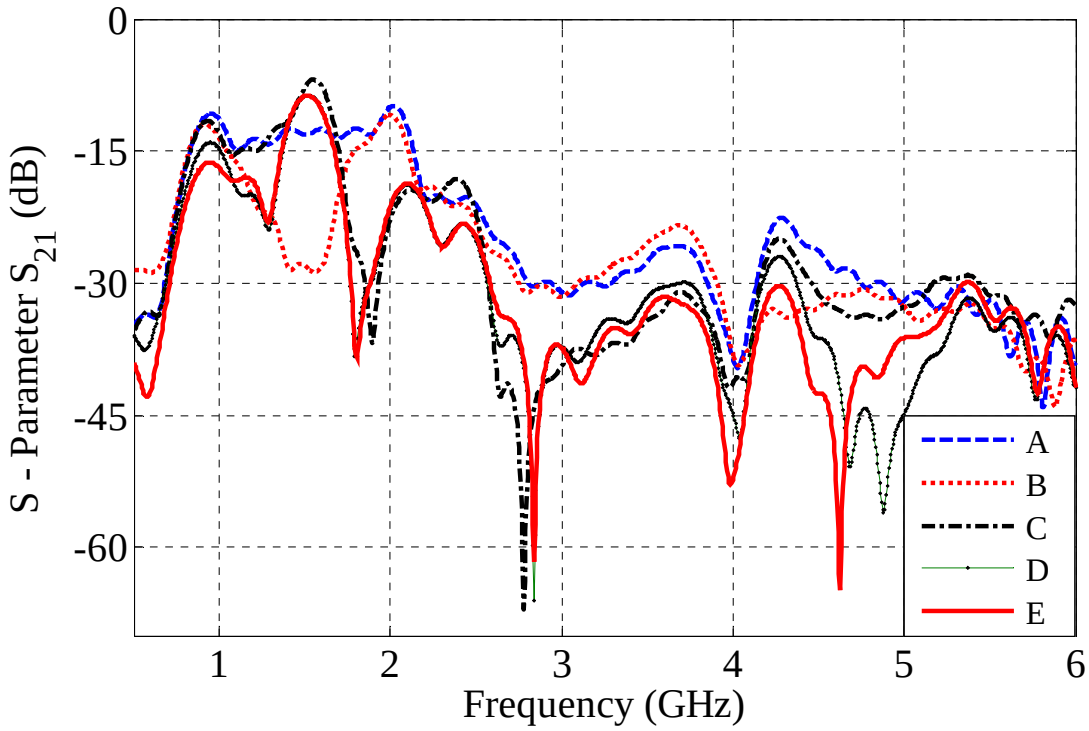

Figure 4.8: Effect of decoupling structure on the S-parameters (S_{21}) of the quad-band MIMO multi-branch monopole antennas.

The effect of the decoupling structure on the gain and efficiency of quad-band MIMO multi-branch monopole antennas can be visualized by looking at the simulated values mentioned in Table 4.1. It can be seen that the gains and efficiencies of the proposed

MIMO antennas remain acceptable. The decoupling structure reflects the radiation patterns of the MIMO antennas without majorly affecting their radiation characteristics. This results in highly de-correlated radiation patterns thus improving the isolation performance.

Table 4.1: Effect of decoupling structure on the gains
and efficiencies of the quad-band MIMO multi-branch monopole antennas.

Freq. (GHz)	**Simulated Efficiency (% age)**		**Simulated Gain (dBi)**	
	With Decoupling	**Without Decoupling**	**With Decoupling**	**Without Decoupling**
0.90	82.4	74.9	1.80	1.27
2.10	82.9	72.5	3.51	2.08
3.50	69.4	82.3	4.43	5.35
5.40	61.8	72.1	2.79	3.04

(b) Parametric Analysis on the length of the ground slot:

A parametric analysis of the antenna was performed on the length of the ground slot etched on the bottom layer of the substrate. The length of the slot in the proposed design is 40 mm. A parametric analysis was performed by varying the length from 30 mm to 50 mm and the effect is plotted in terms of the S-parameters of the MIMO antennas. The effect of varying slot length on S_{11} is shown in Figure 4.9, whereas, the effect of the change in length on the isolation performance of the MIMO antennas is shown in Figure 4.10.

From Figure 4.9, it is seen that there is no noticeable change in 6 dB bandwidth of the MIMO antennas when the slot length is varied from 30 mm to 50 mm. However, by changing the slot length, the isolation between the antennas is largely improved as shown in Figure 4.10. The isolation is poorer than 15 dB at slot lengths of 30 mm to 35 mm and it is better than 15 dB at the slot lengths of 40 mm to 50 mm. A slot length of 40 mm is selected to achieve an optimum combination of isolation and return loss.

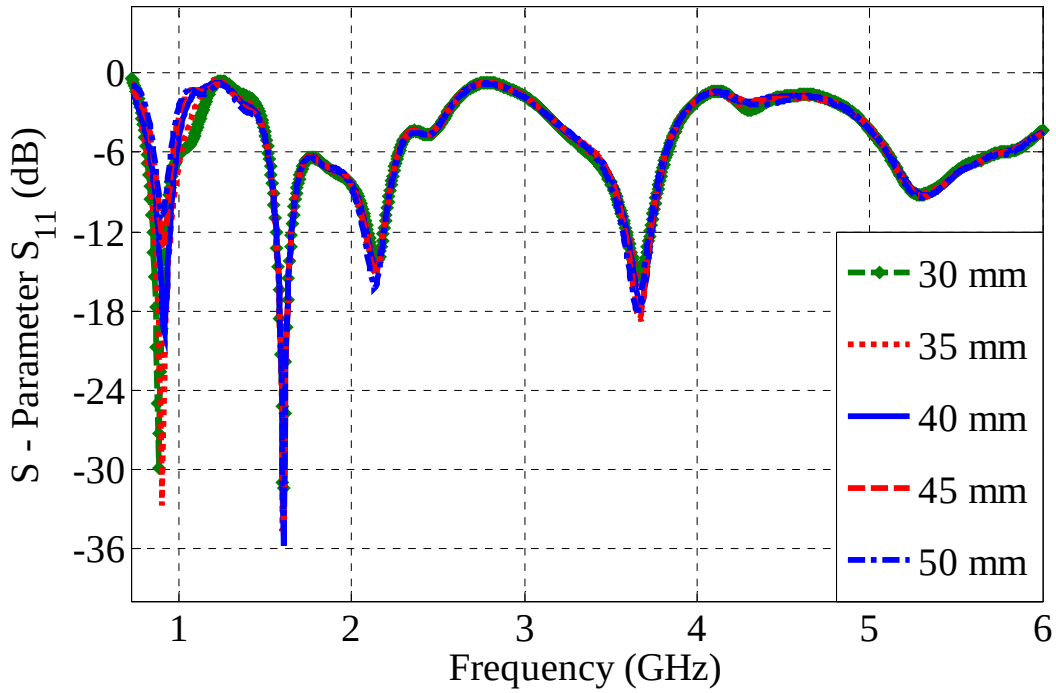

Figure 4.9: Effect of changing the slot length on the s-parameters (S_{11}) of the quad-band MIMO multi-branch monopole Antennas.

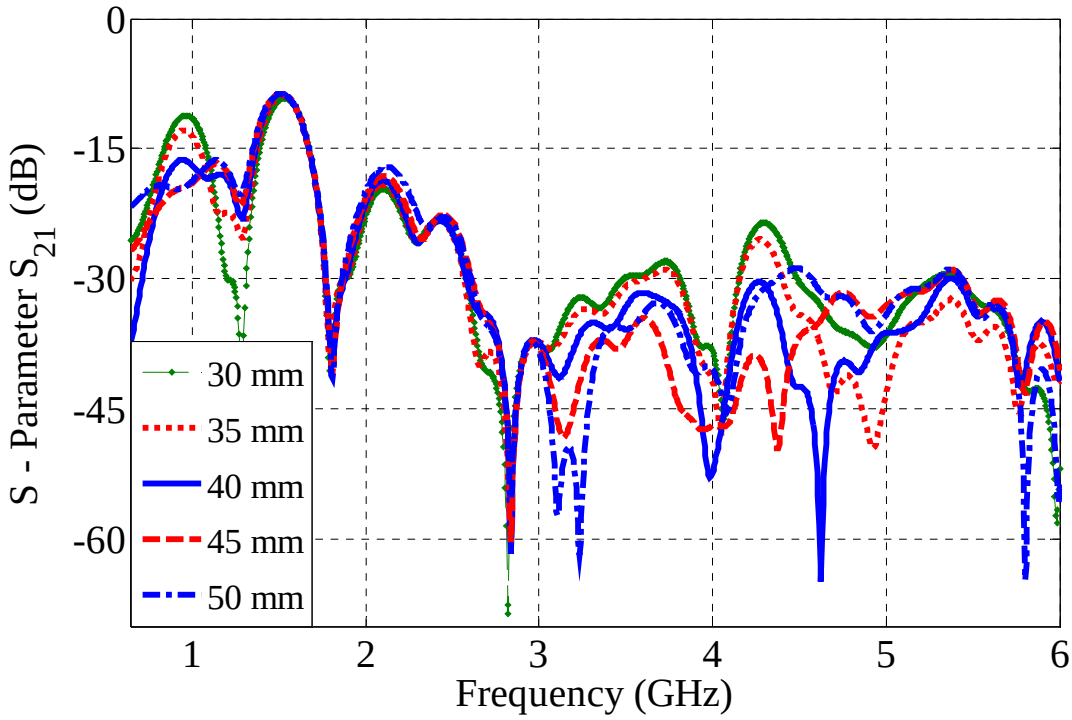

Figure 4.10: Effect of changing the slot length on the s-parameters (S_{21}) of the quad-band MIMO multi-branch monopole Antennas.

4.1.4 Simulation and Experimental Results:

This section presents the simulation and experimental results with the aid of comparison and analysis.

(a) S – Parameters:

The S-parameter curves of the MIMO antennas are shown in Figures 4.11 and 4.12. The S-parameters of only one antenna are shown as both are identical. It can be seen from Figure 4.11 that each MIMO antenna is radiating in four different frequency bands when referenced to a return loss of 6 dB. The first band ranges from 835 MHz to 961 MHz covering the 2G GSM 850/900, 3G HSDPA 800/850/900 and 4G LTE bands 5, 8, 19 with a resonance at 911 MHz. The second band ranges from 1656 MHz to 2272 MHz covering the 2G GSM 1800/1900, 3G HSDPA 1700/1900/2100 and 4G LTE bands 1-4, 25, 30 and WLAN 802.11 b/g/n. The third band ranges from 3346 MHz to 3816 MHz covering WiMAX 3.4 GHz and WLAN 802.11y. Likewise, the fourth band is between 5099 MHz and 5796 MHz covering WLAN 802.11 a/n. The antennas cover most of the cellular bands in the range of 0.8 GHz – 6.0 GHz. The frequency of each cellular service is given in appendix I.

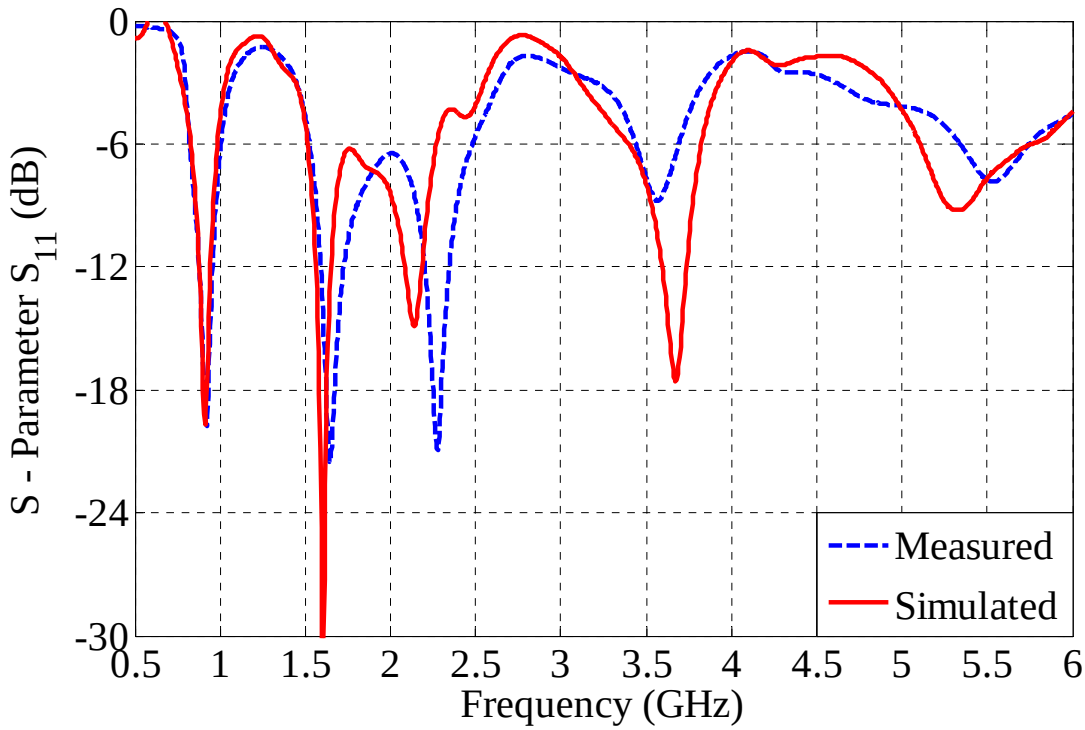

Figure 4.11: S-parameters (S_{11}) of the quad-band MIMO multi-branch monopole antennas.

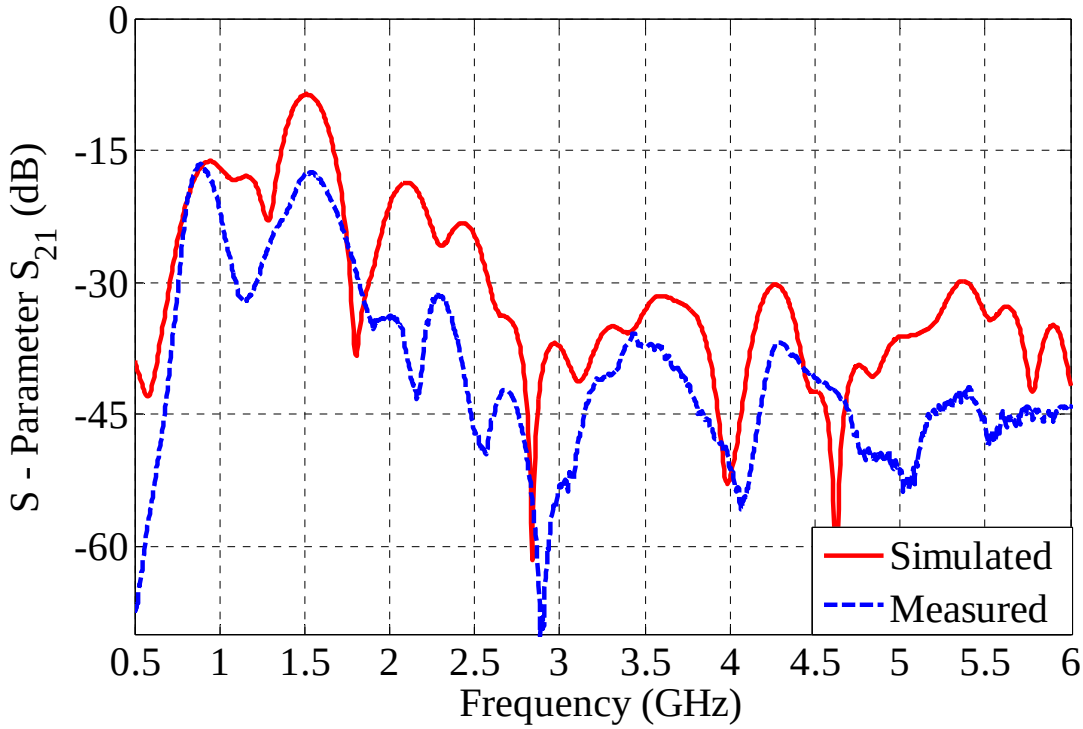

Figure 4.12: S-parameters (S_{21}) of the quad-band MIMO multi-branch monopole antennas.

The simulated S-parameters of the quad-band MIMO multi-branch monopole antennas show good agreement with the measurements. However a minor shift of frequency has been observed in the measurement results which mainly occurred due to the fabrication imperfections and the tolerances in the substrate dielectric properties.

The decoupling structure between the two antennas results in a good isolation in both simulation and measurements. The S_{21} curves shown in Figure 4.12 depict that the isolation between the MIMO antennas is better than 15 dB over all the frequency bands. A further analysis of the decoupling structure will be included in a later section.

(b) Radiation Patterns:

The simulated 3D radiation patterns of the quad-band MIMO multi-branch monopole antennas are obtained by simulating the model in CST® Microwave studio. Figure 4.13 shows the 3D radiation patterns at different frequencies.

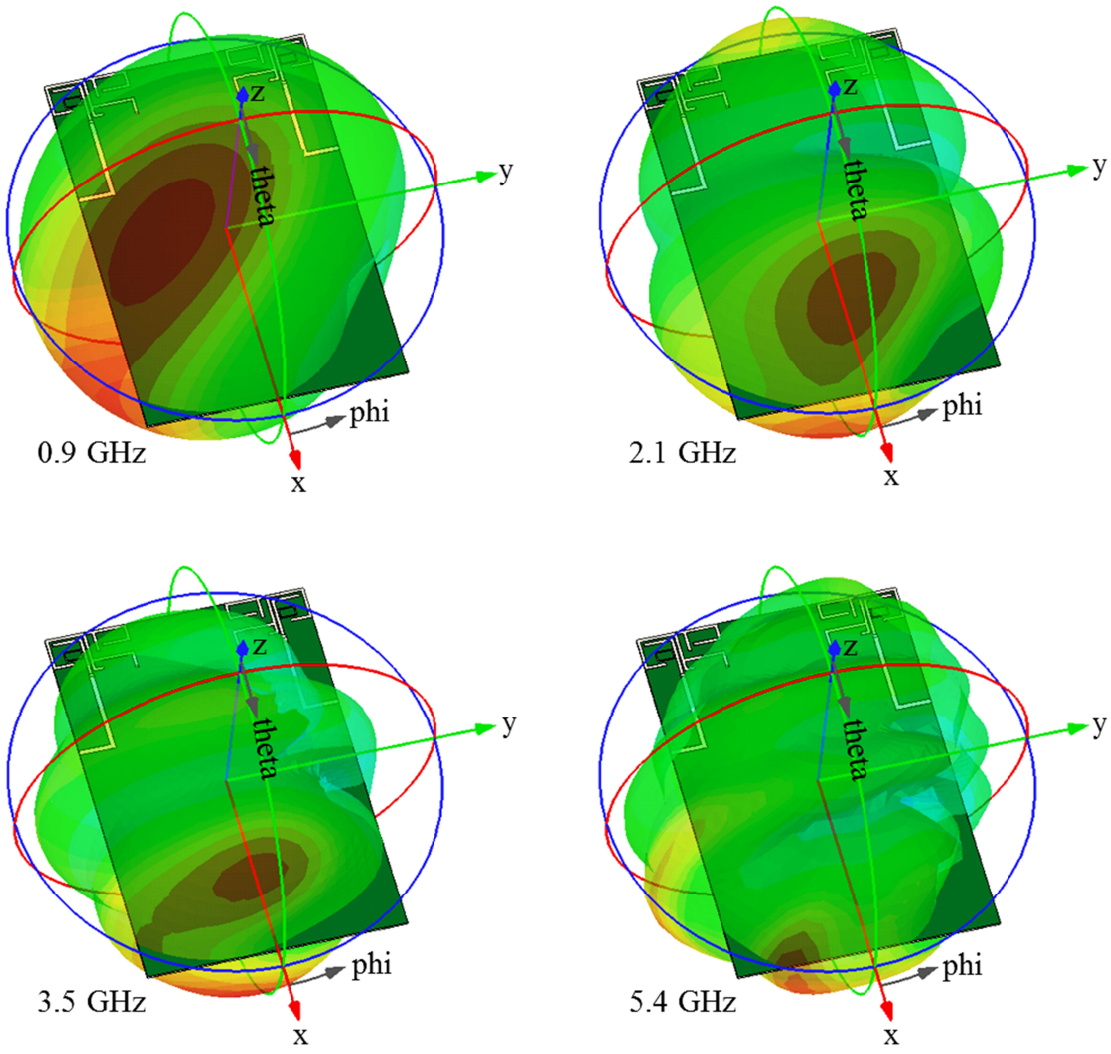

Figure 4.13: Simulated 3D Radiation patterns of the quad-band MIMO multi-branch monopole antennas.

For the measurement of the radiation patterns, the antennas were placed inside the anechoic chamber at QMUL. The co-polar (*phi*) and cross-polar (*theta*) components of the radiation patterns are plotted in both x-z and y-z planes at the resonant frequencies of the MIMO antennas. Figure 4.14 presents the polar plots comparing simulated co-polar (*phi*) and cross-polar (*theta*) radiation patterns with measurement in both x-z and y-z planes. The radiation pattern measurements of only one antenna have been performed while match terminating the other port with a 50Ω load. This is because the two antennas are identical. The simulated and measured radiation patterns strongly agree with only minor discrepancies which may have occurred due to the imperfections in the fabrication and the measurement setup.

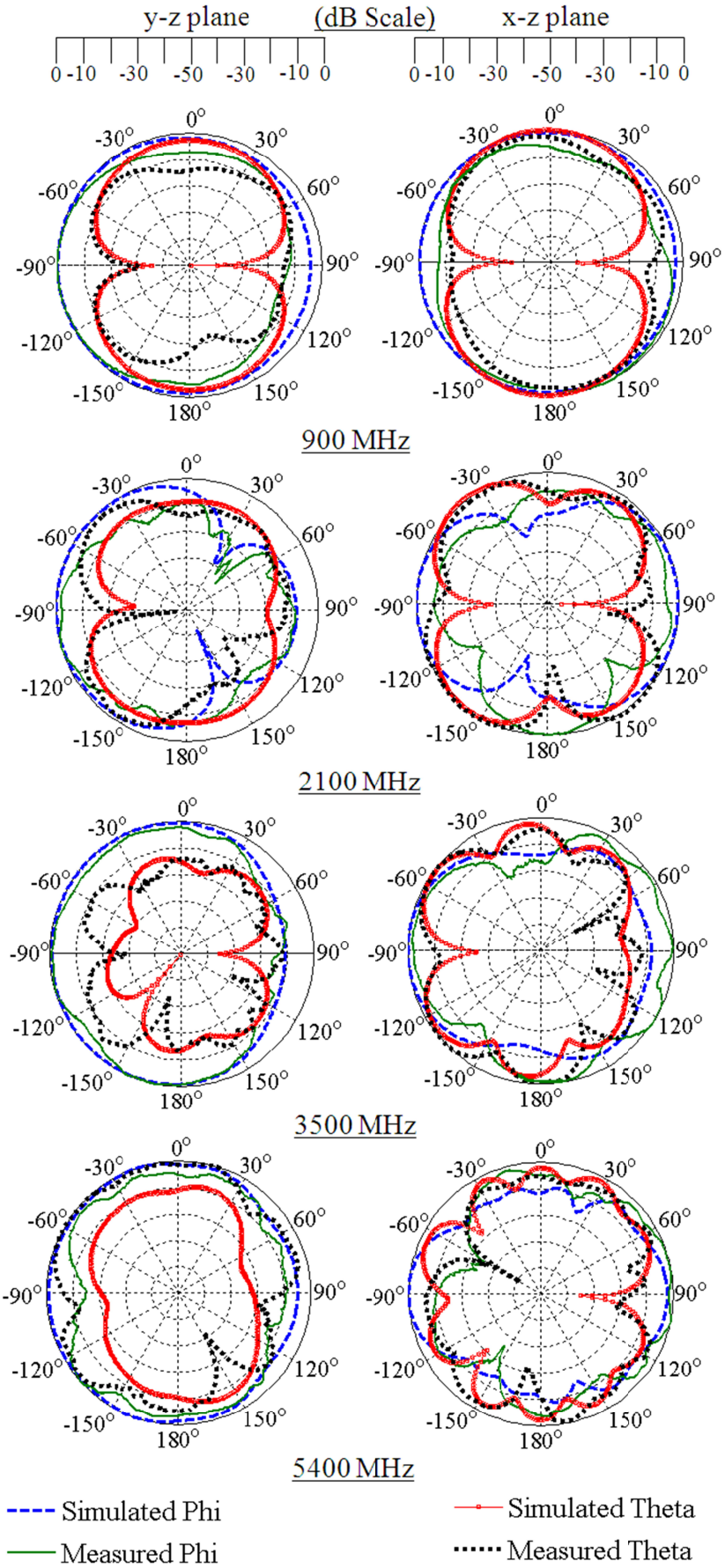

Figure 4.14: Polar plots of the normalized radiation patterns of the quad-band MIMO multi-branch monopole antennas.

(c) Gains of the quad-band MIMO multi-branch monopole antennas:

The simulated gains of the multi-branch MIMO antennas were obtained from CST® Microwave studio, whereas, the measured gains were evaluated by the gain comparison method using a standard gain antenna (SGA) and the antenna under test (AUT) [3]. The gain of the AUT can then be calculated from:

$$Gain_{AUT}\,(dBi) = Gain_{SGA}\,(dBi) + 10log\frac{P_1}{P_2} \qquad (4.1)$$

where, P_1 is the power received by the antenna under test and P_2 is the power received by the standard gain antenna. The simulated and measured gains of the MIMO antennas at different frequencies are presented in Table 4.2 and show a good agreement. However, a slight variation in the simulated and experimental values of the gains exists due to the possible fabrication imperfections.

Table 4.2: Gains of the quad-band MIMO multi-branch monopole antennas

Frequency	**Gain (dBi)**	
	Simulated	**Measured**
0.90 GHz	1.80	1.70
2.10 GHz	3.51	2.10
3.50 GHz	4.43	3.20
5.40 GHz	2.79	1.63

(d) Efficiencies of the MIMO antennas:

The simulated efficiencies of the multi-branch MIMO antennas were extracted from the simulations in CST® Microwave studio. The measured efficiency at different frequencies is evaluated using the Wheeler Cap method [4] which was initially developed by H.A. Wheeler in 1959 who utilized the concept of a radiansphere for the measurement of the radiation efficiency. The radiansphere is the boundary between the near field and the far field. The wheeler cap method was performed by taking two measurements, one with the antenna under test inside the cap, and the other with the antenna in free space. In each case the input impedance of the antenna was measured and efficiency was calculated by:

$$Efficiency\,(\eta) = \frac{R_1 - R_2}{R_1} \qquad (4.2)$$

where, R_1 is the real part of the input impedance without the cap and R_2 is the real part of the input impedance of the antenna inside the cap. The distance of the antenna from each wall of the cap should be at least $\lambda/2\pi$. The size of the cap used in the experiment is 30 x 50 cm^2. A photograph of the measurement setup made at QMUL is shown in Figure 4.15.

The simulated and measured efficiencies of the multi-branch MIMO antennas at different frequencies are shown in Table 4.3. The efficiency of only one antenna is calculated as both the antennas are identical. The simulated and experimental results show a reasonable agreement with some discrepancies mainly due to the fabrication imperfections and the measurement setup.

Figure 4.15: A photograph of the Wheeler Cap measurement setup for the evaluation of antenna efficiency.

Table 4.3: Efficiencies of the quad-band MIMO multi-branch monopole antennas.

Frequency	**Total Efficiency (%age)**	
	Simulated	**Measured**
0.90 GHz	82.4	76.3
2.10 GHz	82.9	73.1
3.50 GHz	69.4	63.2
5.40 GHz	61.8	55.3

(e) Diversity Analysis:

MIMO improves channel capacity due to the presence of more than one transmission path [5]. Ideally the capacity of a MIMO system increases linearly as the number of antenna elements increases. However, in practical environments it is degraded by the presence of possible coupling between the multiple antennas and also by the nature of the propagation environment [6]-[8]. In order to analyze the diversity performance of the MIMO antennas, the envelope correlation coefficients and the diversity gains were calculated.

Envelope Correlation Coefficient – In MIMO, the parameter which shows the effect of different paths through which waves reach the multiple antennas is the Envelope Correlation Coefficient that is symbolically represented as 'ρ_e'. The value of ρ_e varies between '0' and '1' with a perfect performance at $\rho_e = 0$.

There are two different ways to evaluate the correlation between MIMO antennas. One way is to evaluate ρ_e using the far-field radiation patterns [8], [11]. This method is accurate but it involves complex calculations and is very time consuming [9]-[10]. The equation for the calculation of the envelope correlation coefficient using the far-field radiation pattern is:

$$\rho_e = \frac{\left| \iint_{4\pi} \left[\overrightarrow{F_1}(\theta,\varphi) \bullet \overrightarrow{F_2}^*(\theta,\varphi) \right] d\Omega \right|^2}{\iint_{4\pi} \left| \overrightarrow{F_1}(\theta,\varphi) \right|^2 d\Omega \iint_{4\pi} \left| \overrightarrow{F_2}(\theta,\varphi) \right|^2 d\Omega} \tag{4.3}$$

where $F_i(\theta,\varphi)$ is the far-field radiation pattern with only port 1 excited while match terminating all the other ports with a 50Ω load. The '•' operator in the equation is the Hermitian Product.

A comparatively simpler method for the evaluation of correlation coefficient is by using the S-parameters of the MIMO antennas. The equation by which ρ_e is evaluated using the S-parameters is given as [8]:

$$\rho_e = \frac{|S^*_{11}S_{12} + S^*_{21}S_{22}|^2}{(1 - |S_{11}|^2 - |S_{21}|^2)(1 - |S_{22}|^2 - |S_{12}|^2)} \tag{4.4}$$

The '*' operator in the equation (4.4) represents the complex conjugate. It can be seen that (4.4) is much simpler compared to (4.3) and it involves less calculation. Also, (4.4) provides sufficiently accurate results especially when dealing with rich multipath indoor environments.

The calculated envelope correlation coefficients are shown in Table 4.4. The values are calculated using both the radiation patterns and the S-parameters in order to check the reliability of the S-parameters method. The peak value of the measurement based envelope correlation coefficient over all the frequency bands is observed to be 0.0184, which is well below the acceptable value of 0.7 [12]-[13].

Table 4.4: ρ_e values of the quad-band MIMO multi-branch monopole antennas.

Band	**Peak Envelope Correlation Coefficient (ρ_e)**		
	Using Radiation Pattern	**Using S-parameter**	
	Simulated	**Simulated**	**Measured**
I	0.0186	0.0206	0.0184
II	0.0253	0.0092	0.0008
III	0.0005	0.0003	0.0003
IV	0.0012	0.0006	0.0001

Diversity Gain – MIMO utilizes several diversity techniques. The main concept behind the diversity is that each receiver antenna is able to receive multiple replicas of the transmitted signal. Each replica is received through a different path within the same frequency channel. So a combined received signal will have a higher signal to noise ratio (SNR) as compared to that of the individual received signal. This improvement in the SNR is known as the diversity gain. Diversity gain largely depends on the coupling between MIMO antennas. A better decoupling results in a good diversity gain and vice versa. The diversity gain of two antennas in MIMO should be 10 dB or better and three antennas should be at least 15 dB to give transmission reliability of 99% [14]. To obtain a considerably good or near to ideal value of diversity gain, the correlation between antennas should be very low and ideally zero. According to the research work done by Saunders, the maximum permissible value of correlation should be less than 0.7 so that there is no more than 3 dB loss in the diversity gain [12]-[14].

An approximation of the diversity gain can be obtained by using the envelope correlation coefficient as:

$$G_{Div\,(app)} = G_{Div\,(Max)} * DF \tag{4.5}$$

where, $G_{DIV\,(app)}$ is the apparent value of the diversity gain obtained by multiplying the maximum theoretical value ($G_{DIV\,(Max)}$) of diversity gain by the degradation factor (*DF*). The theoretical values of the diversity gains can be obtained from the plots shown in Figure 4.16 which are based on the equations mentioned in [12] and [14]. The term $P_r\,(\gamma < \gamma_s)$ represents the probability of the instantaneous signal to noise ratio (γ) to fall below the given threshold (γ_s). A reliability of 99% can be represented by the P_r value of 0.01.

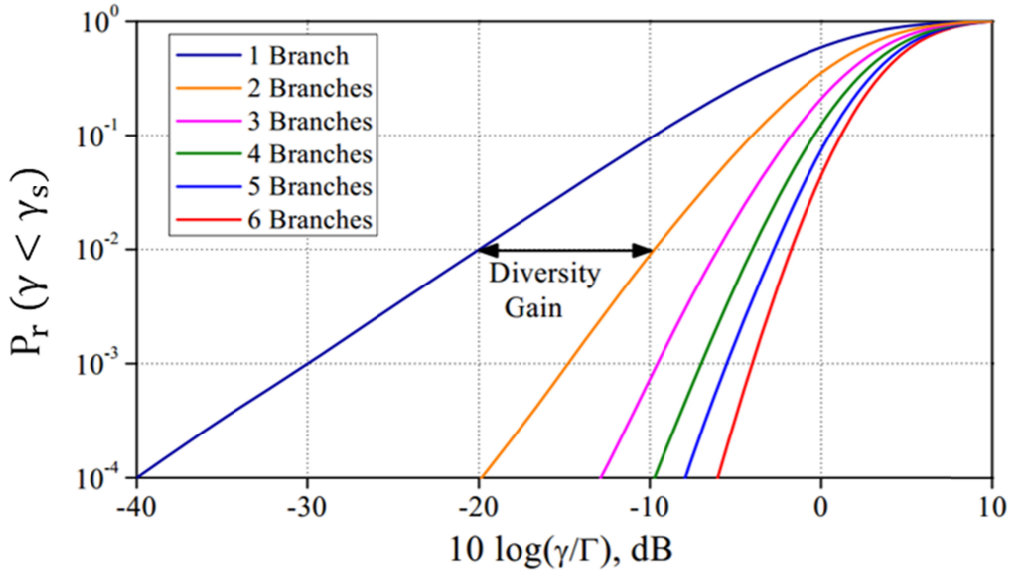

Figure 4.16: Cumulative distribution function of Rayleigh fading signals for the evaluation of the theoretical values of diversity gain.

The degradation factor (DF) can be calculated from the envelop correlation coefficient (ρ_e) by the following equation:

$$DF = \sqrt{1 - \rho_e} \tag{4.6}$$

The effective value of the diversity gain can be obtained by considering the radiation efficiency (η_r) of the antenna and can be expressed as [15]:

$$G_{Div\,(eff)} = G_{Div\,(app)} * \eta_r \tag{4.7}$$

CST® Microwave Studio provides a post processing toolbox for the calculation of the diversity gains. The values of the envelope correlation coefficients and the diversity gains are calculated in both indoor and outdoor environments by simulating the statistical models summarized in [14], [16]-[17]. The simulation parameters used in calculating the envelope correlation coefficients and the diversity gains are shown in Table 4.5, where 'm_v' is the mean elevation angle of the vertically polarized wave, 'm_h' is the mean elevation angle of the horizontally polarized wave, 'σ_v' is the standard deviation of the vertically polarized wave distribution, 'σ_h' is the standard deviation of the horizontally polarized wave distribution and '*XPR*' is the cross polarization ratio between average vertical and horizontal powers.

Table 4.5: Simulation parameters for calculation of the Envelope correlation coefficients and the Diversity gains [14].

Propagation environment	**Simulation parameter**	**Statistical model (Elevation/Azimuth)**	
		Gaussian/Uniform	*Laplacian/Uniform*
Indoor	m_v	10^o	10^o
	m_h	10^o	10^o
	σ_v	15^o	15^o
	σ_h	15^o	15^o
	XPR	5 dB	5 dB
Outdoor	m_v	20^o	20^o
	m_h	20^o	20^o
	σ_v	30^o	30^o
	σ_h	30^o	30^o
	XPR	1 dB	1 dB

The diversity gains mentioned in Table 4.6 are promising and represent a good diversity performance of the MIMO antennas. The values obtained for the quad-band MIMO multi-branch monopole antennas are less than 10 dB. This reduction in the diversity gain is mainly due to less radiation efficiency. The lowest value obtained for the diversity gain is 7.09 dB at 5.40 GHz at which the multi-branch MIMO antennas have lower efficiency as compared to the other frequencies.

Table 4.6: Diversity gains of the quad-band MIMO multi-branch monopole antennas.

Freq. (GHz)	**Envelope Correlation Coefficient**				**Efficiency**	**Effective Diversity Gain (dB)**	
	Indoor Environment		**Outdoor Environment**		η_r	**Indoor Environment**	**Outdoor Environment**
	ρ_e	DF	ρ_e	DF			
0.90	0.0055	0.997	0.0022	0.998	0.86	8.57	8.58
2.10	0.0022	0.999	0.0001	0.999	0.88	8.79	8.79
3.50	0.0004	0.999	0.0014	0.999	0.83	8.29	8.29
5.40	0.0018	0.999	0.0001	0.999	0.71	7.09	7.09

4.2 Wideband MIMO meandered monopole antennas

In this section, a new design of MIMO antennas for mobile handsets is introduced. The proposed antenna is a wideband meandered monopole with a small volume and is designed and optimized through simulations in CST® Microwave Studio. The antenna is modeled and simulated in both single antenna and MIMO configurations. Simulation and measurement results are also analyzed.

4.2.1 Single meandered monopole antenna design:

Figure 4.17 shows the simulated model of the multiband antenna for mobile handsets in single antenna configuration. The volume of the substrate board is 65 x 110 x 0.8 mm^3 with each antenna printed on a no-ground portion of 65 x 15 mm^2. The antenna occupies an area of 24 x 14.5 mm^2. The width of the copper strip is optimized through simulation. The feeding mechanism used is coupled feed with a coupling gap of 1.23 mm. The width of the feed line and the coupling gap have been selected through computer simulations to achieve an optimum impedance bandwidth. The antenna is thus a coupled feed monopole in meandered form and printed on the no-ground portion at the top layer of an FR-4 substrate with relative permittivity of 4.35 and a loss tangent of 0.02.

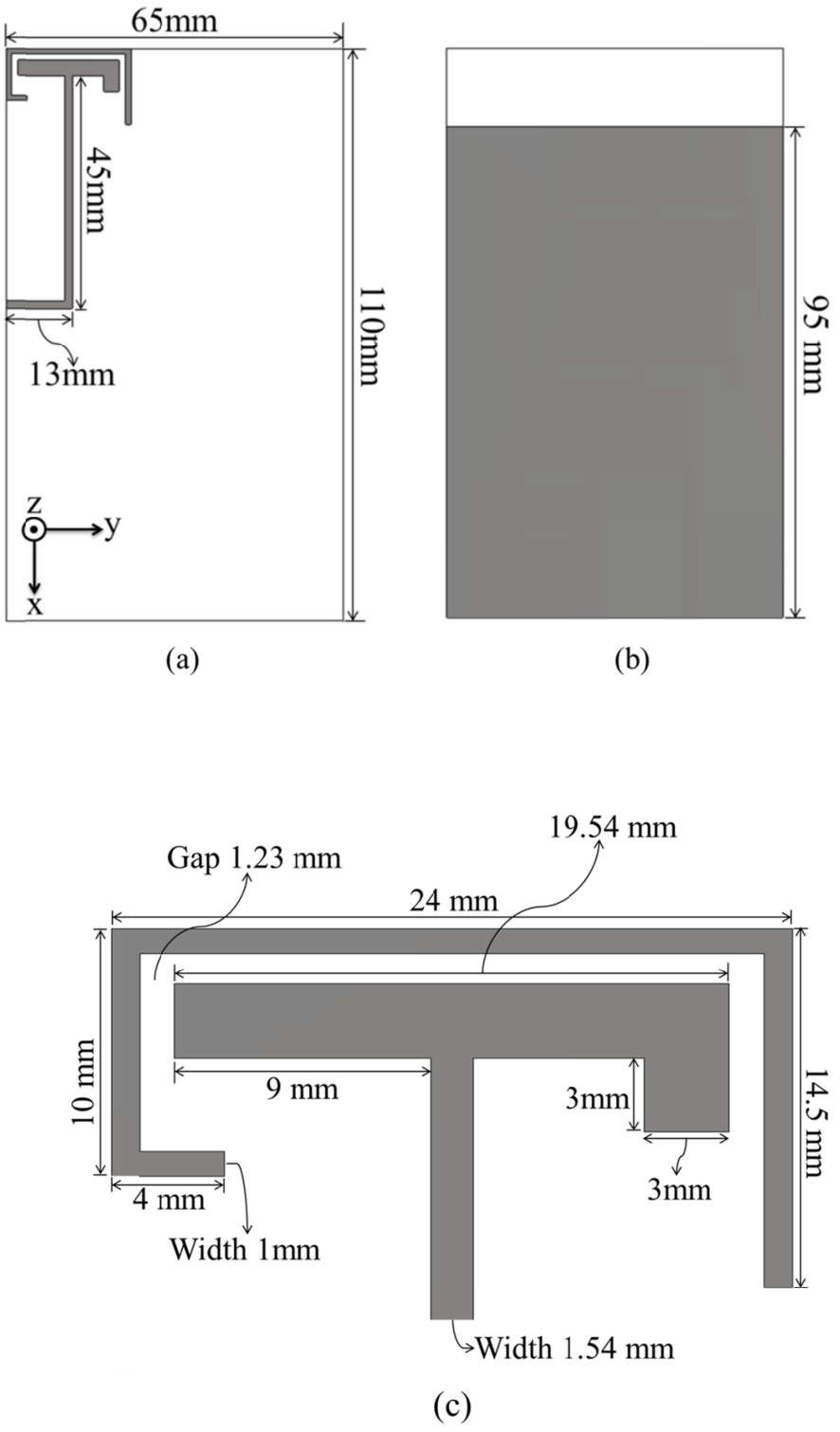

Figure 4.17: Simulated model of the wideband meandered monopole antenna. (a): Top layer. (b): Dimensions of the antenna. (c): Bottom layer.

4.2.2 Working mechanism:

The simulated surface current distributions of the meandered monopole antenna, at 2.05 GHz and 2.45 GHz, are shown in Figure 4.18. It can be seen from the surface current distributions that different portions of the meandered monopole strip are radiating at different frequencies. The total length of the monopole strip is 'A-B-C-D'. The surface current distributions of the antenna tell the information about which part of the antenna is radiating relative to the frequency. It can be seen that at 2.05 GHz the strip length 'B-C-D' is radiating. The combined length of the strip 'B-C-D' is 36.5 mm which is nearly 0.25λ at 2.05 GHz. Likewise, the strips lengths radiating at 2.45 GHz are partially 'A-B' and 'B-C'. The combined length thus obtained is 30 mm which is nearly 0.25λ at 2.45 GHz.

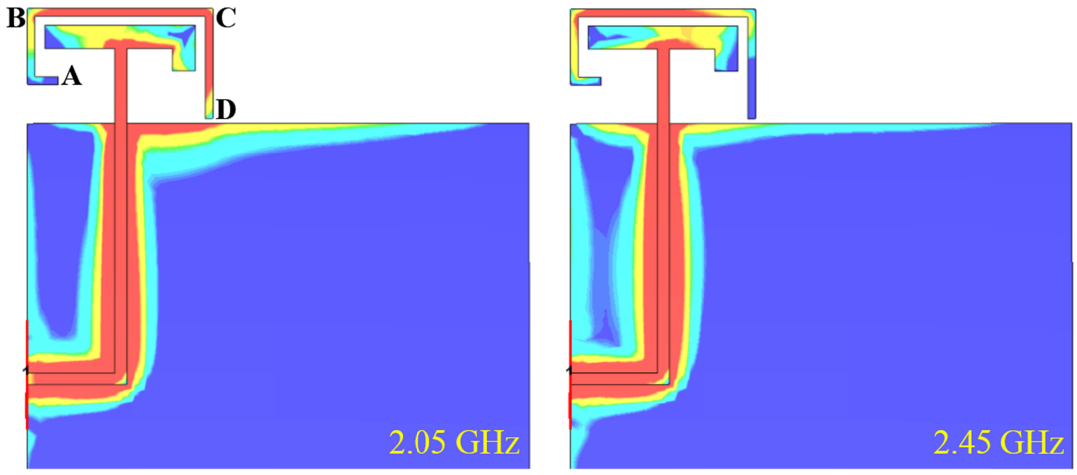

Figure 4.18: Surface current distributions of the wideband meandered monopole antenna at different frequencies.

4.2.3 Simulation Results:

The simulated S_{11} of the antenna is presented in Figure 4.19 which shows that the antenna resonates with a frequency bandwidth of 1.725 – 2.95 GHz, when referenced to a return loss of 6 dB. The antenna is thus capable of covering the 2G GSM 1800/1900, 3G HSDPA 1700/1900/2100, 4G LTE Bands 1-4, 7, 25, 30 (1710 – 2690 MHz) and WLAN 802.11 a/b/g/n 2.45 GHz.

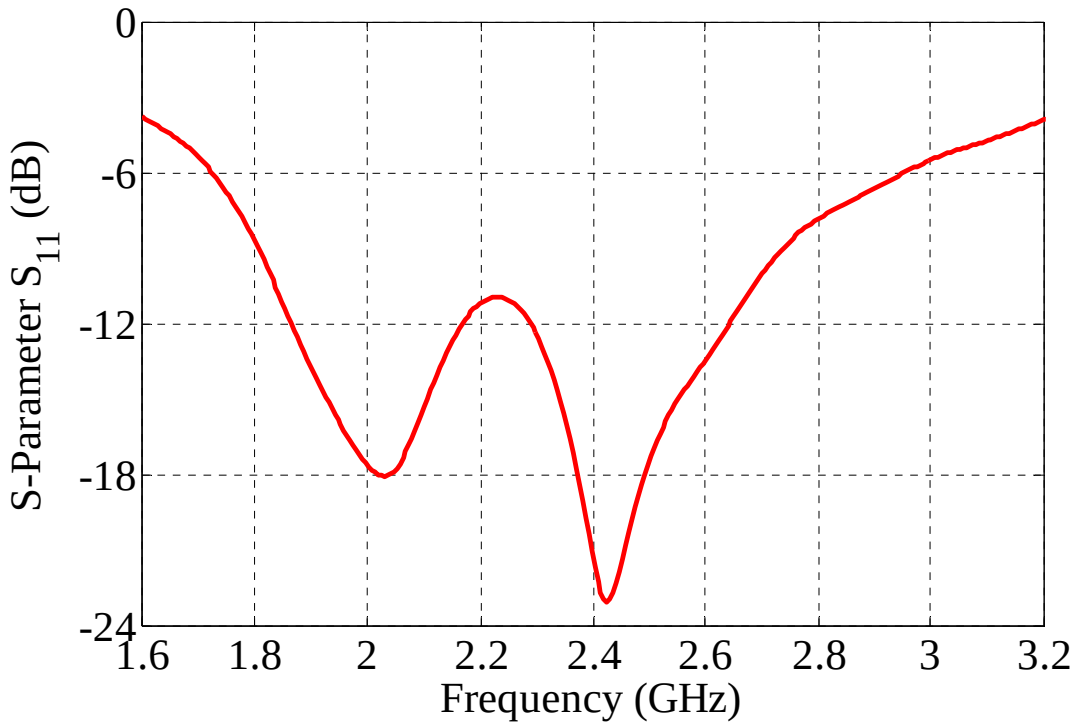

Figure 4.19: Simulated s-parameter of the handset antenna in single antenna configuration.

The antenna possesses a good return loss and covers most of the cellular frequency bands. The geometry of the single antenna configuration and its results make the design suitable for compact mobile handsets. The antenna was also modeled in MIMO configuration and an analysis of the simulation and measurement results is given.

4.2.4 MIMO meandered monopole antennas design:

The simulated model of the wideband meandered monopole antenna for mobile handsets in MIMO configuration is presented in Figure 4.20. The dimensions of the antennas are exactly the same as for the single antenna configuration discussed earlier. The top layer of the substrate is composed of two copies of the meandered monopole antenna arranged diagonally in mirrored configuration. The bottom layer is composed of a dual decoupling structure including inverted-L shaped ground branches that extend into the no-ground portion of the substrate. The width of each inverted-L branch is 2 mm. Two slots of length 20.5 mm and width 2 mm are also cut in the ground plane for achieving better decoupling. For further isolation

improvement, the decoupling structures were also placed diagonally on the bottom layer of the substrate.

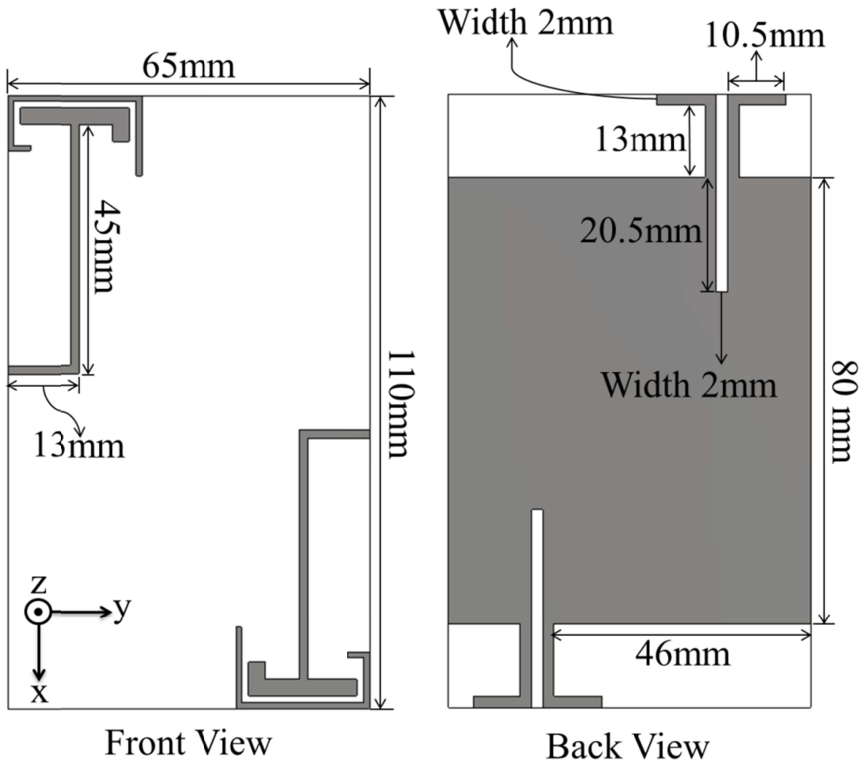

Figure 4.20: Simulated model of the wideband meandered MIMO monopole antennas.

The simulated model of the meandered MIMO monopole antennas was fabricated on FR-4 substrate with relative permittivity of 4.35 and the fabricated prototype is shown in Figure 4.21. For the S-parameter measurement, the antennas were connected to the Agilent® Technologies 2-port network analyzer placed in the antenna laboratory at QMUL. The radiation pattern, gain and efficiency measurements were taken inside anechoic chamber set up at QMUL.

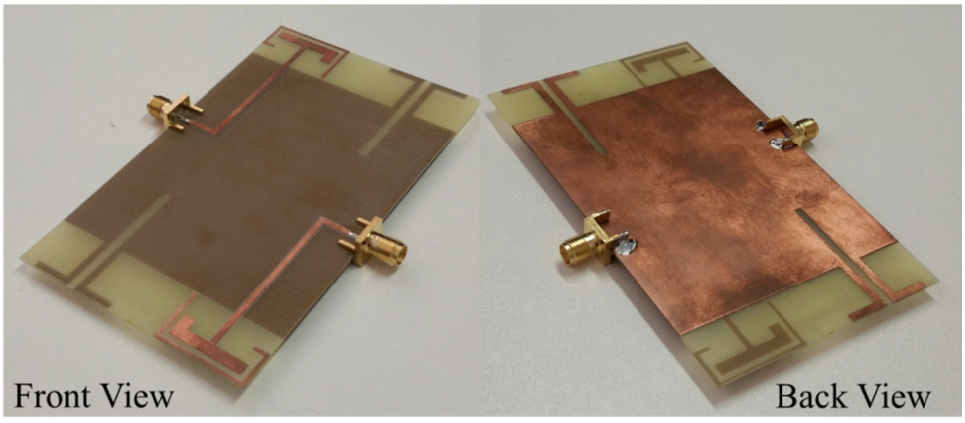

Figure 4.21: Fabricated Prototype of the wideband meandered MIMO monopole antennas.

4.2.5 Effect of decoupling structure:

Different configurations regarding the placement of the MIMO antennas and the arrangement of the decoupling structures are shown in Figure 4.22. These configurations represent the stepwise approach in the design of proposed decoupling structure for achieving an acceptable isolation between the antennas. The graph of S_{21} for each configuration is shown in Figure 4.23. The decoupling structure has no significant impact on S_{11}. However, it can be seen that the isolation performance of the MIMO antennas is best at the configuration 5 in which antennas are placed diagonally on the top layer while the decoupling structures are placed diagonally on the bottom layer of the substrate. All the other configurations result in a poor isolation between the MIMO antennas.

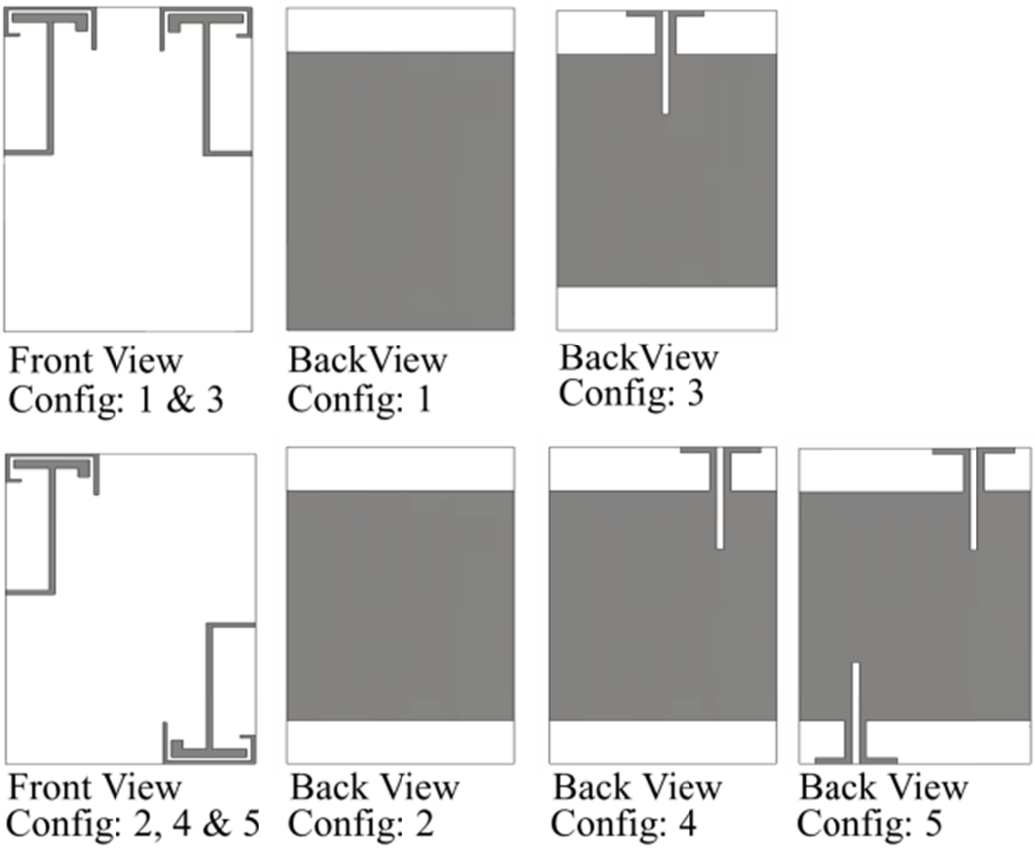

Figure 4.22: Different configurations of the wideband MIMO meandered monopole antennas and the decoupling structure.

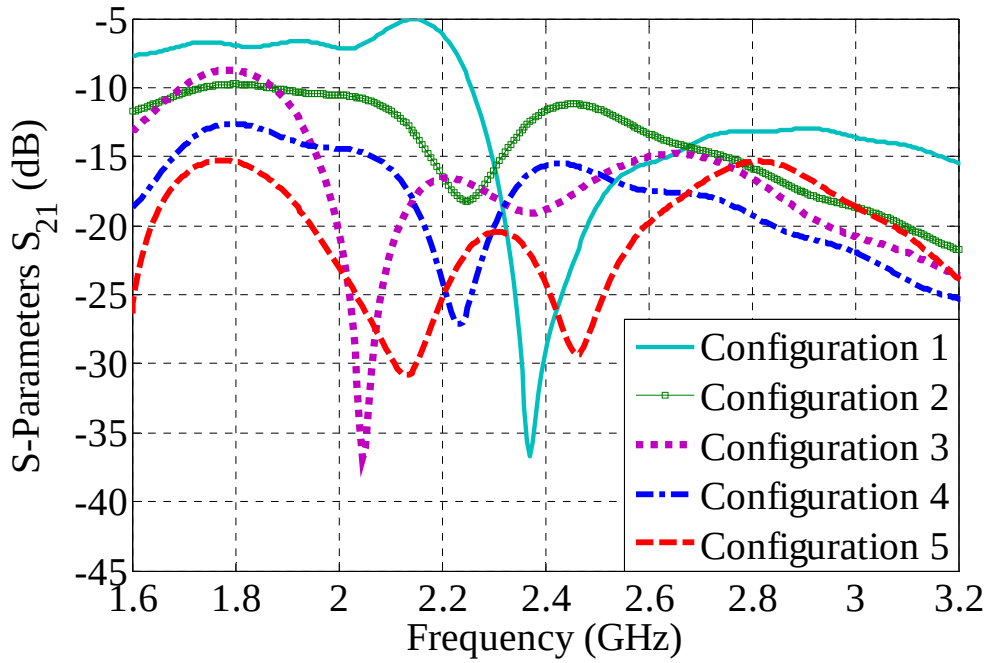

Figure 4.23: Effect of the decoupling structure on the isolation performance of the wideband MIMO meandered monopole antennas.

4.2.6 Simulation and measurement results:

(a) S – Parameters:

The simulated and measured S-parameters of the MIMO meandered monopole antennas are shown in Figure 4.24.

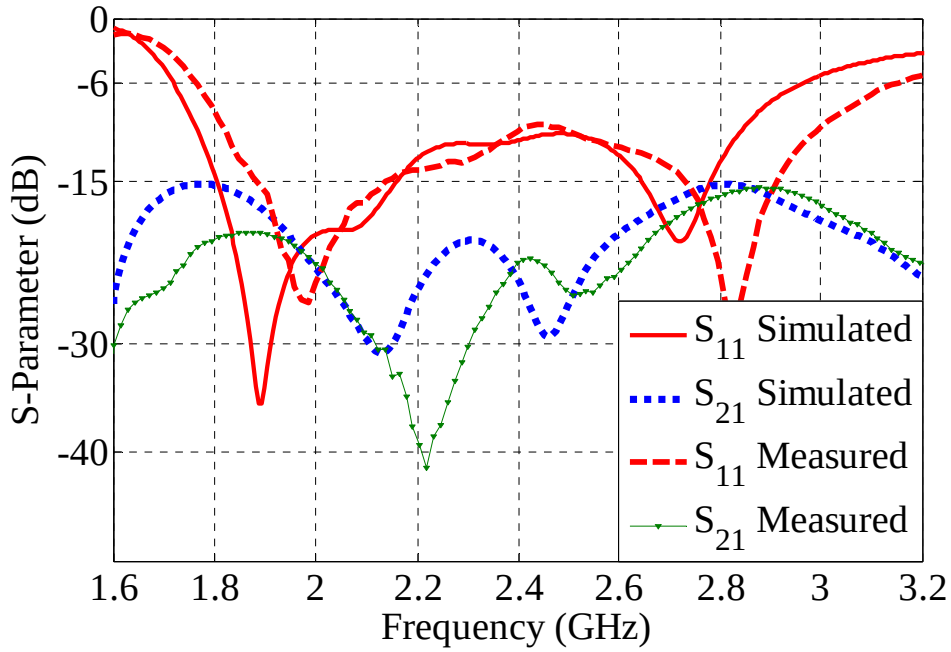

Figure 4.24: S-parameters of the wideband MIMO meandered monopole antennas for mobile handsets.

The simulated S-parameters of the MIMO antennas show a good agreement with measurement. It can be seen that the antenna is resonating with a bandwidth of 1.7-3.2 GHz when referenced to a return loss of 6 dB. The results of the MIMO antennas are nearly same as those of the single antenna configuration. The isolation between the antennas as shown in Figure 4.24 is better than 15 dB which means that the two antennas are radiating independently with acceptably low interference to each other. Each antenna is thus capable of covering the 2G GSM 1800/1900, 3G HSDPA 1700/1900/2100, 4G LTE Bands 1-4, 7, 25, 30 (1710 – 2690 MHz) and WLAN 802.11 a/b/g/n 2.45 GHz.

(b) Radiation patterns:

The simulated antenna radiation patterns are obtained from CST® Microwave studio, whereas, the radiation patterns were measured in the anechoic chamber at QMUL. The co-polar (*phi*) and cross-polar (*theta*) components of the radiation pattern were plotted in both x-z and y-z planes at four different frequencies. Figure 4.25 presents the polar plots comparing simulated radiation patterns with the measured ones.

(c) Current distributions:

The current distribution of the MIMO antennas presented in Figure 4.26 shows that very small amplitude of current is propagating in the ground plane which makes it unlikely to change the radiation properties of the antennas. Also when the antennas will be deployed in a mobile housing with electronic components on board, the operating characteristics such as return loss and bandwidth are anticipated to be unaffected. The decoupling technique used in the design includes the extended ground branches which trap a large amount of current thereby restricting the current from one antenna to the other. Also the ground slots further improve the isolation at all the frequencies covered by the antennas.

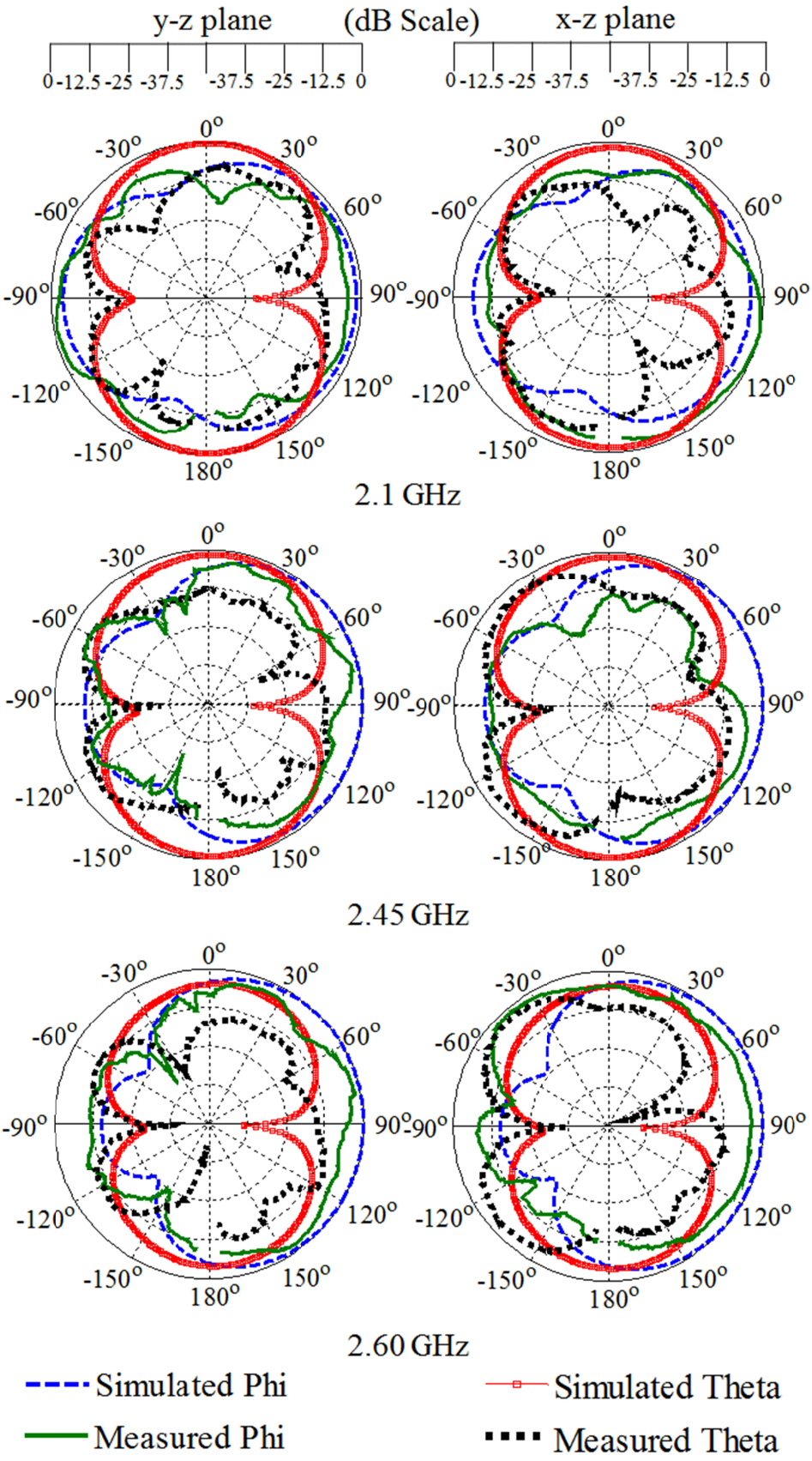

Figure 4.25: Radiation patterns of the wideband MIMO meandered monopole antennas at different frequencies.

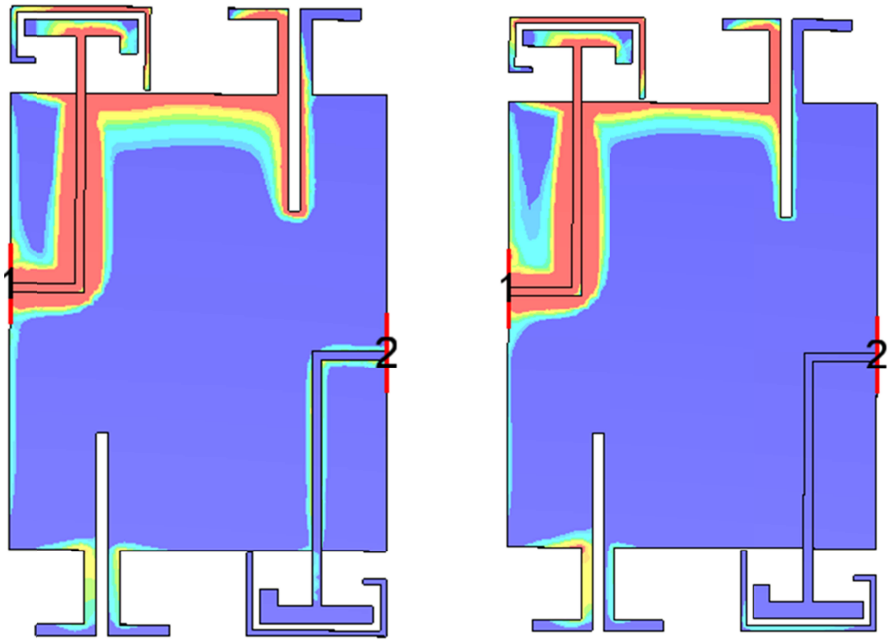

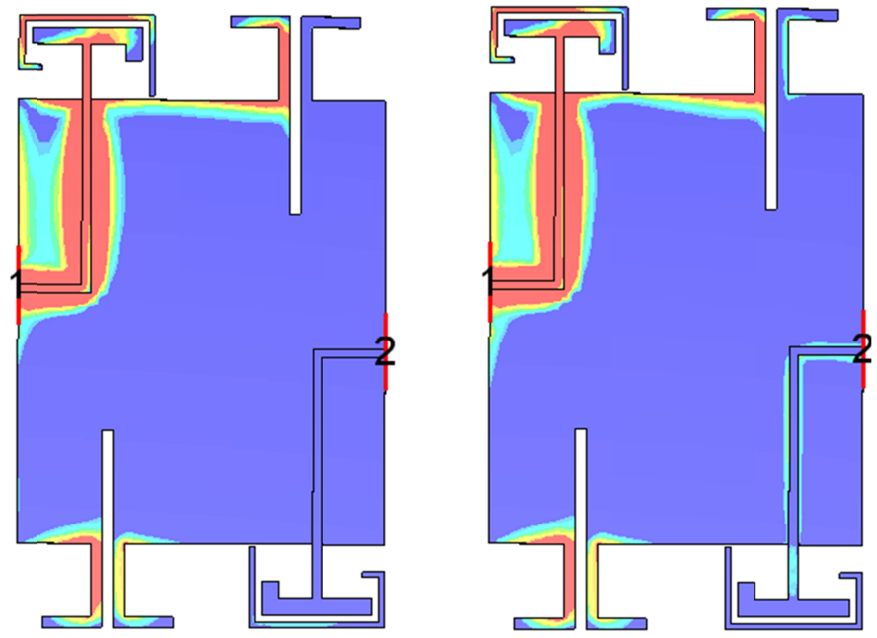

Figure 4.26: Simulated surface current distributions of the wideband MIMO meandered monopole antennas at different frequencies. (Scale: Red: Maximum current; Green: Intermediate current; Blue: Least current)

(d) Antenna Gain and Radiation Efficiency:

The simulated and measured gains and efficiencies of the wideband MIMO meandered monopole antennas at different frequencies are shown in Table 4.7 and show a good agreement. The measured gain is calculated by the Gain Comparison

method [3] and the measured efficiency is evaluated using the Wheeler Cap method [4]. The radiation efficiency depends on the return loss of the antenna. As the return loss gets worse the radiation efficiency gets lower.

(e) Diversity gains and Envelope correlation coefficients:

In order to analyze the diversity performance of the MIMO antennas, the envelope correlation coefficients 'ρ_e' and the diversity gains were calculated. The calculated values of the envelope correlation coefficients are shown in Table 4.7. The values of the envelope correlation coefficients are calculated using the S-parameter formula discussed earlier in this chapter. The peak value of the envelope correlation coefficient over the whole frequency bandwidth is 0.015, which is well below the acceptable value of 0.7 [12]-[13].

Table 4.7: Gains, efficiencies and Envelope correlation coefficients of the wideband MIMO meandered monopole antennas.

Freq. (GHz)	**Gain (dBi)**		**Efficiency (%age)**		**Bandwidth (MHz)**	**ρ_e**	
	Simulated	**Measured**	**Simulated**	**Measured**		**Simulated**	**Measured**
1.90	1.21	1.07	93.9	89.1	1.70 – 1.90	0.015	0.011
2.10	1.99	1.53	92.7	86.2	1.90 – 2.20	0.001	0.001
2.45	2.96	2.73	91.3	82.9	2.40 – 2.70	0.001	0.003
2.60	3.82	4.12	92.6	83.6			

An approximation of the diversity gain can be obtained by using the envelope correlation coefficient. The values of the envelope correlation coefficients and the diversity gains were calculated in both indoor and outdoor environments by simulating the statistical models summarized in [14], [16]-[17]. The diversity gains of the wideband MIMO meandered monopole antennas are mentioned in Table 4.8. The lowest value obtained for the diversity gain is 9.08 dB which is 0.92 dB lower than 10 dB. The antennas thus possess an excellent diversity performance due to a better efficiency than the quad-band MIMO multi-branch monopole antennas.

Table 4.8: Diversity gains of the wideband MIMO meandered monopole antennas.

Freq. (GHz)	**Envelope Correlation Coefficient**				**Efficiency**	**Effective Diversity Gain (dB)**	
	Indoor Environment		**Outdoor Environment**		η_r	**Indoor Environment**	**Outdoor Environment**
	ρ_e	DF	ρ_e	DF			
1.90	0.0510	0.974	0.0161	0.992	0.939	9.15	9.31
2.10	0.0390	0.980	0.0139	0.993	0.927	9.08	9.21
2.45	0.0020	0.999	0.0016	0.999	0.913	9.12	9.12
2.60	0.0004	1.000	0.0001	1.000	0.926	9.26	9.26

4.3 Multiband MIMO meandered loop antennas:

In this section two meandered loop antennas capable of multiband cellular coverage will be presented in MIMO configuration. Details of the design and the results will be discussed.

4.3.1 Antenna design:

The simulated model of the multiband MIMO meandered loop antennas is shown in Figure 4.27. The proposed design is composed of two direct fed MIMO antennas that are meandered to form a loop structure. The end of the loop has been placed at a coupling gap of 0.2 mm that has been selected after simulations in CST® Microwave Studio to achieve a resonance at lower frequency band. The antennas are placed on the top and bottom edges of the substrate. The material used for the substrate is FR-4 with relative permittivity of 4.35 and loss tangent of 0.02. The volume of the substrate board is 70 x 107.5 x 0.8 mm^3 with each antenna occupying an area of 50 x 10 mm^2. The antennas are placed at a gap of 2.5 mm from the top and bottom edges of the substrate to achieve better return loss and good isolation between the MIMO antennas. However, being closely spaced the meandered loop antennas do not show an acceptable isolation due to which a decoupling structure is designed consisting of two ground slots that are etched in mirrored symmetry. The lengths and widths of the slots have been selected from a repetitive parametric analysis to achieve an optimum radiation performance of the MIMO antennas. This leads to an isolation better than 12 dB between the MIMO antennas while achieving multiband operation with a good return loss performance. A prototype of the design was also fabricated and shown in

Figure 4.28. The antenna was fabricated manually by cutting the designed pattern from a 0.1 mm thick copper sheet using a sharp cutter. It is anticipated that there will be certain discrepancies due to the fabrication imperfections and the uncertainties in the material properties.

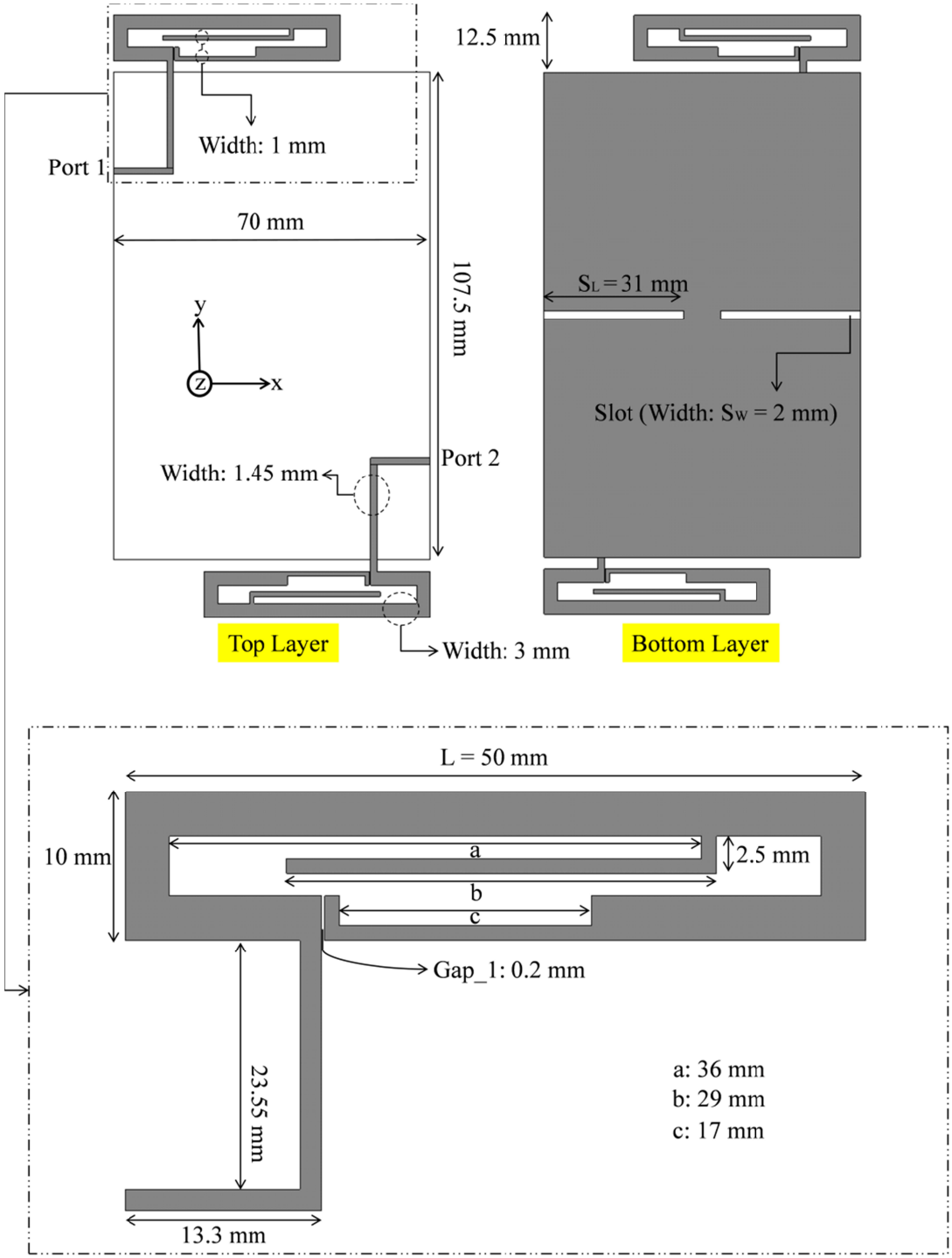

Figure 4.27: Simulated model of the multiband MIMO meandered loop antennas.

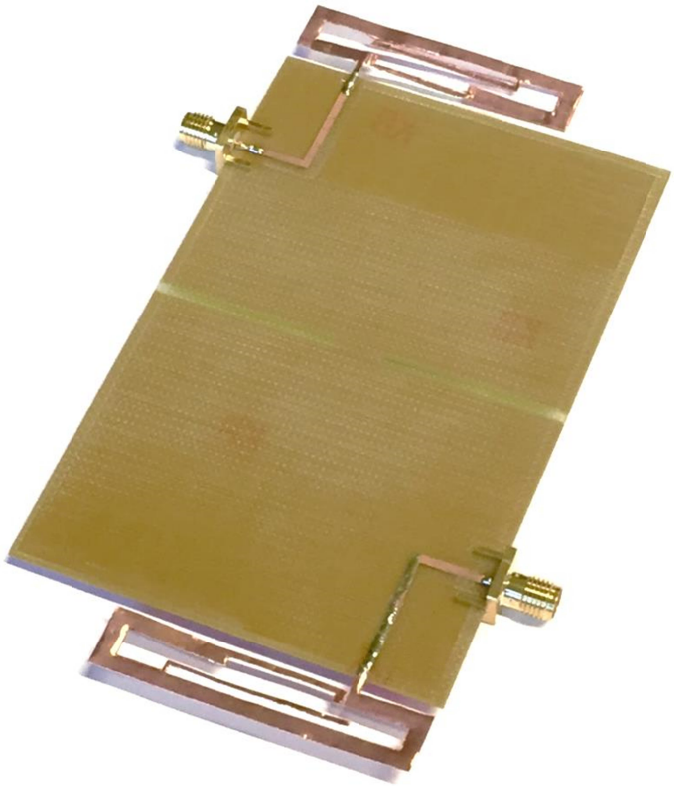

Figure 4.28: Fabricated prototype of the multiband MIMO meandered loop antennas for mobile handsets.

4.3.2 Working mechanism:

Each antenna in the MIMO is folded to form a loop structure. This can be validated from the simulated surface current distributions shown in Figure 4.29. For example, at 0.75 GHz the strip length contributing to the radiation is 'a-b-c-d-e-f' which makes a loop type structure. This loop structure is largely dependent on the Gap_1 which is 0.2 mm. This gap of 0.2 mm has been extracted through optimization in CST® Microwave Studio for achieving a resonance at the lower frequency band. Changing this gap will lead to a different current distribution thereby not achieving a lower resonance. The combined length of the microstrip radiating at 0.75 GHz is 108 mm which is nearly 0.25λ at 0.75 GHz. At 2.05 GHz the strip length of the antenna contributing to the radiation is 'm-n-d-e-f'. The combined length of 'm-n-d-e-f' is 80 mm which is nearly 0.5λ at 2.05 GHz. At 2.6 GHz the strip length of the antenna contributing to the radiation is 'm-n'. However, small portions of strips 'c-d' and 'e-f' also contribute to the radiation thus improving the bandwidth. The length of strip 'm-n' radiating at 2.6 GHz is 28 mm which is nearly 0.25λ at 2.60 GHz. Likewise, at 3.25 GHz the strip length of the antenna contributing to the radiation is mainly 'a-b-c'. The

combined length thus calculated is 22 mm which is nearly 0.25λ at 3.25 GHz. The decoupling between the antennas is achieved by introducing horizontal ground slots at the bottom layer of the substrate. The length and width of the ground slots have been chosen from a parametric study in the computer simulations. The isolation achieved with this simple decoupling structure is better than 12 dB. Also, the structure of the meandered loop antennas and their placement above the edges of the substrate improves the isolation.

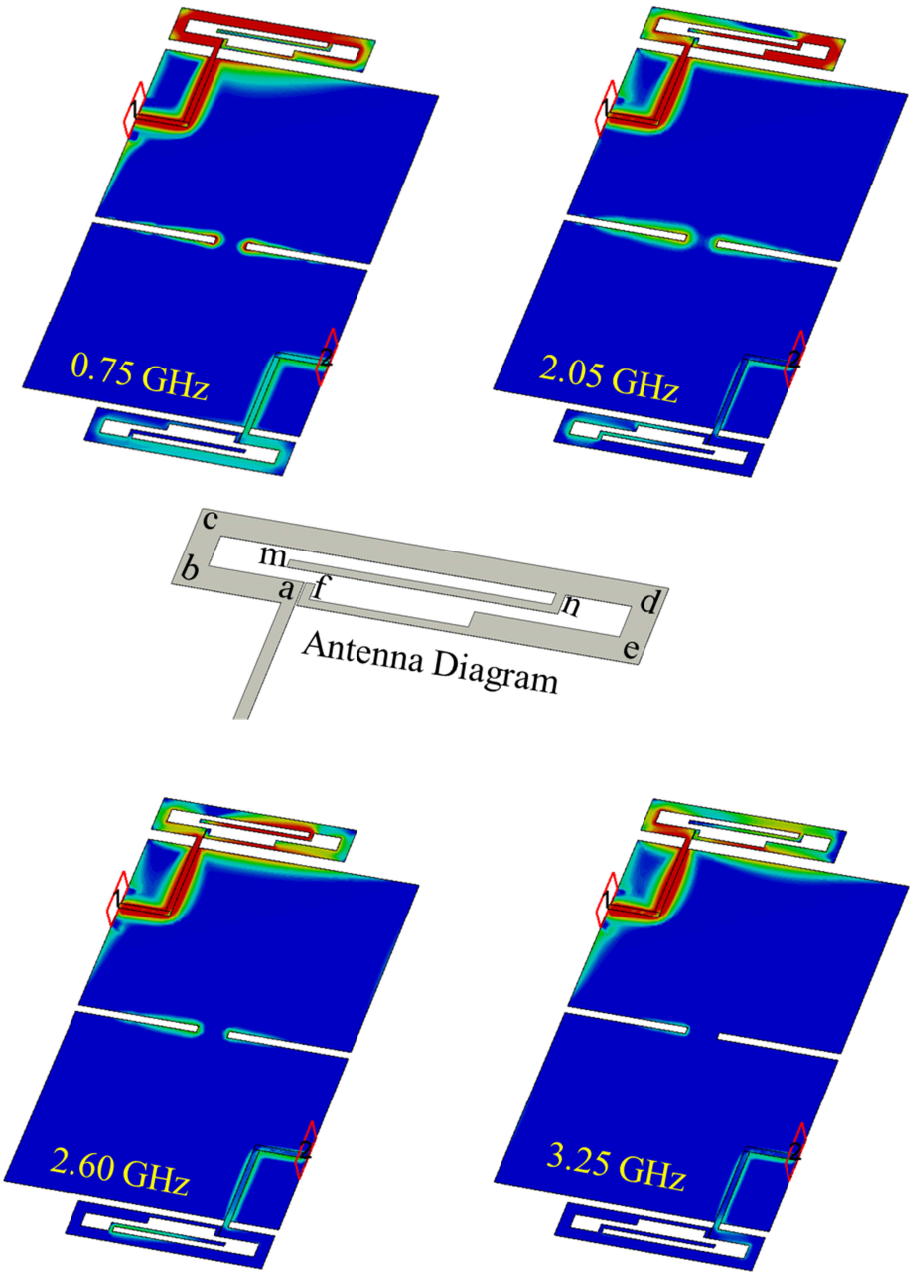

Figure 4.29: Surface current distributions of the multiband MIMO meandered loop antennas at different frequencies. (Scale: Red: Maximum current; Green: Intermediate current; Blue: Least current)

4.3.3 Parametric Study:

(a) Parametric analysis on the antenna design:

A parametric analysis was performed on the design of the multiband MIMO meandered loop antennas. The parameters which have been studied in this parametric analysis are the length 'L', length 'b' and the position of the inverted L branch 'a' as shown in Figure 4.27. The effect of altering these dimensions imposes a minute change in the isolation parameter (S_{21}), whereas, S_{11} is largely affected by changing these lengths. The effect of changing the length 'L' on S_{11} is shown in Figure 4.30, whereas, the effects of changing the parameters 'b' and 'a' on S_{11} are shown in Figure 4.31 and Figure 4.32 respectively. The parametric analysis was performed by changing the lengths in step of 0.1 mm. However, only a few values have been shown here for ease of presentation and understanding.

The length 'L' contributes to the radiation at the lower band (680 – 912 MHz). By altering this length, the 6 dB bandwidth can be changed to the desired range. All the other bands are less affected by changing the length 'L'. As the value of 'L' increases, the frequency shifts to lower value as compared to smaller 'L' values. Also the return loss is affected by changing the length 'L'. It can be seen from Figure 4.30 that L = 50 mm gives the optimum bandwidth and return loss.

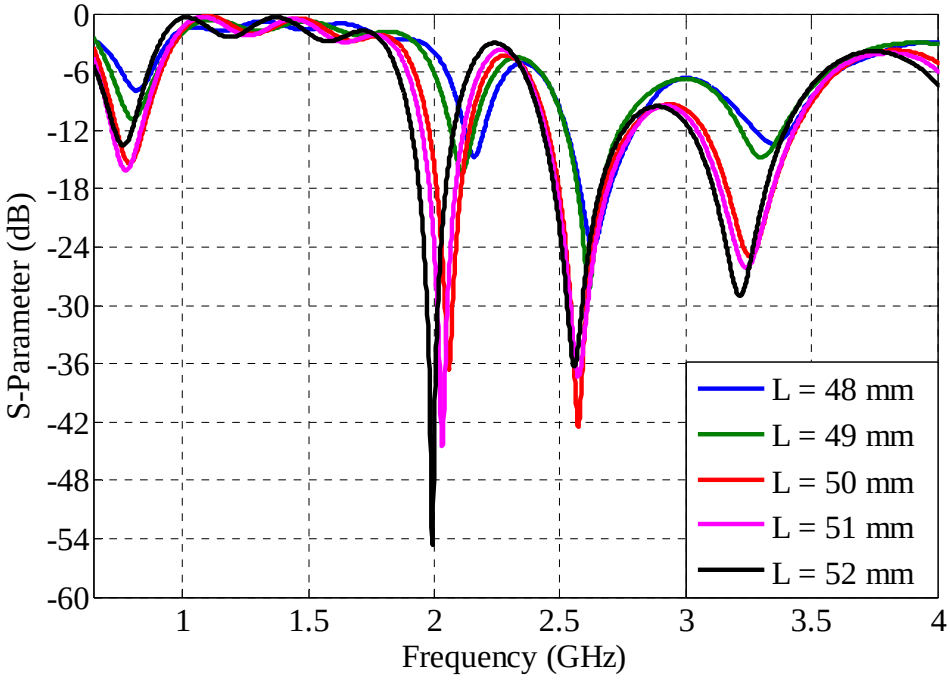

Figure 4.30: Effect of change in length 'L' on the s-parameter (S_{11}) of the multiband MIMO meandered loop antennas.

The length 'b' contributes to the radiation at 2.05 GHz achieving a bandwidth of 1920 – 2203 MHz. By changing this length, the 6 dB bandwidth can be shifted to a different range. However, as this branch is directly connected to the main branch 'L' so it affects the overall return loss of the antenna. It can be seen from Figure 4.31 that b = 29 mm gives a better bandwidth at 2.05 GHz and a better return loss at the other frequencies.

The inverted L branch that contributes to the radiation at 2.05 GHz is directly connected to the main length L which means that the return loss and efficiencies of both microstrip lines are largely dependent on each other. The position of the inverted L strip has been selected very carefully in order to achieve a good return loss not only at 2.05 GHz but also at 0.79 GHz. Also being directly connected to the main branch length 'L', the inverted L branch directly affects the efficiency of the antenna at the lower band which in turn affects the gain of the antenna. It can be seen from Figure 4.32 that a = 36 mm gives an optimum 6 dB bandwidth at all the frequency bands of the proposed loop antennas. The total efficiency at 0.79 GHz for a = 36 mm is 60% which is much better than at other values of 'a'.

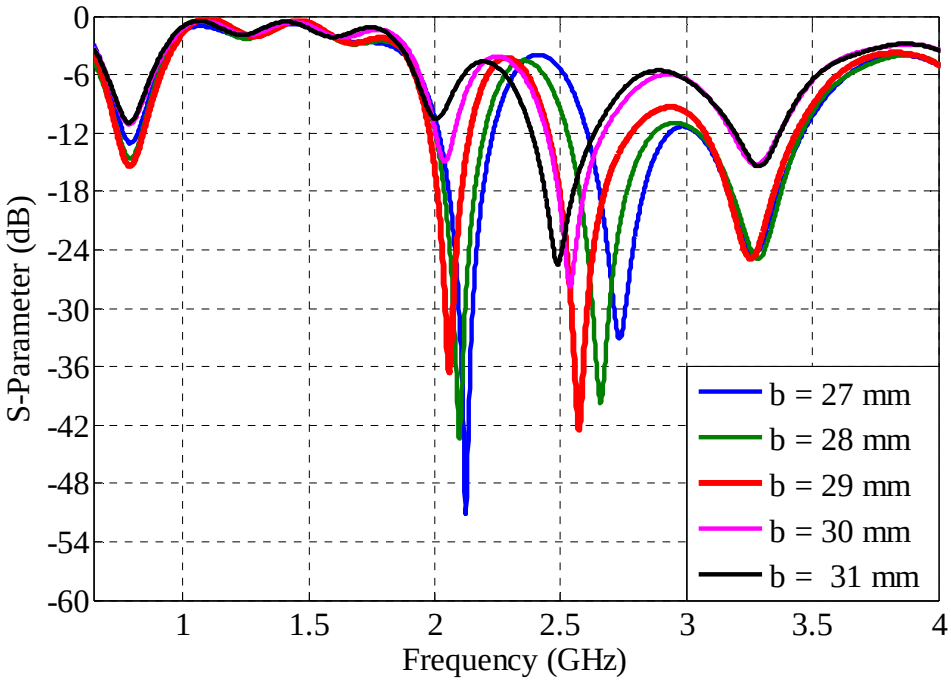

Figure 4.31: Effect of change in length 'b' on the s-parameter (S_{11}) of the multiband MIMO meandered loop antennas.

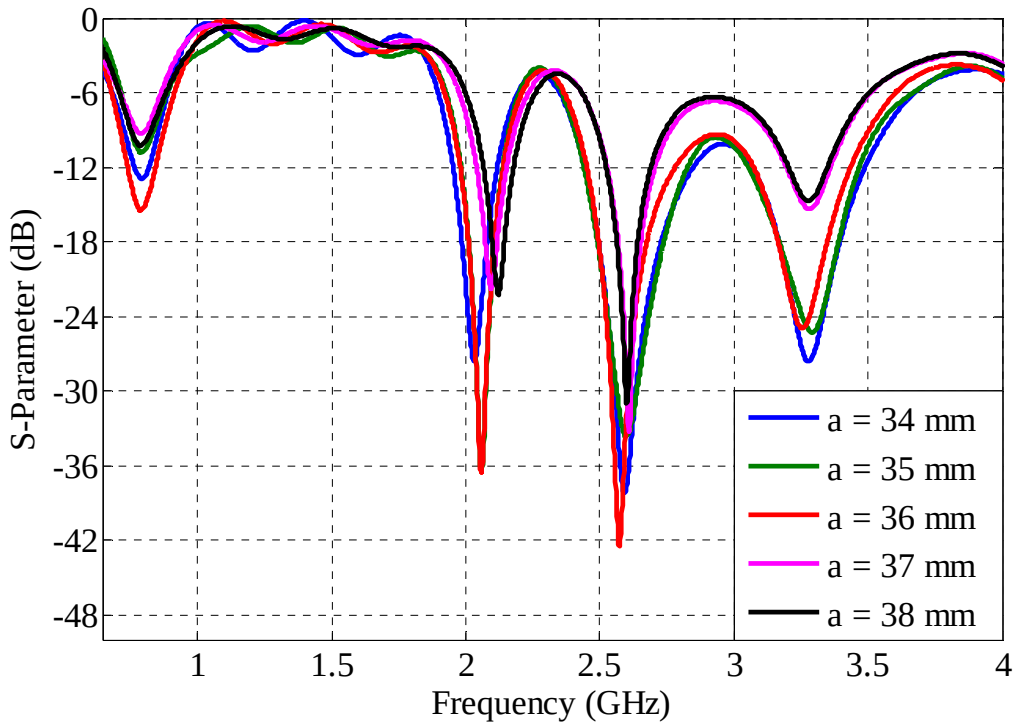

Figure 4.32: Effect of change in parameter 'a' on the s-parameter (S_{11}) of the multiband MIMO meandered loop antennas.

(b) Parametric analysis of the decoupling structure:

A parametric analysis was also performed on the decoupling structure between the multiband MIMO meandered loop antennas. The decoupling structure proposed in this design is two horizontal slots etched into the ground plane in mirrored symmetry. The length 'S_L' and the width 'S_W' of the slot largely affect the isolation performance of the MIMO antennas whereas, the effect on 6 dB bandwidths is minor. The effect of changing the length of the ground slots on the return loss and isolation is shown in Figure 4.33, whereas, the effect by changing the width of the slots is shown in Figure 4.34. It can be seen from the S_{11} curves that the 6 dB bandwidths of the antennas stay nearly the same by changing the length of the slot. However, the width of the slot changes the return loss but the 6 dB bandwidths almost stay the same. It can be seen from the S_{21} curves that the isolation between the antennas is different for each value of the slot length and the slot width. These parameters were therefore extracted from the simulation analysis to achieve optimum values of the return loss and the isolation. The parameter values, S_L = 31 mm and S_W = 2 mm, provide the best combination of return loss and isolation.

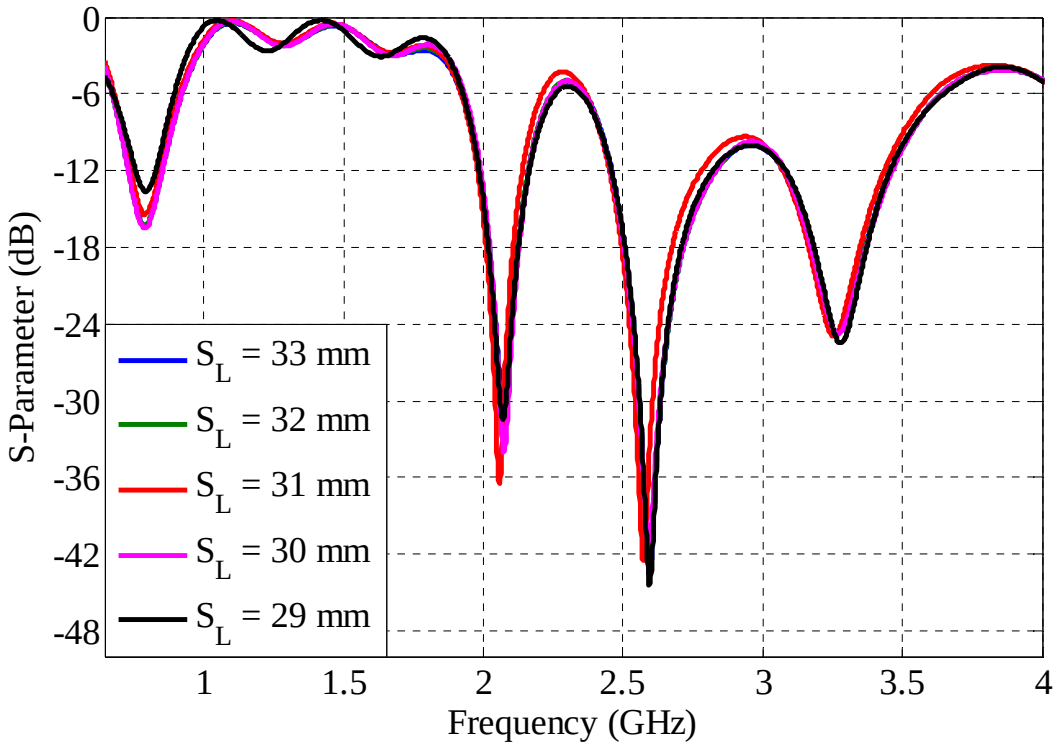

(a)

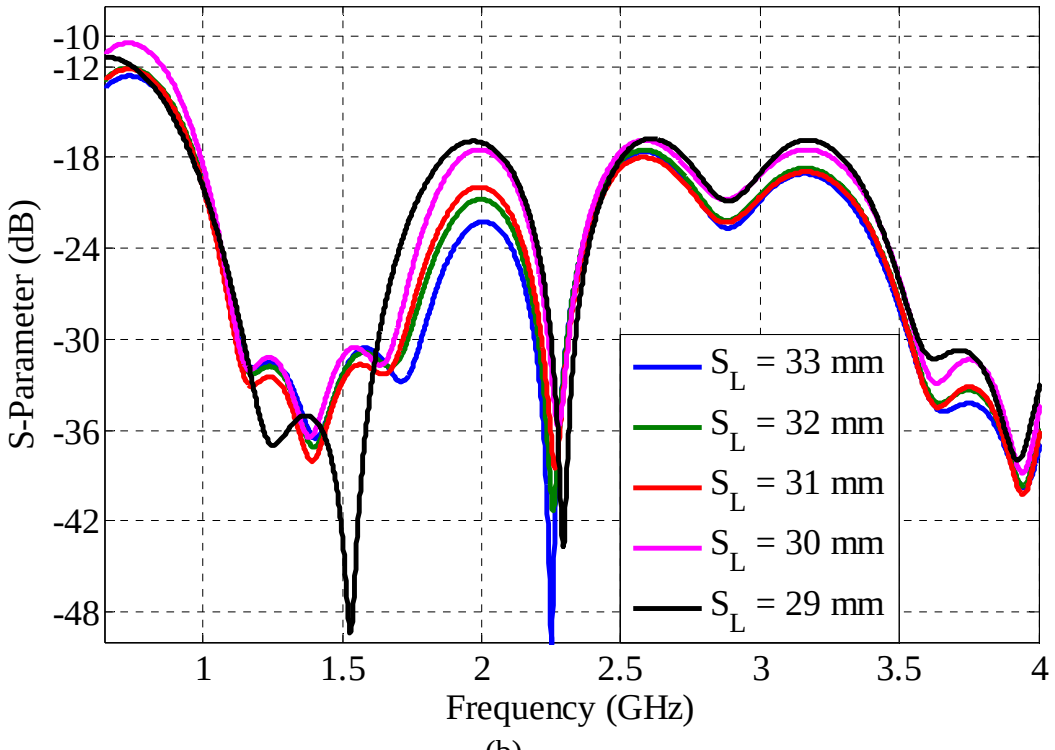

(b)

Figure 4.33: Effect of change in length 'S_L' on the S-parameters of the multiband MIMO meandered loop antennas. (a): Effect on S_{11}. (b): Effect on S_{21}.

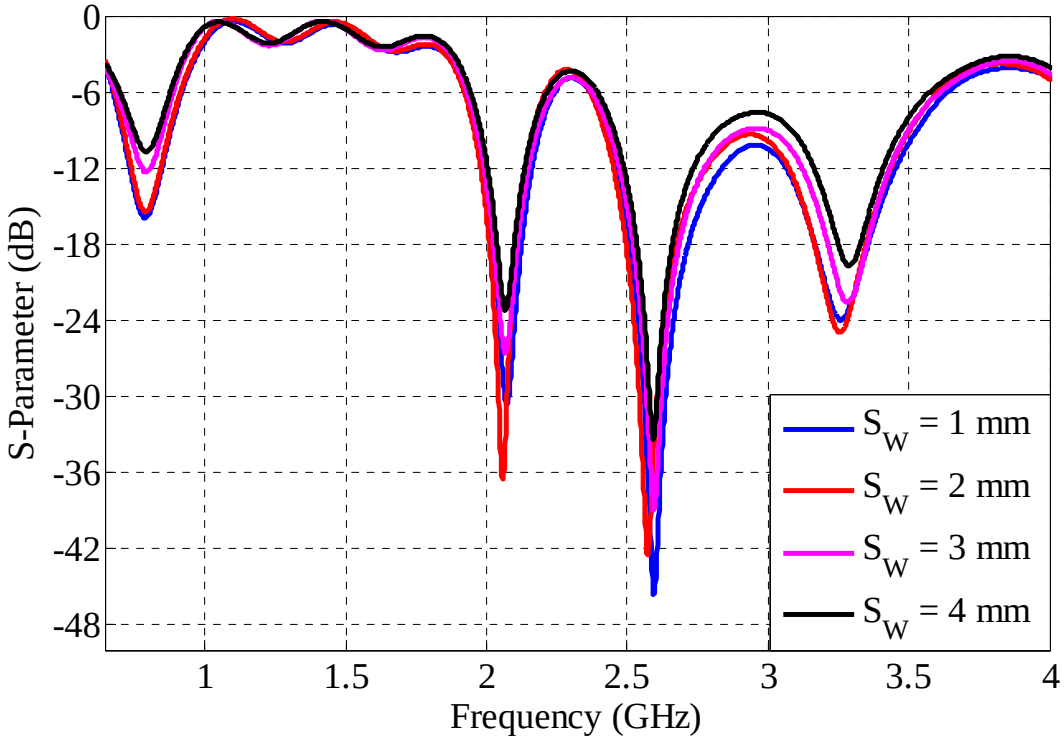

(a)

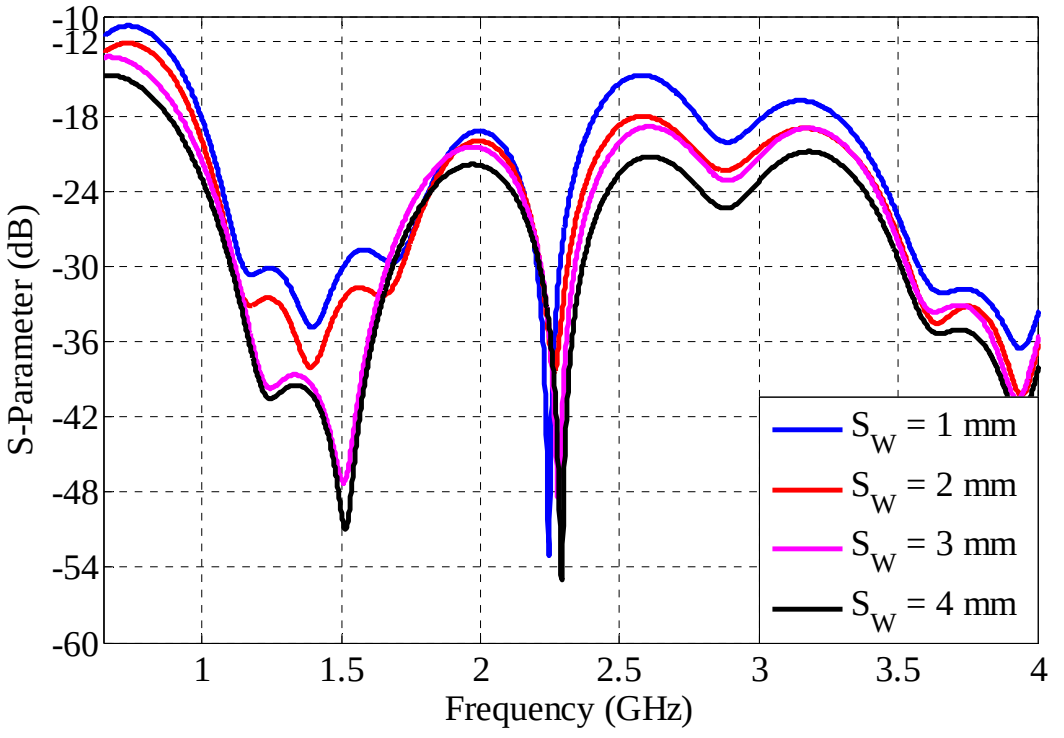

(b)

Figure 4.34: Effect of change in width 'S_w' on the S-parameters of the multiband MIMO meandered loop antennas. (a): Effect on S_{11}. (b): Effect on S_{21}.

4.3.4 Results and discussions:

The antennas were simulated in CST® Microwave Studio and the simulation results of the S-parameters and radiation patterns were extracted. Whereas, testing of the antennas was performed in the antenna laboratory at QMUL. The simulation and the measurement results were then post processed in Matlab® for ease of analysis and comparison.

(a) S-parameters:

The simulated and measured S-parameters of the multiband MIMO meandered loop antennas are shown in Figure 4.35. Only one antenna is considered as the two antennas are identical.

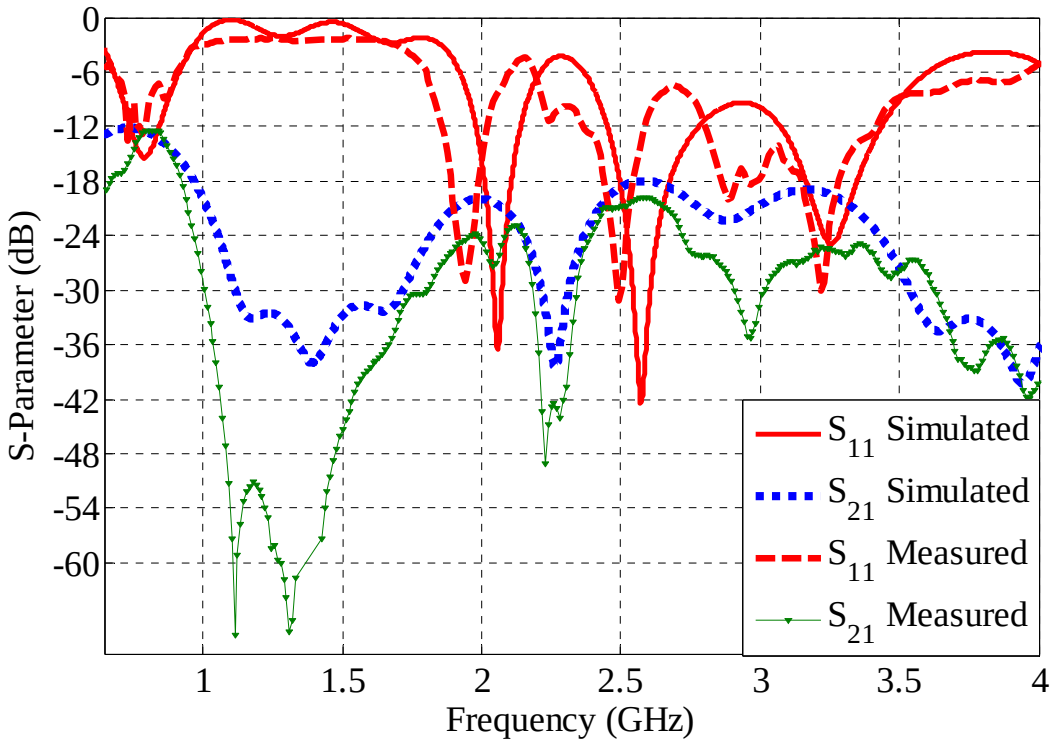

Figure 4.35: S-parameters of the multiband MIMO meandered loop antennas for mobile handsets.

Each antenna of the MIMO pair is resonating in three frequency bands ranging from 680 – 912 MHz, 1920 – 2203 MHz and 2380 – 3603 MHz when referenced to a return loss of 6 dB. The antennas are thus capable of covering the 2G GSM 850/1900, 3G HSDPA 800/850/2100, 4G LTE bands 1-2, 7, 30 (1920 – 2690 MHz), LTE bands 5, 12-13, 17-20, 26, 28 (680 – 912 MHz), WLAN 802.11 a/b/g/n 2.45 GHz and WLAN 802.11h (3400 – 3600 MHz). The isolation achieved between the antennas is better

than 12 dB in the lower band and better than 15 dB in the upper frequency bands. The simulated and measured S-parameters agree well with some discrepancies. A minor shift of frequency has been observed due to the imperfections in the fabrication process. The return loss and isolation performance of the antennas makes the design suitable to be implemented in modern handsets.

(b) Radiation patterns:

The simulated 3D radiation patterns of the multiband MIMO meandered loop antennas are shown in Figure 4.36.

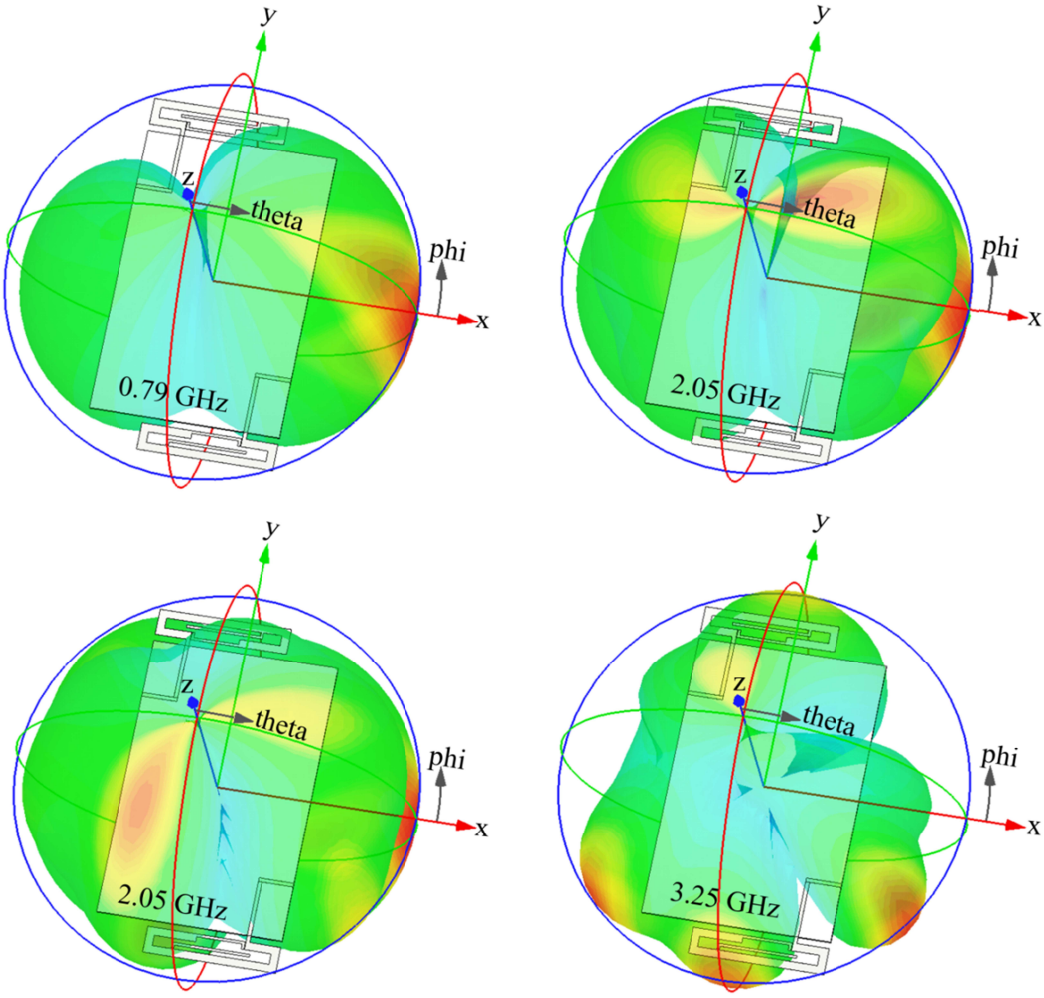

Figure 4.36: Simulated 3D radiation patterns of the multiband MIMO meandered loop antennas for mobile handsets.

The radiation patterns were measured in the anechoic chamber in the antenna laboratory at QMUL. The radiation patterns of only one antenna are plotted as the two antennas of the MIMO configuration are identical. The simulation and the measurement data files were post processed in Matlab® for ease of comparison. The

normalized co-polar (*phi*) and cross-polar (*theta*) components of the radiation pattern are plotted in both x-z and y-z planes at four different frequencies as presented in Figures 4.37 and 4.38. The simulated and measured radiation patterns agree with some discrepancies.

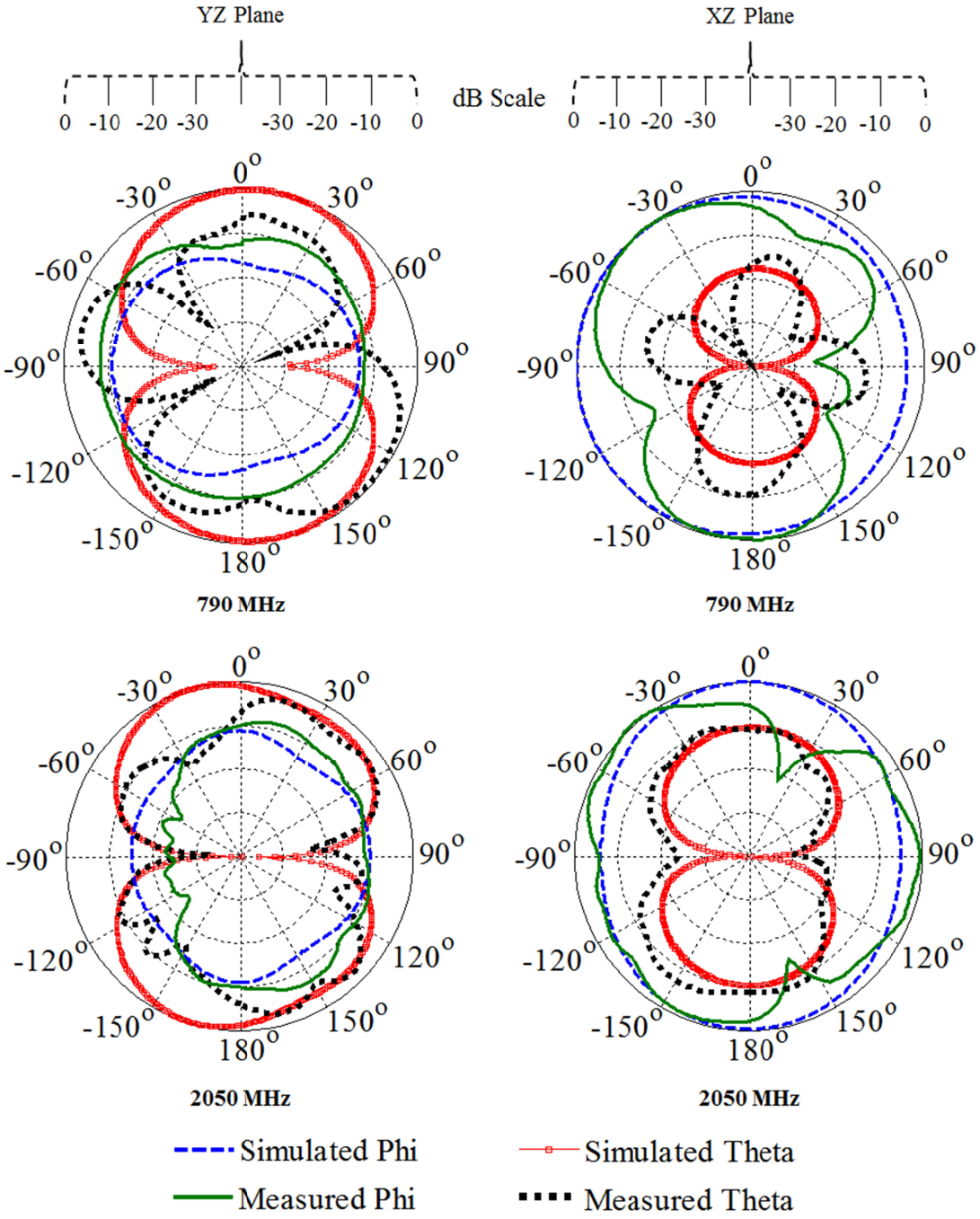

Figure 4.37: 2D Radiation patterns of the multiband MIMO meandered loop antennas at 0.79 GHz and 2.05 GHz.

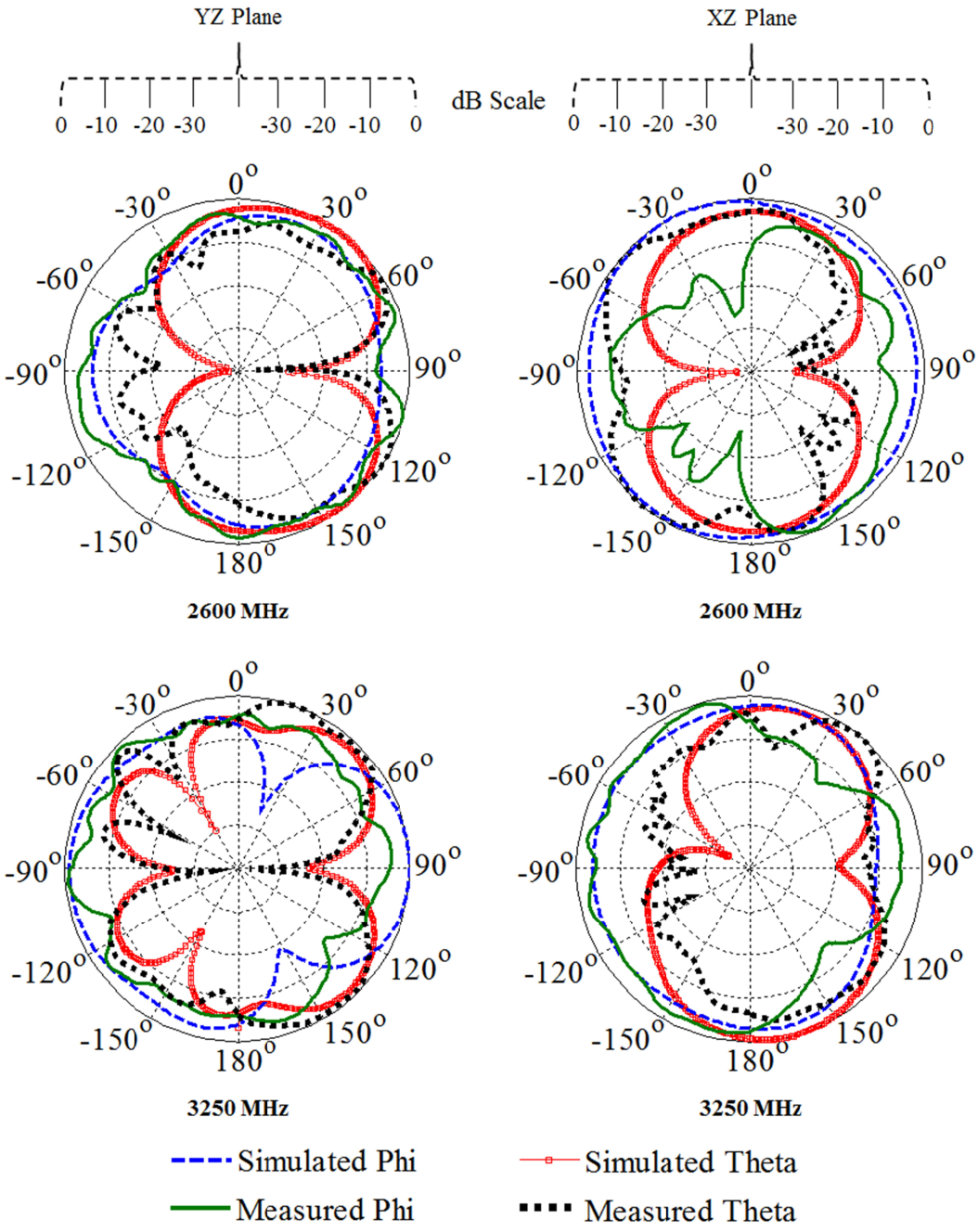

Figure 4.38: 2D Radiation patterns of the multiband MIMO meandered loop antennas at 2.60 GHz and 3.25 GHz.

(c) Antennas gain and efficiency:

The gains and efficiencies of the multiband MIMO meandered loop antennas at different frequencies are shown in Table 4.9. The simulated gains and efficiencies have been extracted from the simulations in CST® Microwave studio. The measured gain was calculated using the gain comparison method [3], whereas, the efficiency was measured using the Wheeler Cap method [4]. The gains and efficiencies of only one antenna are tabulated as the two antennas are identical.

(d) Envelope correlation coefficients:

In order to analyze the diversity performance of the MIMO antennas, the envelope correlation coefficient 'ρ_e' is calculated at different frequencies. The values have been calculated by using the S-parameters method and shown in Table 4.9. The peak values are well below the acceptable value of 0.7 [12]-[13].

Table 4.9: Gains, efficiencies and envelope correlation coefficients of the multiband MIMO meandered loop antennas.

Freq. (GHz)	**Gain (dBi)**		**Total Efficiency (% age)**		**Bandwidth (MHz)**	**Envelope Correlation Coefficient (ρ_e)**
	Sim.	**Mea.**	**Sim.**	**Mea.**		
0.79	1.28	0.93	60	53	680 – 912	0.0810
2.05	3.75	2.73	90	76	1920 – 2203	0.0070
2.60	4.43	3.52	98	81	2380 – 2700	0.0001
3.25	3.39	2.92	90	83	3400 – 3603	0.0007

(e) Diversity gains:

The diversity gains of the multiband MIMO meandered loop antennas are shown in Table 4.10. The values of the diversity gains are calculated in both indoor and outdoor environments by simulating the statistical models summarized in [16]-[17] using CST® Microwave Studio. The diversity gains mentioned in Table 4.10 are promising and represent a good diversity performance of the MIMO antennas. The lowest value obtained for the diversity gain is 6.62 dB at 0.79 GHz. This is due to lower radiation efficiency and a poorer envelope correlation coefficient at 0.79 GHz as compared to the upper frequencies.

Table 4.10: Diversity gains of the multiband MIMO meandered loop antennas.

Freq. (GHz)	**Envelope Correlation Coefficient**				**Radiation Efficiency**	**Effective Diversity Gain (dB)**	
	Indoor Environment		**Outdoor Environment**		η_r	**Indoor Environment**	**Outdoor Environment**
	ρ_e	DF	ρ_e	DF			
0.79	0.2203	0.883	0.0909	0.953	0.75	6.62	7.15
2.05	0.1344	0.930	0.0597	0.970	0.91	8.46	8.83
2.60	0.0002	0.999	0.0004	0.999	0.99	9.89	9.89
3.25	0.0221	0.883	0.0089	0.996	0.93	8.21	9.26

Summary

Three designs of MIMO antennas are presented in this chapter and a comparison of the designs is shown in table 4.11. The first design is for compact and multiband MIMO antennas based on a multi-branch monopole configuration. The antennas cover the 2G GSM 850/900/1800/1900, 3G HSDPA 800/850/900/1700/1900/2100 and 4G LTE bands 1-5, 8, 19, 25, 30, WLAN 802.11 a/b/g/y/n and WiMAX 3.4 GHz. The proposed design consists of two identical printed antennas that are etched on the top layer of an FR-4 substrate and a decoupling structure is etched on the bottom layer. The decoupling structure consists of slots in the ground plane and the inverted L-shaped metallic branches that extend from the ground plane into the non-grounded portion. Detailed analyses on the simulation and measurement results have been carried out. Both the simulation and the measurements have corroborated a good performance of the MIMO antennas. The isolation achieved is better than 15 dB in the lower band and better than 20 dB in the upper frequency bandwidths, leading to the envelope correlation coefficient of less than 0.0184.

The second design is of compact MIMO antennas based on meandered monopole configuration. The antennas are capable of covering 2G GSM 1800/1900, 3G HSDPA 1700/1900/2100, 4G LTE Bands 1-4, 7, 25, 30 (1710 – 2690 MHz) and WLAN 802.11 a/b/g/n. The design presented in this work is composed of two diagonally printed monopole antennas and a dual decoupling structure. The simulation and the measurement results agree thus validating a good performance of the MIMO antennas. The isolation achieved is better than 15 dB leading to the envelope correlation coefficient of less than 0.015.

The third design is composed of two symmetrically positioned loop antennas placed at the top and bottom edges of the FR-4 substrate. The antennas are microstrip antennas meandered to form a loop structure. For the improvement of isolation, two slots are etched at the bottom layer of the substrate. The isolation thus achieved is better than 12 dB leading to a good diversity performance of the MIMO antennas. Each antenna is capable of covering 2G GSM 850/1900, 3G HSDPA 800/850/2100, 4G LTE bands 1-2, 5, 7, 12-13, 17-20, 26, 28, 30 and WLAN 802.11 a/b/g/h/n 2.45 GHz and WLAN 802.11h (3400 – 3600 MHz). The s-parameters and the radiation results have presented a good performance of the MIMO antennas. The antenna designs presented

in this chapter are compact and can be implemented in next generation mobile handsets.

Table 4.11: Summary of the proposed MIMO antenna designs for mobile handsets.

MIMO Design	6dB Bandwidths (MHz)	Freq. (GHz)	Gain (dB)		Efficiency (%)		Isolation (dB)		Diversity Gain (dB)	
			Sim.	*Mea.*	*Sim.*	*Mea.*	*Sim.*	*Mea.*	*Indoor*	*Outdoor*
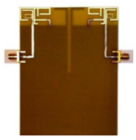	835 – 961	0.90	1.80	1.70	82.4	76.3	16	17	8.57	8.58
	1656 – 2272	2.10	3.51	2.10	82.9	73.1	20	35	8.79	8.79
	3346 – 3814	3.50	4.43	3.20	69.4	63.2	33	38	8.29	8.29
	5099 – 5798	5.40	2.79	1.63	61.8	55.3	30	41	7.09	7.09
Substrate: 85 x 125 mm^2 Antenna: 26.3 x 16 mm^2	**Average →**		3.13	2.16	74.1	66.9	24.8	32.8	8.19	8.19
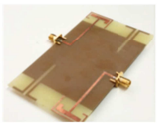	1700 – 3200	1.90	1.21	1.07	93.9	89.1	17.3	20.3	9.15	9.31
		2.10	1.99	1.53	92.7	86.2	27.8	28.5	9.08	9.21
		2.45	2.96	2.73	91.3	82.9	27.8	23.3	9.12	9.12
		2.60	3.82	4.12	92.6	83.6	20.3	24	9.26	9.26
Substrate: 65 x 110 mm^2 Antenna: 24 x 14.5 mm^2	**Average →**		2.50	2.36	92.6	85.5	23.3	24.0	9.15	9.23
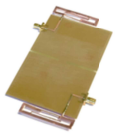	680 – 912	0.79	1.28	0.93	60	53	13	13	6.62	7.15
	1920 – 2203	2.05	3.75	2.73	90	76	21	27	8.46	8.83
	2380 – 3603	2.60	4.43	3.52	98	81	17	21	9.89	9.89
		3.25	3.39	2.92	90	83	20	26	8.21	9.26
Substrate: 70 x 107.5 mm^2 Antenna: 50 x 10 mm^2	**Average →**		3.21	2.53	84.5	73.3	17.8	21.8	8.30	8.78

References

[1] Jie Ma; Ying Zeng Yin; Jing Li Guo; You Huo Huang; , "Miniature Printed Octaband Monopole Antenna for Mobile Phones," Antennas and Wireless Propagation Letters, IEEE , vol.9, pp.1033-1036, 2010

[2] CST® Microwave Studio, Computer Simulation Technology Homepage [Online]. Available: http://www.cst.com, Version, 2013.04, Release, Oct 04, 2013

[3] Balanis, C. A., "Antenna Theory Analysis and Design", Edition, 3rd, A John Wiley & Sons, Inc., Publication, ISBN 0-471-66782-X, 2005.

[4] Pozar, David M.; Kaufman, B., "Comparison of three methods for the measurement of printed antenna efficiency," Antennas and Propagation, IEEE Transactions on , vol.36, no.1, pp.136,139, Jan 1988.

[5] G. J. Foschini and M. J. Gans, “On Limits of Wireless Communications in a Fading Environment When Using Multiple Antennas,” Wireless Personal Communications, Vol. 6, 1998, pp. 311-335.

[6] R. Janaswamy, “Effects of Mutual Coupling on the Capacity of Fixed Length Linear Arrays,” IEEE Antennas and Wireless Propagation Letters, Vol. 1, 2002, pp. 157-160.

[7] R. G. Vaughan and J. B. Andersen, “Antenna Diversity in Mobile Communications,” IEEE Transactions on Vehicular Technology, Vol. 36, 1987, pp. 149-172.

[8] R. G. Vaughan, “Signals in Mobile Communications,” IEEE Transactions on Vehicular Technology, Vol. 35, 1986, pp. 133-145.

[9] G. Lebrun, S. Spiteri and M. Faulkner, “MIMO Complexity Reduction through Antenna Selection,” Proceedings on Australian Telecommun Cooperative Research Center, ANNAC’03, Vol. 5, 2003.

[10] S. Jacobs and C. P. Bean, “Fine Particles, Thin Films and Exchange Anisotropy,” In Magnetism, G. T. Rado and H. Suhl, Eds., Academic, New York, Vol. 3, 1963, pp. 271-350.

[11] J. Blanch, J. Romeu and I. Cordella, “Exact Representation of Antenna System Diversity Performance from In-put Parameter Description,” Electronics Letters, Vol. 39, 2003, pp. 705-707.

[12] S.R. Saunders, “Antennas and propagation for wireless communication systems”, Wiley, 1999.

[13] M. Schwartz, W. R. Bennet and S. Stein, “Communication systems and techniques”, McGraw Hill, 1996.

[14] C. C. Chiau , “Study of the Diversity Antenna Array for the MIMO Wireless communication Systems”, Ph.D. Thesis, Queen Mary University of London, April 2006.

[15] K. Fijimoto, J. R. James, "Mobile Antenna System Handbook", Artech House, 2000.

[16] V. Plicanic, “Antenna Diversity Studies and Evaluation”, Master Thesis, LUND University in cooperation with Ericsson Mobile Communications AB, May 2004.

[17] Z. Ying, “Characterization of multi-channel antenna performance for mobile terminal by using near field and far field parameters,” COST 273 TD (04) (095) Goteborg, Sweden, June, 2004.

[18] Radio Electronics, Resources and analysis for electronic engineers, “LTE frequency bands and spectrum allocations”, Available at: http://www.radio-electronics.com/info /cellular telecomms/lte-long-term-evolution/lte-frequency-spectrum.php.

CHAPTER 5
MIMO ANTENNAS FOR MOBILE TABLETS

This chapter presents MIMO antennas for tablet applications. The antennas are designed and optimized through simulations in CST® Microwave Studio [1] and are modeled in single antenna and MIMO configurations. This chapter will include simulation and measurement results along with the simulation analysis of the proposed MIMO antennas.

5.1 MIMO antennas for 2G/3G mobile tablets:

This section presents the design and results of MIMO antennas for tablet applications. The antennas are modeled in four element MIMO configuration and cover the 2G and 3G cellular frequency bands.

5.1.1 Design and modelling of single antenna configuration:

The simulation model of a multiband antenna for mobile tablets is presented in Figure 5.1. The design is given in single antenna configuration and is composed of a coupled fed monopole in meandered form etched on the top layer of the substrate. The substrate used is FR-4 with relative permittivity of 4.4 and loss tangent of 0.02.

The volume of the substrate is 230 x 176 x 0.8 mm^3 with each antenna printed on the no-ground area which is 230 x 15 mm^2. The antenna occupies an area of 75 x 11 mm^2 and the width of the copper strip is selected through optimization in CST® Microwave Studio. The feeding mechanism used in the design is coupled feed with a coupling gap of 1.23 mm. The width of the feed line and the coupling gap have been selected through computer simulations to achieve an optimum impedance bandwidth. The

proposed antenna is then simulated and tested for a comparison between simulation and measurement results.

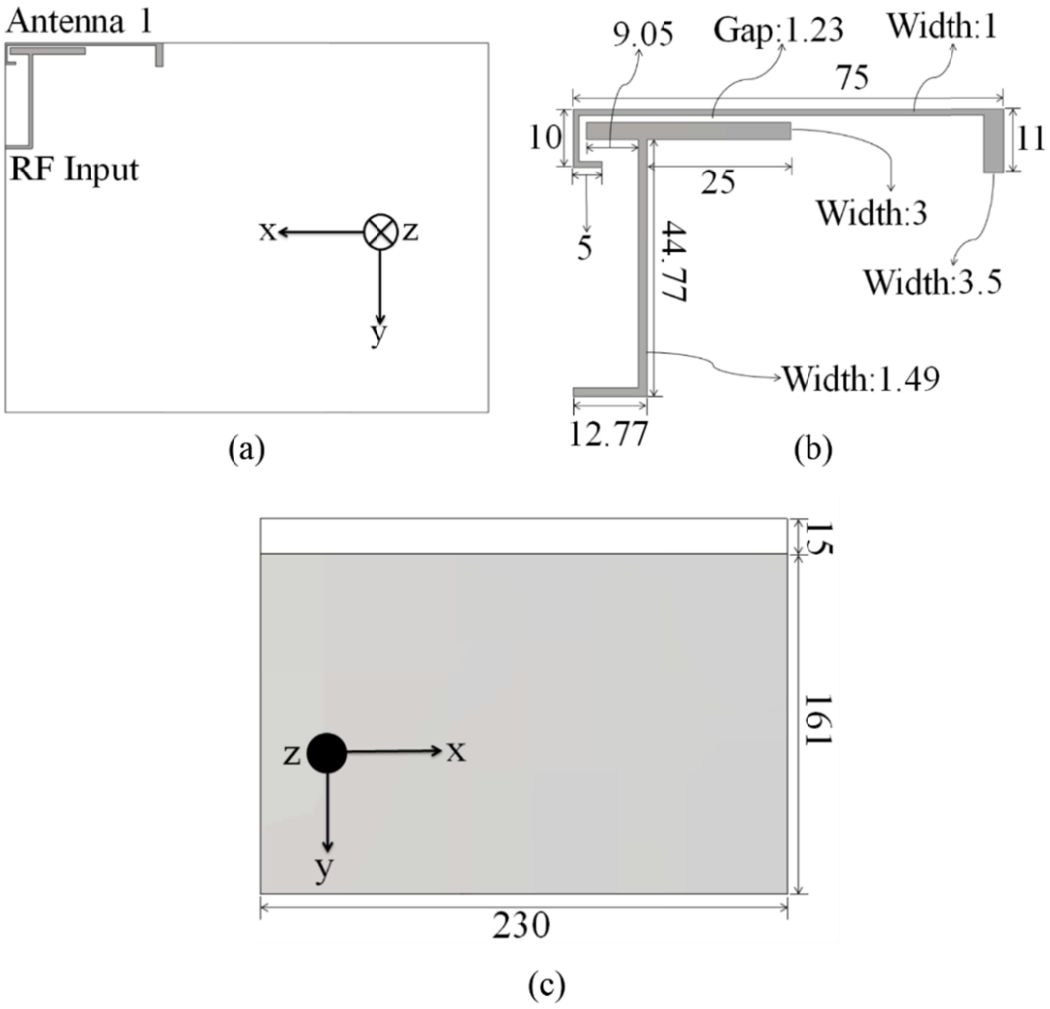

Figure 5.1: Simulated model of the antenna for mobile tablets in single antenna configuration. (a): Top layer. (b): Dimensions of the antenna. (c): Bottom layer.

5.1.2 Working mechanism:

The simulated surface current distributions of the antenna in single antenna configuration are shown in Figure 5.2. The antenna is composed of a monopole strip that is meandered for a compact volume. It can be seen from the surface current distributions that different sections of the antenna are radiating at different frequencies. The whole length of the monopole strip is mentioned as 'A-B-C-D-E' in the diagram. The radiating length of the antenna at a particular frequency can be obtained by calculating the length of the red section in the current distribution.

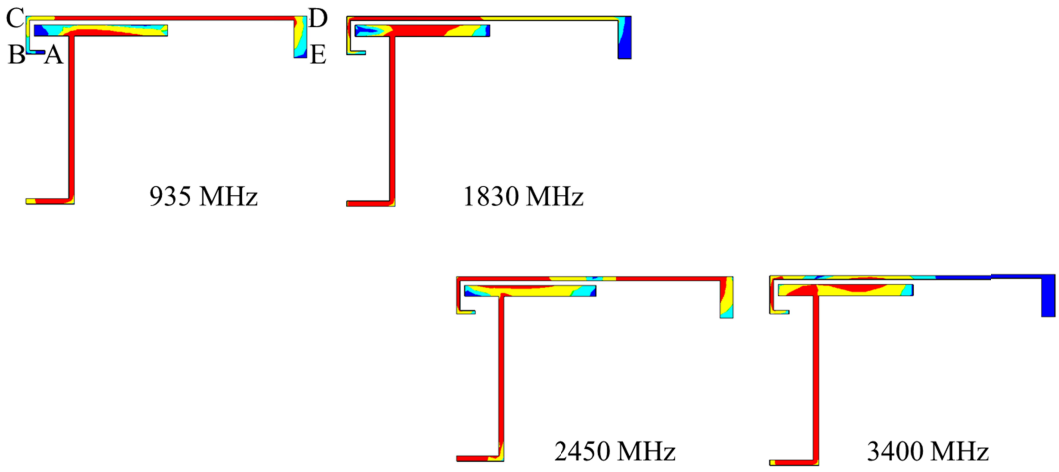

Figure 5.2: Surface current distributions of the proposed antenna at different frequencies. (Scale: Red: Maximum current; Green: Intermediate current; Blue: Least current)

At 935 MHz, the strip length 'C-D' is predominantly radiating with a 6dB bandwidth of 850-1007 MHz. The combined length of 'C-D' is 75 mm which is nearly 0.25λ at 935 MHz. Likewise, at 1.83 GHz, the strip lengths contributing to the radiation are 'B-C' and partially 'C-D' giving a bandwidth of 1628-2100 MHz. The combined length thus calculated is 41 mm which is almost 0.25λ at 1830 MHz. At 2.45 GHz, two sections of strip length 'B-C-D-E' are radiating. Each comprises a length of 35 mm which is nearly 0.25λ at 2.45 GHz. Lastly, at 3.4 GHz, the microstrip strip lengths contributing to the radiation are 'B-C' and a small section of 'C-D', each having a length of length of 18 mm which is nearly 0.25λ at 3.4 GHz.

5.1.3 Simulation Results:

The simulated return loss of the antenna (S_{11}) is shown in Figure 5.3. It can be seen that the antenna is resonating in four different frequency bands when referenced to a return loss of 6 dB. The antenna covers 2G GSM 900/1800/1900, 3G HSDPA 900/1700/1800/1900, WLAN 802.11n 2.45 GHz and WiMAX 3.4 GHz. The frequency information of each cellular service is mentioned in appendix I.

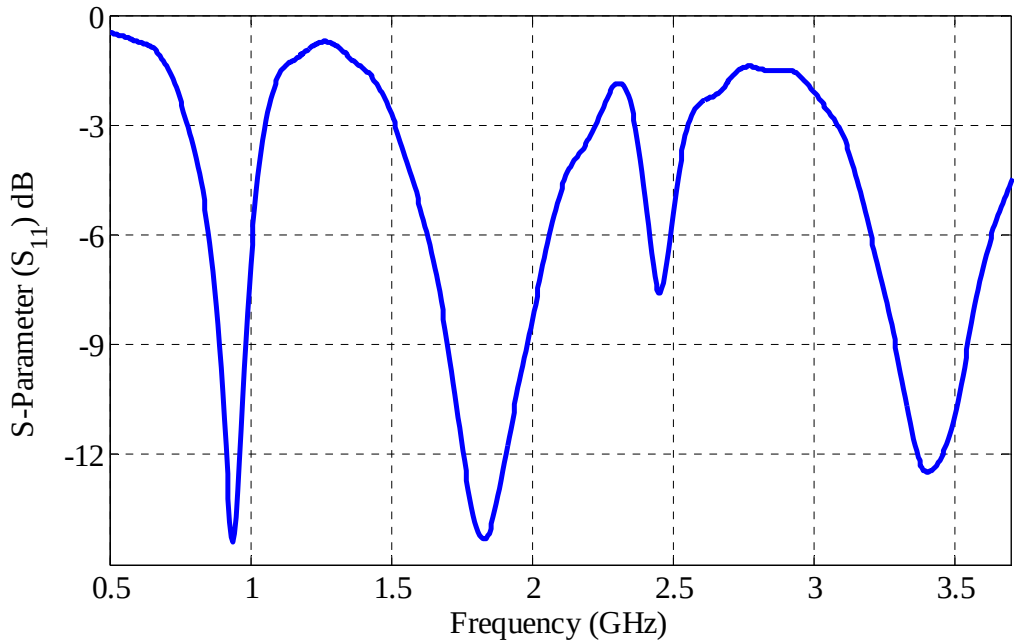

Figure 5.3: Simulated return loss (S_{11}) of the antenna for 2G/3G mobile tablets in single antenna configuration.

The antenna possesses good return loss and covers most of the 2G and 3G cellular frequency bands. The antenna was also modeled in a 4 x 4 MIMO configuration and an analysis of the simulation and measurement results is provided.

5.1.4 Design and modelling of tablet antenna in 4x4 MIMO configuration:

Figure 5.4 shows the drawing of the multiband antenna for mobile tablets in 4x4 MIMO configuration. The dimensions of the MIMO antennas are exactly the same as used for the single antenna configuration discussed in section 5.1.1.

The top layer of the substrate is composed of four copies of the monopole antenna printed in mirror configuration at each corner of the substrate. The bottom layer is composed of the dual decoupling structure for reducing the coupling between the MIMO antennas. The decoupling structure consists of two metallic strips of length 54 mm and width 2.5 mm that are placed at a coupling gap of 0.27 mm from the ground plane. These metallic branches provide a coupling path for the current, thus limiting its flow from one antenna to the other antennas. For further improvement of isolation between the MIMO antennas, two horizontal and six vertical slots have been etched into the ground plane to make the isolation between each antenna pair better than 15 dB.

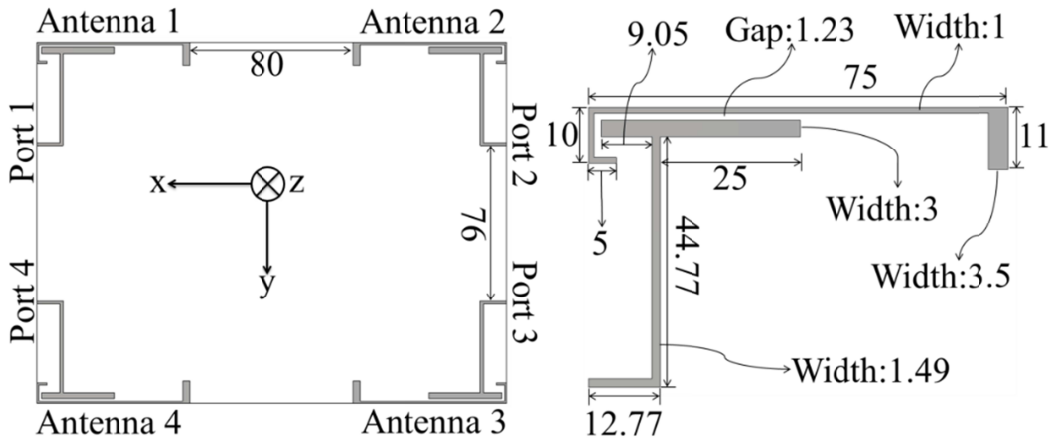

(a)

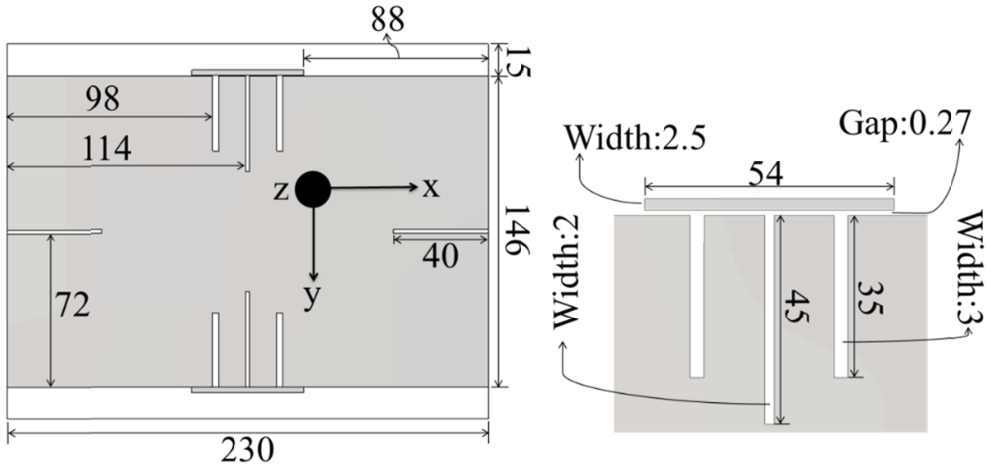

(b)

Figure 5.4: Simulated model of the 4x4 MIMO antennas for 2G/3G mobile tablets. (Units: mm). (a): Front View. (b): Back View.

The simulated model of the MIMO antennas is fabricated on FR-4 substrate with permittivity of 4.4. The fabricated prototype is shown in Figure 5.5. For the measurements of the S-parameters, the antennas were connected to the Agilent® Technologies 2-port network analyzer in the antenna laboratory at Queen Mary, University of London (QMUL). While the radiation pattern and gain measurements were performed inside the anechoic chamber at QMUL.

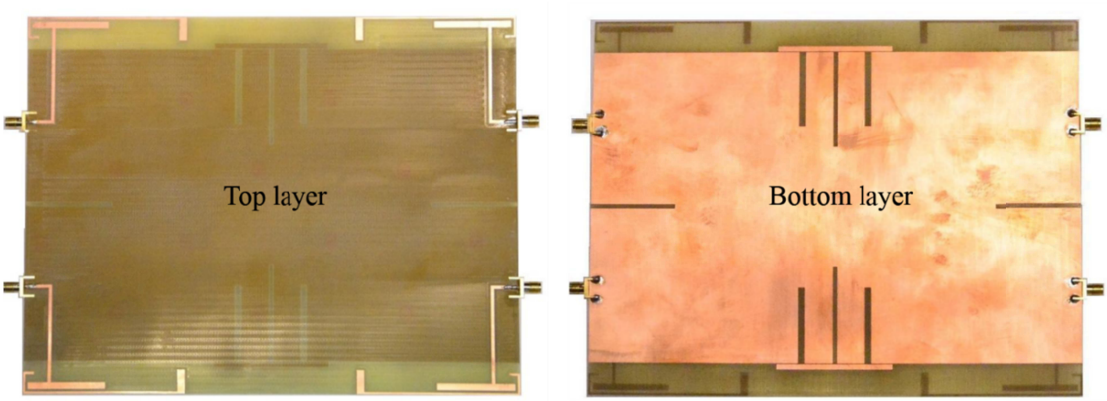

Figure 5.5: Fabricated prototype of the 4x4 MIMO antennas for 2G/3G mobile tablets.

5.1.5 Study of the decoupling structure between 4x4 MIMO antennas:

Different configurations regarding the decoupling structure at the bottom layer of the substrate are shown in Figure 5.6. These configurations represent the stepwise approach for achieving an acceptable isolation between the MIMO antennas. The isolation is best at configuration 6 which is the proposed configuration of the decoupling structure. All other configurations lead to a poor isolation between the 4x4 MIMO antennas. This can be visualized from the surface current distributions shown in Figure 5.8 which are equally-scaled and plotted at 935 MHz. This is because the isolation at a lower frequency is more challenging as compared to the upper frequencies. It can be seen that the horizontal metallic strips majorly improve the isolation by blocking the current from one antenna to reach the other antennas. The isolation between antennas is further improved by introducing slots in the ground plane. However, without the decoupling strips the isolation is very poor as a large amount of current starts flowing between the antennas. So the strips and the slots together make the isolation better than 15 dB. The isolation curves for each configuration are shown in Figure 5.7. It can be seen that the isolation achieved is best at the configuration 6.

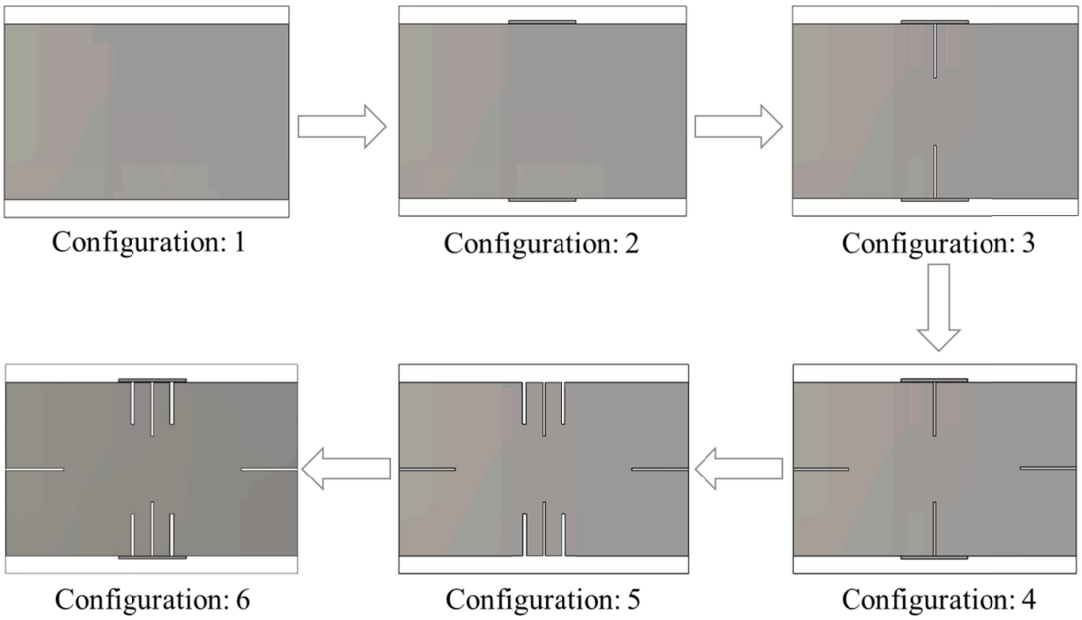

Figure 5.6: Different configurations of the decoupling structure between the 4x4 MIMO antennas.

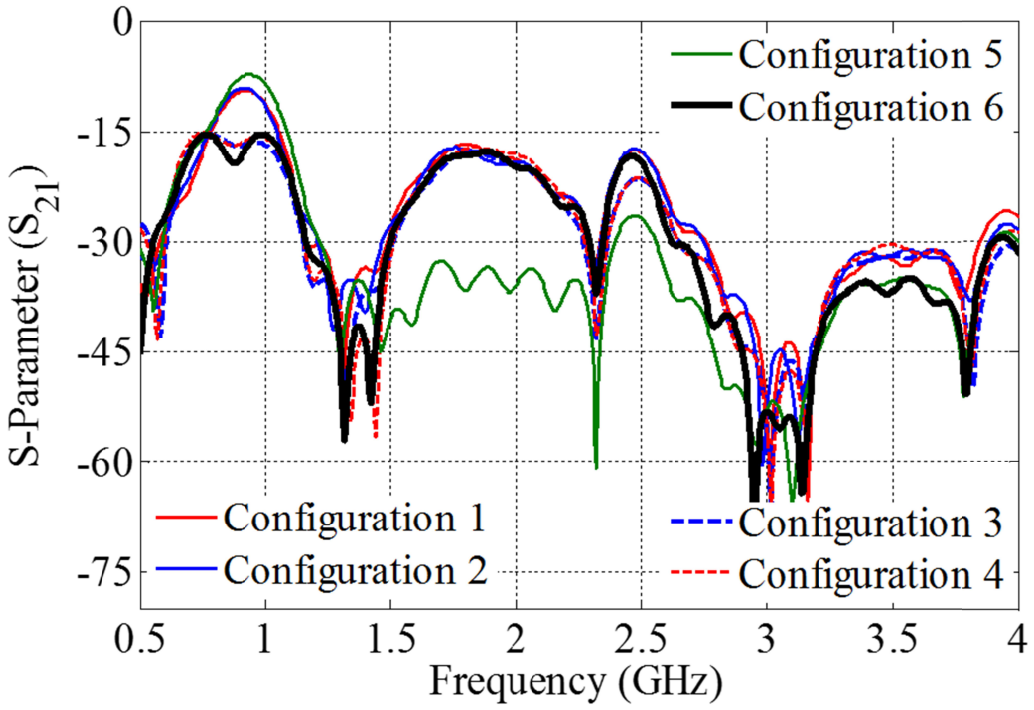

Figure 5.7: Effect of the decoupling structure on the isolation between the 4x4 MIMO antennas.

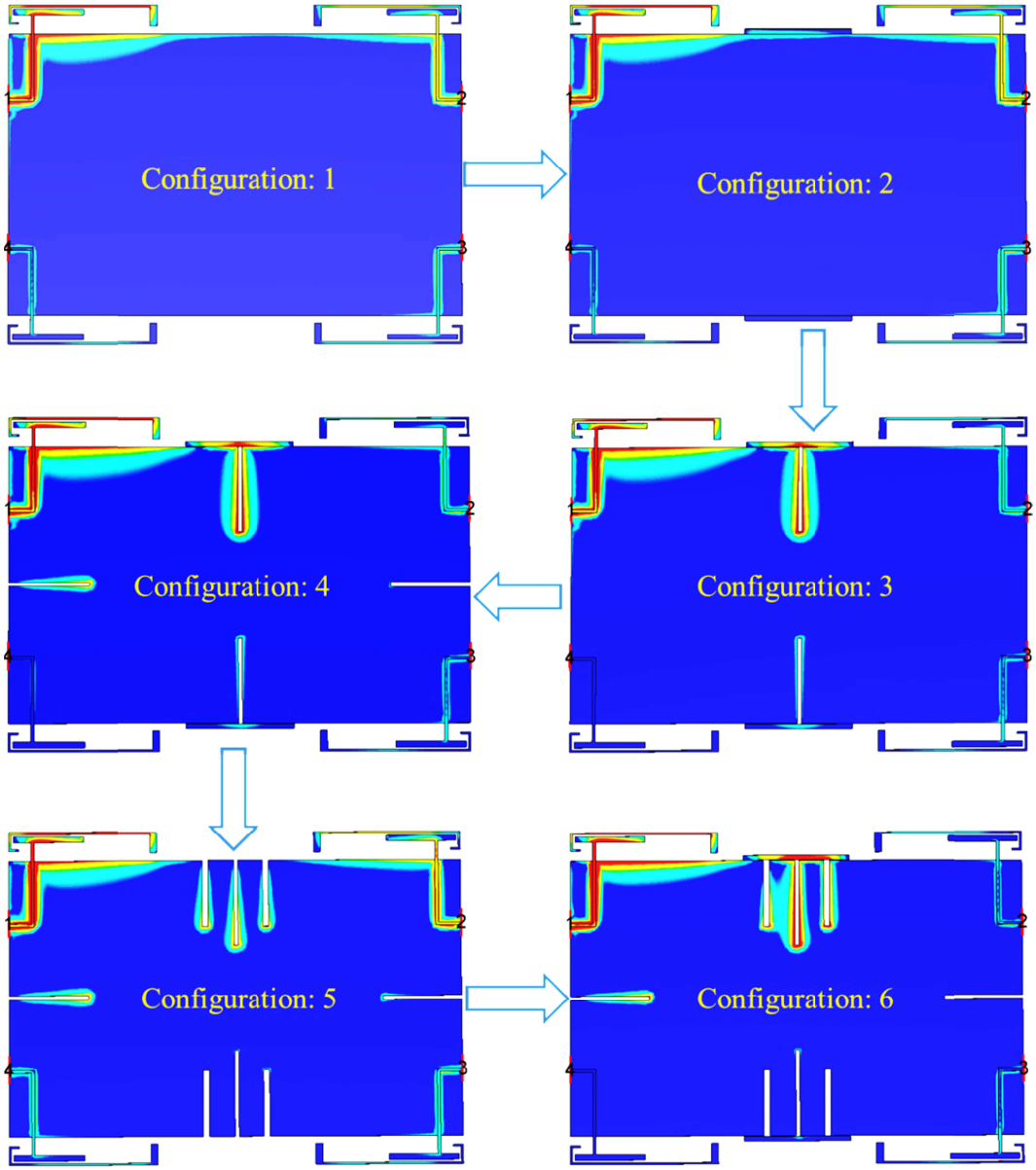

Figure 5.8: Effect of the decoupling structure on the current distribution of the 4x4 MIMO antennas. [Frequency: 935 MHz]

5.1.6 Simulation and measurement results of the 4x4 tablet antennas:

(a) S-parameters:

The simulated and measured s-parameters of the 4x4 MIMO antennas are shown in Figure 5.9. The S-parameters of only one antenna are shown as all were identical. The simulated S-parameters of the MIMO antennas show good agreement with measurement and were nearly the same as for the single antenna. The decoupling performance of the MIMO antennas is represented as S_{21}, S_{31} and S_{41} in Figure 5.9. The isolation achieved is better than 15 dB over all the frequency bands covered by

the antennas. Each antenna is thus capable of covering 2G GSM 900/1800/1900, 3G HSDPA 900/1700/1800/1900, WLAN 802.11n 2.45 GHz and WiMAX 3.4 GHz.

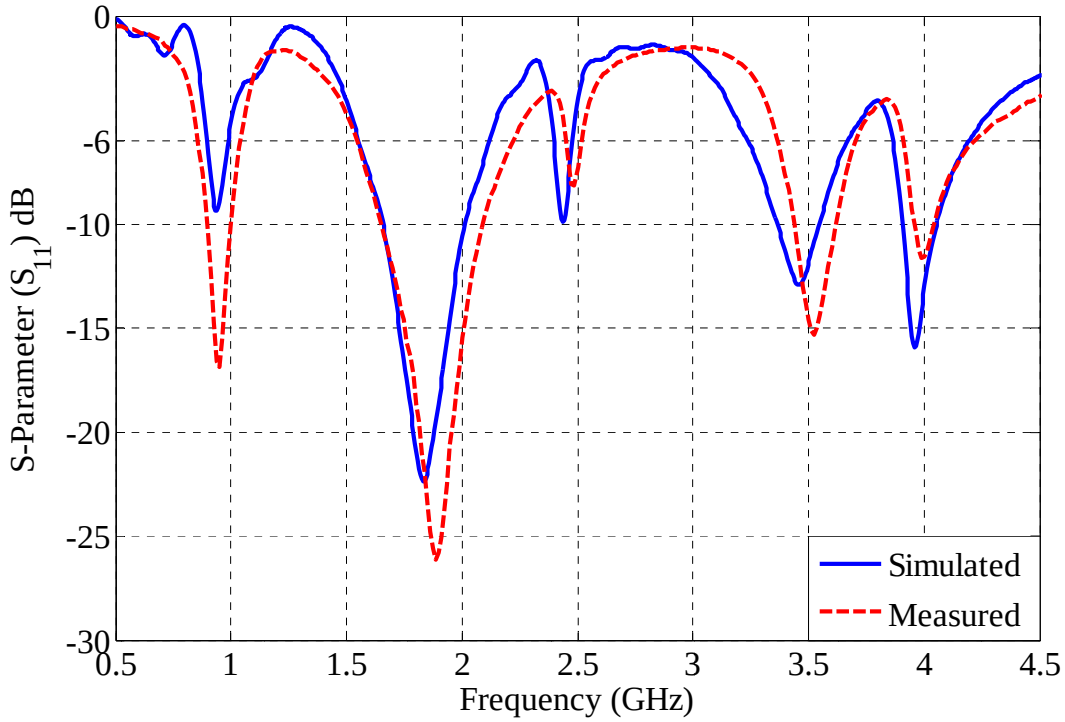

(a)

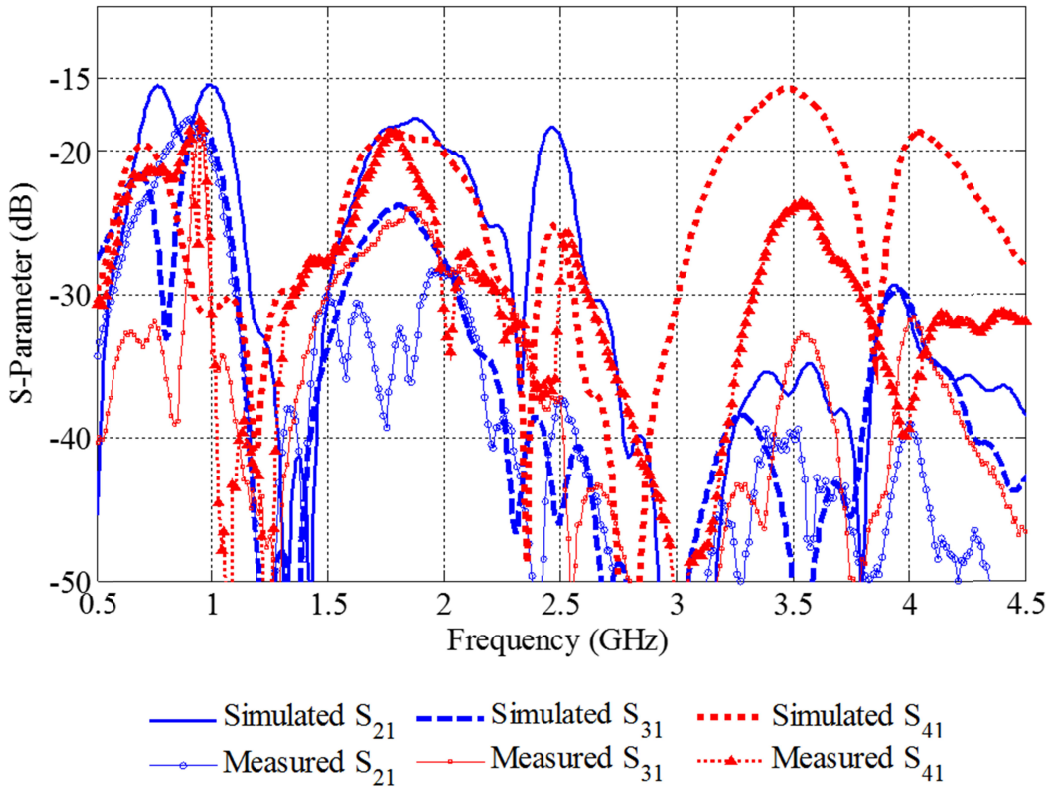

(b)

Figure 5.9: S-parameters of the 4x4 MIMO antennas for 2G/3G mobile tablets. (a): Return loss. (b): Isolation performance.

(b) Current distributions:

The current distributions of the 4x4 MIMO antennas are presented in Figure 5.10. The decoupling technique includes metallic strips that are placed with a small gap from the ground plane. These strips couple a large amount of current thereby restricting the current from one antenna to reach the other antennas. Also the horizontal and vertical slots further improve the isolation at all frequencies. The amount of current propagating in the ground plane is also minor. The radiating lengths of the MIMO antennas are nearly the same as those for the single antenna configuration.

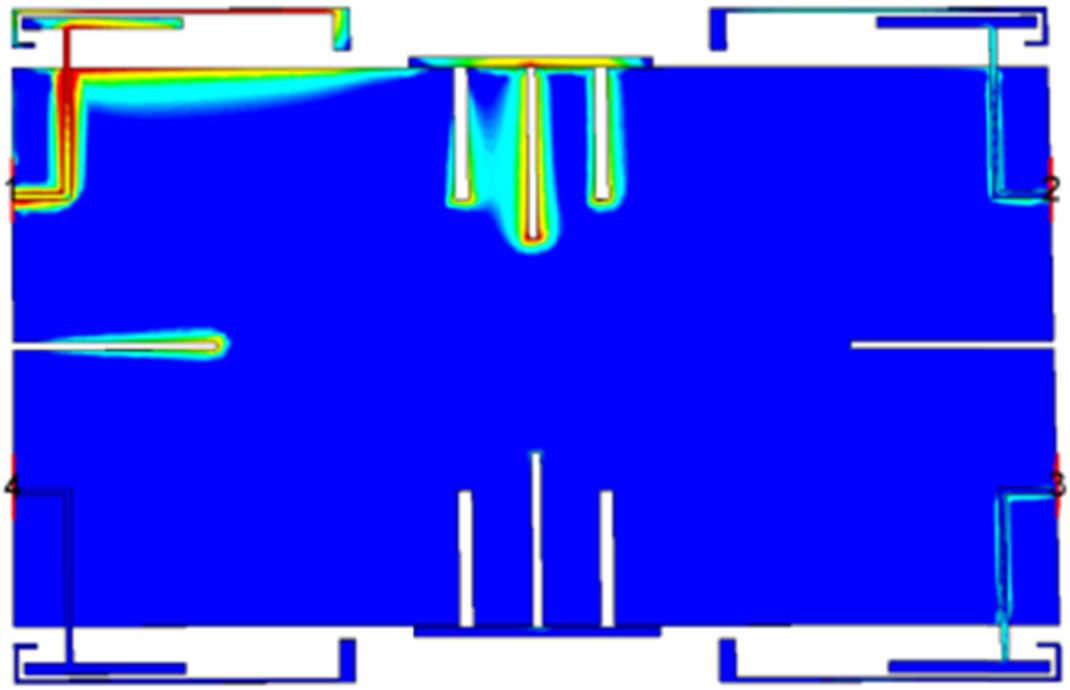

(a)

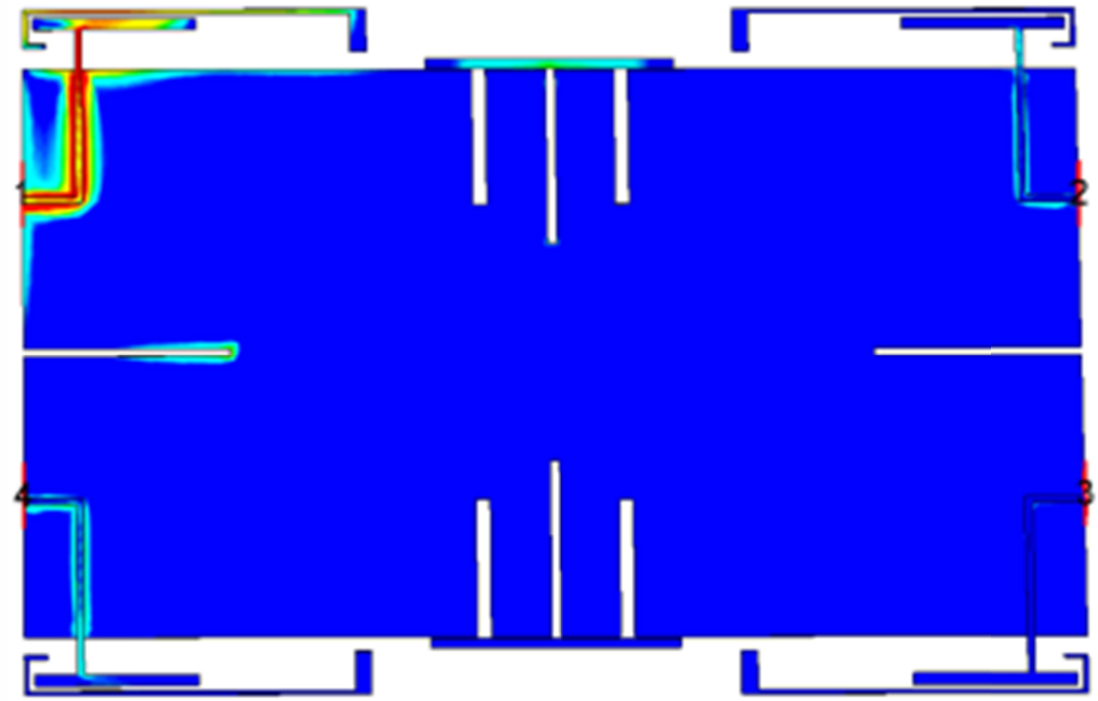

(b)

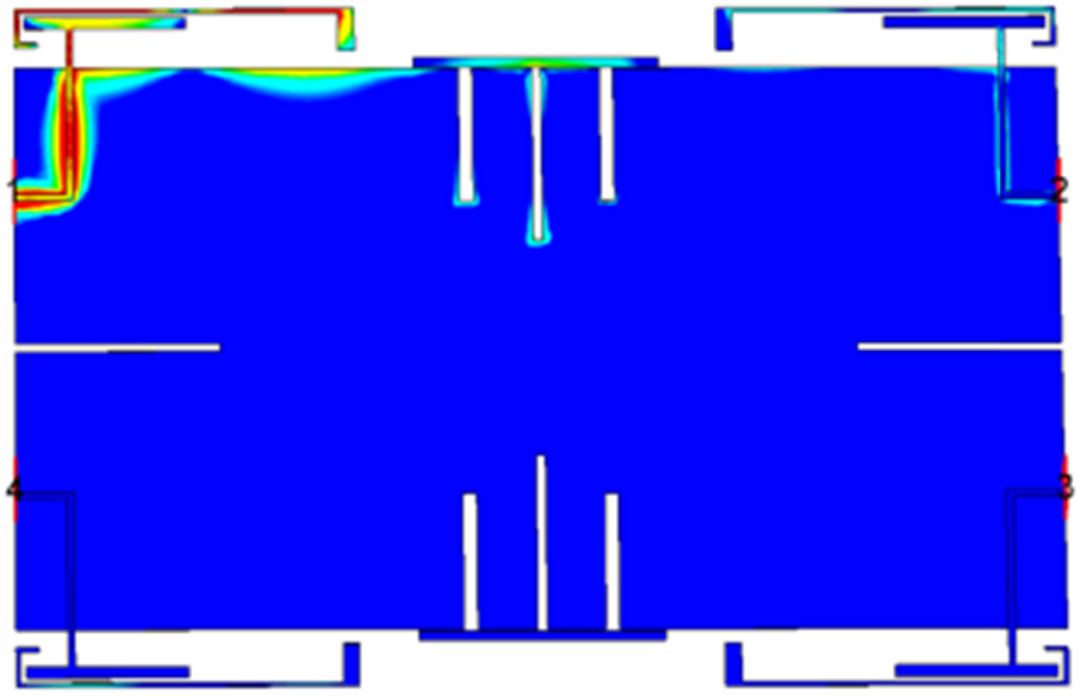

(c)

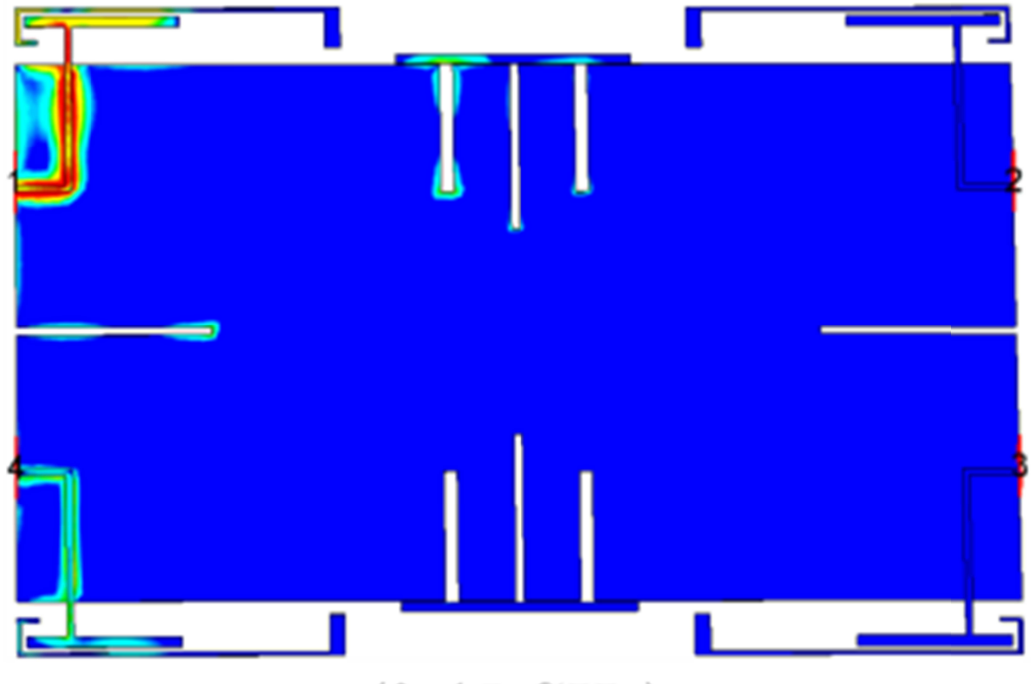

(d)

Figure 5.10: Simulated surface current distributions of the 4x4 MIMO antennas for 2G/3G mobile tablets. (a): At 935 MHz. (a): At 1830 MHz. (a): At 2450 MHz. (a): At 3400 MHz. (Scale: Red: Maximum current; Green: Intermediate current; Blue: Least current)

(c) MIMO antennas Gain and Efficiency:

The gains and efficiencies of the 4x4 MIMO antennas at different frequencies are shown in Table 5.1. The simulated and measured gains of the antenna show a good agreement. The measured gain was calculated by the Gain Comparison method [2]. The measured efficiency was not calculated due to the unavailability of the measurement setup. The gains of only one antenna are tabulated as all the antennas are symmetric.

Table 5.1: Gains, efficiencies and envelope correlation coefficients of the 4x4 MIMO antennas for 2G/3G mobile tablets.

Freq. (MHz)	**Gain (dBi)**		**Efficiency (% age)**	**Bandwidths (MHz)**	**ρe**	
	Sim.	**Meas.**			**Sim.**	**Meas.**
935	1.53	1.22	92.2	0896 – 0987	0.080	0.004
1830	3.61	3.33	95.3	1554 – 2118	0.027	0.004
2450	2.24	1.87	78.3	2397 – 2479	0.009	0.001
3400	3.16	2.85	85.2	3240 – 3665	0.028	0.005

(d) Diversity analysis:

In order to analyze the diversity performance of the MIMO antennas, the envelope correlation coefficients 'ρ_e' and the diversity gains were calculated. The envelope correlation coefficients are calculated using the S-parameters formula discussed in Chapter 4. The peak values have been selected after simulating the MIMO antennas in CST Microwave Studio®. It can be seen from Table 5.1 that the peak value of the envelope correlation coefficient over all the cellular frequency bands covered by the antennas is observed to be 0.08, which is well below the maximum acceptable value of 0.7 [3]-[4].

The diversity gains of the 4x4 MIMO antennas in both indoor and outdoor environments are calculated using the method discussed in Chapter 4. CST® Microwave Studio provides a post processing toolbox for the calculation of the diversity gains. The values of the envelope correlation coefficients and the diversity gains were calculated in both indoor and outdoor environments by simulating the statistical models summarized in [5]-[6]. The diversity gains of the 4x4 MIMO antennas are mentioned in Table 5.2. The values obtained are less than 15 dB and this reduction in the diversity gain is mainly due to less radiation efficiency. The diversity performance of the 4x4 MIMO antennas is better in indoor environment as compared to outdoor environment due to a lower cross polarization ratio (*XPR*). The lowest value obtained for the diversity gain is 11.71 dB at 2.45 GHz. The antennas possess an acceptable diversity performance and can further be improved.

Table 5.2: Diversity gains of the 4x4 MIMO antennas for 2G/3G mobile tablets.

Freq. (MHz)	**Envelope Correlation Coefficient**				**Efficiency**	**Effective Diversity Gain (dB)**	
	Indoor Environment		**Outdoor Environment**		η_r	**Indoor Environment**	**Outdoor Environment**
	ρ_e	DF	ρ_e	DF			
0935	0.0003	0.9998	0.0006	0.9997	0.922	13.82	13.82
1830	0.0100	0.9949	0.0081	0.9959	0.953	14.22	14.24
2450	0.0023	0.9988	0.0049	0.9975	0.783	11.73	11.71
3400	0.0003	0.9998	0.0027	0.9986	0.852	13.82	12.76

5.2 Meandered monopole MIMO antennas for 4G tablets:

This section presents the design and results of MIMO antennas for 4G mobile tablets. Antennas are modeled in MIMO configuration and cover 4G LTE cellular frequency bands.

5.2.1 Design and modelling of the MIMO antennas:

The top layer of the simulation model is shown in Figure 5.11 and the bottom layer in Figure 5.12. The proposed design is composed of two pairs of MIMO antennas in meandered monopole configuration. Each pair is designed to cover separate frequency bands. The pair covering 4G cellular services is composed of two direct fed monopole antennas whereas, the pair covering 2G and 3G cellular services consists of two coupled feed monopoles in meandered form. The antennas are printed on the upper and lower no-ground areas of the substrate. The material used for the substrate is FR-4 with relative permittivity of 4.35 and loss tangent of 0.02. The volume of the substrate is 230 x 176 x 0.8 mm^3 with each pair printed on a no-ground portion of 230 x 15 mm^2. The antenna for 4G cellular coverage occupies an area of 75 x 10 mm^2, whereas, the antenna for 2G and 3G cellular coverage occupies the area of 75 x 11 mm^2. The antennas are printed in diagonal symmetry to achieve a good isolation performance. However, being closely spaced the antennas did not show an acceptable isolation and due to this a decoupling structure was etched on the bottom layer of the substrate.

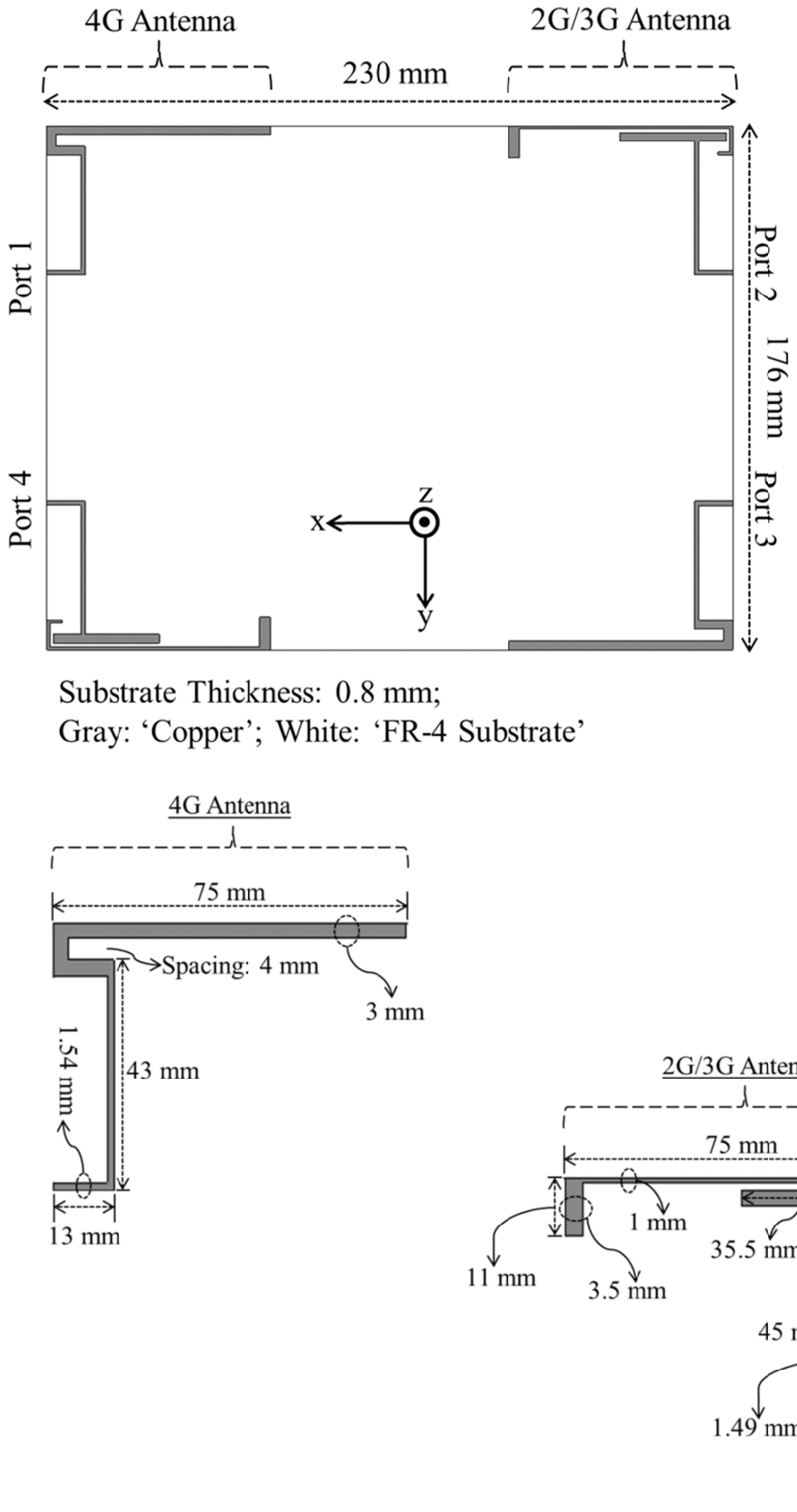

Figure 5.11: Top layer of the simulated model of the meandered monopole MIMO antennas for 4G mobile tablets.

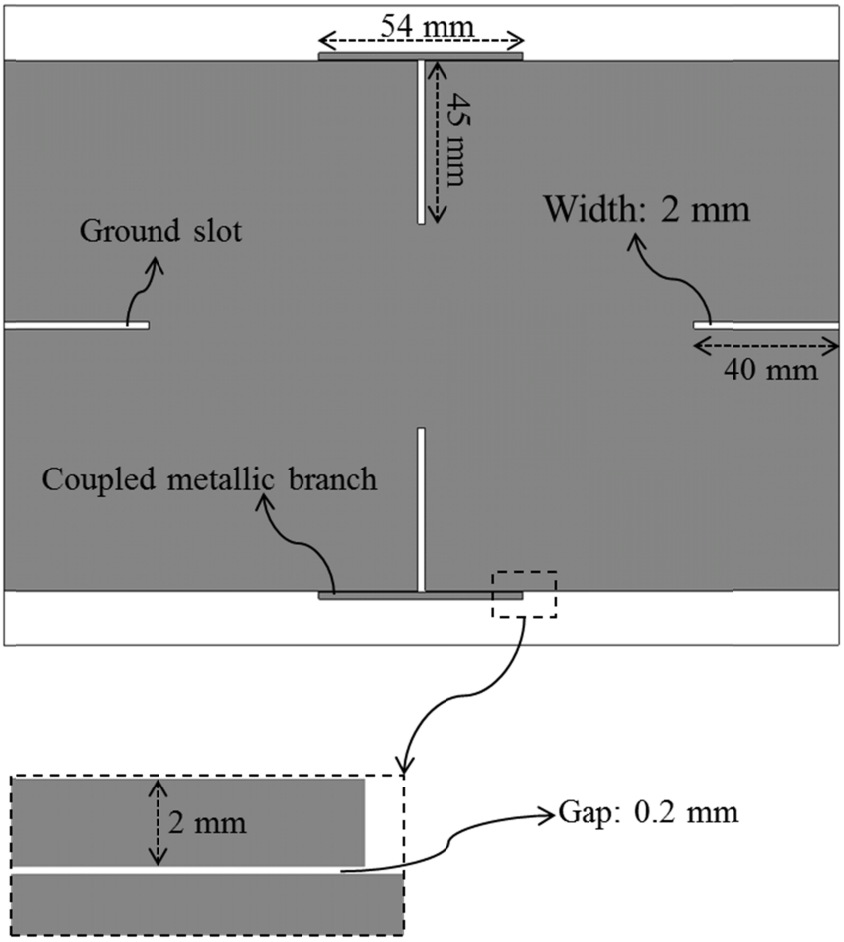

Figure 5.12: Bottom layer of the simulated model of the meandered monopole MIMO antennas for 4G mobile tablets.

The model shown in Figure 5.12 presents a dual decoupling structure composed of the ground slots and coupled metallic extensions. The coupled metallic extensions are placed at a gap of 0.2 mm from the ground plane. This provides a coupling path for the current and thus limits the current to flow from one antenna to the other antennas. For further improvement in isolation between the MIMO antennas, four slots have been etched in pairs into the ground plane. Each pair is composed of two slots arranged in mirrored configuration to make the isolation between each antenna pair better than 15 dB. A prototype of the MIMO antennas is shown in Figure 5.13. The proposed design offers more simplicity and covers more cellular frequencies than the 4x4 MIMO antennas presented earlier in this chapter.

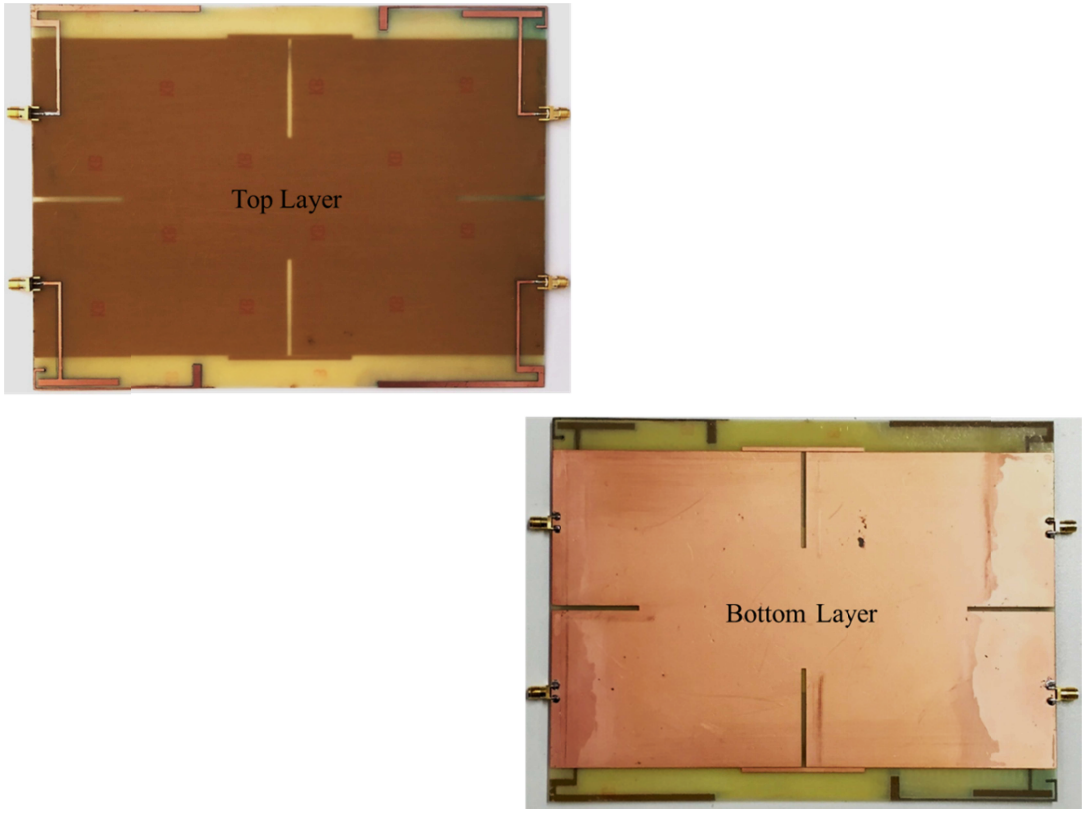

Figure 5.13: Fabricated prototype of the meandered monopole MIMO antennas for 4G mobile tablets.

5.2.2 Working mechanism:

The meandered monopole MIMO antennas presented in this design are printed in pairs with one pair primarily designed to cover 2G/3G cellular services and the other pair for 4G frequency bands. The radiating lengths can be calculated from the simulated current distributions shown in Figure 5.14. For example, at 0.75 GHz the strip length of the 4G antenna contributing to the radiation is 'a-b-c-d'. The combined length of 'a-b-c-d' is 92 mm which is nearly 0.25λ at 0.75 GHz. At 0.93 GHz the strip length of the 3G antenna contributing to the radiation is 'c-d-e'. The combined length thus calculated is 83 mm which is nearly 0.25λ at 0.93 GHz. The decoupling between antennas is achieved by introducing ground slots and additional coupled branches at the bottom layer of the substrate. Being placed at a gap of 0.2 mm, the coupled branches draw a large amount of current thereby restricting the current from one antenna to reach the other antennas. This largely improves the isolation achieving a good diversity performance.

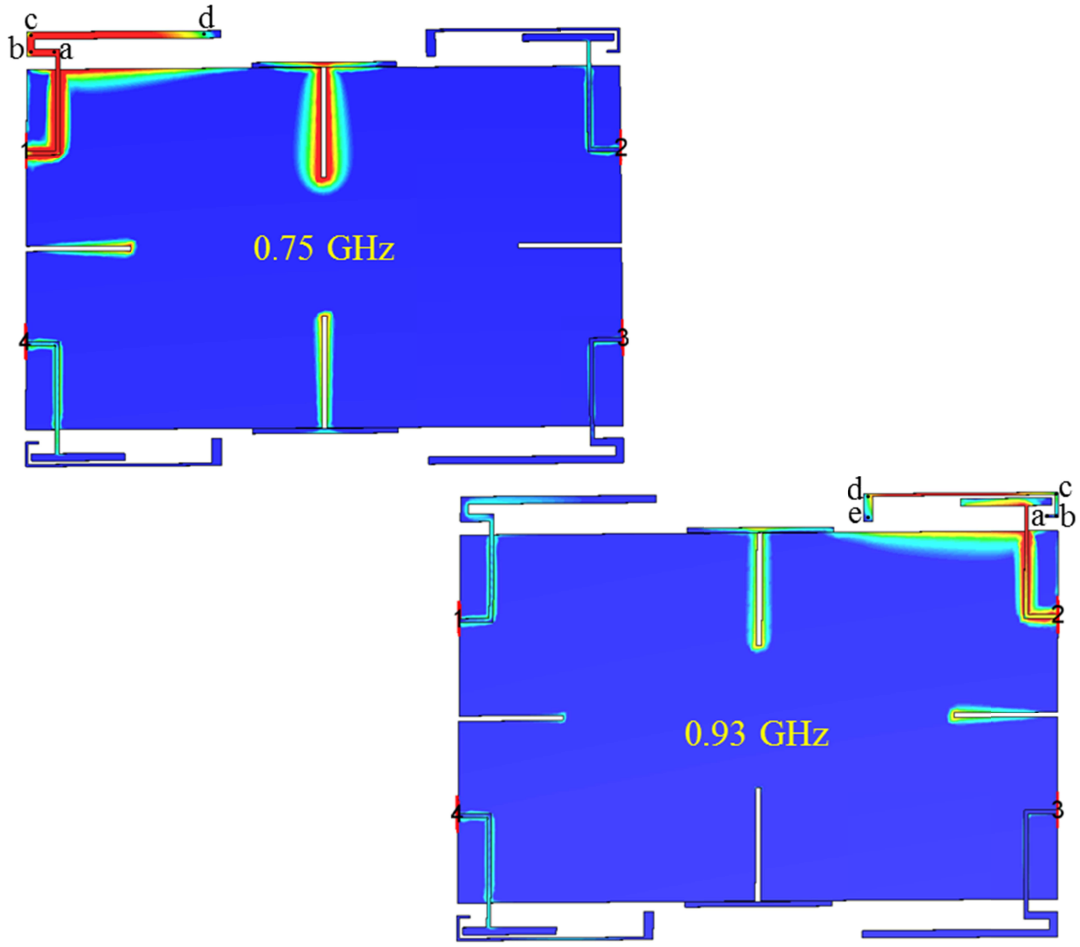

Figure 5.14: Surface current distributions of the meandered monopole MIMO antennas for 4G tablets at different frequencies. (Scale: Red: Maximum current; Green: Intermediate current; Blue: Least current)

5.2.3 Simulation and measurement results:

The meandered monopole MIMO antennas were simulated in CST® Microwave Studio and the simulated S-parameters and radiation patterns were extracted. For the S-parameter measurements, the antennas were connected to the Agilent® Technologies 2-port network analyzer in the antenna laboratory at QMUL. The radiation pattern and gain measurements were performed inside the anechoic chamber at QMUL. The simulation and measurement results were then post processed in Matlab® for ease of analysis and comparison.

(a) S-parameters:

The simulated and measured S-parameters of the meandered monopole MIMO antennas are shown in Figure 5.15. The S-parameters of only one antenna in each pair are shown as the two antennas in each pair are identical.

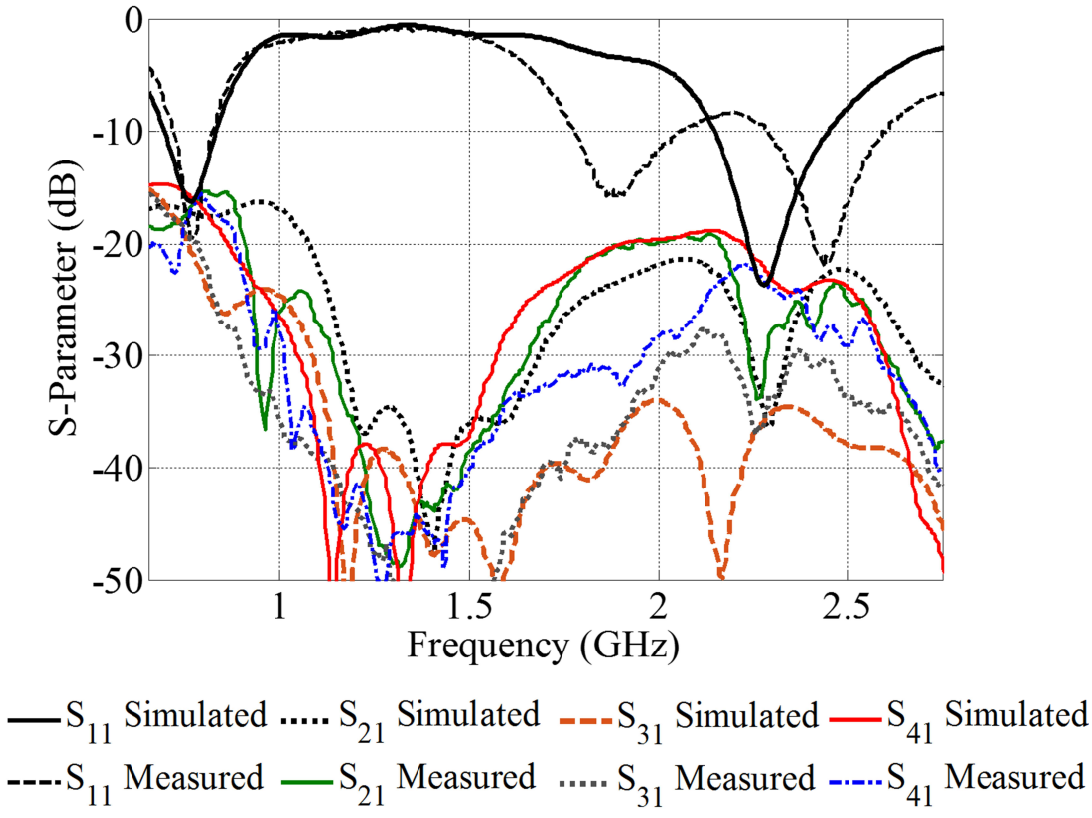

(a)

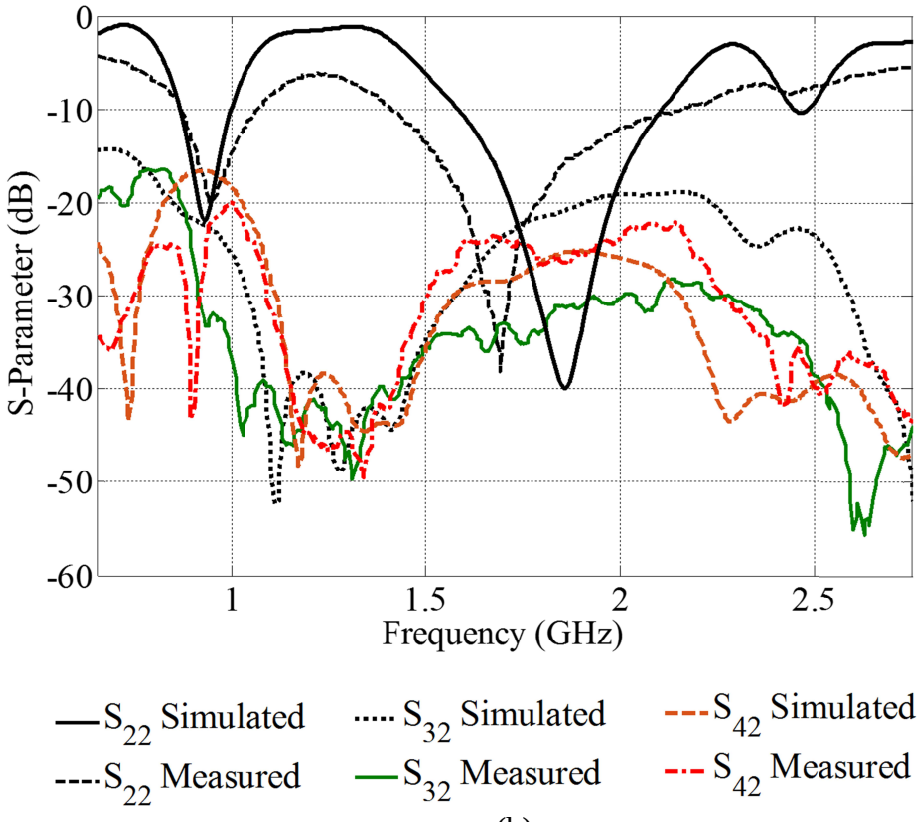

(b)

Figure 5.15: S-parameters of the meandered monopole MIMO antennas for mobile tablets. (a): S-parameters of 4G antenna pair. (b): S-parameters of 3G antenna pair.

The simulated S-parameters show a good agreement with measurement. Each antenna of the 4G pair resonates in two frequency bands ranging from 680 MHz to 865 MHz and 2073 MHz to 2557 MHz when referenced to a return loss of 6 dB. The antennas are thus capable of covering 4G LTE bands 12-13, 17-18, 20, 28-29 (680 – 865 MHz), 4G LTE band 30 (2305 – 2360 MHz) and WLAN 802.11n 2.45 GHz (4 x4 MIMO). Likewise, each antenna of the 3G pair resonates in three frequency bands ranging from 830 MHz to 998 MHz, 1503 MHz to 2183 MHz and 2380 MHz to 2550 MHz. The antennas therefore cover 2G GSM 850/900/1800/1900 and 3G HSDPA 800/850 /900/1700/1900/2100 cellular frequency bands. In combination, the MIMO antennas cover numerous commercial 2G, 3G and 4G cellular frequency bands with a measured isolation better than 15 dB over all the frequency bands accommodated by the MIMO pairs. The return loss and isolation results corroborate a good performance of the MIMO antennas.

(b) Radiation patterns:

The simulated 3D radiation patterns of the meandered monopole MIMO antennas are shown in Figure 5.16. The radiation patterns were measured inside the anechoic chamber at QMUL. The co-polar (*phi*) and cross-polar (*theta*) components of the radiation pattern are plotted in both x-z and y-z planes at different frequencies. Figure 5.17 presents the polar plots comparing simulated radiation patterns with the measured ones for the 4G MIMO antennas. Whereas, Figure 5.18 presents the polar plots comparing simulated radiation patterns with the measured ones for the 2G/3G MIMO antennas. The simulated radiation patterns agree well with the measured ones. However, there are some discrepancies which mainly occurred due to the fabrication imperfections, substrate tolerances and the measurement setup.

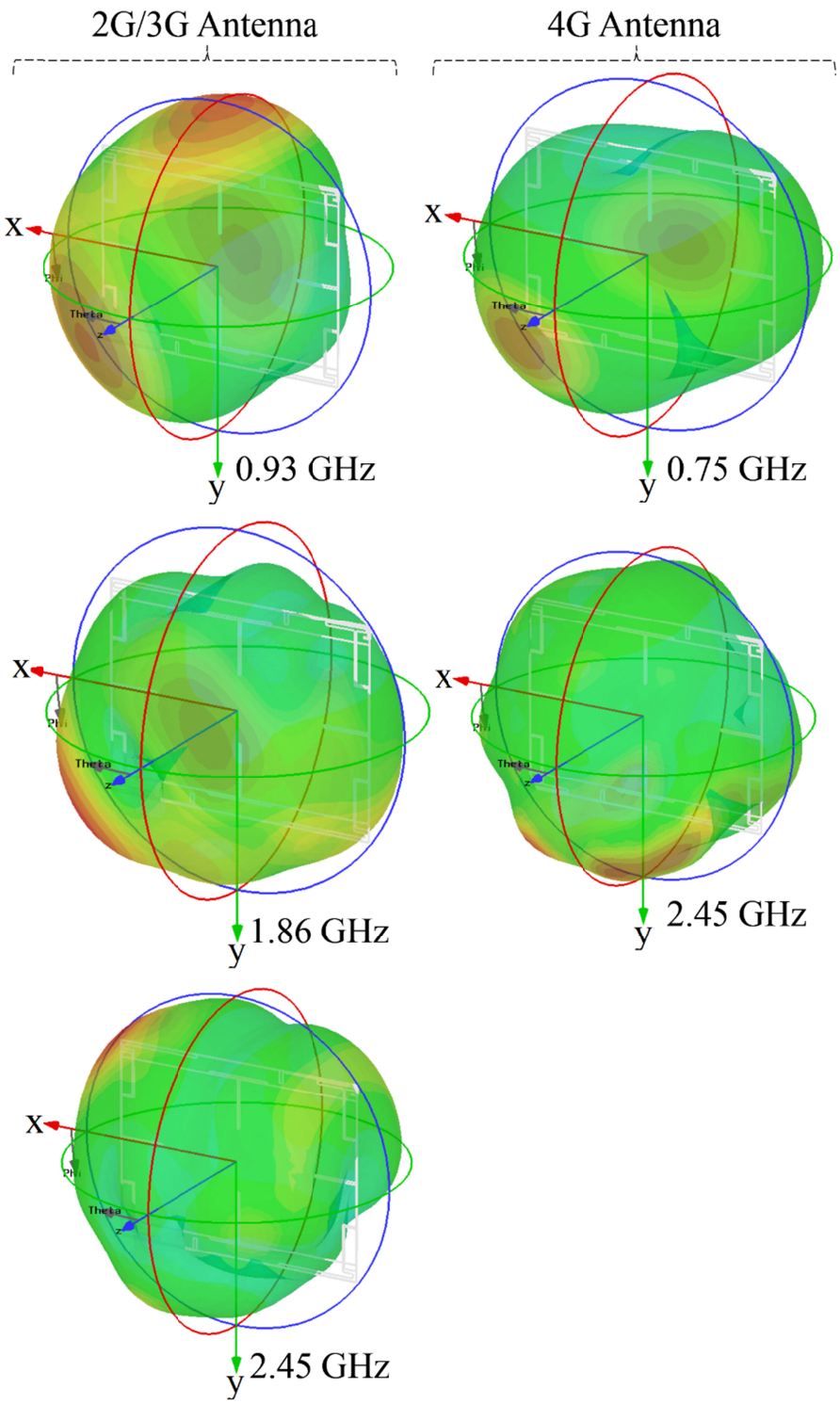

Figure 5.16: Simulated 3D Radiation patterns of the meandered monopole MIMO antennas for 4G mobile tablets.

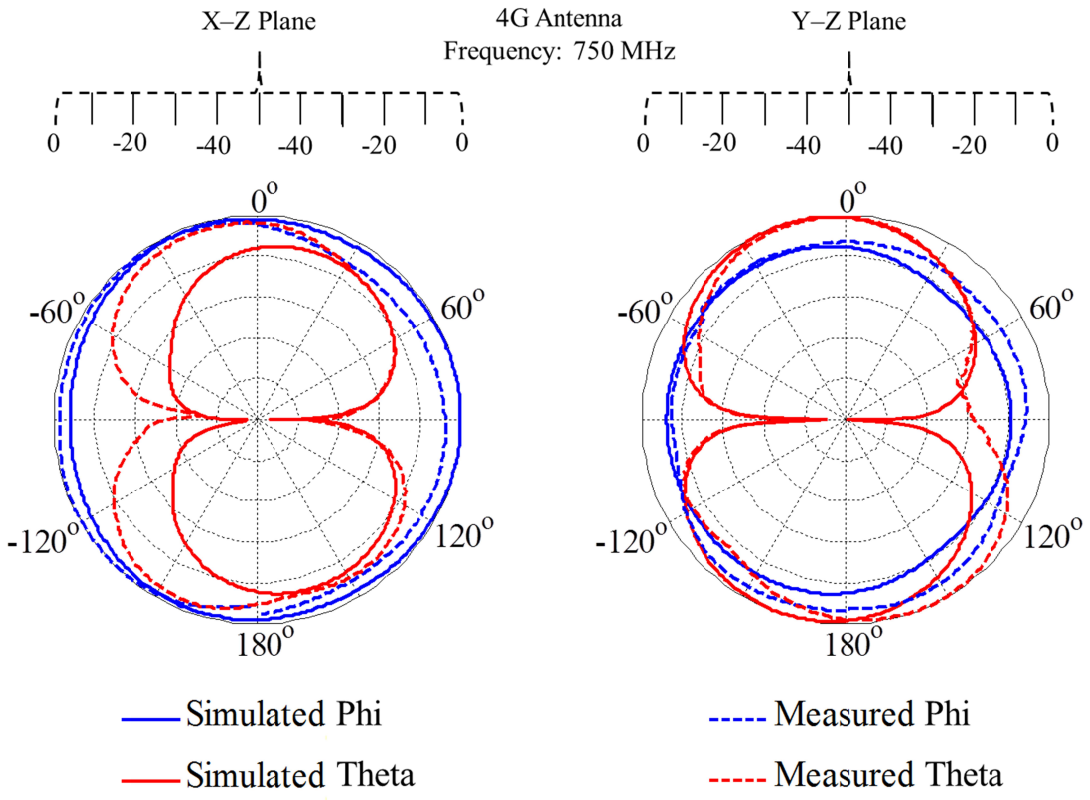

Figure 5.17: 2D radiation patterns of the 4G pair of the meandered monopole MIMO antennas.

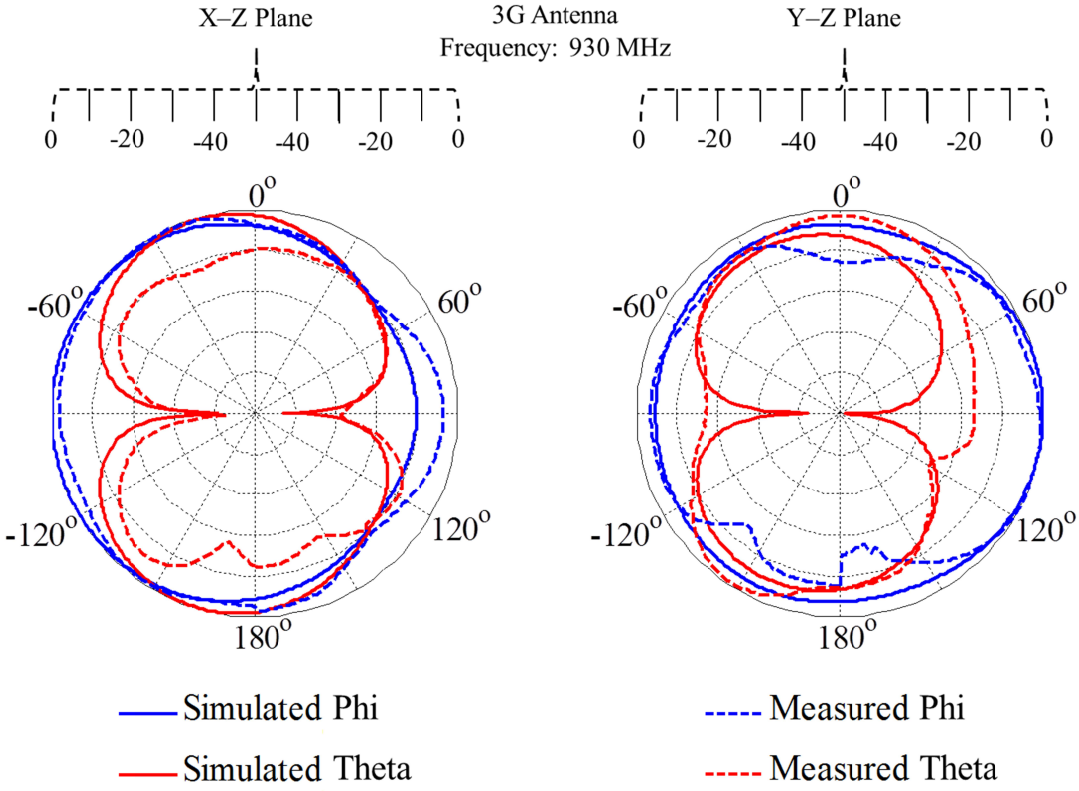

(a)

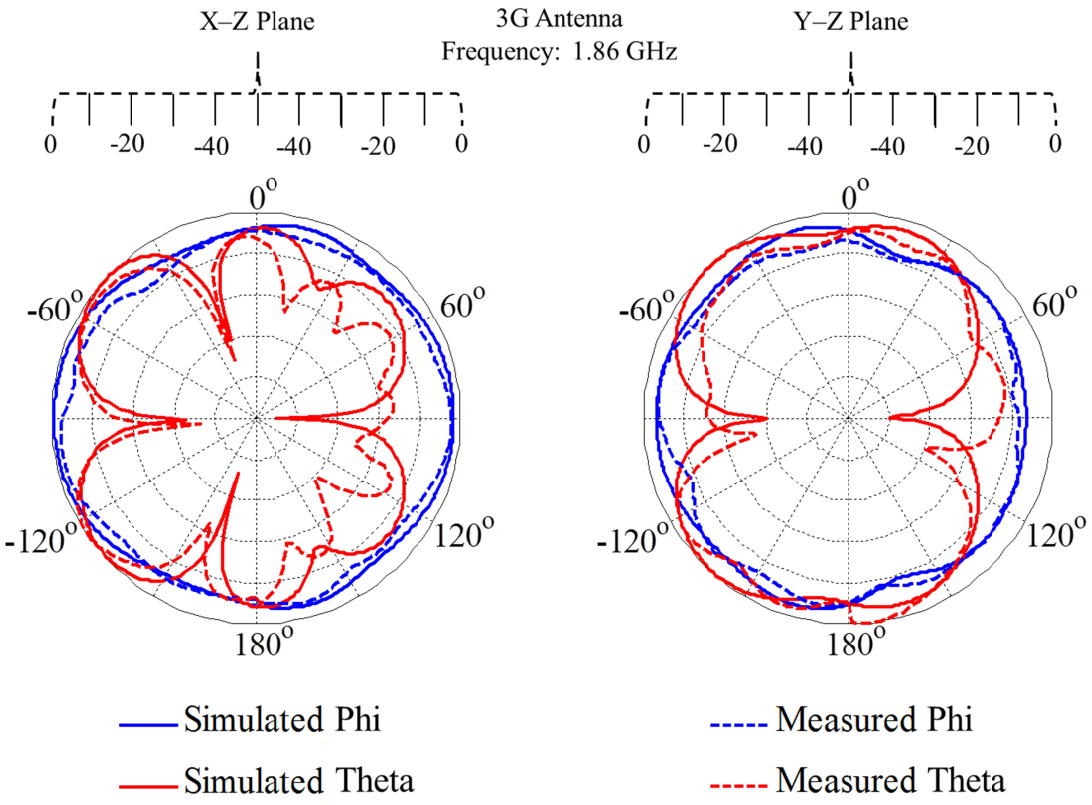

(b)

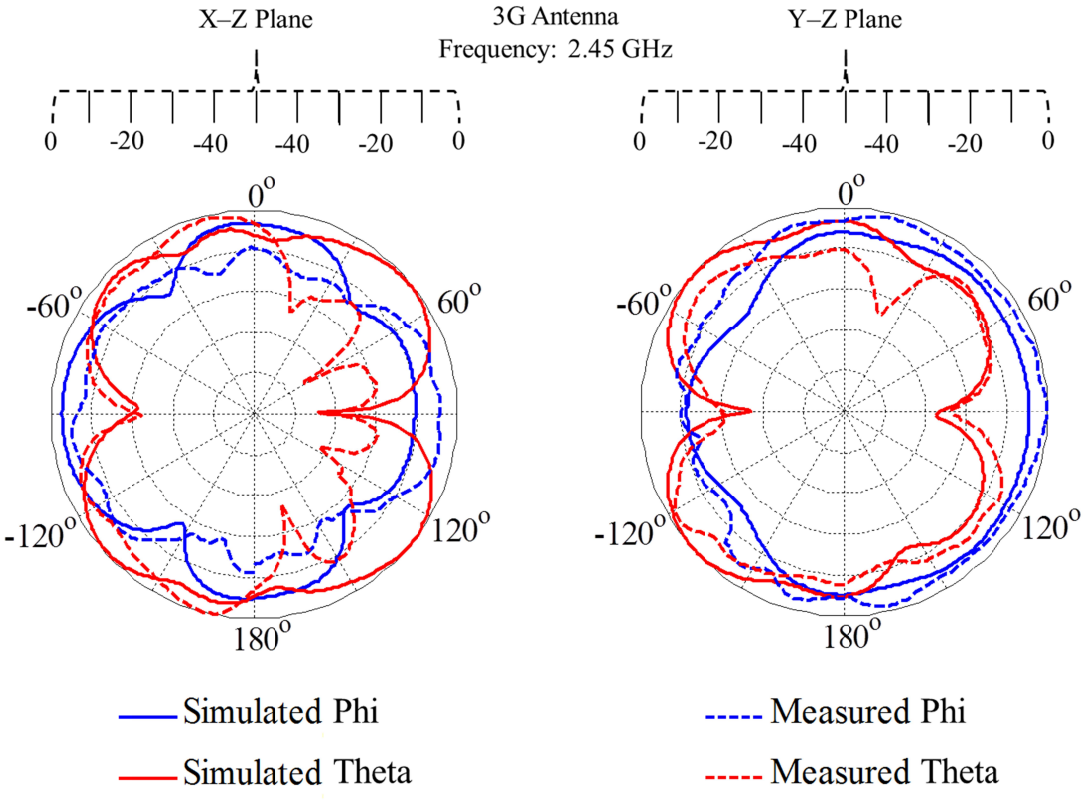

(c)

Figure 5.18: 2D radiation patterns of the 3G pair of the meandered monopole MIMO antennas. (a): At 930 MHz. (b): At1860 MHz. (c): At 2450 MHz.

(c) Antenna Gain and Efficiency:

The gains and efficiencies of the meandered monopole MIMO antennas for 4G tablets are shown in Table 5.3. The simulated and measured gains of the antenna show a good agreement. The measured gain is calculated by the Gain Comparison method [2]. The measured efficiency is not calculated due to the unavailability of the measurement setup. The gains and efficiencies of only one antenna in each pair are tabulated as both the antennas are identical.

Table 5.3: Gains and efficiencies of the proposed meandered monopole MIMO antennas for 4G mobile tablets.

Frequency (GHz)	**Gain (dBi)**		**Total Efficiency (% age)**
	Simulated	**Measured**	
0.75 (4G Antenna)	0.89	0.61	47.8
0.93 (3G Antenna)	3.12	2.75	86.7
1.86 (3G Antenna)	5.26	4.32	94.2
2.45 (3G Antenna)	2.47	1.89	61.1

(d) Envelope correlation coefficients:

In order to analyze the diversity performance of the meandered monopole MIMO antennas, the envelope correlation coefficients 'ρ_e' were calculated and are shown in Figure 5.19. The envelope correlation coefficients were calculated using the S-parameters formula discussed in Chapter 4. It can be seen from the graph that the peak points are well below the maximum acceptable value of 0.7 [3]-[4]. This is due to a good isolation between the antennas which enhances the diversity performance.

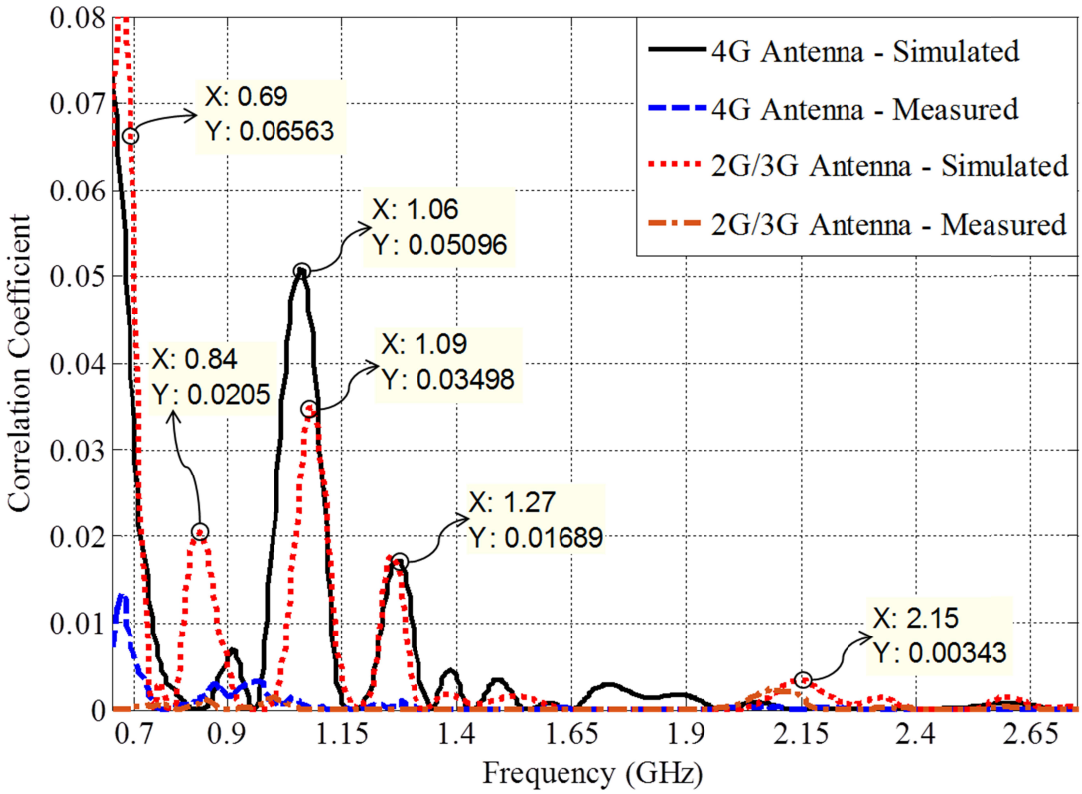

Figure 5.19: Envelope correlation coefficients of the meandered monopole MIMO antennas for mobile tablets.

Summary

Two designs of multiband antennas, capable of covering 2G, 3G and 4G cellular frequencies, for tablet applications were presented in this chapter. A comparison of the designs is shown in Table 5.4. A design of 4x4 MIMO antennas for covering 2G and 3G cellular frequencies was presented in the first section whereas, a MIMO design for 4G tablets was presented in the second section. The designs were based on a meandered monopole configuration. The design for 2G/3G cellular tablets is composed of four symmetrically placed coupled feed monopole antennas printed on the top layer of the substrate and a decoupling structure is etched at the bottom layer. The MIMO design for 4G tablets is composed of four antennas that were printed in pairs and placed diagonally in the no-ground area of the substrate. Each pair was designed to cover different cellular frequencies with one pair covering 4G LTE and the other covering 2G and 3G frequency bands. The simulation and measurement results have corroborated a good performance of the MIMO designs. The isolation achieved in both designs is better than 15 dB in all frequency bandwidths

accommodated by the antennas. The antennas are compact with good cellular coverage making them suitable for implementation in cellular tablets and PDAs.

Table 5.4: Comparison of the proposed MIMO antenna designs for mobile tablets.

MIMO Design	6dB Bandwidths (MHz)	Freq. (GHz)	Gain (dB)		Efficiency (%)	Minimum Isolation (dB)		Envelope Correlation Coefficient
			Sim.	*Mea.*		*Sim.*	*Mea.*	
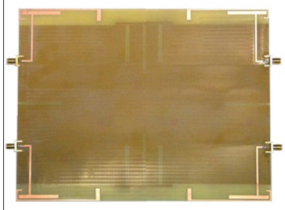	0896 – 0987	0.93	1.53	1.22	92.2	17.2	18.8	0.080
	1554 – 2118	1.86	3.61	3.33	95.3	18.1	36.1	0.027
	2397 – 2479	2.45	2.24	1.87	78.3	18.6	19.8	0.009
	3240 – 3665	3.40	3.16	2.85	85.2	16.3	26.2	0.028
- 4x4 MIMO Antennas - Substrate: 230 x 176 mm² - Antenna: 75 x 11 mm²	**Average →**		2.64	2.32	87.7	17.6	25.2	0.049
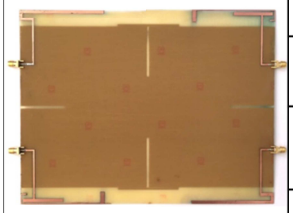	0680 – 0865	0.75	0.89	0.61	47.8	15.6	17.5	0.0075
	830 – 998	0.93	3.12	2.75	86.7	16.6	26.1	0.0008
	1503 – 2183	1.86	5.26	4.32	94.2	20.8	26.1	0.0002
	2073 – 2557	2.45	2.47	1.89	61.1	22.9	34.3	0.0001
	2380 – 2550							
- 4 Antennas; 2 MIMO Pairs - Substrate: 230 x 176 mm² - Antenna 4G: 75 x 10 mm² - Antenna 3G: 75 x 11 mm²	**Average →**		2.94	2.39	72.5	19.0	26.0	0.0022

References

[1] CST® Microwave Studio, Computer Simulation Technology Homepage [Online]. Available: http://www.cst.com, Version, 2013.04, Release, Oct 04, 2013

[2] Balanis, C. A., "Antenna Theory Analysis and Design", Edition, 3rd, A John Wiley & Sons, Inc., Publication, ISBN 0-471-66782-X, 2005.

[3] S.R. Saunders, “Antennas and propagation for wireless communication systems”, Wiley, 1999.

[4] M. Schwartz, W. R. Bennet and S. Stein, “Communication systems and techniques”, McGraw Hill, 1996.

[5] V. Plicanic, “Antenna Diversity Studies and Evaluation”, Master Thesis, LUND University in cooperation with Ericsson Mobile Communications AB, May 2004.

[6] Z. Ying, “Characterization of multi-channel antenna performance for mobile terminal by using near field and far field parameters,” COST 273 TD (04) (095) Goteborg, Sweden, June, 2004.

CHAPTER 6

PATTERN RECONFIGURABLE MIMO ANTENNAS FOR MOBILE HANDSETS

In this chapter a design composed of two MIMO antennas, modelled and optimized through simulations in CST Microwave Studio®, is presented [1]. The antennas are pattern reconfigurable and cover multiple cellular frequencies with acceptable isolation performance. Details of the design and the results will be discussed in later sections.

6.1 Design and modelling of the pattern reconfigurable MIMO antennas:

6.1.1 Antenna design:

The simulated model of pattern reconfigurable MIMO antennas for mobile handsets is presented in Figure 6.1. The proposed design is composed of two MIMO antennas in meandered monopole configuration. The antennas are printed on the no-ground areas along the longer edges of the substrate. The material used for the substrate is FR-4 with relative permittivity of 4.35 and loss tangent of 0.02. The volume of the substrate board is 120 x 65 x 1.6 mm^3. Each antenna is printed on a no-ground part of 120 x 15 mm^2 and occupies an area of 26.5 x 14.5 mm^2. The antennas are printed in diagonal symmetry to achieve a good isolation performance. The top layer of the substrate is composed of two antennas while the ground plane is etched on the bottom layer presented as dashed red line in the Figure 6.1. Each antenna of the MIMO configuration is coupled fed monopole in meandered form. The coupling gap and the

dimensions of the monopole have been selected through optimization in CST® Microwave Studio. The antennas are made pattern reconfigurable by connecting and disconnecting a 4.5 x 2 mm^2 metallic strip using Infineon BAR 50-02V p-i-n diode switches. The p-i-n diode switches exhibit an area of 1 x 0.8 mm^2 and are soldered in Gap_1. The lumped components model of the diode switch is shown in Figure 6.2. The diode has a resistance of 3Ω and inductance of 0.6 nH in the forward biased mode, whereas, when reverse biased it has a resistance, capacitance and inductance of 5000Ω, 0.15pF and 0.6nH respectively. A variable DC power supply is used to bias the p-i-n diode with a voltage of 0.95V and a current of 20mA. The metallic strip can be connected or disconnected to alter the surface current distributions thereby achieving pattern reconfigurability. The biasing wires run through the bottom layer of the substrate and are connected to the antennas through via holes. Coilcraft fixed value RF inductors are placed in Gap_2 to choke the RF current from flowing into the biasing wires. The value of the inductance is 56 nH that was selected through optimization in CST Microwave Studio®. A prototype of the MIMO antennas was developed and shown in Figure 6.3.

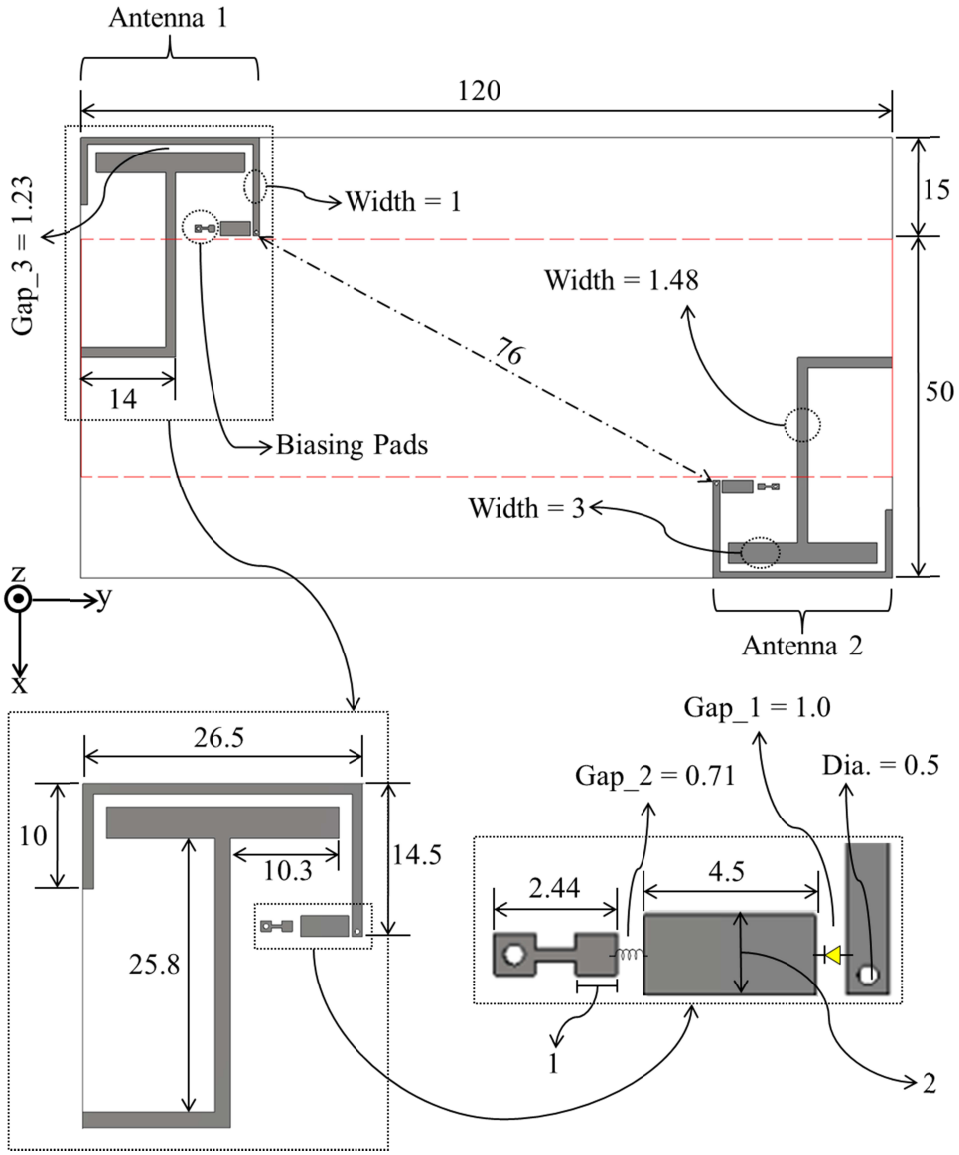

Figure 6.1: Simulated model of the pattern reconfigurable MIMO antennas for mobile handsets.

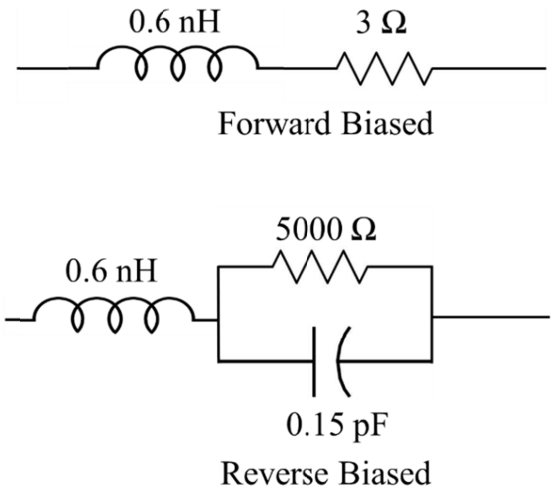

Figure 6.2: Lumped components representation for the Infineon BAR 50-02V switch.

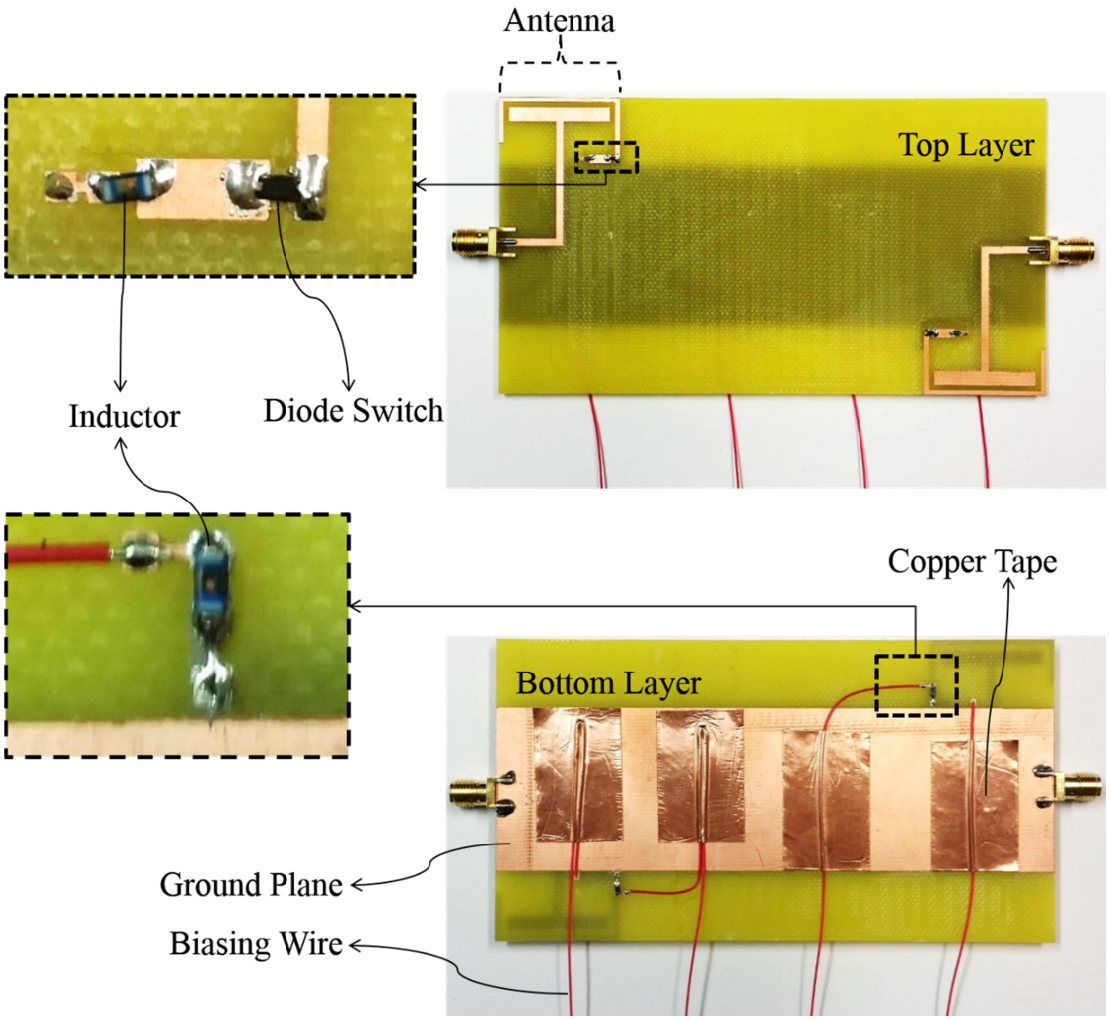

Figure 6.3: Fabricated prototype of the pattern reconfigurable MIMO antennas for mobile handsets.

6.1.2 Working mechanism:

The MIMO antennas proposed in this work are monopoles that are meandered for a compact volume. Each antenna is connected to an extended metallic branch printed with a gap of 1 mm. The connection between the antenna and the metallic branch can be made using the p-i-n diode switch. The p-i-n diode switch exhibits strict size and temperature limits which made it not suitable to be soldered in traditional way. The soldering of the p-i-n diode is thus done using the conductive epoxy. The biasing wires are attached to the variable DC power supply to connect or disconnect the p-i-n diode for achieving 'ON' and 'OFF' states. When the p-i-n diode is turned to the 'ON' state, a shorting path is established and the strip starts radiating. This can be seen from the current distribution shown in Figure 6.4. The amount of current through

the metallic strip in the 'OFF' state of p-i-n diode is less as compared to the current in the 'ON' state of the p-i-n diode. The variation in the amount of current passing through the metallic strip changes the surface current distribution of the antenna which in turn shifts the radiation pattern. The antennas are pattern reconfigurable in the bandwidth of 1.9–2.1 GHz.

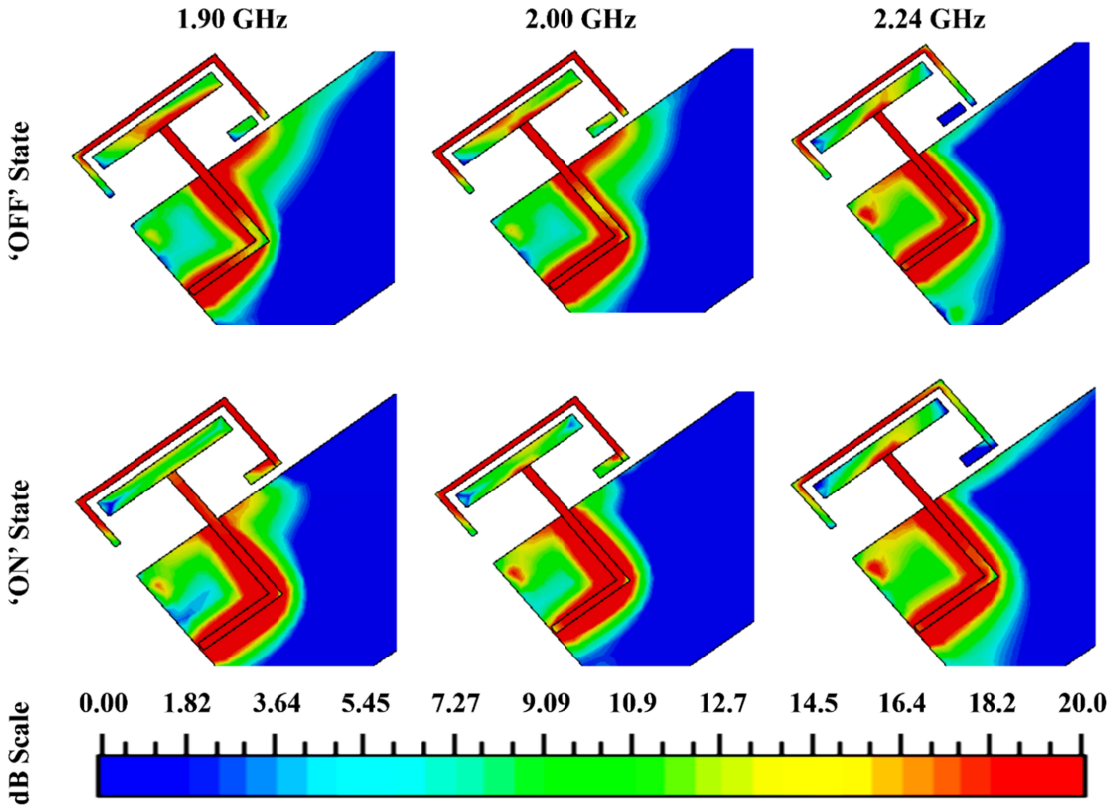

Figure 6.4: Surface current distributions of the pattern reconfigurable MIMO antennas at different frequencies.

6.1.3 Simulation and measurement results:

The antennas were simulated in CST® Microwave Studio and the simulation results of the s-parameters and radiation patterns were extracted. For the measurement of the S-parameters, the antennas were connected to the Agilent® Technologies 2-port network analyzer placed in the antenna laboratory at Queen Mary, University of London (QMUL). While the radiation pattern, gain and efficiency measurements were taken in the anechoic chamber at QMUL. A photograph of the measurement setup is shown in Figure 6.5. The antenna was simulated and tested in both 'ON' and 'OFF' states of the p-i-n diode. The simulation and measurement results were then post processed in Matlab® for the ease of analysis and comparison.

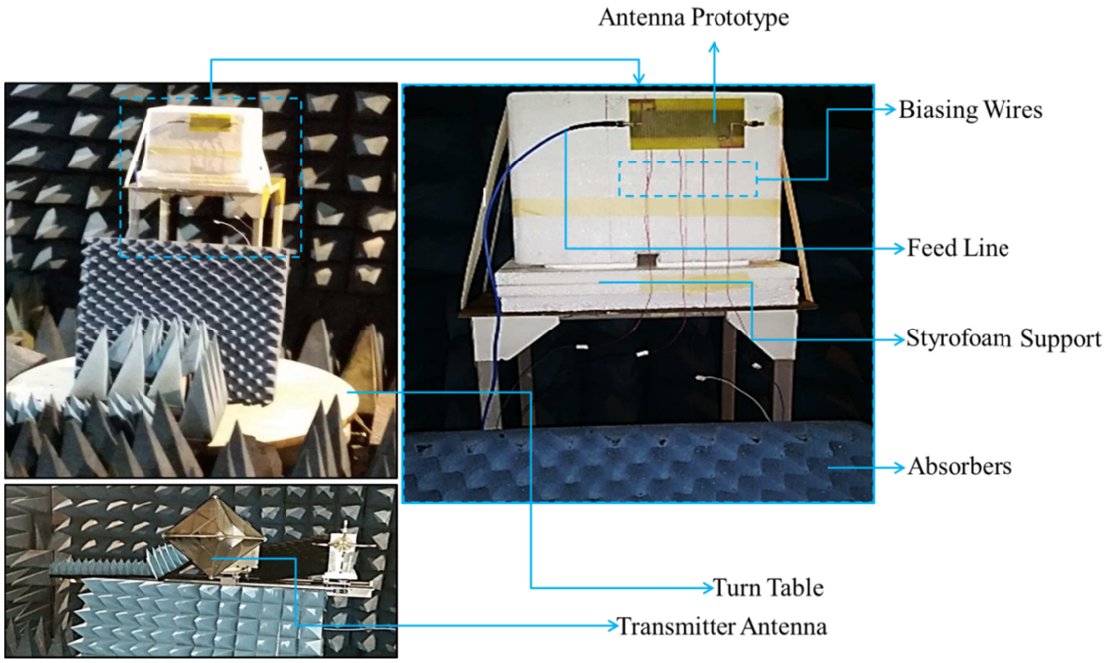

Figure 6.5: A photograph of the measurement setup inside the anechoic chamber at QMUL.

(a) S-parameters:

The simulated and measured S-parameters of the MIMO antennas are shown in Figure 6.6. The s-parameters of only one antenna in are shown as the two antennas are identical.

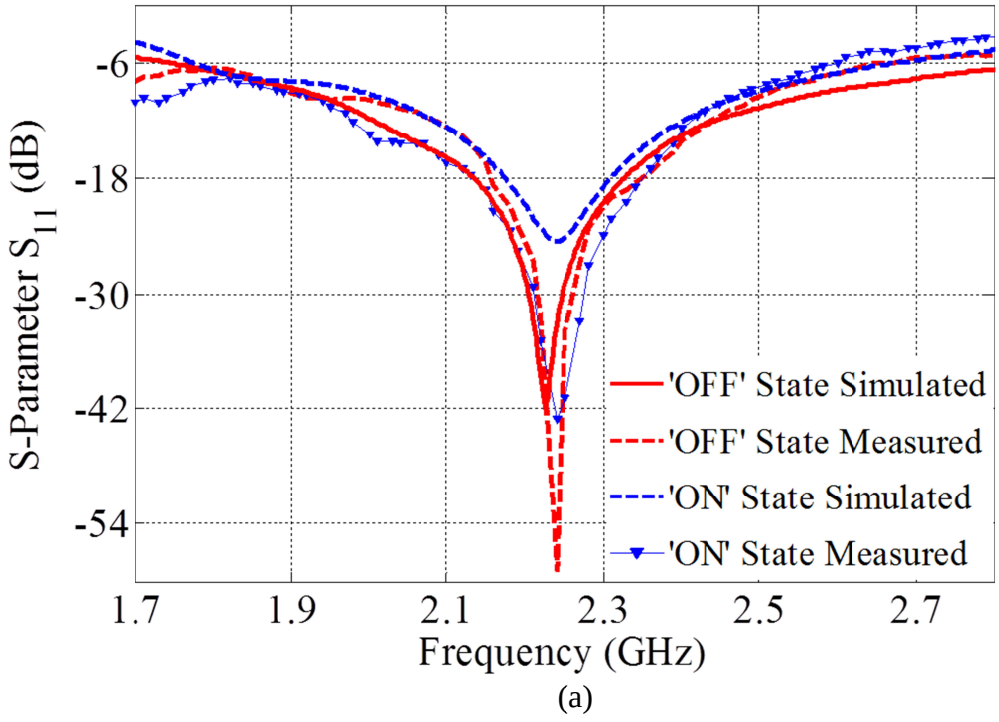

(a)

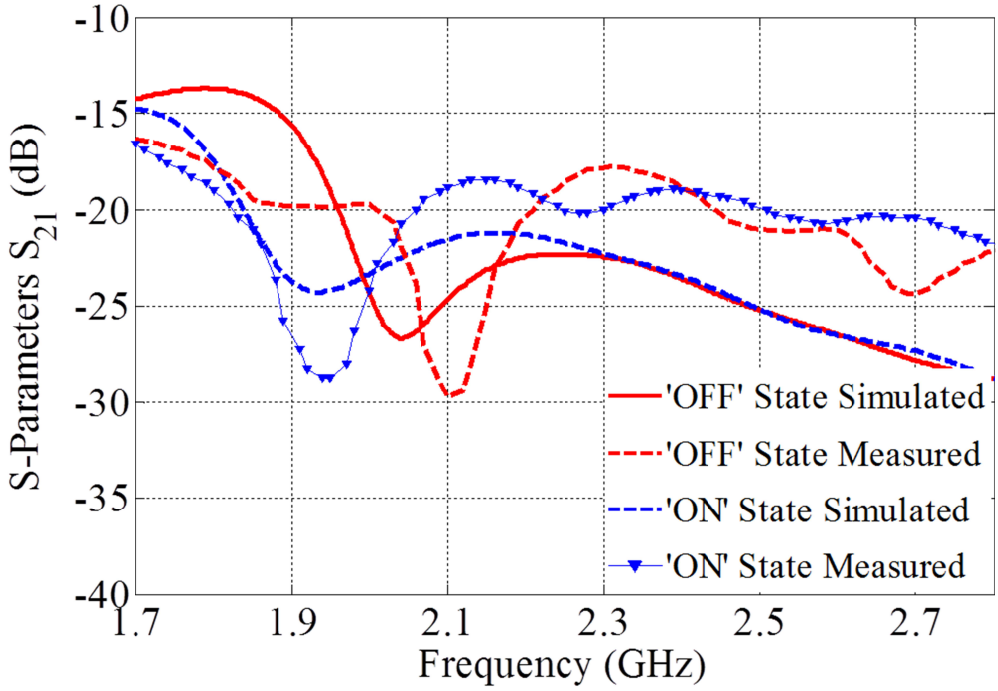

(b)

Figure 6.6: S-parameters of the pattern reconfigurable MIMO antennas for mobile handsets. (a): Return loss. (b): Isolation performance.

The simulated s-parameters of the MIMO antennas show good agreement with the measured ones. However, a minor shift in the frequency was observed due to the measurement setup and the tolerances in the material properties. Each antenna of the MIMO configuration resonated in a 6 dB bandwidth of 1.75 – 2.67 GHz. The MIMO antennas are thus capable of covering GSM 1800 (1.71-1.88 GHz), GSM 1900 (1.85-1.99GHz), UMTS (1910-2170 MHz), WLAN (2.4-2.48 GHz), LTE band number 2-4, 9-10, 15-16, 23, 30 (1.70-2.36 GHz) and LTE band 7 (2.5-2.69 GHz). Isolation curves for the MIMO antennas are shown in Figure 6.6 (b). The MIMO antennas exhibited a measured isolation better than 18 dB in the whole frequency bandwidth. This is due to the placement of the antennas in diagonal configuration which isolated them in the farfield. The diagonal separation between the antennas is 76 mm which is nearly 0.6 λ at the resonant frequency of 2.23 GHz. The farfield distance of each MIMO antenna can be calculated by using the longest dimension of the antenna which is its vertical length. The vertical length of the antenna is 32.5 mm which gives a farfield distance of 15.7 mm. The antennas are thus placed in each other's farfield and being in mirrored configuration the antennas radiate in opposite directions. Also the diagonal configuration makes them highly isolated in polarization thereby enhancing the

decoupling performance. This results in a low correlation between the farfields of the antennas leading to a better isolation as compared to the other configurations. Simulations have shown that the isolation between the proposed MIMO antennas improves by increasing the diagonal spacing.

(b) Radiation Patterns:

The simulated 3D radiation patterns of the reconfigurable MIMO antennas in both 'ON' and 'OFF' states at different frequencies are shown in Figure 6.7. The 'ON' state radiation patterns of the MIMO antennas are different from the radiation patterns in the 'OFF' state. This can be validated from the current distribution shown in figure 6.4. The magnitude of the current flowing in the upper edge of the ground plane in the 'OFF' is more than the current in in the 'ON' state. Also, the amount of current flowing through the metallic strip increases as the p-i-n diode is turned 'ON'. These changes in the flow of current generate pattern reconfigurability from the MIMO antennas.

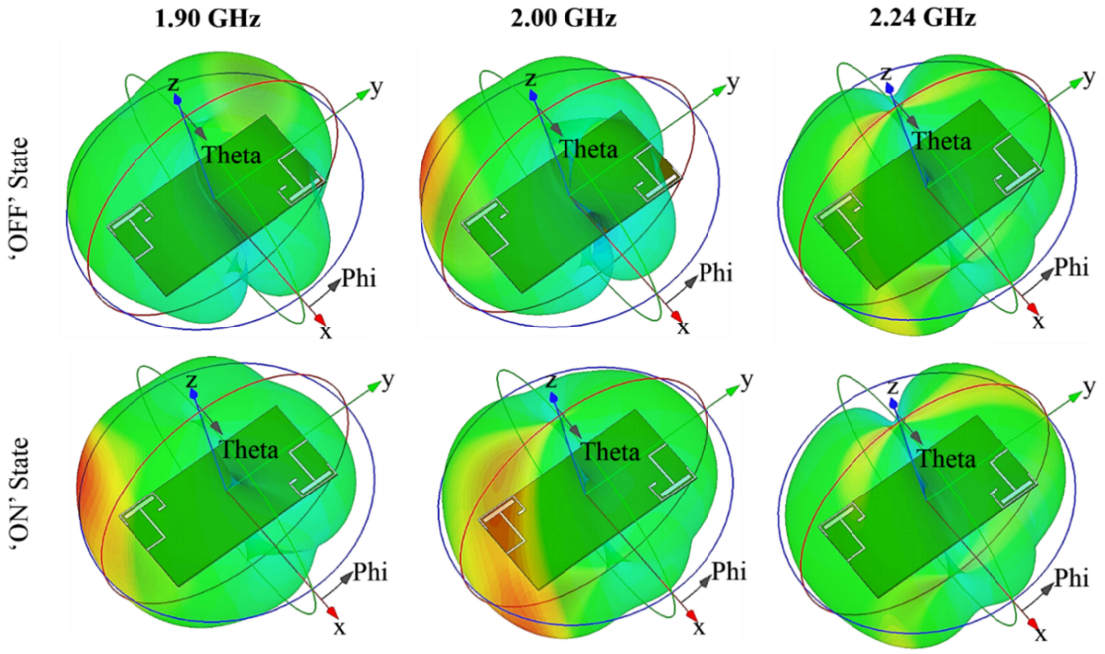

Figure 6.7: Simulated 3D radiation patterns of the pattern reconfigurable MIMO antennas.

The measurement of the radiation patterns was performed in both logical states of the diode switch while placing the antennas in x-z and y-z planes. The polar plots comparing the normalized radiation patterns are shown in figure 6.8 and figure 6.9.

The p-i-n diode is biased using a variable DC power supply with current set to 20 mA and voltage to 0.95 V. The radiation patterns of only one antenna are shown as the two antennas of the MIMO configuration are symmetrical. The simulated and measured radiation patterns agree with some discrepancies which occurred mainly due to the fabrication limitations and the measurement procedure which involves the use of biasing wires, connection cables and RF connectors.

It can be seen that the shape of the radiation pattern in the ‘ON’ state of p-i-n diode is different from that in the ‘OFF’ state. The antennas are pattern reconfigurable in the bandwidth of 1.9–2.1 GHz.

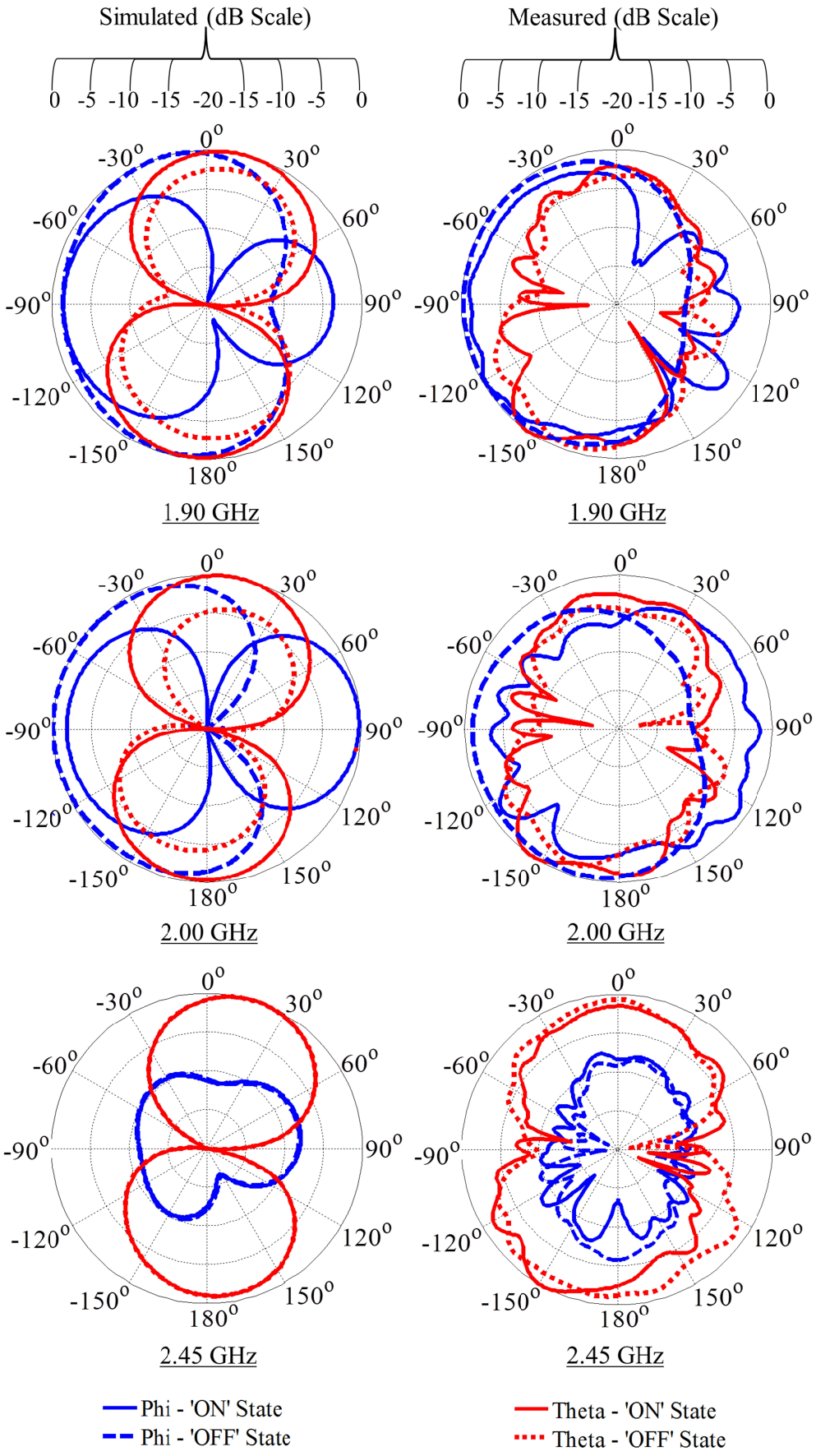

Figure 6.8: Radiation patterns of the pattern reconfigurable MIMO antennas in *x-z* plane.

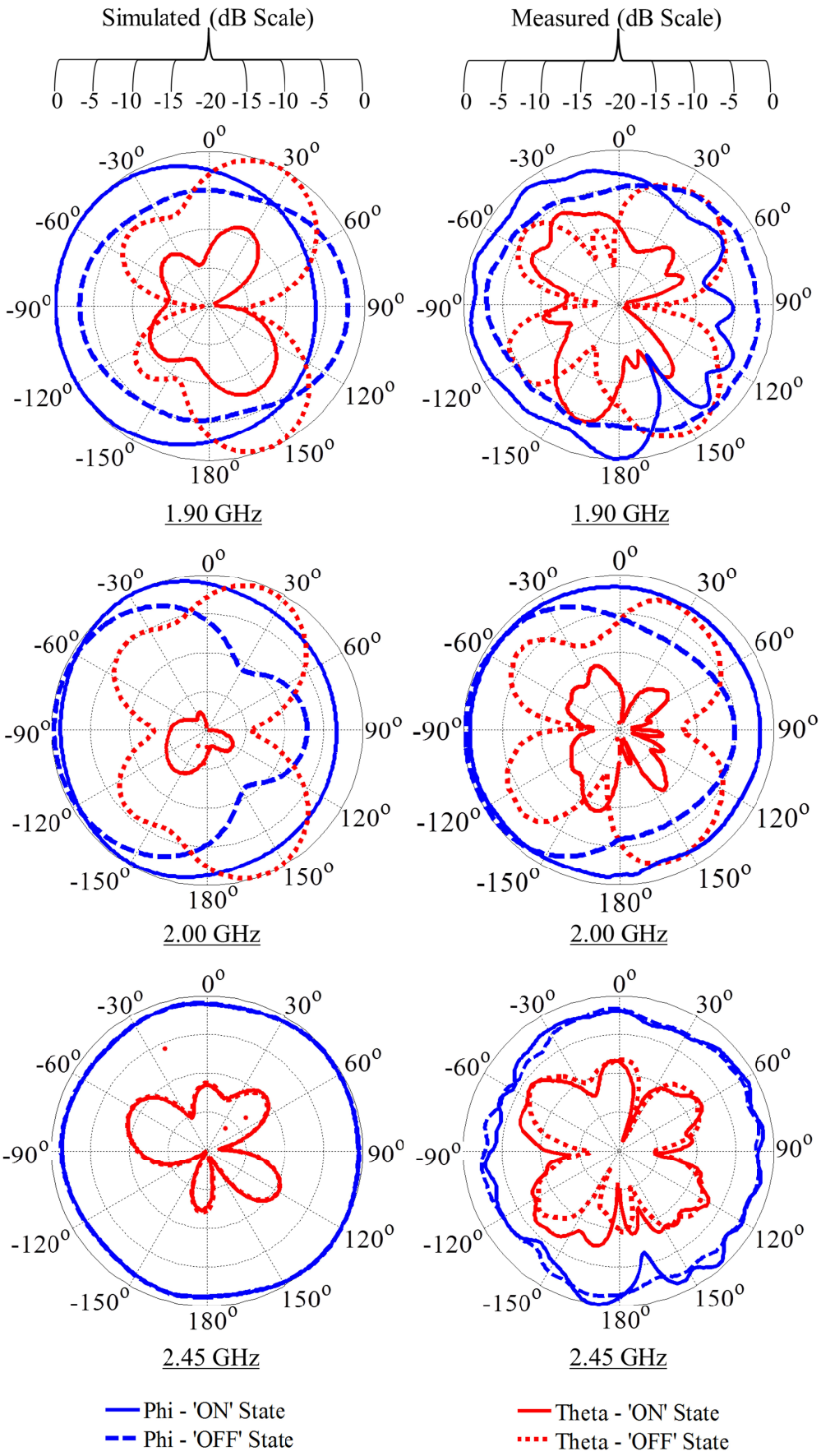

Figure 6.9: Radiation patterns of the pattern reconfigurable MIMO antennas in *y-z* plane.

(c) Gains and Efficiencies

The simulated and measured gains and efficiencies of the pattern reconfigurable MIMO antennas at different frequencies are listed in Tables 6.1 and 6.2 respectively. The measured gain is calculated by the gain comparison method using a standard gain horn. Whereas, the efficiencies are measured using the Wheeler Cap Method. The simulated and measured values of the gains and efficiencies corroborate a good performance of the MIMO antennas. It can be seen from Table 6.2 that the value of efficiency at 2.24 GHz is higher than the efficiency at 1.80 GHz. This is because the return loss at 1.80 GHz is poorer than the return loss at 2.24 GHz. A good return loss ensures a better efficiency and vice versa.

Table 6.1: Gains of the pattern reconfigurable MIMO antennas.

Frequency (GHz)	**Gain (dBi)**			
	'ON' State		**'OFF' State**	
	Simulated	**Measured**	**Simulated**	**Measured**
1.80	1.17	0.96	1.60	1.31
1.90	1.54	1.19	1.47	1.12
2.24	1.84	1.53	1.76	1.64
2.45	1.24	0.92	1.12	0.83

Table 6.2: Efficiencies of the pattern reconfigurable MIMO antennas.

Frequency (GHz)	**Total Efficiency (% age)**			
	'ON' State		**'OFF' State**	
	Simulated	**Measured**	**Simulated**	**Measured**
1.80	53	46	62	56
1.90	71	64	63	58
2.24	81	75	81	73
2.45	70	63	68	64

(d) Diversity Gain

The diversity gains of the pattern reconfigurable MIMO antennas at different frequencies were evaluated using statistical models summarized in [5]-[7]. The diversity gains were calculated in both indoor and outdoor environments using the post processing toolbox in CST® Microwave Studio. The effective values of diversity gain mentioned in Tables 6.3 and 6.4 represent a good diversity performance of the MIMO antennas. This is because the antennas exhibit a good isolation which reduces the correlation coefficient thereby increasing the diversity gain. Also, the average

radiation efficiency of the reconfigurable MIMO antennas is more than 85% which further improves the diversity performance. The diversity gain of the reconfigurable MIMO antennas is better than 8 dB in the 'ON' state and 7 dB in the 'OFF' state.

Table 6.3: Diversity gains of the reconfigurable MIMO antennas in the 'ON' state.

Freq. (GHz)	**Envelope Correlation Coefficient**				**Radiation Efficiency**	**Effective Diversity Gain (dB)**	
	Indoor Environment		**Outdoor Environment**		η_r	**Indoor Environment**	**Outdoor Environment**
	ρ_e	DF	ρ_e	DF			
1.80	0.047	0.976	0.023	0.988	83	8.10	8.20
1.90	0.052	0.973	0.025	0.987	89	8.66	8.78
2.24	0.051	0.974	0.054	0.972	85	8.28	8.26
2.45	0.013	0.993	0.028	0.986	82	8.14	8.09

Table 6.4: Diversity gains of the reconfigurable MIMO antennas in the 'OFF' state.

Freq. (GHz)	**Envelope Correlation Coefficient**				**Radiation Efficiency**	**Effective Diversity Gain (dB)**	
	Indoor Environment		**Outdoor Environment**		η_r	**Indoor Environment**	**Outdoor Environment**
	ρ_e	DF	ρ_e	DF			
1.80	0.262	0.859	0.181	0.905	89	7.65	8.05
1.90	0.176	0.908	0.135	0.930	88	7.99	8.18
2.24	0.044	0.978	0.044	0.978	84	8.22	8.61
2.45	0.013	0.993	0.027	0.986	81	8.04	7.99

6.1.4 Parametric Analysis:

A parametric analysis was performed on the feed gap by changing its value from 0.83 mm to 1.63 mm and the effect on the s-parameter was observed. Another parametric analysis was carried out on the length and width of the extended metallic strip which contributes to the reconfigurability of the radiation pattern. The parametric analysis is only performed in the 'ON' state of the p-i-n diode when the metallic strip contributes to the reconfigurability of the radiation pattern. Each parametric analysis will be discussed in later subsections.

(a) Coupling Gap of the Feed

A parametric analysis was carried out on the coupling gap of the feed. This gap is represented as Gap_3 in the antenna design. It can be seen from the S-parameter

curves in figure 6.10 that a gap of 1.23 mm gives a better 6 dB bandwidth and a better return loss performance when compared to the other values of the coupling gap.

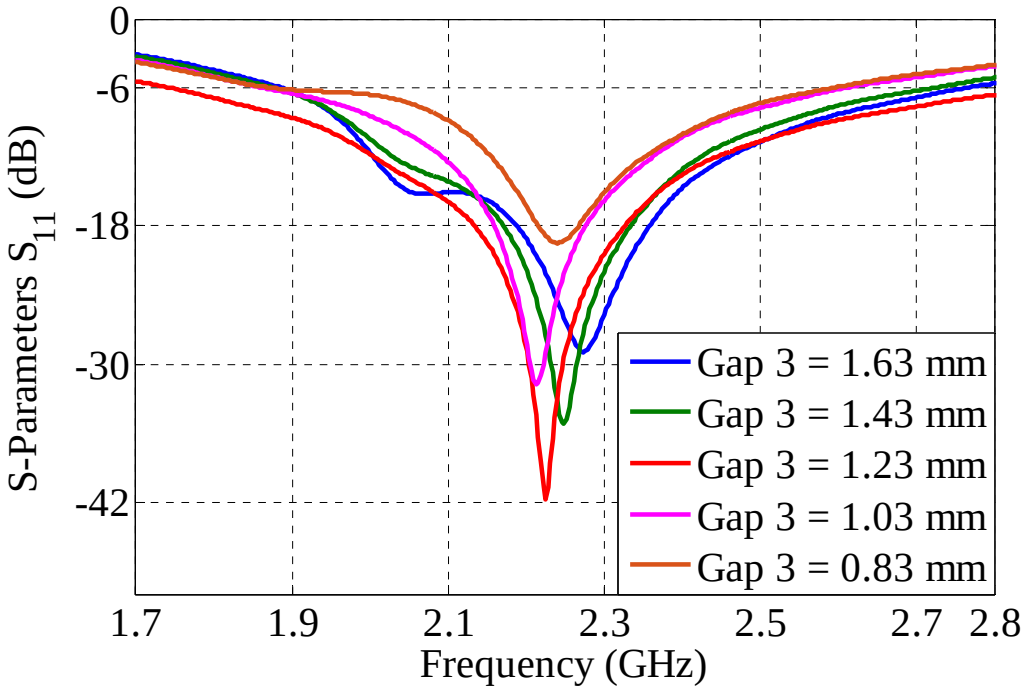

Figure 6.10: Effect on the return loss by varying the coupling gap of the reconfigurable antenna's feed.

(b) Length of extended metallic strip:

A parametric analysis was also performed on the length of the extended metallic strip which contributes to the reconfigurability of the radiation pattern. The length of the strip was changed from 0 mm to 4.5 mm. It can be seen from figure 6.11 (a) that the effect of change in length on the return loss is almost negligible and the 6 dB bandwidth stays nearly the same. The width is kept at the proposed value of 2 mm.

The effect of the variation of length on the radiation pattern is presented in figure 6.11 (b) which shows that the change of length controls the directivity of antenna. The radiation patterns are plotted at 1.90 GHz at which antennas are showing pattern reconfigurability. The length of 4.5 mm is selected as it gives a considerable change in the directivity without altering the frequency bandwidth. Also, if the length of the extended metallic strip is controlled using the diode switches, the radiation pattern reconfigurability can be achieved in more than one direction. This can be seen from figure 6.11 (b) that the direction of maximum radiation is different at each value of length.

(c) Width of extended metallic strip:

Another analysis was done on the width of extended metallic strip which contributes to the pattern reconfigurability. The width was changed from 1 mm to 4 mm and it can be seen from figure 6.12 that the effect of change in width on the return loss and the radiation patterns is almost negligible. The radiation patterns are plotted at 1.90 GHz and the length is kept at the proposed value of 4.5 mm.

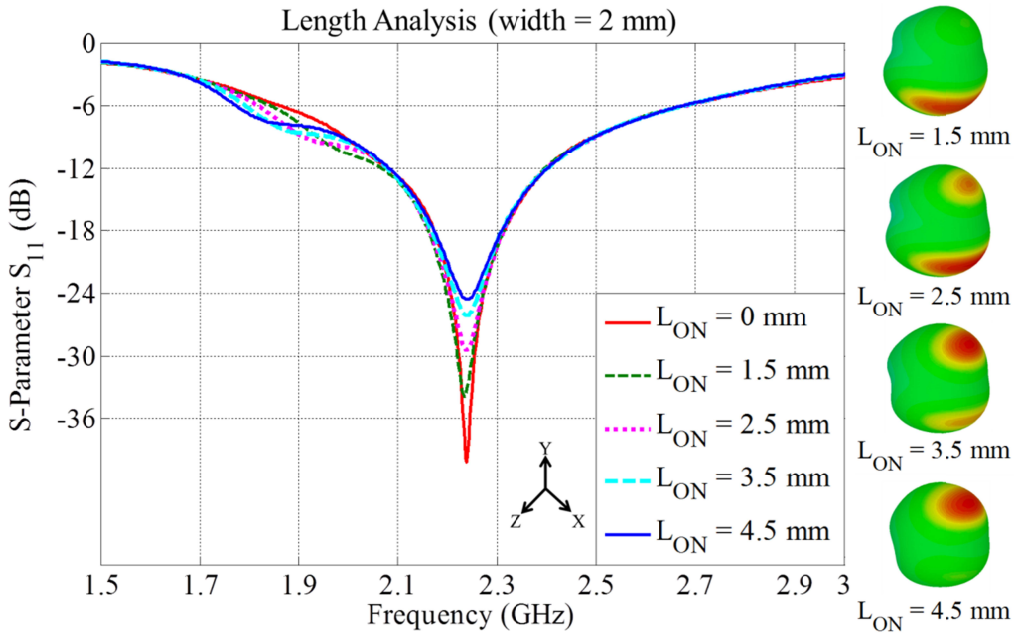

Figure 6.11: Effect on the return loss and the radiation pattern by changing the length of the extended metallic strip of the reconfigurable antenna.

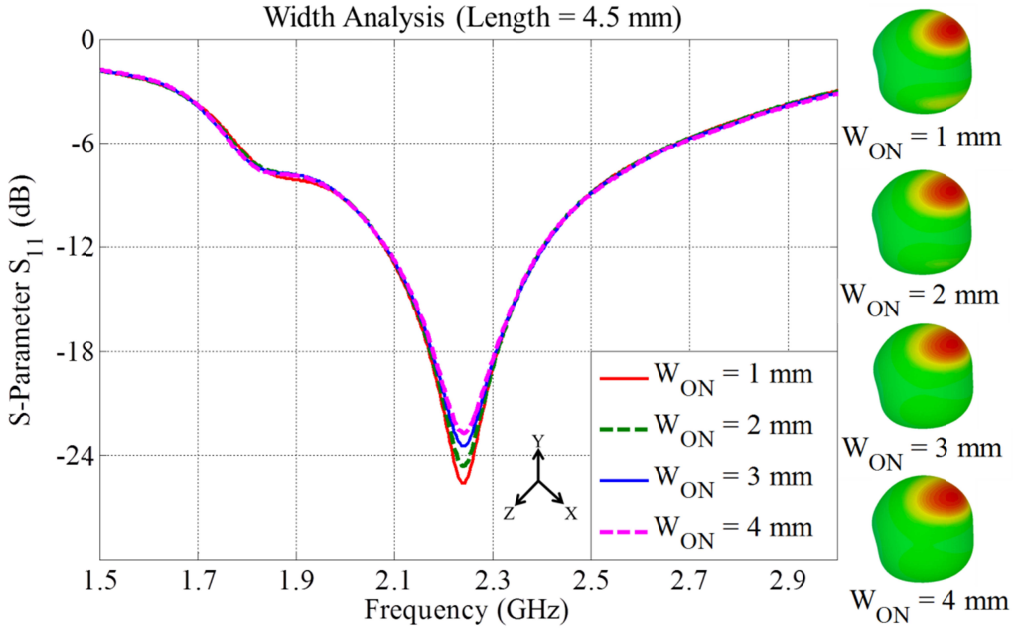

Figure 6.12: Effect on the (a): return loss and (b): the radiation pattern by changing the width of the extended metallic strip of the reconfigurable antenna.

Summary

A pair of printed pattern reconfigurable MIMO antennas for mobile handsets was presented in this chapter. The antennas are meandered monopoles fed through coupling for a compact volume. Each antenna is wideband covering GSM 1800/1900, UMTS, WLAN, and several LTE frequency bands. Each antenna is capable of pattern reconfigurability in the bandwidth of 1.9-2.1 GHz. The pattern reconfigurability is achieved by connecting or disconnecting the extended metallic strip using the p-i-n diode switch. The simulation and measurement results show good agreement with some discrepancies. The measured decoupling between MIMO antennas is better than 18 dB for all the cellular frequency bands covered by the antennas. The design proposed in this work represents a good example of pattern reconfigurable antennas for new generation smartphones. However, modified designs can be made in future to cover cellular frequency bands below 1 GHz.

References

[1] CST® Microwave Studio, Computer Simulation Technology Homepage [Online]. Available: http://www.cst.com, Version, 2013.04, Release, Oct 04, 2013

[2] Balanis, C. A., "Antenna Theory Analysis and Design", Edition, 3rd, A John Wiley & Sons, Inc., Publication, ISBN 0-471-66782-X, 2005.

[3] S.R. Saunders, “Antennas and propagation for wireless communication systems”, Wiley, 1999.

[4] M. Schwartz, W. R. Bennet and S. Stein, “Communication systems and techniques”, McGraw Hill, 1996.

[5] V. Plicanic, “Antenna Diversity Studies and Evaluation”, Master Thesis, LUND University in cooperation with Ericsson Mobile Communications AB, May 2004.

[6] Z. Ying, “Characterization of multi-channel antenna performance for mobile terminal by using near field and far field parameters,” COST 273 TD (04) (095) Goteborg, Sweden, June, 2004.

[7] C. C. Chiau , “Study of the Diversity Antenna Array for the MIMO Wireless communication Systems”, Ph.D. Thesis, Queen Mary University of London, April 2006.

CHAPTER 7
CONCLUSIONS AND FUTURE WORK

In this chapter the antenna designs presented in the research work will be concluded and the future works will be discussed. A summary of all the designs will also be given.

7.1 Conclusions

This report presented several new designs of multiband antennas for wireless terminals such as mobile phones and tablets. Three designs of MIMO antennas for mobile handsets and two designs of MIMO antennas for tablet applications have been presented. Moreover, a design of pattern reconfigurable MIMO antennas for smartphone applications was also proposed. The designs are based on meandered and multi-branch monopole configurations. The antennas are direct and coupled fed with the coupling gap being optimized to achieve a good impedance bandwidth. It has been observed that the frequency bandwidth for coupled fed antennas is better than the direct fed designs. However, for achieving a resonance at frequency below 1 GHz, direct fed antennas are better as they achieve a better return loss as compared to the coupled fed antennas.

Two designs of coupled fed monopole antennas based on meandered and multi-branch configuration were presented for mobile handsets. The antennas were presented in MIMO configuration with simple decoupling structure etched on the bottom layer of the substrate. The decoupling technique used in these designs involved ground slots and inverted L-shaped metallic extensions in the ground plane.

This achieves isolation better than 15 dB over all the frequency bandwidths accommodated by the antennas. The antennas cover 2G, 3G and 4G cellular services. A compact antenna for covering 4G LTE frequency bands was also presented. The design is composed of two antennas placed at a gap of 2.5 mm from the shorter edges of the substrate. Each antenna is composed of monopole strip that is meandered to form a loop structure. Additionally, an inverted L-shaped branch is also added to widen the bandwidths at the upper and lower frequency bands thus enabling the antenna to cover 2G and 3G cellular services. The antennas cover most of the 4G cellular frequencies with isolation better than 12 dB.

One of the designs of MIMO antennas presented for tablet applications is composed of four identical antennas etched at the no-ground corners of the substrate. The overall volume of the substrate is almost the same as most of the commercially available tablets. The decoupling technique used in the design is composed of six vertical and two horizontal slots in the ground plane. Additionally, two metallic branches are also placed in coupling with the ground plane. These branches couple a large amount of current flowing between the ports thus enhancing the isolation especially at the lower frequency bands. The proposed antennas however cover only 2G and 3G cellular frequency bands. In order to cover 4G LTE as well, another design of the MIMO antennas was presented for tablet applications. This design is composed of four antennas with two antennas making MIMO pair for 4G LTE and the other two antennas make MIMO pair for covering 2G and 3G cellular services. The antennas are arranged in diagonal symmetry for the enhancement of isolation.

The reconfigurable antenna design presented in the report is composed of two simple and compact meandered monopole antennas with additional metallic branches. Each metallic branch can be connected and disconnected using p-i-n diode switch. This allows the current to flow into the metallic branch thus achieving pattern reconfigurability. The antennas are placed diagonally in mirrored configuration to reduce the farfield correlation thus improving the isolation performance. The MIMO antennas are pattern reconfigurable in the frequency range of 1.9-2.1 GHz. The proposed design is compact and covers most of the cellular frequency bands.

All the antennas were designed and fabricated on FR-4 substrate with dielectric constant of 4.3-4.4 and loss tangent of 0.02. The antennas were designed and simulated in CST® Microwave Studio, whereas, the testing and measurements were performed in the antenna laboratory at Queen Mary university of London. It has been observed the simulation and measurement results agree with some discrepancies which mainly occurred due to the tolerances in the substrate properties and the measurement setup. The key parameters discussed in the report include s-parameters, radiation pattern, gain, efficiency, envelope correlation coefficient and the diversity gain. The simulated and measured results were post processed in Matlab® for the purpose of analysis and comparison. A detailed parametric analysis was also included at the end of each chapter to understand the effect of changing various dimensions on the results of the antenna. The dimensions of each design have been tuned for achieving an optimum combination of the return loss and isolation.

The antenna designs presented in this research work are compact with simple decoupling techniques. The design methodology is based on meandered microstrip configurations to achieve compact monopole and loop type structures. This makes the designs suitable for slim mobile handsets. The decoupling techniques are mainly based on ground slots and extended metallic branches to increase the isolation between multiple antennas in a compact volume. The antennas that have been presented for handset and tablet applications resonate in multiple frequency bandwidths and cover most of the cellular frequencies majorly 2G GSM, 3G HSDPA, WLAN and 4G LTE frequency bands. A summary of the antenna designs is shown in Table 7.1. It has been observed that the achievement of isolation better than 15 dB at frequency bands below 1 GHz is a challenging task. This is due to the increased correlation between MIMO antennas which largely reduces the efficiency and gain. The isolation achieved for most of the antenna designs is better than 15 dB. The designs and the results make the antennas suitable for next generation mobile terminals.

Table 7.1: Summary of the proposed antenna designs.

Antenna Design	Main Features	Cellular Coverage
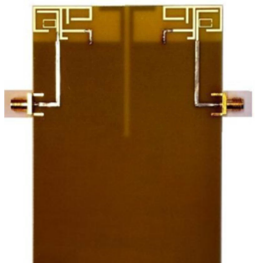	- Two MIMO antennas - Printed - Based on multi-branch monopole configuration - Decoupling – Ground slot and inverted L ground extensions - Suitable for smartphones and phablets - Four 6 dB bandwidths - Isolation better than 15 dB	- 2G GSM 850/900/1800/1900 - 3G HSDPA 800/850/900/1700/1900/2100 - 4G LTE Bands 5, 8, 19, (824 – 960 MHz) - 4G LTE Bands 1-4, 25, 30 (1710 – 2360 MHz) - WLAN 802.11 b/g/n 2.45 GHz - WLAN 802.11 a/n 5 GHz - WiMAX 3.4 GHz - WLAN 802.11y
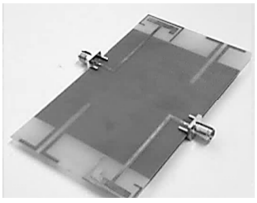	- Two MIMO antennas - Printed and compact - Based on meandered monopole configuration - Decoupling – Dual decoupling with ground slots and inverted L ground extensions - Suitable for smartphones - Wide 6 dB bandwidth - Isolation better than 15 dB	- 2G GSM 1800/1900 - 3G HSDPA 1700/1900/2100 - 4G LTE Bands 1-4, 7, 25, 30 (1710 – 2690 MHz) - WLAN 802.11 a/b/g/n 2.45 GHz
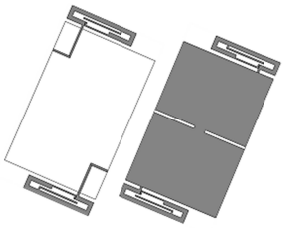	- Two MIMO antennas - Simple geometry - Loop configuration - Ground slots for isolation enhancement - Suitable for smartphones - Three 6 dB bandwidths - Isolation better than 12 dB in the bands below 1 GHz and 15 dB in the upper frequency bands	- 2G GSM 850/1900 - 3G HSDPA 800/850/2100 - 4G LTE Bands 1-2, 7, 30 (1920 – 2690 MHz), 5, 12-13, 17-20, 26, 28 (680 – 912 MHz) - WLAN 802.11 a/b/g/n 2.45 GHz
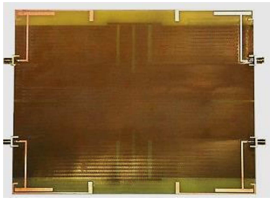	- Four MIMO antennas - Printed and coupled fed - Based on meandered monopole configuration - Ground slots and coupled metallic branches for decoupling - Suitable for tablets - Four 6 dB bandwidths - Isolation better than 15 dB	- 2G GSM 900/1800/1900 - 3G HSDPA 900/1700/1800/1900 - WLAN 802.11n 2.45 GHz - WiMAX 3.4 GHz
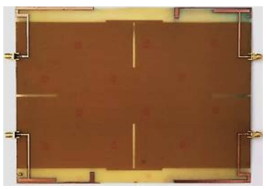	- Four MIMO antennas with two pairs - Two antennas for 2G/3G and two antennas for 4G cellular coverage - Printed - Simpler decoupling technique - Suitable for tablets - Three 6 dB bandwidths for 3G pair - Two 6 dB bandwidths for 4G pair - Isolation better than 15 dB	- 4G LTE band 12-13, 17-18, 20, 28-29 (680 – 865 MHz) - 4G LTE band 30 (2305 – 2360 MHz) - WLAN 802.11n 2.45 GHz (4 x4 MIMO) - 2G GSM 850/900/1800/1900 - 3G HSDPA 800/850/900/1700/1900/2100
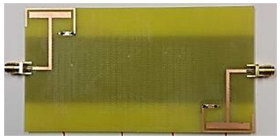	- Two printed MIMO antennas - Pattern reconfigurable - Meandered monopoles with additional metallic branches switched through p-i-n diode - Wide 6 dB bandwidth - Isolation better than 18 dB	- 2G GSM 1800/1900 - 3G HSDPA 1900/2100 - 4G LTE Bands 1-4, 7, 25, 30 (1750 – 2670 MHz) - WLAN 802.11 a/b/g/n 2.45 GHz - WLAN 802.11h (3.4 – 3.6 GHz)

7.2 Future works

The designs proposed in this thesis are of compact and multiband antennas for mobile terminals such as smartphones and tablets. However, improvements in the proposed designs should be studied and developed in the future. The tasks for the future work can be summarized as:

- Development of techniques to improve antenna efficiency for all the designs.
- Development of techniques to further reduce the overall size of antenna. This will make it possible to place more than two MIMO antennas with in a compact handset.
- Study and implementation of methods to evaluate the losses due to the head and hand. Also there are numerous positions in which user holds the mobile handset. The gain and efficiency at each position will be evaluated along with the S-parameters.
- Many commercial mobile handsets have metal casings which may induce certain limitations and losses in the antenna designs. It is therefore necessary to study these limitations in the future work. This may involve the tuning of the proposed antenna designs for achieving a better return loss and isolation performance at all the cellular frequency bands.

APPENDIX I: LIST OF CELLULAR FREQUENCIES

Table I: List of second generation (2G) cellular frequency bands

Band Name	**Frequency**
GSM 850	824 – 894 MHz
GSM 900	890 – 960 MHz
GSM 1800	1710 – 1880 MHz
GSM 1900	1850 – 1990 MHz

Table II: List of third generation (3G) cellular frequency bands

Band Name	**Frequency**
HSDPA 800	830 – 890 MHz
HSDPA 850	814 – 894 MHz
HSDPA 900	880 – 960 MHz
HSDPA 1700	1710 – 2170 MHz
HSDPA 1900	1850 – 1990 MHz
HSDPA 2100	1920 – 2170 MHz
UMTS 2100	1920 – 2170 MHz

Table III: List of cellular frequency bands (4G LTE)

Name	**Band Number**	**Frequency Range**
4G LTE 2100	1	1920 – 2100 MHz
4G LTE 1900	2	1850 – 1990 MHz
4G LTE 1800	3	1710 – 1880 MHz
4G LTE 1700/2100	4	1710 – 2155 MHz
4G LTE 850	5	824 – 894 MHz
4G LTE 2600	7	2500 – 2690 MHz
4G LTE 900	8	880 – 960 MHz
4G LTE 700	12	698 – 746 MHz
4G LTE 700	13	746 – 787 MHz
4G LTE 700	17	704 – 746 MHz
4G LTE 800	18	815 – 875 MHz
4G LTE 800	19	830 – 890 MHz
4G LTE 800	20	791 – 862 MHz
4G LTE 1900	25	1850 – 1995 MHz
4G LTE 850	26	814 – 894 MHz
4G LTE 700	28	703 – 803 MHz
4G LTE 700	29	717 – 728 MHz
4G LTE 2300	30	2305 – 2360 MHz

Table IV: List of data networks used in cellular communication

Data Networks	**Frequency**
WLAN 802.11 b/g/n	2400 – 2480 MHz
WLAN 802.11 a/ac/n	5150 – 5350 MHz / 5470 – 5825 MHz
WLAN 802.11y in US	3655 – 3695 MHz
WiMAX 3.4 GHz	3400 – 3600 MHz